UNIVERSITY OF LIVERPOOL

A Computational Fluid Dynamics Analysis of the Distraction Forces Experienced by Stent-Grafts following Fenestrated Endovascular Aneurysm Repair

Thesis submitted in accordance with the requirements of the University of Liverpool for the degree of Doctor of Medicine

By

Steven Mark Jones

February 2016

Acknowledgments

I would like thank Professor Robert Poole, Professor Rachel Williams and Mr Robert Fisher for their supervision and guidance.

The idea of examining the relationship between angulation and force came from initial discussions with Dr Thien How and I am very pleased to have had the opportunity to work with him in the early stages.

I am grateful for additional advice from Professor Rao Vallabhaneni and Professor Richard McWilliams.

I would like to acknowledge the Vascular Research Fund at the Royal Liverpool Hospital for the financial contributions used to purchase both the software and hardware essential for this research.

Many thanks to Dr Andrew England for collaborating on the migration analysis and thanks also to Mr James Scurr, Mr Robin Calderwood, Miss Rana Canavati and Mr Alistair Millen for their participation in the angle measurement study.

Outputs

SM Jones, RJ Poole, TV How, RL Williams, RG McWilliams, JA Brennan, SR Vallabhaneni, RK Fisher Computational fluid dynamic analysis of the effect of morphologic features on distraction forces in fenestrated stent grafts *J Vasc Surg* 2014;60:1648-56

SM Jones, RJ Poole, TV How, RL Williams, RG McWilliams, JA Brennan, SR Vallabhaneni, RK Fisher Computational Fluid Dynamic (CFD) analysis of the Distraction Forces Experienced by Stent-Grafts following fEVAR. Presented at BJS prize session, Vascular Society of Great Britain and Ireland, Manchester, 27th November 2013

SM Jones, RJ Poole, TV How, RL Williams, RK Fisher Haemodynamic evidence that ectatic visceral aortas and narrow iliacs may be a recipe for failure following fenestrated Endovascular Aneurysm Repair (fEVAR). Presented to the British Society of Endovascular Therapy, Warwickshire, 27th June 2013

SM Jones, RJ Poole, TV How, RL Williams, RK Fisher Pilot study of Computational Fluid Dynamics in the Analysis of Distraction Force post fenestrated Endovascular Aneurysm Repair. Awarded the prize for best presentation at the European Society for Vascular Surgery Spring Meeting, Frankfurt, 24th May 2013

SM Jones, RJ Poole, TV How, RL Williams, RK Fisher Computational Fluid Dynamics following fEVAR. Novel Image Processing and Meshing method published online at http://www.simpleware.com/industries/case-studies

Abstract

Introduction

One option for repair of abdominal aortic aneurysms with inadequate length of infrarenal neck is fenestrated Endovascular Aneurysm Repair. Significant complications may be caused by stent-graft migration and component distraction which are both resisted by fixation force and provoked by haemodynamic distraction force.

The hypotheses tested in this thesis are that larger angulation of vessels is associated with greater distraction force and that greater distraction force is associated with higher incidence of migration and component distraction.

Method

Interobserver variation of a new method of angle measurement was compared with the standard method currently in use in our unit. Computer models of complete fenestrated stent-grafts and their individual components (proximal body, distal body and limb extensions) were then constructed based on the postoperative computed tomography scans of 54 patients. Computational Fluid Dynamic analysis in steady state was used to quantify the distraction force acting on each device. Blood pressure was kept constant at 160mmHg and the impact of morphological features upon distraction force was assessed. To test the second hypothesis, patient-specific blood pressures were used to obtain *in situ* distraction forces that were then related to the incidence of migration and component distraction.

Results

There were no significant differences between the old and new methods of angle measurement (p=.723, WSR).

Inlet cross-sectional area (XSA) exhibited a strong, positive correlation with total RDF in complete stent-grafts, proximal body and distal body components. Outlet

angulation ≥45° was significantly associated with greater total RDF in complete stent-grafts and limb extension components (Median total RDF in complete stent-grafts with angle <45° = 2.6N vs 6.2N in those ≥45°, p<.001. Limb extensions: 1.4N vs 2.1N, p=.004, MWU).

There was no significant difference between total RDF acting on the proximal or distal bodies that underwent migration or component distraction versus those that did not. Limb extensions that were observed to migrate were exposed to significantly greater total RDF compared to those that did not migrate (Median total RDF 2.9N, range 2.7-6.3N versus 1.6N, range 0.4-3.8N, p=.003, MWU).

Conclusions

For a given blood pressure XSA was the most important morphological determinant of total RDF. Outlet angulation of complete stent-grafts and limb extensions was associated with significantly greater total RDF. In limb extensions, greater distraction force was significantly associated with migration. The results suggest caution when planning distal seal in ectatic iliac vessels.

Contents

List of Figures

List of Tables

Glossary

AAA	Abdominal Aortic Aneurysm
AGM	Anterior Gold radiopaque Marker (of proximal body)
ARF	Acute Renal Failure
ASA	American Society of Anaesthesiologists (classification)
AUI	Aorto-Uni Iliac stent-graft
BMI	Body Mass Index
BP	Blood Pressure
CA	Coeliac Axis
CFD	Computational Fluid Dynamics
CIA	Common Iliac Artery
CLL	Central Luminal Line
CT	Computed Tomography
DGM	Distal Gold radiopaque Marker (of proximal body)
DICOM	Digital Imaging and Communications in Medicine
eGFR	estimated Glomerular Filtration Rate
EIA	External Iliac Artery
EVAR	EndoVascular Aneurysm Repair
fEVAR	fenestrated EndoVascular Aneurysm Repair
FTAV	Friedman's Two-way Analysis of Variance
GRAE	Graft-Related Adverse Events
IFU	Instructions For Use
IIA	Internal Iliac Artery
IQR	Interquartile Range
LiVES	Liverpool Vascular and Endovascular Service

MI	Myocardial Infarction
MiPPR	Maximum Intensity Projection
MMPs	Matrix Metalloproteinases
MSOF	Multisystem Organ Failure
MWU	Mann-Whitney U test
NARC	Non-Aneurysm-Related Causes
PGM	Proximal Gold radiopaque Marker (of distal body)
RA	Renal Artery
RDF	Resultant Distraction Force
ROI	Region Of Interest
SMA	Superior Mesenteric Artery
WSR	Wilcoxon matched-pair Signed-Rank test
W:L	Window:Level
XSA	Cross-Sectional Area
3D	Three-Dimensional

1 Abdominal Aortic Aneurysms (AAA)

Aneurysms are dilatations of localised segments of the arterial system. The most common type of large vessel aneurysm is an abdominal aortic aneurysm (AAA). Macroscopically AAAs involve all layers of the arterial wall and usually taper at both ends, they are therefore described as 'true', 'fusiform' aneurysms. 95% are infrarenal arising distal to the renal arteries as illustrated in Figure 1.1 (1).

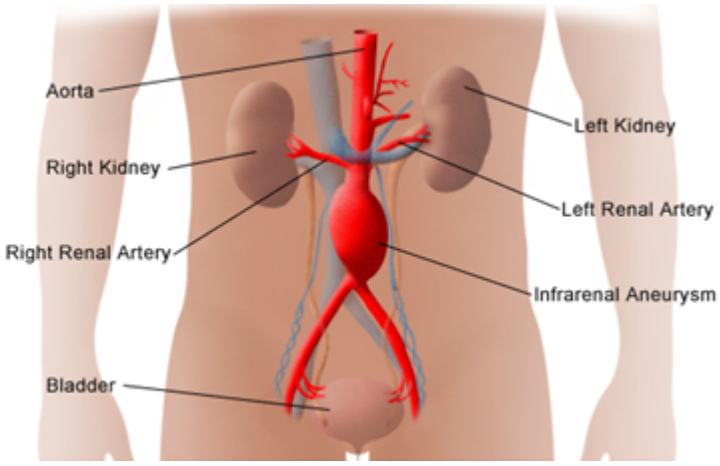

Figure 1.1 Infrarenal abdominal aortic aneurysm.
Image from Stanford Health Care (2)

1.1 Epidemiology

AAA disease is more common in men where the prevalence is 4.9% of those aged 65-74 years (3). It was the direct cause of 3535 deaths in England and Wales during 2013 (4).

1.2 Aetiology and pathogenesis

AAAs are sometimes attributed to atherosclerosis. The main risk factors are the same for both diseases (smoking, hypertension, hypercholesterolaemia, age and male sex (5)) but the true aetiology of AAA disease is likely to be multifactorial

with complex interaction between environmental and genetic factors. Matrix metalloproteinases (MMPs) have been implicated in the degradation of the aortic wall and a transition at one locus of the MMP9 gene may provide some explanation of the strong link to the increased incidence observed with a positive family history (6).

AAA disease is characterised by loss of elastin and smooth muscle cells from the aortic media. Inflammation leads to excessive collagen deposition and thickening of the arterial wall (7). These abnormalities reduce the tensile strength of the vessel to withstand the forces imposed by arterial blood pressure. The structural changes associated with Marfan's and Ehlers-Danlos syndromes may have the same end result in terms of aortic wall weakening and dilatation but remain separate clinical entities.

1.3 Clinical presentation

AAA is usually asymptomatic. The natural history is of gradual expansion and eventual rupture which classically presents as severe abdominal or back pain and hypovolaemic shock. At this point mortality approaches 80-90% (8).

1.4 Screening

Screening for AAA with an abdominal ultrasound scan significantly reduces both the rate of aneurysm rupture (9) and all-cause mortality (3). It has also been proven to be cost effective (10) and the NHS Abdominal Aortic Aneurysm Screen Programme (NAAASP) has now been introduced throughout the UK to offer ultrasound imaging to all men aged 65 years. The initial yield rate of this screening programme appears to be less than was originally forecast (11), possibly due to more recent primary care emphasis on blood pressure control

and smoking cessation (12) as well as increased use of cross-sectional imaging by other medical specialities.

1.5 Treatment threshold

No benefit has been found from repair of AAA <55mm (13) therefore following diagnosis most patients enter a surveillance programme. As the AAA nears the treatment threshold of 55mm a computed tomography (CT) scan is usually performed to identify whether it is anatomically suitable for endovascular or open repair. This treatment threshold is based on comparison of the risk of rupture with the risk of open repair. At 40-55mm diameter a AAA has approximately 0.6% risk of rupture per year (13) and 2.7-5.8% operative mortality from elective repair (13, 14). For AAA of up to 60mm diameter the risk of rupture is 10.3% (15) with no increase in mortality from elective repair (2.1-6.3%) (13, 14).

1.6 Open repair

The aim of open AAA repair is to replace the aneurysmal segment with a synthetic Dacron graft. Adequate access is usually achieved with a midline laparotomy or large transverse abdominal incision. The small bowel is packed into the right side of the abdomen and the aneurysm is identified at the base of its mesentery. Mobilisation of the duodenum and dissection through the connective tissue in front of the infrarenal aorta is undertaken to expose a segment of normal aorta on which to apply a cross clamp. This normal segment of aorta or 'aneurysm neck' is also used as the site for the proximal anastomosis. Inadequate length of infrarenal neck obviates the need to either clamp above one or both renal arteries or in some cases above all of the visceral vessels. The

more proximal the anastomosis, the more complex the dissection and reconstruction becomes and the more potential morbidity is introduced.

Depending on whether the aneurysm extends into the iliac vessels or is confined to the abdominal aorta a tube or bifurcated graft is anastomosed to normal arterial tissue using an 'inlay' technique with a continuous monofilament suture as is shown schematically in Figure 1.2.

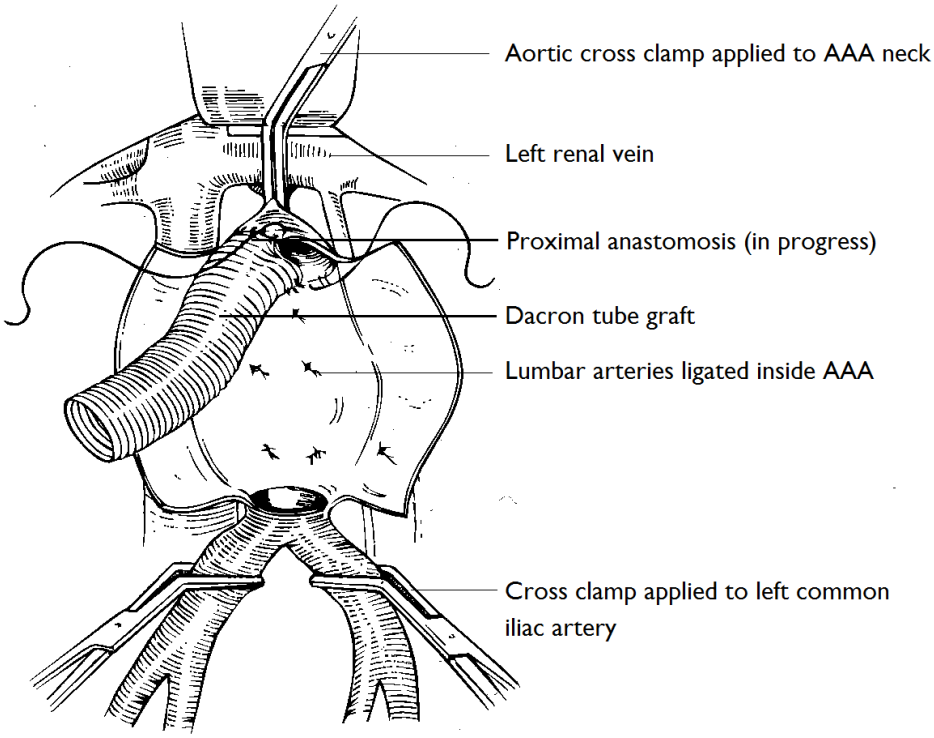

Figure 1.2 Inlay repair of abdominal aortic aneurysm with Dacron tube graft. Image adapted from Kirk and Winslet (16)

1.6.1 Mortality and morbidity of open repair

In 2008, Vascunet (a collaboration of European Vascular registries) reported 7.5% mortality for elective AAA repair. This compared unfavourably with most other countries and prompted the introduction of a AAA Quality Improvement Programme, the aim of which was to reduce mortality to 3.5% by 2013 (17). National Vascular Database (NVD) figures from 2013 estimated elective

infrarenal AAA mortality had fallen to 2.4% with significant improvements seen in data governance (18). The incidence of the more common postoperative complications include chest infection (36.8%), impaired renal function (11.2%) with 6.0% requiring some form of renal replacement therapy, respiratory failure (8.4%), myocardial infarction (MI, 7.5%), cardiac failure (5.5%), major haemorrhage (4.8%), wound infection (4.7%), bowel ischaemia (2.4%) and lower limb ischaemia (3.5%). Graft infection is a rare (0.8%) but potentially fatal complication of open repair (19).

1.7 Endovascular Aneurysm Repair (EVAR)

An alternative to open repair is Endovascular Aneurysm Repair (EVAR). First described by Parodi in 1991 (20) EVAR involves introduction of a stent-graft into the aorta via small incisions in the groin through which the femoral arteries are accessed. The device itself usually consists of a stainless steel or nitinol stent framework sutured or bonded to a polyester (Dacron) or polytetrafluoroethylene (PTFE) graft fabric. The aneurysm is relined as shown in Figure 1.3 using one or more modular stent-graft components and is excluded from the circulation.

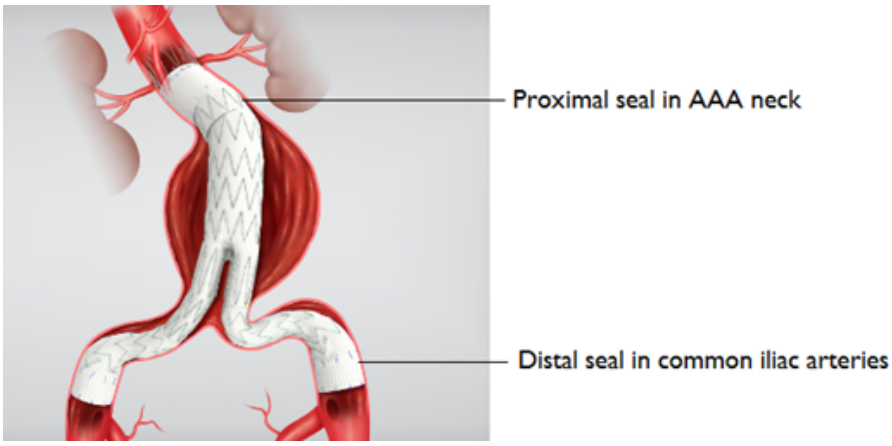

Figure 1.3 Endovascular aneurysm repair performed with a standard Zenith stent-graft. Image from Cook Medical Inc. (21)

The principles of this technique have remained unchanged throughout more than 20 years of stent-graft development. Successful endovascular repair requires adequate access vessels and sufficient length of normal artery proximal and distal to the aneurysm in which to achieve a seal (see Figure 1.3). 'Seal' is the haemostatic apposition of graft fabric to the vessel wall achieved via the radial force of the metal stents.

As devices have evolved so morphological restrictions have been overcome. An infrarenal neck length of 10mm and a common iliac artery length of 15mm are now adequate for proximal and distal seal with the Endurant stent-graft (Medtronic Inc., Minneapolis, USA). The Aorfix (Lombard Medical PLC, Oxfordshire, UK) can be deployed in vessels with up to 90° angulation and lower profile devices like the Zenith LP (Cook Medical Inc. Bloomington, USA) with reduced diameter delivery systems allow access via more challenging ilio-femoral vessels. Overall, modern standard EVAR devices can now be used in up to 63% of cases of AAA (22).

1.7.1 Mortality and morbidity of EVAR

In 2006, 132 (29%) AAA repairs in the UK were performed with EVAR versus 1580 (44%) in 2008 (19). The increasing use of EVAR is likely to be a contributory factor to the reduction in overall mortality for elective AAA repair in the UK over the last ten years.

The EVAR trial reported a significantly lower 30 day mortality from EVAR vs open repair (1.8% vs 4.3%, p=.02) (23) and similar initial results were observed in two other large scale randomised controlled trials (24, 25). Only the French ACE trial failed to show any difference between EVAR and open repair (26). The early survival benefit seen in the EVAR trial was eventually lost due in part to the incidence of late rupture in the endovascular group (23).

EVAR is not associated with lower rates of non-fatal MI, stroke or renal failure despite it being inherently less invasive than open repair (23). Its main

disadvantage is the incidence of graft-related adverse events (GRAE, section 2.8.3) and the need for secondary intervention which are both significantly higher following EVAR (12.6 and 5.1 events per 100 person years respectively) as compared with open repair (2.5 and 1.7 events per 100 person years, p<.0001) (23). This higher incidence necessitates a long-term surveillance programme of imaging to ensure the aneurysm remains excluded from the circulation and to recognise early changes associated with graft failure before clinical consequences occur. A recent health economic analysis suggested that because of these disadvantages EVAR may not currently be cost-effective based on UK standards (27).

1.7.2 Follow-up

There has been a move away from contrast-enhanced CT imaging in the surveillance of standard stent-grafts in order to reduce both radiation exposure – estimated to account for one solid tumour per year in large volume EVAR centres (28) – and contrast induced nephropathy (incidence of 1.25-11% following intravenous contrast use) (29). One approach is to use non-contrast enhanced CT which eliminates the risk of nephropathy and reduces radiation exposure (30). An alternative is duplex surveillance (31). In each case, changes in aneurysm sac volume or diameter trigger further evaluation with contrast-enhanced CT to assess for endoleak and to check stent-graft and seal-zone integrity.

More recently Contrast-Enhanced Ultrasound (CEUS) has been shown to have similar accuracy to contrast-enhanced CT for the detection of endoleak (32). It may therefore have an adjunctive role in EVAR follow-up (33). It does not however provide a structural assessment of stent-graft or seal-zone integrity.

1.7.3 Complications

The main complications that follow-up protocols are designed to detect are:

1.7.3.1 Endoleak

White *et al. (34)* defined endoleak as:

> *"...a condition defined by the persistence of blood flow outside the lumen of the [stent-] graft but within an aneurysm sac or adjacent vascular segment being treated by the [stent-] graft" (34).*

The current standard classification system was published the following year (35) and is represented pictorially in Figure 1.4.

Type I endoleak: blood flow into the aneurysm at the proximal or distal seal-zones. Later further classified as Ia: proximal or Ib: distal. Type I endoleaks carry a high risk of aneurysm expansion and subsequent rupture, they are therefore treated aggressively whenever possible with endovascular extension or open reintervention.

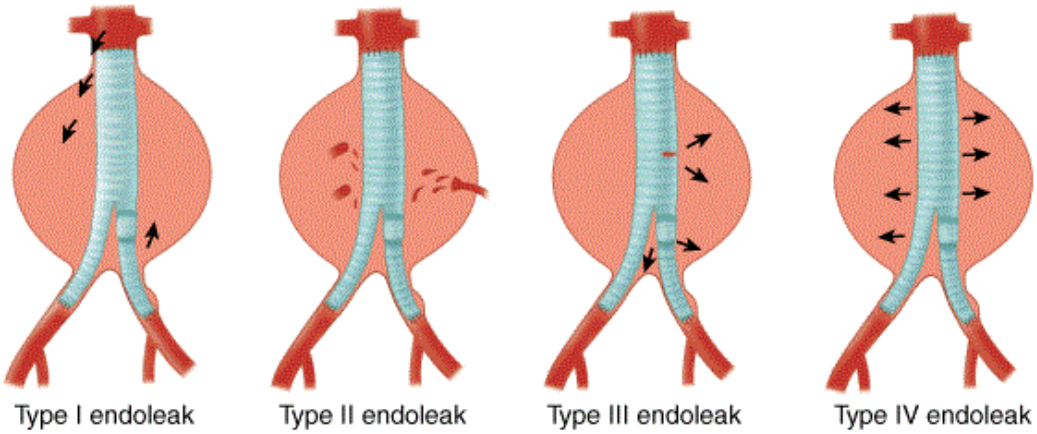

Figure 1.4 Endoleak Classification.
Image from Brunicardi *et al.* (36)

Type II endoleak: retrograde flow into the aneurysm from patent aortic branches i.e. lumbar arteries or inferior mesenteric artery (IMA). Controversy still exists about the significance of type II endoleaks but most are treated conservatively unless associated with continual increases in AAA diameter (37).

Type III endoleak: blood flow into the aneurysm from the junction between stent-graft components or from defects in the graft fabric. Later classified as IIIa: junctional or IIIb: fabric defect. Diagnosis of type IIIb endoleak is often difficult but reintervention in the form of relining or conversion to open repair may be required to prevent AAA expansion and rupture (38).

Type IV endoleak: blood flow into the aneurysm through the normal porosity of the stent-graft fabric in the immediate postoperative period. In practice the incidence of this type of endoleak is now very low due to the availability of modern low porosity fabrics.

Type V endoleak or endotension are terms that have been proposed since the initial White *et al.* classification to describe a pressurised aneurysm following EVAR in the absence of demonstrable flow outside of the stent-graft (39, 40).

1.7.3.2 Migration

Migration is thought to be the commonest mode of failure following standard EVAR (41). Definitions of migration include movement of the stent-graft >10mm relative to an anatomical landmark, movement >5mm or any degree of migration leading to symptoms or requiring therapy (40, 42). Migration can describe distal movement of the proximal seal-zone or proximal movement of the distal seal-zone, both of which have the potential for type I endoleak with the risk of aneurysm expansion and rupture. Distally there are the added risks of limb kinking and occlusion.

Migration is provoked by haemodynamic distraction force and resisted by the fixation force of each stent-graft component (43, 44). The radial force of sealing stents and the presence of barbs or stented fenestrations contribute to fixation force, whilst vessel-related factors such as atherosclerotic disease, thrombus, angulation and progressive dilation may adversely affect the adequacy of fixation (45-52).

1.7.3.3 Limb occlusion

Proximal migration of the iliac limb component may induce kinking. Severe kinking may cause a reduction in vessel cross-sectional area with haemodynamic changes such as increases in peak systolic velocity that can be diagnosed on duplex scanning. Limb kinking may progress to thrombosis and occlusion with clinical implications of lower limb ischaemia.

1.8 Aneurysms not suitable for EVAR

Despite many technological advances in stent-graft design, approximately a third of AAA patients may still be anatomically unsuitable for standard EVAR. The majority of these (76%) are 'juxtarenal' aneurysms with inadequate infrarenal neck length for proximal seal (22).

1.8.1 Juxtarenal aneurysms

Juxtarenal aneurysms involve the infrarenal aorta adjacent to or including the lower margin of the lowest renal artery ostium (53). The exact definition has evolved with the expanding indications for standard EVAR and can differ between publications (54). Generally a juxtarenal aneurysm is not suitable for repair with a standard EVAR device due to an inadequate length of infrarenal neck and therefore another treatment option must be found. Choices include:

1. Conservative management. The aim of any aneurysm repair is to prolong life by preventing rupture. If life expectancy is limited due to other significant co-morbidities then repair may be futile and may actually become the cause of death if attempted. In these situations an informed decision not to treat made in partnership with the patient may be appropriate.
2. Standard EVAR outside of the manufacturer's instructions for use (so called 'off label' use). This may be associated with higher incidence of type I

endoleak at one year (55) and graft thrombosis (45) although other studies show no difference in outcome (56).

3. Open repair with infrarenal cross clamp or the associated higher morbidity of interrenal/suprarenal cross clamping and renal re-implantation (57).
4. Complex endovascular techniques such as fenestrated Endovascular Anuerysm Repair (fEVAR). This approach is described in detail in chapter two.

1.9 Summary

AAA disease affects 4.9% of men aged 65-74 years. Screening and appropriate elective treatment can prevent rupture thus avoiding a mortality of 80%. In the UK increasing numbers of elective aneurysm repairs are being performed by endovascular techniques. Although this reduces 30 day mortality from 4.3% to 1.8%, these benefits are lost in the long-term due to late stent-graft failure. Postoperative surveillance programmes are designed to recognise the signs of this early and allow secondary intervention to be carried out. A third of all AAA are not suitable for the standard endovascular approach and one option for these patients is a fenestrated Endovascular Aneurysm Repair (fEVAR).

2 Fenestrated Endovascular Aneurysm Repair (fEVAR)

2.1 Introduction

fEVAR provides an endovascular option for the treatment of AAA with necks that are unsuitable for standard EVAR. The first two cases were described by Park *et al.* in 1996 (58) who used stainless steel and PTFE stent-grafts with a single 'home-made' fenestration for the inferior mesenteric artery and right renal artery. One year later the Perth Endovascular Group were deploying the first customised fenestrated versions of the Zenith stent-graft manufactured by Cook Medical Inc. (Bloomington, USA) (59). The Zenith fenestrated stent-graft has become the most commonly used fenestrated device worldwide and shares many features with its standard counterpart. The three-piece modular system (Figure 2.1) consists of a proximal fenestrated body (A), a distal bifurcated body (B) and at least one iliac limb extension (C). These components will subsequently be referred to as 'proximal body', 'distal body' and 'limb extension'.

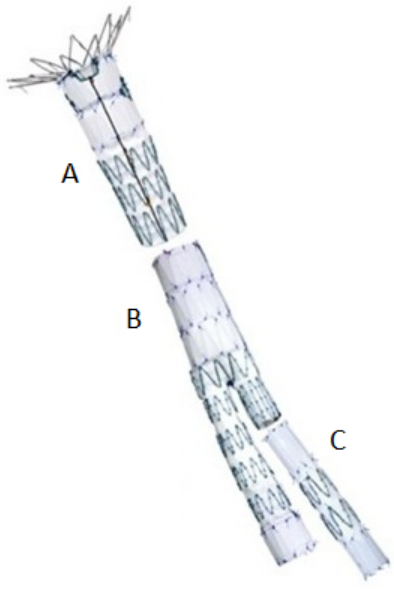

Figure 2.1 Zenith Fenestrated Stent-graft. A: Proximal body, B: Distal body, C: Limb extension. Image adapted from Cook Medical Inc. (60)

2.2 Stent-graft configuration

All three components of the Zenith fenestrated stent-graft are made with the same full thickness woven polyester fabric (Dacron) that is used in the standard version. The fabric is sutured to self-expanding Gianturco stainless steel z-stents using both polyester and polypropylene suture material. The bare metal suprarenal stents have the same barbs as the standard infrarenal device placed at 3mm increments around the radius however they are situated on the additional proximal body component rather than the bifurcated component.

2.2.1 Proximal body

The tubular proximal body component has custom made fenestrations cut into the Dacron fabric to maintain flow to the visceral vessels. Each fenestration is re-enforced with a nitinol ring and is bounded by 2mm high gold radiopaque markers (GM) at the 12, 3, 6 and 9 o'clock positions as shown in Figure 2.2. Fenestrations can be large (8, 10 or 12mm diameter) or small (6 or 8mm high x 6mm wide) and are located around the circumference of the proximal body seal-zone as defined by radial clock face position and distance from the proximal fabric edge.

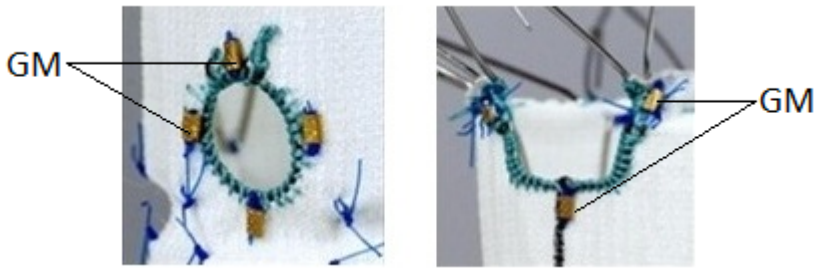

Figure 2.2 Fenestration (left) and Scallop (right). GM: Gold radiopaque Marker. Image adapted from Cook Medical Inc. (60)

Visceral vessels less than 10mm away from the intended position of the proximal fabric edge can usually be accommodated by a scallop. Scallops are 'U'-shaped fabric defects bounded by three radiopaque markers as shown in Figure 2.2.

Without nitinol re-enforcement, fenestrations and scallops may not fully deploy with the rest of the stent-graft. The fenestrations would therefore be difficult to cannulate and the scallop may continue to slowly open to its full extent with the risk of fabric 'shuttering' across target vessels. The mean number of fenestrations per patient in available case series is 2.5 with the most common configuration being a scallop for the superior mesenteric artery (SMA) and two small fenestrations for the renal arteries (59, 61-68). Earlier publications generally describe fewer fenestrations per patient. Semmens' series of fEVAR in Western Australia for instance recruited patients from as early as 1997 and used single fenestration devices in 43.1% of patients (59).

Proximal seal is achieved in the visceral segment with one, or more usually two self-expanding sealing stents located *inside* the graft material and available in diameters from 24 to 36mm in 2mm increments. Oversizing by 10% is standard. Proximal bodies are available in lengths from 94 to 137mm but all now have a distal diameter of 22mm to accommodate the 24mm diameter proximal end of the distal, bifurcated body component. The distal diameter of the proximal body was changed from 24mm to 22mm in 2005 possibly following the experience of the American centres where 16 adjunctive stents/stent-grafts were needed in a total of 119 fEVARs (13.4%) to treat type IIIa endoleaks between the proximal and distal bodies (64). The relative weakness of this junction was intended to allow some inter-component distraction so that not all of the distraction forces experienced at the bifurcation were transmitted to the proximal body. The net effect of this modification was to strengthen the junction between the proximal and distal body.

Diameter reducing ties allow the proximal body to be constrained to approximately 30% of its full diameter during deployment. This feature is illustrated in Figure 2.3 and enables manipulation of the component within the visceral aorta for alignment of fenestrations with their intended target vessels. It also preserves blood flow around the proximal body during the often time

consuming step of target vessel cannulation (69, 70). Removal of the stainless steel wire from the centre of the ties allows the proximal body to expand to its full extent.

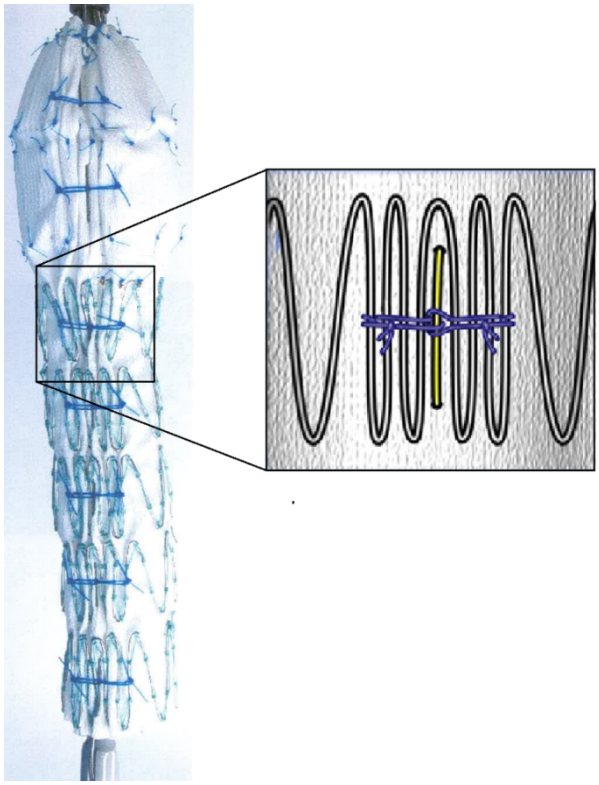

Figure 2.3 Posterior view of a proximal fenestrated body with diameter reducing ties to all stents (blue). Close up shows stainless steel wire (yellow). Image adapted from Oderich *et al.* (70)

2.2.2 Distal body

The distal bifurcated component has a variable body length (76-124mm), ipsilateral limb length (28-62mm) and ipsilateral limb diameter (12-24mm). Overlap within the proximal body should be at least 36mm or two stent lengths although 54mm (three stents) is preferable and offers more resistance to component distraction. The contralateral gate is the segment intended for overlap with the iliac limb extension. It is a standard 23mm long by 12mm diameter and is marked by a radiopaque 'tick' to aid accurate deployment and catheterisation.

2.2.3 Limb extensions

Iliac limb extensions are available in lengths of 39-122mm and distal diameters of 9-24mm to allow ipsi or contralateral extension into the common or external iliac artery. The recommended 22mm overlap with the contralateral gate is built into the sizing therefore a limb extension of 39mm is actually 61mm in total length. Distal seal is achieved via the radial force of one sealing stent.

A three-piece modular design enables application of this technology to a large variation of aorto-iliac anatomy. Figure 2.4 shows the three stent-graft components combined to exclude a juxtarenal aneurysm from the circulation while maintaining flow to the SMA (scallop) and renal arteries (stented fenestrations).

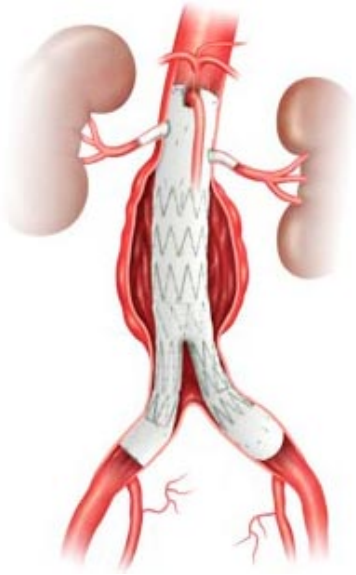

Figure 2.4 A juxtarenal aneurysm treated with a Zenith Fenestrated Stent-graft. Image from Cook Medical Inc. (60)

2.3 Indications for use (fEVAR)

2.3.1 Neck length

The Zenith fenestrated stent-graft is one option for AAAs with a diameter of 55mm or above that are not suitable for standard EVAR. One survey of UK vascular surgeons involved in a fEVAR programme reported that even in the presence of adverse neck features such as short length, conicity, excess angulation and thrombus lining most would still chose standard EVAR outside of the manufactures instructions for used (IFU). The same survey reported that fEVAR was supported in AAAs not at all suitable for standard EVAR due to short or no infrarenal neck. In these types of more complex aneurysms the consensus for fEVAR was stronger in patients under 85 years of age and in aneurysms greater than 60mm diameter (71).

For fEVAR within IFU the manufacturers specify that the infrarenal neck should be non-aneurysmal and at least 4mm long (72). The average neck length of patients receiving fEVAR worldwide is 6.9mm (range 0-14.4) based on five series of a total 346 patients (48, 62, 64, 65, 67).

2.3.2 Neck diameter and angulation

Neck diameter should be 19-31mm as measured from the outer wall of the vessel and there should be no angulation in excess of 45° including the angle between the flow axis of the suprarenal aorta and the AAA neck and between the neck and the aneurysm itself. Excess angulation greatly increases the difficulty of orientation and cannulation of the fenestrations.

2.3.3 Iliac arteries

Distal seal-zones must be at least 30mm in length and 9-21mm diameter (ipsilateral) or 7-21mm diameter (contralateral) as measured from the outer wall of the vessel. Adequate femoral and iliac artery access is a prerequisite although

access vessel issues (stenosis, angulation or aneurysmal enlargement) only preclude less than 4% of AAA patients from endovascular treatment (22).

2.3.4 Benefits

fEVAR is a useful option for hostile abdomens, i.e. those with stomas or scarring from previous surgery. Access via groin incisions avoids the need to re-enter the abdominal cavity and traverse complex peritoneal adhesions. Avoiding the physiological insult of a large laparotomy may also be beneficial when the patient has significant cardio-respiratory co-morbidity.

2.3.5 Contraindications

Physical limitations upon what can be manufactured may provide contraindication to fEVAR. For instance the necessary arrangement of fenestrations when visceral vessels are in close proximity to each other may be impossible to incorporate into the stent-graft design. Other contraindications include sensitivity to any of the materials used in the manufacture of the stent-graft or introduction system and systemic or local infection likely to increase the chance of stent-graft infection. In clinical practice this latter contraindication is sometimes overlooked and stent-grafts can be used to stabilise mycotic aneurysms following rupture (73).

2.3.6 Other considerations

In addition to the manufacturers indications the high cost of the device (average £17,000 per fEVAR) demands careful case by case evaluation based upon a reasonable life expectancy and an unacceptably high risk from open AAA repair. An initial cost effectiveness analysis has reported a two-fold higher total cost at 30 days associated with fEVAR in comparison with open repair (74).

2.4 Planning

Accurate assessment of aneurysm morphology is essential before fEVAR is undertaken. This requires high resolution cross-sectional imaging usually in the form of a helical computerised tomography (CT). Axial images can be reconstructed to provide three-dimensional (3D) images that can then be manipulated using a suitable workstation. This process enables measurements to be taken in the correct planes and allows the surgeon to build-up a mental image of the spatial arrangement of the aneurysm and major vessels that should aid deployment and cannulation. Although the 2011 guidelines on the management of AAA from the European Society for Vascular Surgery (75) did not recommend the use of a 3D workstation, weak evidence does suggest that it may reduce the incidence of type I endoleak following standard EVAR (76). In the planning of fenestrated EVAR the 3D workstation becomes a vital tool to define the position of the visceral vessels. A planning pro forma (Appendix 8.1) is supplied by the manufacturer and is used to standardise the information gathering and device selection process.

Custom-made fenestrated stent-grafts take approximately six weeks to manufacture and supply which precludes the treatment of haemodynamically stable ruptures and conveys a theoretical risk of rupture whilst awaiting treatment. Recently 'off-the-shelf' devices have been introduced to reduce the time between planning and deployment. The Zenith p-branch device is an off-the-shelf proximal fenestrated body that is available in two configurations and is potentially applicable to more than 70% of patients requiring fEVAR (77, 78). Early results are comparable with the custom-made devices. The planning stage involves the same measurement of vessel diameters and lengths but the visceral target vessels are then assessed in terms of their relative geometry to the SMA and are plotted on a sizing sheet to determine whether p-branch option A or B is more suitable. The sizing sheet is a two-dimensional projection of the visceral segment/seal-zone of the proximal body and is shown in Figure 2.5.

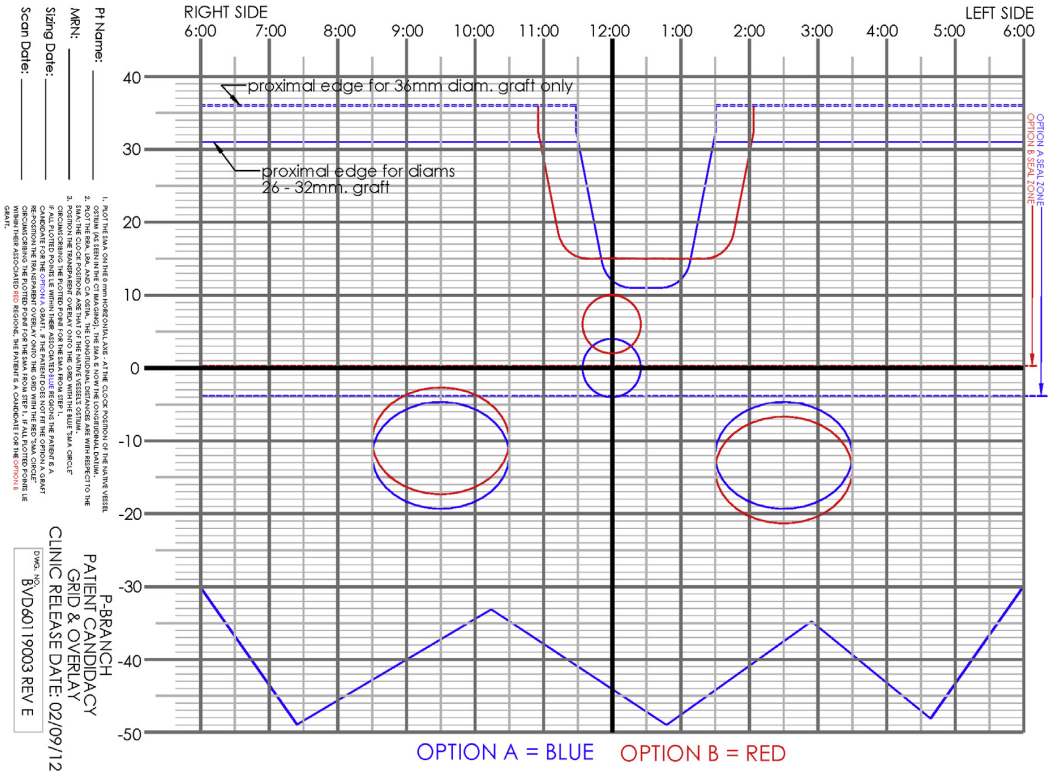

Figure 2.5 Zenith p-branch sizing sheet. Image from Kitagawa *et al.* (77)

2.5 Deployment

2.5.1 Anaesthesia

fEVAR can be performed under general, regional, or local anaesthesia. General anaesthesia is the standard approach in Europe as it removes the potential for any patient movement during the precise deployment of stent-graft components. Of 11 major publications reporting on fEVAR (48, 59, 61-68, 79, 80), four contained details of the anaesthetic regimen. Three European series included a total of 279 patients treated under general (n=221), regional (n=43) and local (n=13) anaesthesia (two unknown) (61, 65, 67). The only US series revealed a 4:1 preference for regional anaesthesia (64).

2.5.2 Access

Bilateral femoral artery access is obtained by either open cut down or percutaneously with ultrasound guidance. Percutaneous access requires either prior placement of a suture-mediated closure device, i.e. Perclose ProGlide (Abbott Vascular, USA) (81) or post procedural surgical closure of the arteriotomy. An alternative to direct surgical closure of the arteriotomy is fascial closure. This involves closure of the fascia lata/femoral sheath superficial to the femoral artery and just distal to the inguinal ligament with a purse string (82). It can be completed through a 25-50mm skin incision and obviates the need to dissect close to the artery which makes any subsequent groin access easier.

Although the proximal body can be deployed from either groin depending on the patient's anatomy the following description uses the right groin as the ipsilateral side.

2.5.2.1 Ipsilateral

Ipsilateral femoral artery puncture is usually performed with an 18-gauge needle through which an 0.035mm wire is advanced into the external iliac artery. The

needle is exchanged for a 9Fr sheath via which a soft tipped guidewire can be inserted under fluoroscopy screening until it lies in the proximal aorta. A catheter is advanced over the wire and the initial wire is exchanged for an extra-stiff wire (Lunderquist, Cook Medical Inc., Bloomington, USA) before the catheter is removed. These steps ensure safe introduction of the extra-stiff wire with the minimum of vessel wall trauma. The extra-stiff wire is necessary to support the stent-graft delivery system.

2.5.2.2 Contralateral

A similar guidewire and needle exchange is used on the contralateral side before the access sheath is exchanged for a 20Fr DrySeal sheath (W. L. Gore & Associates, Inc., USA) via which the multiple target vessel catheters can be introduced. A further puncture and 5Fr sheath is used to deliver an angiography catheter to the level of L1 (i.e. at the level of the visceral vessels).

5000units of unfractionated heparin is administered intravenously before any endovascular manipulation is commenced and Activated Partial Thromboplastin Time (APTT) can be checked during the procedure to allow further boluses to be administered if necessary (83).

2.5.3 Proximal body and target vessel stents

The 9Fr sheath is removed from the ispilateral femoral artery and the proximal body on its delivery system is inserted over the extra-stiff Lunderquist guidewire. The device is orientated for height and rotation based the gold radiopaque markers and then positioned in relation to a pre-selected index visceral vessel with that vessel profiled appropriately (usually the SMA with the image intensifier/C-arm positioned laterally). Once a satisfactory position has been achieved the proximal body is unsheathed and the angiogram is repeated to confirm accurate alignment of the visceral fenestrations. This stage is represented pictorially in Figure 2.6A. In practice the fenestrations are aligned

with the superior aspect of the respective target vessels anticipating a little caudal movement when the barbs of the bare metal stent engage fully with the aortic wall.

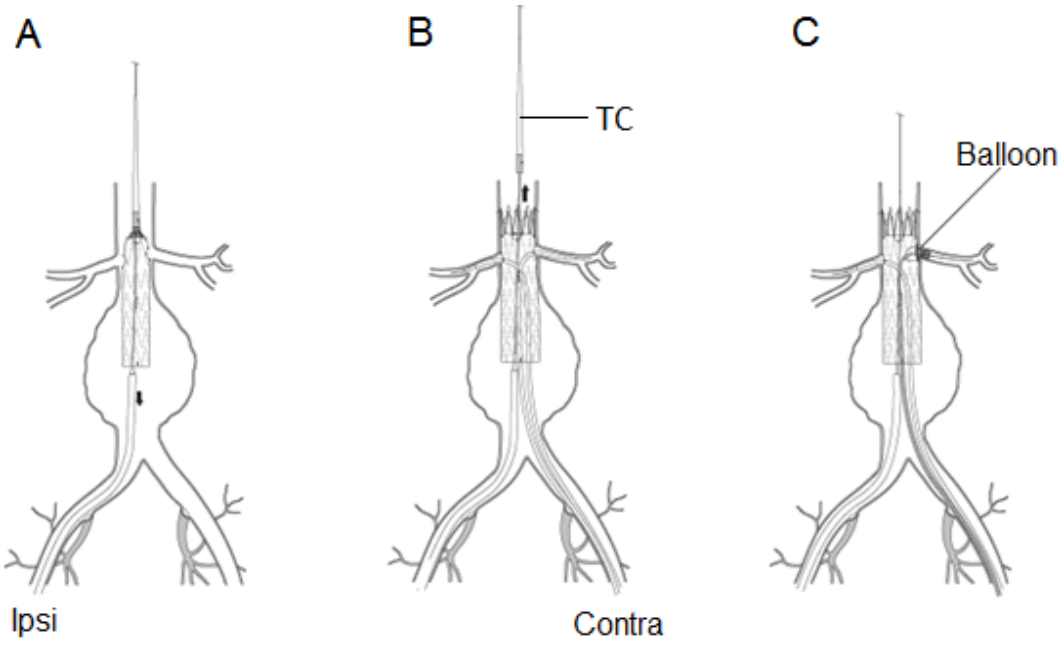

Figure 2.6 Deployment of proximal body and target vessel stents. TC: Top Cap. Image adapted from Cook Medical Inc. (72)

The first visceral vessel is cannulated through its fenestration via the contralateral groin using a Glidewire (Terumo Medical Corp., USA). A further wire-catheter exchange usually with a Rosen wire (Cook Medical Inc., Bloomington, USA) for renal arteries or Amplatz Super Stiff wire (Boston Scientific, France) for the SMA creates a stable platform for introduction of the long 7Fr sheath. A small volume of contrast confirms correct positioning of the sheath in the vessel ostium and the balloon expandable stent is then introduced (but not deployed) with 5mm of its length remaining within the aortic lumen. Once this procedure has been performed for all target vessels the diameter reducing ties and top cap of the delivery system (TC) can be released to fully deploy the proximal body and restore normal blood flow to the limbs (Figure 2.6B). The top cap is retrieved and carefully pulled down away from the visceral

segment to allow more room for deployment of the visceral stents. The C-arm is manoeuvred to provide a perpendicular view of the first target vessel based upon the appearance of its gold radiopaque markers and the corresponding target vessel stent is deployed. An oversized balloon is used to create a flange in the intra-aortic portion of the stent and seal the new vessel ostium. This process is represented in Figure 2.6C with the end result shown in Figure 2.7.

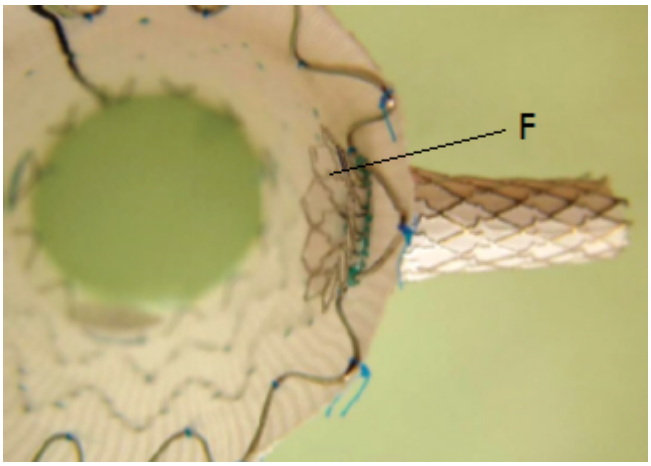

Figure 2.7 Flange (F) created in aortic lumen portion of target vessel stent. Image adapted from Moore *et al.* (83)

A selective angiogram is performed to confirm no disruption of blood flow has occurred and the procedure is repeated for the other target vessels.

2.5.4 Distal body and limb extension

After removal of the target vessel access wires and catheters the angiography catheter is pulled back and another angiogram is taken to mark the position of the aortic bifurcation. The proximal body delivery system is then exchanged for that of the distal body component. It is orientated so that the contralateral gate (CG) indicated by the radiopaque tick marker lies just proximal to the contralateral common iliac artery origin as shown in Figure 2.8. The proximal extent of the distal body is positioned inside the proximal body with two to three stents' overlap, although – in practice – the maximum available length of overlap is desirable. Repeat angiogram confirms the position of the ipsilateral limb in

relation to the internal iliac artery origin before the sheath is withdrawn to deploy the contralateral gate. The proximal stent (PS) remains constrained as shown in Figure 2.8A.

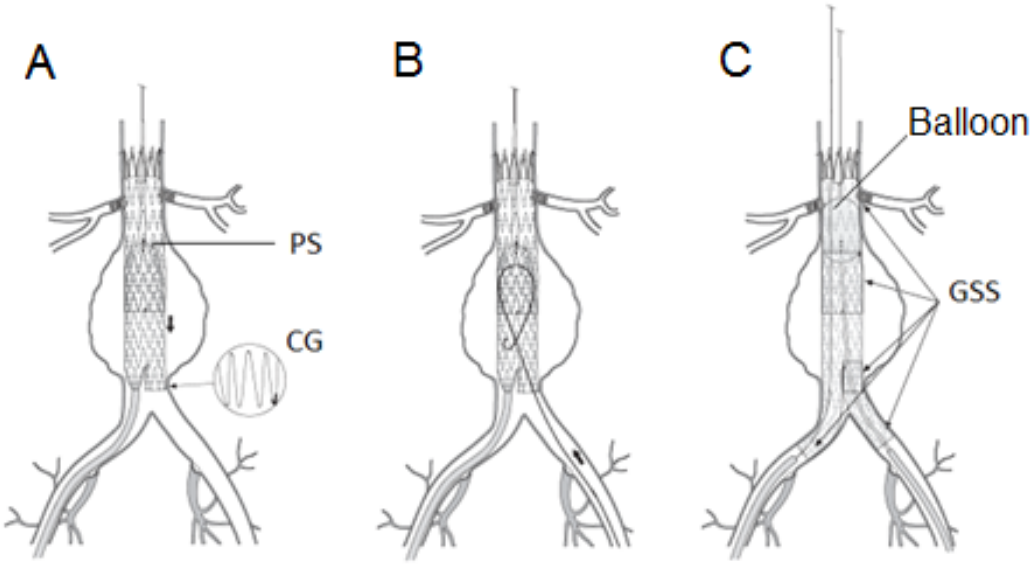

Figure 2.8 Deployment of distal body and limb extension. PS: Proximal Stent, CG: Contralateral Gate, GSS: Graft Sealing Sites. Image adapted from Cook Medical Inc. (72)

The contralateral gate is cannulated from the contralateral side. Due to the proximal constraint of the distal body it should not be possible to advance the guidewire beyond this point (see Figure 2.8B). Further confirmation can be obtained by either rotating a catheter within the body of the graft, taking further angiographic images or inflating a balloon partially inside the contralateral gate and observing the pear shape this causes. The proximal stent of the distal body is then deployed and the contralateral wire and catheter are advanced proximally. The C-arm is moved caudally and obliquely to the right to give perpendicular images of the contralateral common iliac artery. The position of the contralateral *internal* iliac artery is confirmed with a further angiogram. The limb extension delivery system is advanced into the contralateral gate of the distal body to give at least 22mm overlap before deployment.

Balloon dilatation has been shown to significantly improve the fixation of the proximal and distal seal-zones (84), therefore after completing the deployment by releasing the ipsilateral limb of the distal body a moulding balloon is used to secure all of the graft sealing sites (GSS, Figure 2.8C). These include the proximal body seal-zone, proximal body/distal body junction, distal body/limb extension junction, distal ipsilateral seal-zone and distal contralateral seal-zone.

A completion angiogram is taken at the level of the SMA to confirm target vessel patency and exclude type I/III endoleak before all wires and catheters are removed. The groins are then closed in the most appropriate way as outlined in section 2.5.2.

2.6 Intraoperative details

Published fEVAR results reveal a mean procedural time of 232mins (range 80-720) (61-65, 67, 68, 79). The large variability was probably due to some extent on the experience of the operating surgeon or interventionalist but also may have depended heavily upon the complexity of case which ranged from single tubular components and one scallop to multiple limb extensions and four fenestrations. Mean fluoroscopy time was 47mins (range 1-230) and mean contrast volume used was 180mls (range 40-450) (61, 63, 64, 67, 68). Again this reflects the varying complexity of fEVAR with the series that reported the lowest contrast use also reporting the lowest ratio of fenestrations per patient (mean contrast volume used 96.3mls +/- 46.3, ratio of fenestrations per patient 1.9) (68). The mean blood loss was 535mls (range 50-7000) (62-64, 67, 79) which highlights the potential for significant complications such as rupture of stenosed iliac arteries (4.5% of patients in one series) (61) or perforation of target vessels.

There was considerable variation between studies in terms of the number of adjunctive procedures performed. One Swedish series reported more than one

adjunctive procedure per patient including 18 proximal extensions or cuffs for type I endoleak in a cohort of 52 patients (48). The most recent multicentre study reported a 16.5% rate of adjunctive procedures with only three extensions or cuffs for type I endoleak (79).

2.7 Follow-up

Although duplex alone can be used for follow-up of standard EVAR, the anatomical complexities of fenestrated endovascular repair means that contrast-enhanced CT remains the gold standard. The current surveillance protocol for our unit comprises a baseline abdominal x-ray postoperatively and then a duplex, contrast enhanced CT and venous blood sampling for estimated glomerular filtration rate (eGFR) at one month. Clinical review is usually performed at approximately six weeks with these results. A further duplex, contrast enhanced CT and eGFR are performed at six months and the patient then enters a yearly surveillance programme with abdominal x-ray, duplex, contrast-enhanced CT and eGFR. Contrast Enhanced Ultrasound (CEUS) is used selectively to obtain further characterisation of endoleaks incompletely diagnosed at CT (32, 33).

2.8 Complications

The fEVAR follow-up regimen is designed to identify all of the complications previously detailed for standard EVAR and described in section 1.7.3 with the following additions:

2.8.1 Migration and target vessel compromise

The implications of migration could be considered to be more severe following fEVAR compared with standard EVAR. Target vessel loss may lead to renal failure or bowel ischaemia as well as type I endoleak with the potential risks of AAA

expansion and rupture. Even small amounts of caudal migration of the proximal body risks impingement of the superior aspect of the re-enforced fenestrations upon the visceral stents leading to stenosis and in severe cases stent fracture or occlusion (67). Technical difficulties during deployment or unforeseen interactions with the native aorta may both lead to stent distortion (85) however small amounts of radial misalignment of fenestrations may be well tolerated without adverse effect (86). Compromise of scalloped target vessels may result from shuttering of the scallop across the vessel as a result of planning or deployment error (85, 87).

2.8.2 Endoleak and component distraction

Type IIIa endoleak is possible at more sites than with standard EVAR due to the greater modularity of the fenestrated device. The junction between target vessel stents and the proximal body, between proximal and distal bodies as well as the distal body and iliac limb extension are all potential sites for endoleak. CT and plain film images are therefore examined for any evidence of component distraction and CT and duplex are used to assess for any endoleak originating from these junctions.

2.8.3 Graft-related adverse events

Following fenestrated endovascular aneurysm repair the term ‘graft-related adverse events’ (GRAE) refers to migration, component distraction target vessel compromise type I and III endoleak, or limb stenosis.

2.9 Results to date

Apart from the aforementioned single or multicentre series of fEVAR there have also been nine review articles summarising the worldwide experience (54, 88-95). The most recent systematic review from Queen Mary Hospital, Hong Kong includes 817 patients (less than a third of the estimated number of fenestrated

stent-grafts deployed worldwide) (93). Fifty six of these patients received Ventana (Endologix Inc., Irvine, USA) or Anaconda (Vascutek, Inchinnan, Scotland) fenestrated devices (93). By including the multicentre GLOBALSTAR initiative (79) and excluding potential duplication of patients (66, 96-100) the number of reported outcomes for the Zenith fenestrated stent-graft totals 1028 (59, 61-65, 67, 68, 79, 80). The overall median follow-up remains less than 20 months (range 0-94). Since the initial review of fEVAR outcomes was performed for inclusion in this thesis there have been two small single centre series with less than ten fEVAR patients in each (101, 102), and two others where fEVAR outcomes were reported alongside open repair or alternative endovascular techniques (103, 104). The Swedish and French series (61, 105) have been expanded by 100 patients (106) and updated (107) and outcomes from another 139 patients treated at the Cleveland Clinic, Ohio, USA have also been published (108). The following review of outcomes is based on the original combined cohort from ten publications (59, 61-65, 67, 68, 79, 80).

2.9.1 30-day Outcomes

2.9.1.1 Mortality

Overall cumulative 30-day mortality was 23 patients from 1028 (2.2% range 0.8-3.7%). Five more patients died during the initial admission after 30 days therefore the global cumulative perioperative mortality for fEVAR was 2.6% (range 0.8-4.4%). Causes of death included distal embolisation, mesenteric ischaemia, multisystem organ failure (one case following major bleeding from access vessel rupture and one following conversion to open repair), myocardial infarction, major haemorrhage (from a perforated kidney), pulmonary oedema and possible pulmonary embolism.

In comparison with open repair of juxtarenal aneurysms, a recent comprehensive systematic review and meta-analysis of 1575 open and 751 fEVAR patients reported no significant difference in mortality (4.1% for open and fEVAR, p=.822)

despite fEVAR patients being significantly older with a significantly higher rate of pre-existing renal and respiratory insufficiency, cardiac dysfunction and diabetes (94). It must be recognised however that a significant amount of heterogeneity exists even within AAAs regarded as juxtarenal. For example some juxtarenal aneurysms unsuitable for standard EVAR may be suitable for open repair with an infrarenal clamp. Others require inter or suprarenal or even supracoeliac aortic cross clamping.

One direct comparison from a single centre study reported outcomes in 107 patients who underwent open repair or fEVAR. It showed a risk-adjusted absolute risk reduction of death of 9.5% for fEVAR as compared with open surgery (109).

2.9.1.2 Conversion to open repair

Only two patients in all fEVAR studies (0.2%) were reported as needing open conversion at the time of initial repair. The first was during treatment of a juxtarenal aneurysm above a previously placed standard infrarenal stent-graft where difficulty in retrieving the top cap resulted in crushing of the renal stents. The patient spent eight days in ICU but was discharged at 22 days in 'good' condition (67). The second was due to occlusion of the aortic bifurcation following successful deployment of the proximal body and renal stents. This patient died at 4-5 days postoperatively of multisystem organ failure (61).

2.9.1.3 Primary success and primary technical success

Four studies reported primary success defined as successful deployment of the stent-graft without surgical conversion, mortality or limb and target vessel occlusion (59, 62, 65, 79). Only two studies reported primary technical success which in addition to the requirements for primary success included the absence of limb stenosis and type I/III endoleak in the first 30 days (63, 65, 68). It is likely that some of the reported 'primary' technical success also included 'assisted' technical success but this concept was not mentioned in any study despite the large numbers of adjunctive manoeuvres used in some. Overall primary success was 92.7% and primary technical success 90.7%.

2.9.1.4 Target vessel loss

Overall target vessel patency was 2391 of 2435 target vessels (98.2%, range 90.5-100%). Some studies reported this at completion, at 24 hours or at 30 days (59, 61, 62, 64, 65, 67, 68, 79).

2.9.1.5 Primary Endoleak

The lower 'primary technical success' rate (90.7%) compared to the 'primary success' rate (92.7%) was due to the incidence of type I/III endoleak at completion and during the first 30 days. In nine studies of a total 921 fEVAR patients there were 41 type I and 13 type III endoleaks diagnosed. Some were successfully treated with adjunctive manoeuvres such as ballooning and palmaz stent/cuff deployment. Treatment of primary graft-related endoleak is summarised in Table 2.1 (59, 61-65, 67, 68, 79). Whilst it cannot be confirmed that all endoleaks occurred in separate patients, the *approximate* overall rate of primary graft-related endoleak following fEVAR was 5.9% (range per series 2-10.1%).

Table 2.1 Summary of primary graft-related endoleak

Endoleak	n	Treatment
Type Ia	34	8 Giant Palmaz stents (1 requiring further fenestrated cuff extension) 1 open conversion at 9 months 1 AAA sac embolization 10 conservatively treated (7 resolved; 2 persisted requiring 1 fenestrated cuff, the other refused treatment; 1 unknown) 14 treatment unknown (79)
Type Ib	6	1 IIA coil embolization and extension to EIA 2 palmaz stent 3 treatment unknown (79)
Other	1	persistent type Ia from standard EVAR following fenestrated extension (65). Conservative treatment with complete resolution
Type IIIa renal ostium	5	3 covered target vessel stents 2 treatment unknown
Type IIIa proximal-distal body junction	7	1 extension cuff 2 giant Palmaz stents (1 recurred requiring AUI + cross over bypass) 1 relining 2 conservative (both resolved) 1 treatment unknown
Type IIIa distal body - limb extension junction	1	Treatment unknown

AUI: Aorto-Uni Iliac stent-graft, EIA: External iliac artery, IIA: Internal iliac artery, RA: Renal artery

Five other patients with seven type IIIa endoleaks from the Troisi *et al.* (80) series were not included in Table 2.1. All were due to failure of target vessel cannulation but it was not stated whether these endoleaks were present upon completion angiography or were diagnosed at early follow-up. Because all five received secondary intervention between one and 18 months following the initial procedure they have been included in the secondary endoleak section 2.9.2.3.

2.9.1.6 Renal failure

The likely causes of renal failure following fenestrated endovascular aneurysm repair include contrast induced nephropathy, embolisation, technical error or renal artery/renal stent stenosis and occlusion during follow-up. Renal failure occurred in 14.1% of patients with 1.8% of all patients requiring dialysis (59, 61-65, 67, 68) however the exact definition of renal failure often differed between publications or was absent entirely. Even the two most recent studies to look specifically at the incidence of renal failure following fenestrated endovascular aneurysm repair used different definitions (>50% or >25% increase in creatinine) (110, 111). In these two studies dialysis was required in 3% and 5.9% of patients, temporarily in all but one case. Although the latter series included 38 patients treated with branched stent-grafts as well as 187 fenestrated devices, no significant difference was found in terms of incidence of acute renal failure (ARF) or need for dialysis between the two groups. Postoperative ARF was significantly associated with preoperative chronic renal failure, metformin use and longer procedure time although not with higher volumes of contrast (111).

2.9.1.7 Other significant morbidity

2.9.1.7.1 Surgical or procedure related:

There were seven cases of spinal ischaemia (cumulative incidence 0.8%) of whom five suffered permanent loss or reduction in function (59, 61, 79). This is much lower than the 9.7% rate of paraplegia/paraparesis reported following

endovascular treatment of thoraco-abdominal aneurysms and is probably a result of less aorta being lined with stent-graft (112). The only series to include nine branched stent-grafts with fenestrated repairs reported no persistent neurological complications (80).

Other procedural related complications included lower limb ischaemia from internal iliac artery coverage or limb extension occlusion/stenosis, non-fatal bowel ischaemia, additional wounds for access or control of haemorrhage, additional puncture sites (i.e. brachial), haematoma and pseudoaneurysm, peripheral embolism, wound infection, stent-graft infection and seroma.

2.9.1.7.2 Medical:

Non-fatal myocardial infarction, acute coronary syndrome, atrial fibrillation, stroke/transient ischaemic attack, pneumonia, urine retention and urinary tract infection have all been reported following fEVAR.

2.9.1.8 Early reintervention

Three studies reported reintervention rates within the first 30 days (64, 67, 79). Three others provided enough information for this to be calculated (61, 68, 80). Overall 51 of 841 patients (6.1%) required a range of early reinterventions that included the aforementioned procedures for graft-related endoleak (see Table 2.1); target vessel bypass for occlusion and stenosis; target vessel coil embolization for perforation; thromboembolectomy and peripheral bypass for acute ischaemia; laparotomy or diagnostic laparoscopy for concern regarding abdominal pathology; repair of brachial and femoral psuedoaneurysm; evacuation of haematoma; ureteric stent for hydronephrosis and cardiac pacemaker insertion for bradycardia.

2.9.1.9 Length of hospital stay

Overall median length of hospital stay was five days (range 1-100 days). Median ICU stay was one day (range 0-38 days) but this was based on only three studies (482 patients) (61, 62, 79).

2.9.2 Outcomes during follow-up after 30 days

Definitions of early, short, mid and long term follow-up vary. For standard EVAR 'early' has been defined as 30 days to one year, 'short' as one to five years, 'midterm' as five to ten years and 'long term' as more than ten years (113). Fenestrated repair however is a younger discipline therefore most authors described early reintervention as being between 0 and 30 days postoperatively. Median follow-up of 15 months (range 2-53) has been described as midterm (61). It is inevitable that as experience progresses these definitions will continue to be revised.

2.9.2.1 Mortality after 30 days

Eight of the ten studies reported mortality after 30 days (59, 61-64, 67, 68, 79). One other gave enough information for this to be calculated (65). Overall mortality after 30 days during a median follow up of 17.4 months (range 0-87) was 10.9% (range 3.6-23.8%).

The only AAA related deaths during this follow-up were in the German series that included 63 patients and had a median follow-up of 14 months (range 6-77) (68). One patient died following rupture at ten months. He was not suitable for any intervention due to comorbidities and whilst the rupture was attributed to type I endoleak none was found either at six month follow-up or upon acute presentation. The other AAA related death was due to an aorto-duodenal fistula at 72 months. This series also included the only 'late' conversion to open repair performed successfully at nine months due to a persistent proximal type I endoleak (68).

Five studies reported freedom from all mortality by Kaplan-Meier analysis (61, 63, 67, 68, 79). This ranged from 89% at 36 months (79) to 58.5% at 60 months (67). The latter figure from the Dutch single centre study was based on only 14 remaining patients at risk at that time interval.

2.9.2.2 Target vessel loss during follow-up

Of the 2435 target vessels patent following the primary procedure in nine studies, 72 (3%) occluded during follow-up (59, 61-65, 67, 68, 79). Troisi *et al.* described another five target vessel occlusions but did not state the overall number of target vessels in their 107 patients. Because the definition of primary target vessel patency varied (to include either completion imaging, 24 hour or 30 day postoperative periods) a more accurate indicator of target vessel loss may be Kaplan-Meier analysis over the longer term. Reported freedom from target vessel loss was: 95% at 36 months (79), 93% at 60 months (67) and 92% at 77 months (68).

More recently the Dutch group has published target vessel follow-up data on 138 fEVAR patients treated between 2001 and 2011. Four year patency for all target vessels was 91.9%. For stented target vessels only this figure was 88.6%. It was noted that after 2005 covered stents became the stent of choice for fenestrated target vessels as opposed to the uncovered stents more commonly used prior to this. No difference in patency was noted between the two types of stent. Renal stent stenosis occurred more frequently in uncovered stents than in covered stents (p=.004) and uncovered stents were significantly more likely to fracture (10.3% versus 1.2% p=.01) (114).

Causes of target vessel compromise included proximal body migration, native vessel characteristics (i.e. progressive stenosis or unsatisfactory initial stent position due to acute vessel angulation) and iatrogenic causes (i.e. intentional coverage of a target vessel to abolish a type III endoleak at the real ostium).

Historically, occlusions were observed in scalloped target vessels (59). A possible mechanism for this was incomplete initial deployment of the scallop due to oversizing of the stent-graft. Rotational forces acting upon it would then cause shuttering of the fabric across the target vessel ostium. Stenting of scallops was a potential protective mechanism but the need for this was superseded by nitinol re-enforcement of the scallop edge.

2.9.2.3 Secondary endoleak

The reported incidence of secondary or late type I/III endoleak was low in most studies. Troisi *et al.* (80) however described a disproportionate six late type I and 10 late type III endoleaks in their series. This was the only series to include branched (n=9), and hybrid repairs (n=2) as well as fenestrated stent-grafts (n=96). The initial type of repair was specified for secondary type I but not type III endoleaks (80).

2.9.2.3.1 Secondary type I endoleaks

There were nine proximal type I endoleaks reported in a total of 961 patients. One was a recurrence at one year of a conservatively treated primary type Ia endoleak. It was successfully treated the second time with proximal extension and re-stenting of the left renal artery (64). Another occurred at 18 months and led to an increase in AAA diameter. This was treated with aortic cuff and chimney stent to the SMA (61). The third was at an unknown time after the initial fEVAR and was treated conservatively due to no observed changes in AAA diameter (48).

Another six cases – all from the fenestrated patients included in Troisi *et al's* series (80) – were associated with stent-graft migration and renal stent fracture (two with bilateral fractures). Mean time to diagnosis of these six late type I endoleaks was two years following the initial procedure. Treatment and outcomes are described in Table 2.2.

One review examining type I endoleaks in fenestrated and branched endovascular aneurysm repairs showed that this complication was much more likely in conical visceral sealing zones (i.e. those with >10% increase in diameter from cranial to caudal. Type Ia endoleak was associated with increased aneurysm related mortality (115).

2.9.2.3.2 Secondary type III endoleaks

Most type IIIa endoleaks were between renal artery fenestrations and the AAA sac. Seven of these were due to initial failure of cannulation therefore could be considered type I endoleaks. One was sealed at six months with loss of the renal artery (68), another was treated at 12 months with an aortic cuff (61). Two were stented successfully at two and 18 months (80), the other three had failed attempts at stenting at one, two and four months and then required either coverage with a stent-graft, Amplatzer plug (St. Jude Medical, USA) embolization or open renal artery ligation with ilio-renal bypass (80).

Six type IIIa endoleaks occurred between the junction of the renal stent and the proximal body fenestration. One required re-stenting at 13 months following unsuccessful angioplasty 11 months earlier (79). The other five were due to dislocation of a target vessel stent (four SMA and one renal artery). These were all successfully treated with further stenting at a median time of eight months following the primary procedure (range 2-14 months) (80).

Two other type IIIa endoleaks occurred between the proximal and distal bodies, one at 12 months and the other (a complete disconnection) at 20 months. Both were treated with further stent-grafts (67, 68).

2.9.2.4 Migration

There were 13 confirmed cases of proximal body migration in 8 of the 10 series (48, 59, 62, 64, 65, 67, 68, 80). Cumulative incidence of migration was therefore 2.3% in a total of 565 patients. These cases are summarised in Table 2.2.

The Dutch series (67) described two other cases of *suspected* migration and Semmens *et al.* (59) reported four cases of target vessel loss due to shuttering that they describe as rotational migration. Migration was not reported in the French series (61) and although Kristmundsson *et al.* (63) also did not report on migration, Chisci *et al.* (48) reported no migration in the same patient cohort. The GLOBASTAR database described freedom from migration by Kaplan-Meier analysis of 92% and 88% at two and three years respectively (79). This was similar to the 92% freedom from migration at three years reported by Troisi *et al.* (80).

A core lab analysis of follow-up imaging from 154 fenestrated endovascular aneurysm repairs showed that migration ≥4mm can be found in 21% of proximal bodies (116). Median time to diagnosis varied greatly between one and 88.7 months (median 11.8 months) and the presence of migration was not associated with a greater incidence of graft-related adverse events or reintervention.

Table 2.2 Summary of proximal body migration

Author	Total no. of fEVAR in series	Migration (n)	Extent (mm)	Time post fEVAR (months)
O'Neill (64)	119	**1**	3	-
Outcome: Crushing and occlusion of renal stent successfully re-stented (117)				
Ziegler (68)	63	**2**	-	<14 (1 at 6 days)
Outcome: One type IIIa endoleak (renal ostium). Both migrations resulted in target vessel occlusion in unsecured fenestrations				
Scurr (65)	45	**2**	-	-
Outcome: Deformation and angulation of target vessel stents				
Greenberg (118)	30	**1**	6	24
Outcome: Crushing of renal stent successfully re-stented				
Verhoeven (67)	100	**1**	<5	24
Outcome: Renal artery occlusion and creatinine rise >30%				
Troisi (80)	96	**6**	-	Mean 24 Range 4-45
Outcome: 6 graft-related endoleaks with 8 renal stent fractures. Successful treatment in 3 cases with balloon dilatation and renal stent. Unsuccessful recanalization of renal arteries in 3 cases with 2 persistent type I endoleaks and 3 patients requiring permanent dialysis (1 despite hepato-renal bypass).				

2.9.2.5 Component Distraction

Component distraction refers to the movement of a component in relation to another into which it has been deployed. It may eventually result in complete dislocation. Seven examples of component distraction were found in six of the major series and are summarised in Table 2.3 (59, 64, 65, 67, 68, 80).

Table 2.3 Summary of component distraction

Author	Recruit-ment period	Total no. in series	Component distraction (n)	Time post fEVAR (months)	Outcome
O'Neill (64)	2001-2005	119	**1**	24	Successful extension cuff
Semmens (59)	1997-2004	58	**2**	-	Both treated with additional stent-graft when <1 stent overlap
Ziegler (68)	1999-2006	63	**2** (1 with type IIIa endoleak)	<14	Both treated with bridging stents
Scurr (65)	2003-2006	45	**1**	28	Successful bridging cuff
Verhoeven (67)	2001-2009	100	**1** (Complete dislocation)	20	Treated with thoracic stent-graft

Four publications made no mention of either component distraction, dislocation or separation (61-63, 79). The cumulative incidence of component distraction was therefore approximately 1.5% of a total 481 patients. There were a very small number of tubular single-piece and custom-made stent-grafts deployed in some of the series that lacked modularity and would not have been susceptible to this complication.

One further example was described by Resch *et al.* (119) in 2010 where complete dislocation of the distal body component led to type IIIa endoleak and rupture. This patient was converted to open repair (119).

An analysis of component movement and distraction from the Cleveland Clinic was published in 2008. Many of the patients included would have been part of the O'Neill series (64) that initially reported only one example of this complication (see Table 2.3). After analysis of 106 patients' CT images, 14 were found to have >10mm movement between components. Eight required secondary intervention including one open conversion due to rupture (120). Although there were an unknown number of branched stent-grafts included in the analysis, the results suggest that there may be an underlying incidence of sub-clinical component distraction higher than that reported in the clinical series (120).

O'Neill's series (64) was one of only two to recruit all patients prior to 2005 when the distal diameter of the proximal body was changed by the manufacturer from 24mm to 22mm. The proximal diameter of the distal body remained 24mm. The aim was to reduce the chance of component distraction by creating a more secure fixation between the two components. Less component distraction may be expected following this change.

2.9.2.6 Limb complications

2.9.2.6.1 Limb migration

Proximal migration of the limb extension was not reported in any of the publications however the core lab analysis by England *et al.* (116) identified 34 examples of iliac limb migration ≥4mm in a total of 259 limbs (13%) (116).

2.9.2.6.2 Limb occlusion

Seven late limb occlusions were reported in four of the series (1.2% cumulative incidence by patient) (67, 68, 79, 80). There were also five examples within the first 30 days (61, 79, 80). Removal of the extra-stiff wire before the completion angiogram is performed is one way to ensure kinked or tortuous anatomy is identified early (80). In this setting judicious use of adjunctive stents has been shown to reduce limb occlusion rates (121). Freedom from late limb occlusion by Kaplan-Meier analysis was 96% and 85% at two and three years respectively (79).

2.9.3 Reintervention

Three series reported freedom from reintervention by Kaplan-Meier analysis (48, 61, 68). This varied between 81% at 3 years (61) to 75.3% at over six years (68). GLOBASTAR reported freedom from *late* secondary intervention (i.e. not including reinterventions within the first 30 days) of 70% at three years (79).

2.10 Summary

Fenestrated Endovascular Aneurysm Repair using the modular Zenith fenestrated stent-graft is an alternative to open juxtarenal aneurysm repair for patients with suitable anatomy. It avoids the higher perioperative mortality of open surgery and obviates the need to negotiate hostile abdomens with multiple previous operative scars. It does however require long term radiological follow-up to ensure that the stent-graft components remain intact and continue to exclude the aneurysm from the circulation. Graft-related adverse events such as migration, component distraction, type I/III endoleak, target vessel compromise, and limb stenosis may all require reintervention to maintain the structural integrity of the repair.

The published clinical results in the short and medium term are favourable however longer term results are not available and this lack of data as well as an awareness of the financial costs need to be considered when advising patients on treatment options.

3 Rationale for Investigations

Migration of stent-graft components following fenestrated Endovascular Aneurysm Repair is a serious complication observed in up to 12% of patients at three years (79). Clinical sequelae of proximal body migration include target vessel loss leading to renal failure or bowel ischaemia and graft-related endoleak that risks aneurysm expansion and rupture. Movement of the distal body and migration of limb extensions may lead to limb thrombosis, and type Ib or IIIa endoleak with the subsequent risk of AAA expansion and rupture.

Understanding what factors increase the chance of stent-graft migration may allow targeted intensive follow-up to be undertaken or guide the patient and surgeon toward an alternative choice of intervention for those at high risk.

3.1 Fixation force

Migration is resisted by the fixation force of a stent-graft component i.e. the force holding it in place inside the vessel. Two main factors affect fixation force:

1. The physical properties of the stent-graft;
2. The characteristics of the vessel into which the stent-graft is deployed.

Physical properties include adjunctive fixation aids such as suprarenal bare metal stents, hooks, barbs or stented fenestrations as well as the radial force of the sealing stents themselves. Radial force is determined by the type of metal and the configuration of the stent. Incorporation of the graft fabric into the native vessel is probably less important (122). The proportion to which these physical properties contribute to fixation force is difficult to define as few commercially available stent-grafts differ by only one feature.

3.1.1 Proximal fixation

The most relevant comparison of proximal fixation force was made by Zhou *et al.* (123) who compared a standard Zenith stent-graft (Figure 3.1D) with a one-fenestration proximal body deployed in wet, pressurised bovine aorta segments. Both had stainless steel gianturco design sealing stents, a stainless steel bare metal stent with barbs and the same Dacron fabric. The stent-grafts were distracted from the aortas using a force gauge. The addition of one stented fenestration increased the overall fixation force from 10.8N +/-1.7N to 28.2N +/-1.6N (approximately 262%) (123).

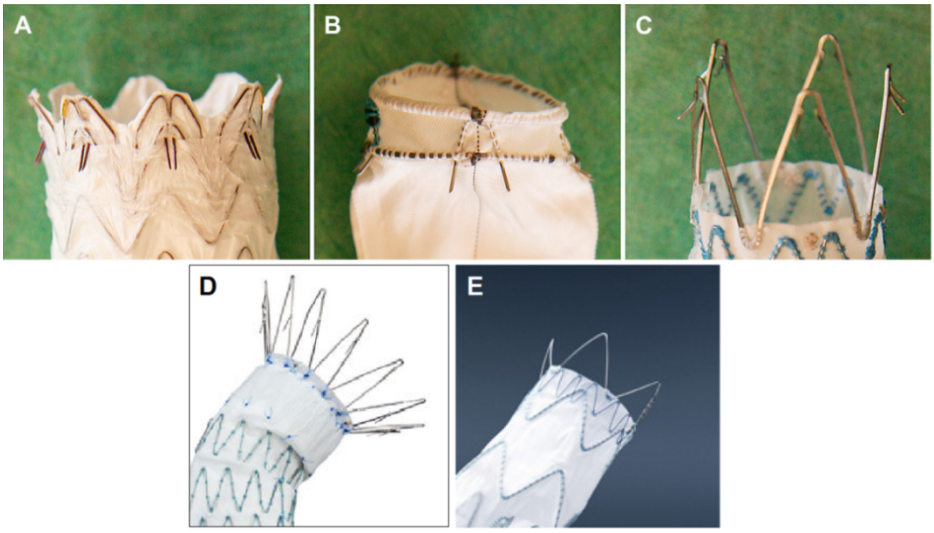

Figure 3.1 Proximal stent-graft design. A: Excluder (W.L. Gore & Associates Inc., Flagstaff, USA), B: Anaconda (Vascutek, Inchinnan, Scotland), C: Endurant (Medtronic, Minneapolis, USA), D: Zenith (Cook Medical Inc., Bloomington, USA), E: Talent (Medtronic, Minneapolis, USA). A-C from Bosman *et al.* (124), D-E adapted from respective manufacturers (125, 126)

Resch *et al.* (127) reported a median proximal fixation force of 24N (23-26.5N) for the standard Zenith device in a segment of human cadaveric aorta but other studies using the complete standard stent-graft as opposed to the truncated proximal end have yielded even higher results (46.7N +/-5.4N in ovine aorta (128) and 39.3N +/-1.6N in human aorta (84)). These results suggest that secure iliac fixation and columnar stability also contribute to the strength of the

proximal seal. Experimental data using stent-grafts deployed in an *in vivo* ovine model support this finding (129), as do clinical follow-up studies from Stanford University School of Medicine (130-132). Although forces greater than 28.2N may be required to completely displace the proximal body of a Zenith fenestrated stent-graft, a lower *initial* fixation force of 11.5N +/-1.5N was also described (123). When forces of this magnitude were applied to the proximal body an initial phase of migration (<5mm) was observed that corresponded to full engagement of the barbs with the aortic wall. At this point overall fixation force had to be overcome to produce further movement. Verhoeven e*t al.* (67) considered migration of <5mm to be the cause of at least two cases of target vessel compromise and experimental work has shown that the median force required to produce stenosis of the commonly used target vessel stent (Atrium Advanta V12, Maquet Ltd., UK) is similar to this initial fixation force. When 9.3N of force (interquartile range, IQR 0.9N) was applied perpendicular to the long axis of the stent a 50% stenosis resulted. 13.2N (IQR 1.6N) caused a 75% stenosis (133).

The Endurant stent-graft (Figure 3.1C, Medtronic, Minneapolis, USA) has a similar m-shaped stent configuration to that of the z-shaped gianturco sealing stent of the Zenith device. It also has a bare metal stent with barbs. The main difference is that the stents are made from an alloy of nickel and titanium (nitinol) that gives more flexibility and thermal memory than stainless steel. It is therefore more resistant to elastic deformation and is more likely to re-expand to its initial shape than stainless steel under the same compressive force. Conversely it exerts less radial force on the internal surface of the vessel into which it is deployed (134). One experimental study in human cadaveric aorta found that the Zenith had approximately 7.6N (24%) more fixation force than the Endurant (39.3N +/-1.6N vs 31.8N +/- 2.3N). The most likely reason for this was the different properties of the metals (84).

Nitinol without barbs has a lower fixation force. This was shown by Linsen *et al.* (135) using a similar experimental set up to that of Zhou *et al.* (123). The proximal end of a standard Talent stent-graft (Figure 3.1E, Medtronic, Minneapolis, USA) and a modified, two-stented fenestration Talent stent-graft were both distracted from human cadaveric aortas with simulated aneurysms. The median fixation force was 4.7N (range 3.8-6.4N) and 17N (14.8-19.7N) respectively with some of the higher force generated by the increased surface area of contact afforded by using the visceral aorta as a seal-zone (135).

Further evidence for the beneficial effect of barbs comes from observing the lack of engagement that excess oversizing causes. In one study where custom-made stent-grafts were imaged post deployment before distraction was performed, greater than 30% oversizing resulted in only approximately a third of barbs penetrating the aortic wall. This compared with 89% penetration with 10% oversizing and led to 41% less fixation force (136). Sternbergh *et al.* (137) linked >30% oversizing to a significant 14-fold increase in migration as compared with <30% oversizing in the participants of the (standard) Zenith multicentre trial (137).

The importance of stent design is best illustrated by comparing the nitinol fish-mouth ring stents of the Anaconda stent-graft (Vascutek, Inchinnan, Scotland Figure 3.1B) with the more traditional z/m-shaped nitinol of the Excluder (W. L. Gore & Associates Inc., Flagstaff, USA Figure 3.1A). Both are devoid of suprarenal fixation and both have small barbs near the proximal extent of the fabric (woven polyester and PTFE respectively). The anaconda device displayed approximately 13.6N (60%) more fixation force than the Excluder (84). The impact of stent design on radial force has also been shown on a smaller scale in 3mm diameter coronary stents (138).

By contrast to the magnitude of fixation displayed by endovascular stent-grafts, a hand-sewn anastomosis as performed during open aneurysm repair has a

fixation force of between 89.2N and 150N (127, 135). At this force the aorta was seen to tear before any disruption of the anastomosis occurred.

All of these experimental designs investigated fixation force under ideal deployment conditions. At worst there were small amounts of calcified atherosclerotic plaque in the human aortas used. One pullout study examined the effect of 10mm versus 15mm of proximal neck length and showed that although fixation force was less with the shorter seal-zone, the difference was only significant for the Excluder device and not for the Ananconda or Endurant (124).

A number of clinical follow-up studies have investigated the effect of adverse neck morphology upon the consequences of poor fixation. Thrombus lining of the aneurysm neck might be expected to reduce the fixation force of the proximal stent-graft by interfering with barb engagement and providing a less than stable surface for purchase of the sealing stents. This should result in a higher rate of migration however, after correction for the type of stent-graft, one analysis of 396 patients following standard EVAR showed no difference in the rate of migration with or without neck thrombus (139). Although outcomes may not be affected in the early postoperative period (140), large diameter, angulated necks have been linked to a higher incidence of migration (45, 46, 49, 50, 141) as well as more type I endoleak (46, 50, 51, 141, 142), postoperative complications and reinterventions (48, 51, 52, 142) in the longer term.

3.1.2 Inter-component fixation

Two *in vitro* models using Zenith stent-grafts give some insight into the important factors affecting the inter-component fixation force. In the absence of barbs and without the influence of native vessel characteristics the most important factor at this junction is the radial force of the stents. Scurr *et al.* (143) showed that with a two stent (35mm) overlap the distal body of a Zenith fenestrated stent-graft was fixed within the proximal body at a median force of

approximately 6.5N (IQR 4.8-7.2N) (143). Liffman *et al.* (144) showed that by bringing more surface area of the two components into contact (i.e. increasing the overlap) the same junction could be stabilised against the effects of pressure differences in a pulsatile flow model (144).

The strength of the iliac limb and contralateral gate fixation was reported by Cina *et al.* (145), for the Zenith device this was approximately 3.5N +/-0.1N. This force was more than for the Excluder (2.5N +/-0.5N) but less than for Talent (6.3N +/-0.6N) and Anaconda devices (4.7N +/-0.4N to 13N +/- 0.4N) (145).

3.1.3 Distal fixation

In a pullout study in cadaveric human vessels the similar z/m distal stent design of the Endurant (Figure 3.2C), and Talent (E) resulted in a similar distal fixation force to the Zenith (D) despite the difference in materials (9.7N +/-0.4N and 9.2N +/-1.3N versus 9.6N +/-1.5N) (84).

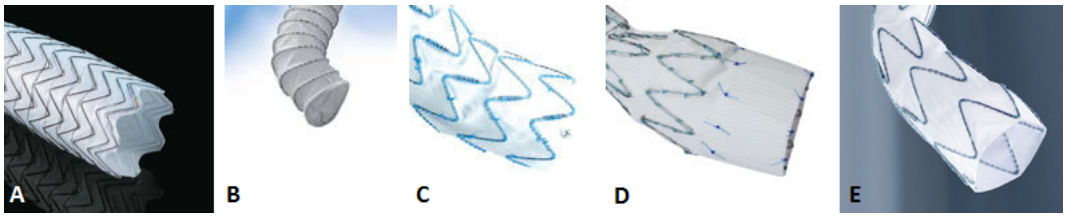

Figure 3.2 Distal sealing stent design. A: Excluder (146), B: Anaconda (147), C: Endurant (148), D: Zenith (125), E: Talent (126)

The Excluder (Figure 3.2A) with more numerous stents and the anaconda (B) with circular stents had greater distal fixation forces of 10.5N +/-0.4N and 14.6N +/-0.7N respectively.

Previous work from our unit has shown a link between the length of distal seal (i.e. iliac engagement) and the incidence of distal endoleak, limb kinking and occlusion (149, 150). Other studies however have shown no adverse outcomes with other vessel characteristics that may affect fixation force such as large diameter (151, 152) and a greater degree of iliac angulation (153).

3.2 Distraction force

Haemodynamic distraction force is derived from blood pressure (normal force or stress) and blood flow (shear stress). The overall effect of distraction force is to act against fixation force, provoking migration or movement of stent-graft components. Quantification of the effect of vessel morphology and physiological factors upon *in situ* distraction force would improve understanding of this important physical concept. Further to this, if *in situ* distraction force could be linked to stent-graft movement then high-risk morphology could be identified early giving the clinician an option to arrange more intensive follow up or chose alternative intervention.

3.3 Determining distraction force

Distraction force can be determined using three main techniques:

1. Experimental (desktop) models (144, 154-157);
2. Analytical (theoretical) models (43, 44, 158);
3. Computational Fluid Dynamics (CFD) models (41, 159-165).

3.3.1 Experimental models

Experimental models enable the effects of pulsatile blood flow to be analysed (154) but even the construction of a rudimentary desktop model is time-consuming and provides little patient-specific information about the forces likely to be encountered *in situ*. Experimental models have been used to show the linear relationship between blood pressure and distraction force (154, 155). Liffman *et al.* (144) used them to show the effect of pulse pressure on modular distraction with varying lengths of overlap and Corbett *et al.* (156) documented the greater longitudinal force generated with increasing bifurcation angle and increasing tortuosity (i.e. out-of-plane limb angulation).

3.3.2 Analytical models

Analytical or theoretical models provide an excellent opportunity to assess the impact of changing one variable at a time on distraction force. Most are based on simple 'Bernoulli-type' approaches in combination with the principles of continuity (conservation of mass) and linear momentum to fluid flow.

The linear momentum equation is a form of Newton's 2nd law of motion which states:

"The rate of change of momentum is parallel and directly proportional to force, is in the direction of that force and is inversely proportional to its mass".

If momentum remains constant the net forces must be zero, therefore changes in momentum can be used to calculate force. The following theoretical model was used by Mohan *et al.* (44) to determine distraction force in a simple bifurcated tube representing the aorta and iliac vessels.

$$f_x = P_1A_1 + \rho A_1 U_1^2 - \rho \frac{A_1^2}{2A_2} U_1^2 \cos\theta - 2A_2 \cos\theta \left[P_1 + \rho \frac{U_1^2}{2} \left(1 - \frac{A_1^2}{4A_2^2} \right) \right] \quad \textbf{(3.1)}$$

The main determinants of distraction force (f_x) were: Inlet pressure (P_1), inlet cross-sectional area (A_1), blood density (ρ), inflow velocity (U_1), outlet cross-sectional area (A_2), and outlet angle (θ). Pressure and inlet cross-sectional area had a linear relationship with distraction force. Outlet angle was only found to increase distraction force when greater than 20°. Density and velocity of flow were relatively less important as the pressure terms dominate. More complex analytical models have been used for determining distraction force (43, 158). Some include terms for asymmetrical flow division and gravity but all are limited by only providing a one dimensional representation of flow in simplified bifurcated geometries at one particular point in time along a pulse wave.

3.3.3 Computational Fluid Dynamics (CFD)

Computational Fluid Dynamics (CFD) simulates real fluid flow by using numerical methods to solve the Navier-Stokes equations. The Navier-Stokes equations are partial differential equations derived from Newton's second law that describe the interrelationship between flow variables in Newtonian fluids (166). In relation to blood flow where temperature is constant and flow is incompressible (i.e. density is constant) these equations may be simplified into the following continuity equation (3.2) and the conservation of momentum equation (3.3)

$$\frac{\partial u}{\partial x}+\frac{\partial v}{\partial y}+\frac{\partial w}{\partial z}=0 \qquad \textbf{(3.2)}$$

where *u, v* and *w* represent velocity components in the *x, y* and *z* axes.

$$\underbrace{\frac{\partial u}{\partial t}+u\frac{\partial u}{\partial x}+v\frac{\partial u}{\partial y}+w\frac{\partial u}{\partial z}}_{\text{Inertia}}=\underbrace{-\frac{1}{\rho}\frac{\partial p}{\partial x}}_{\text{Pressure Gradient}}+\underbrace{\frac{\mu}{\rho}\left(\frac{\partial^2 u}{\partial x^2}+\frac{\partial^2 u}{\partial y^2}+\frac{\partial^2 u}{\partial z^2}\right)}_{\text{Viscous}}$$

$$\frac{\partial v}{\partial t}+u\frac{\partial v}{\partial x}+v\frac{\partial v}{\partial y}+w\frac{\partial v}{\partial z}=-\frac{1}{\rho}\frac{\partial p}{\partial y}+\frac{\mu}{\rho}\left(\frac{\partial^2 v}{\partial x^2}+\frac{\partial^2 v}{\partial y^2}+\frac{\partial^2 v}{\partial z^2}\right)$$

$$\frac{\partial w}{\partial t}+u\frac{\partial w}{\partial x}+v\frac{\partial w}{\partial y}+w\frac{\partial w}{\partial z}=-\frac{1}{\rho}\frac{\partial p}{\partial z}+\frac{\mu}{\rho}\left(\frac{\partial^2 w}{\partial x^2}+\frac{\partial^2 w}{\partial y^2}+\frac{\partial^2 w}{\partial z^2}\right) \qquad \textbf{(3.3)}$$

The conservation of momentum equation (3.3) relates inertial terms to the pressure gradient and viscous terms in three directions. ρ represents density, *p:* pressure, μ: viscosity and *t* is time

The CFD software first separates the fluid domain of the model into much smaller elements to make it suitable for numerical evaluation. This process is called discretisation. Boundary conditions including velocity at the model inlet,

pressure (at steady state), fluid viscosity, density, temperature and flow weighting are set. The walls of the model are assumed to be rigid with zero flow velocity (the so-called 'no-slip' condition). The above equations are then solved simultaneously and repeatedly for each element. When the software has achieved an acceptable level of error the model can be interrogated to return values for the forces acting on different parts of the wall.

3.3.3.1 Application to vascular surgery

Rudimentary CFD was being used in medical research during the 1960s when Ray and Davids from the Department of Engineering Mechanics at Pennsylvania State University constructed a computational model with 20 elements to examine the effect of asymmetrical vessel cross-section on shear stress (167). Early applications to vascular surgery involved the modelling of turbulence and shear stress as risk factors for developing atherosclerosis (168) or in the quantification of AAA wall shear stress as a predictor of expansion and rupture (169-171).

Idealised models of stent-grafts – where real-life anatomy is simplified and represented by two or three-dimensional models with curvature in one plane – provide an opportunity to make stepwise changes to morphological parameters and assess the impact upon distraction force. Results of such CFD studies demonstrated a linear relationship between greater distraction force and larger proximal diameter (43, 158, 172), larger proximal:distal diameter ratios and larger bifurcation angle in standard stent-grafts (163). 'Neck angle' was poorly defined but was found to influence distraction force more in the lateral direction than in the antero-posterior direction (163, 172). One study has included an assessment of distraction force acting on an idealised complete fenestrated stent-graft model. Forces of 7.36N were observed at peak systole (159).

More recent developments in computer processing power and the ability to produce computer models of patient-specific geometries from cross-sectional imaging in a relatively short time (173-175) have enabled virtual replicas of life-

like anatomy to be solved by CFD. This has enabled *in situ* distraction forces to be determined without the need for intricate physical models or elaborate desktop flow circuits.

CFD analysis of patient-specific geometry has been used to describe the effect of inlet diameter (41) as well as inlet cross-sectional area (161, 165) upon distraction force. Other morphological parameters found to be associated with greater distraction force include smaller outlet diameter, larger inlet:outlet diameter ratio (172), larger neck angulation (160, 161, 163, 165, 172), iliac angulation (160, 172), bifurcation angle (163), and curvature (160, 164). The largest of these studies reported no significant association between inlet:outlet cross-sectional area ratio or iliac angulation and the magnitude of distraction force (165). All ten stent-graft models in this analysis were standard EVAR devices. Only one study considered distraction force in patient-specific fenestrated Anaconda stent-graft models (161). This was a pulsatile flow analysis that considered the complete stent-graft as one piece. No studies have investigated distraction forces in Zenith fenestrated stent-grafts or considered the stent-graft in terms of its *individual* components.

3.3.3.2 Other findings with CFD

Crossed iliac limbs (the so called 'ballerina' position of stent-graft deployment) has not been shown to increase the distraction force acting upon the stent-graft (176). A minor beneficial effect has been noted with tapering of stent-graft limbs as opposed to sudden diameter changes (177) and some variation has been noted depending on the position of the bifurcation (164).

Incorporation of the mechanical properties of the stent-graft and aneurysm into simulations has shown the possible protective effects of type II endoleak in reducing distraction force (41, 162). It has also shown that compliance of the stent-graft had only a negligible effect upon distraction force and therefore supports the assumption of rigid, 'no-slip' walls for the boundary conditions of

fluid simulations (158, 178). Prior to stent-graft deployment the compliance of the native vessel may be more important. The analytical model developed by Morris *et al.* (158, 178) suggested an approximate 15% increase in distraction force at peak systole between a low compliance model of an elderly aorta and the high compliance of a young aorta (158, 178).

A steeper inflection of the blood pressure waveform was associated with greater distraction force (172) but velocity profile was not found to have a significant effect (179).

3.4 Summary

Stent-graft migration is resisted by fixation force and provoked by haemodynamic distraction force. Experimental, analytical and CFD studies have associated the following factors with greater distraction force:

1. Large inlet cross-sectional area/diameter;
2. Hypertension;
3. Small outlet cross-sectional area;
4. Large proximal:distal diameter ratio;
5. Large bifurcation angle;
6. Large proximal neck angulation;
7. Greater vessel curvature.

Less important contributors include: high volume flow rate, high viscosity and blood density. Analytical models do not allow consideration of complex geometries and experimental models are time-consuming and costly to set up. Once suitably validated, CFD is the ideal method to evaluate the effect of angulation on distraction force in patient-specific geometries. Although CFD methods have been described for the evaluation of distraction force acting on standard stent-grafts and complete fenestrated stent-grafts, no studies have

quantified distraction force for patient-specific stent-graft components. A study of this kind would provide greater understanding of the contribution of morphological factors upon the distraction force. In addition to this if the intuitive link between distraction force and migration can be proven it would justify targeted intensive follow-up of at-risk stent-grafts or help the clinician to avoid placing stent-grafts in high-risk anatomy.

3.5 Project overview

This thesis will use Computational Fluid Dynamic analysis in steady state to quantify *in situ* distraction force for 59 complete fenestrated stent-grafts and their individual components.

In part one blood pressure will be kept constant at 160mmHg to represent peak systole in a hypertensive patient and morphological features will be defined in order to assess their impact on distraction force. In part two, patient-specific blood pressures will be used to obtain *in situ* distraction forces that will then be related to the incidence of migration and component distraction.

3.6 Hypotheses

In fenestrated Endovascular Aneurysm Repair:

1. Larger angulation of vessels is associated with greater distraction force;
2. Greater distraction force is associated with higher incidence of migration and component distraction.

3.7 Limitations

One limitation of a CFD approach is that a number of factors will change between models which may make elucidation of the effect of one particular feature more difficult. Blood will be modelled as a Newtonian fluid. This is a reasonable assumption for the large vessels and high velocity flows present in the aorto-iliac territory (180).

The effect of the blood pressure waveform will not be assessed as pulsatile flow will not be modelled. The effect of endoleak (high AAA sac pressure) and aorta/stent-graft compliance will also not be assessed as this requires simultaneous modelling of tissue mechanical properties.

4 Measurement of Vessel Angulation

4.1 Abstract

4.1.1 Introduction

In order to quantify the effect of aorto-iliac angulation upon distraction force it is first necessary to describe a reproducible and accurate method by which angle measurements can be obtained. No standardised method for measurement of vessel angulation currently exists. The aim of this chapter was to develop a method of angle measurement that would be useful when assessing the link between vessel angulation and distraction force. The interobserver variation of the new method was then compared with the standard method currently in use in our unit for measuring vessel angulation during the EVAR planning process.

4.1.2 Method

Interobserver variation in the measurement of the angle between the suprarenal aorta and the infrarenal neck (α angle) was assessed between five observers using sagittal or coronal reconstructed images of CT scans in the arterial phase on the Leonardo workstation (Siemmens AG, Germany). A protocol for a new method of angle measurement was drawn up with reference to existing literature and was used by the same five observers to measure the same α angles from three-dimensional models created using ScanIP software (Simpleware Ltd, UK). Results were compared using Wilcoxon matched-pair Signed-Rank test (WSR) and Friedman's Two-way Analysis of Variance (FTAV). The application of the protocol was also qualitatively assessed.

4.1.3 Results

The overall median α angle measured with Leonardo was 17° (range 0-56°) vs 19.6° (range 1.4-55.8°) for ScanIP, p=.723 (WSR). There were no significant differences between the two methods of angle measurement. FTAV revealed no

significant differences in α angle measurement between observers using Leonardo (p=.154) or ScanIP (p=.171). Qualitative analysis of the results revealed that although there were no differences in the values recorded, there were major differences in interpretation and application of the protocol between methods and between observers.

4.1.4 Conclusions

Variation between observers measuring α angle was not improved by the use of the new method. It was however at least as good as the current method in common use and can be used to describe angles within the aorto-iliac arteries for the purpose of relating them to haemodynamic forces.

4.2 Introduction

Standard geometric terminology can be used to define important features involved in the measurement of an angle (see Figure 4.1):

Ray: One of a pair of lines that make up an angle. Technically a ray is a line with infinite length but as 'leg' is the alternative term it has been used here to avoid confusion with the anatomical term 'limb'.

Vertex: the point at which the two rays converge. The 'pivot point' of the angle being measured.

Endpoint: the extent of each ray away from the vertex.

Supplementary angle: describes position of the second ray in terms of its deviation from the direction of the first assuming that the first ray runs from endpoint to vertex.

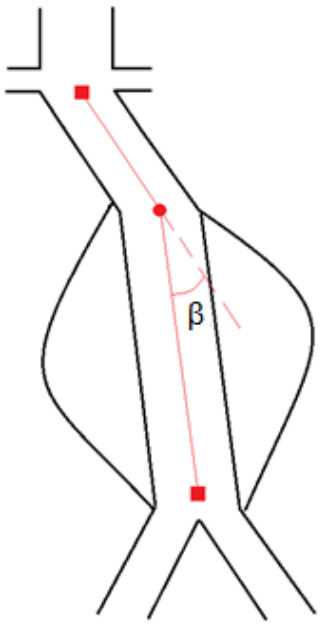

Figure 4.1 Geometric terminology applied to β angle of the aorta

■ : Endpoint of ray, ● : Vertex, β: Supplementary β angle

For accurate angle measurement it is essential that rays follow a Central Luminal Line (CLL). This eliminates error caused by variation in the aortic wall or thrombus lining (See Figure 4.2).

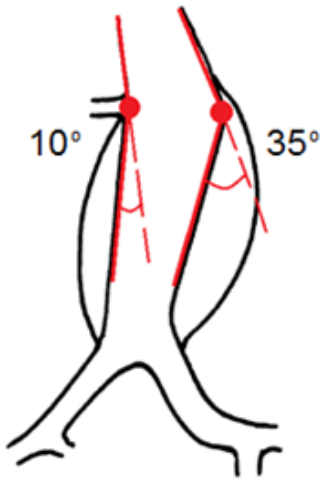

Figure 4.2 Importance of central luminal line: Angle measurement using either aortic wall leads to different results

The position of ray endpoints may also significantly affect the magnitude of the angle being measured (see Figure 4.3).

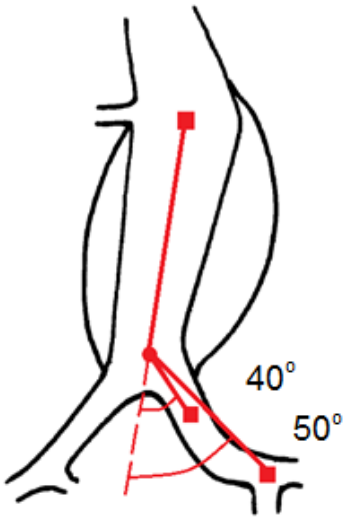

Figure 4.3 Importance of ray endpoints: The choice of mid common iliac artery or bifurcation as the position for distal endpoint leads to different results

4.2.1 Methods for measuring angulation in aorto-iliac arteries

Angulation of the aneurysm neck is one of the morphological features commonly associated with poor outcome after EVAR and most stent-graft Instructions for Use (IFU) include a recommended range for at least one angle within the aorto-iliac territory. Despite this recommendation there is no standard method for the measurement of aorto-iliac angulation. The 2002 EVAR reporting standards document contained no definition of angles or measurement method (40) but a related publication defined four angles (α, β, θ and ϕ) and recommended the use of spatially correct 3D images from which to take measurements (181). The definitions were as follows (see Figure 4.4):

α angle: between the flow axis of the suprarenal aorta and the infrarenal neck.

β angle: between the flow axis of the infrarenal neck and the aneurysm.

Φ/ϕ angle: the most acute angle in the aorta (Φ) and iliac arteries (ϕ).

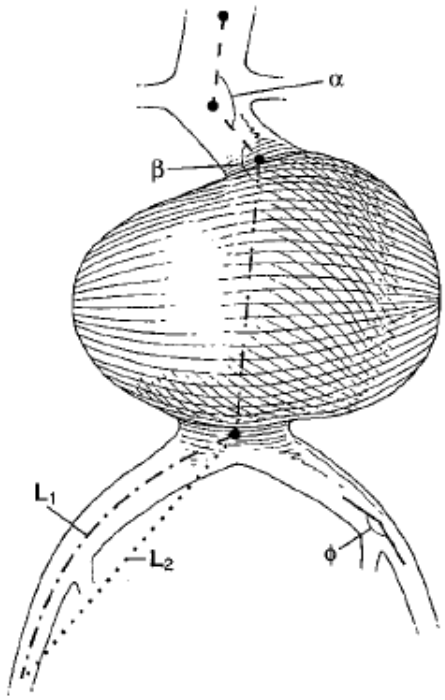

Figure 4.4 α, β and ϕ angle. From Chaikof *et al. (181)*

(L_1 and L_2 are CLL and straight-line distances used to determine the iliac tortuosity index)

It should be noted that in this publication the angles were 'internal' rather than 'supplementary' as is more commonly used. The 'internal' angle describes the difference between the position of first and second ray as if rotation had occurred around the vertex rather than as a deviation from the axis of blood flow. The sum of the internal and supplementary angles is always 180°.

Many other published studies dealing with angulation refer to one or other of these angles but provide little further detail on how measurements were actually obtained. Most of these studies have methodological deficiencies in one or more of the following areas:

1. Angle terminology: Different terms used for the same angles, lack of clear definition of the angles measured or method used (45, 50, 141, 142, 182-184);
2. Comprehensiveness versus applicability: Methods that attempt to describe all angulation within a complex vessel (185-187) are usually too rigid to allow application to variations in aorto-iliac anatomy;
3. Reproducibility: the less precise a method is in describing exactly how to manipulate images and measure an angle the less reproducible the results become (182).

4.2.2 Proposed improvements

Terminology can be improved by using standard terms. Guidelines should be both specific and to some degree adaptable.

All angle measurements considered so far have relied upon placing an angle measuring tool (i.e. a physical or electronic protractor) onto a projection of a 3D image. If the image has not been manipulated to show the desired angle in its maximum projection (i.e. the plane in which the angle appears as large as possible) then an incorrect measurement is inevitable despite accurate application of the measuring tool. 3D calipers that can be applied to the CLL independent of the projection in which the angle is being viewed is a function available in ScanIP (Simpleware Ltd, UK). The approach requires 3D image

reconstruction with CLLs as opposed to coronal and sagittal cross-sectional views (188, 189) but it may reduce the need for and variability caused by pre-measurement image manipulation.

4.2.3 Aim

The aim of this chapter was to develop a method of angle measurement that would be useful when assessing the link between vessel angulation and distraction force. Interobserver variation of this new method was assessed and compared with the current method of angle measurement used for EVAR planning in Liverpool Vascular and Endovascular Service (LiVES).

4.3 Method

4.3.1 Preparation of images

Ten patients who received standard EVAR were chosen at random from a departmental database. Each patient's pre-intervention arterial phase CT scan was anonymised and imported into a commercially available image processing software (ScanIP, Simpleware Ltd, UK). Images were cropped to include the aorto-iliac segment from diaphragm to just distal to the common iliac artery bifurcation.

The lumen and thrombus were segmented based on pixel greyscale density to obtain two Regions of Interest (ROIs, red: lumen, purple: thrombus, see Figure 4.5). The lumen ROI was duplicated and a skeletalisation filter was applied to reduce it to the pixel furthest from the vessel wall in each axial slice thus yielding a CLL (green ROI, Figure 4.5).

The same CT scans were downloaded onto the Leonardo (Siemmens AG, Germany) 3D workstation and anonymised.

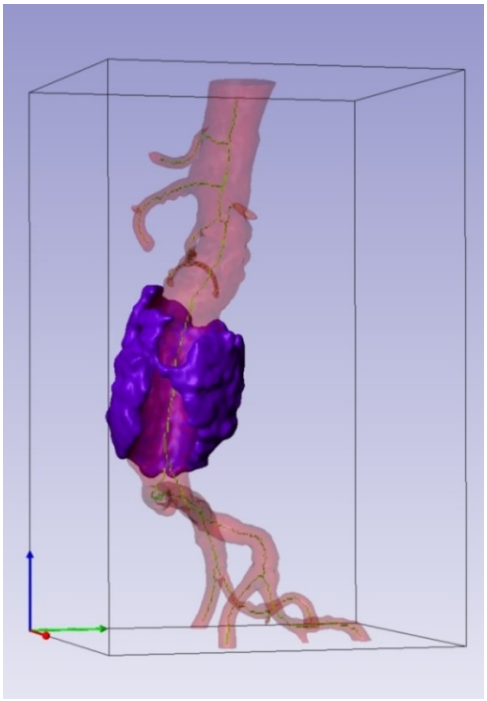

Figure 4.5 Reconstructed image of a patient-specific AAA. Red ROI: lumen, purple: thrombus, green: CLL

4.3.2 Angle measurement

α angles were measured by five observers using both ScanIP and Leonardo workstation. All observers had previous experience of EVAR planning with the Leonardo workstation. Three were researchers enrolled in MD or PhD programs with LiVES and the University of Liverpool, the other two were Specialist Registrars in Vascular Surgery.

4.3.2.1 ScanIP method

Observers were given three test cases to get used to the software. They were then asked to follow the protocol detailed in Appendix 8.2 and measure α angle using 3D calipers applied to the CLL.

α angle was defined as the angle between the axis of blood flow in the neck of the aneurysm (at the seal-zone of the planned standard EVAR) in relation to that

of the aorta immediately proximal to this. The vertex was defined as the major angulation of CLL nearest the lowest renal artery. Proximal endpoint was defined as where the CLL of the superior mesenteric artery joins the aortic CLL and distal endpoint was the most distal point of the CLL along the neck of the aneurysm or the next major angle vertex. The protocol was designed to prescribe the setting of endpoints and vertex whilst leaving some room for application to variations in aneurysm morphology. An advisor was available for technical software issues but not to give any advice regarding application of the protocol.

4.3.2.2 Leonardo method

Observers measured the same angles on the Leonardo workstation with at least 24hrs rest between each method. This workstation uses axial CT slices to reconstruct coronal and sagittal images that can be manipulated in different planes to provide projections of the aortic lumen. Observers were asked to do this in the usual way as for EVAR planning. No CLL was available therefore the angle measuring tool (a two-dimensional electronic caliper) had to be applied over an estimated CLL on the manipulated image in either sagittal or coronal plane that projected the largest angle.

4.3.2.3 Statistical analysis

Variation between methods was assessed by comparing paired angle measurements using Wilcoxon matched-pair Signed-Rank test (WSR). Observers were compared using Friedman's Two-way Analysis of Variance.

4.4 Results

Five observers measured α angle in ten aneurysms (see Table 4.1). Observer four failed to record α angle for aneurysm nine with ScanIP and observer five failed to record α angle for aneurysm two with ScanIP and aneurysm three with Leonardo.

Table 4.1 α angle measurements in degrees made by each observer

Observer		EVAR									
		1	2	3	4	5	6	7	8	9	10
1	Leo	52	5	22	34	13	8	52	9	18	8
	ScanIP	17.5	22.9	17.7	16.3	21.8	13.1	16.5	7.6	31.2	11.4
2	Leo	12	5	16	38	23	18	49	3	28	11
	ScanIP	45.5	19.5	24	25.5	22.5	23	55.8	1.4	28.5	10.7
3	Leo	45	24	16	45	28	30	56	0	31	7
	ScanIP	45.4	19.3	18.4	31.1	20.2	25.6	53.1	7.9	24.6	14
4	Leo	13	21	9	36	18	17	14	7	12	12
	ScanIP	12.9	21.6	4.1	20.5	26.4	13.9	18.5	5.3	-	24.4
5	Leo	54	10	-	37	17	20	13	10	34	15
	ScanIP	15.3	-	3.2	23.4	30.8	8.9	19.6	8.3	26.4	10.3

4.4.1 Analysis by method

The overall median α angle measured with Leonardo was 17° (range 0-56°) versus 19.6° (range 1.4-55.8°) for ScanIP. There were no significant differences between the values obtained using either two methods of angle measurement p=.723 (WSR).

4.4.2 Analysis by observer

Paired data was also analysed between observers using Friedman's Two-way Analysis of Variance. This is similar to Kruskal-Wallis test in that it compares the distribution of multiple groups of non-parametric data for significant differences but can be used when the observations are linked. In this case there were five groups with ten linked observations for each method. There were no significant differences in α angle measurement between observers using Leonardo (p=.154) or ScanIP (p=.171).

4.4.3 Qualitative analysis of images

Even though there was no statistically significant difference in α angles measured by the five observers using the two techniques, examination of the pictures recorded at the time of angle measurement showed variation in application of the protocol. In case one, using the Leonardo method, observers two and four chose to position the vertex at the level of the lowest renal artery on the sagittal image and measure the slight anterior angulation just distal to that point (see Figure 4.6A).

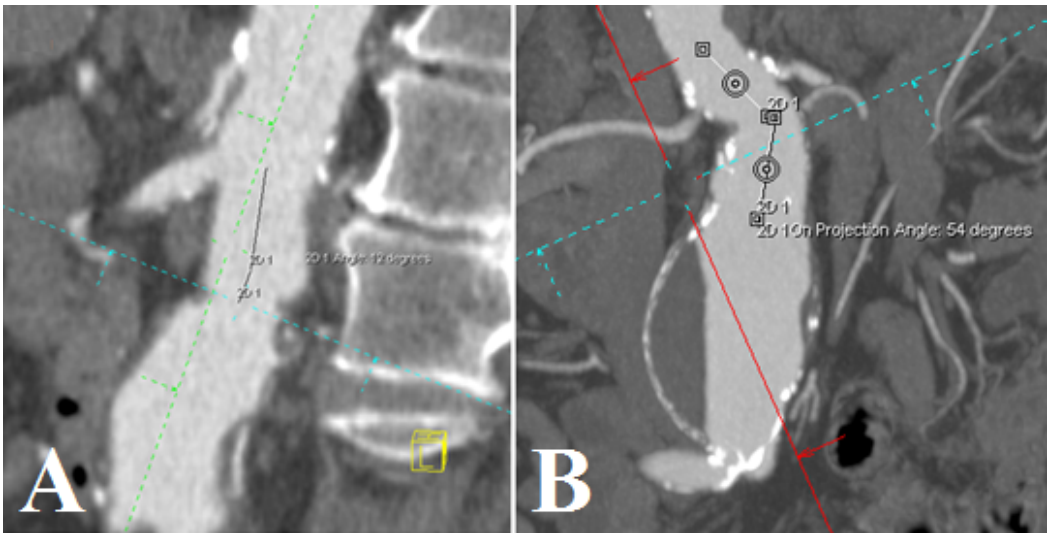

Figure 4.6 Case 1. Two different α angles measured using different images on the Leonardo workstation (A: 12°, B: 54°)

Observers one, three and five chose to use the coronal image and measure lateral angulation (see Figure 4.6B). Case one α angle using Leonardo therefore varied from 12-13° to 45-54°. The same two ways of applying the protocol were also seen with the ScanIP method (see Figure 4.7).

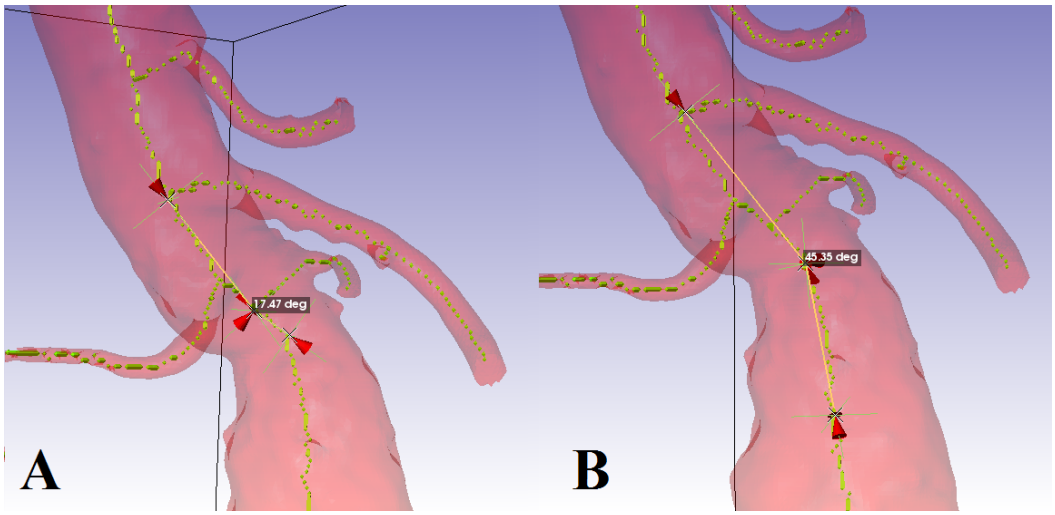

Figure 4.7 Case 1. Two different α angles measured using ScanIP (A: 17°, B: 45°)

Only observers three and four consistently measured the same α angle with both methods in case one. Observers one, four and five chose to use the exact position at which the CLL of the lowest renal artery meets the CLL of the visceral aorta as the vertex (as shown in Figure 4.7A) whereas observers two and three chose the more obvious vertex just distal to this point (Figure 4.7B). The resulting α angle for case one measured using ScanIP was either approximately 17° or 45°.

Case four illustrates how even when the same angle is measured, different methods of image manipulation with the Leonardo method can lead to variation in the resulting α angle (see Figure 4.8). The lower levels of magnification in images A and C compared with B may have contributed some of the variation. The 3D calipers in ScanIP that automatically adhere to the CLL and reduce the need for and variation caused by image manipulation were expected to improve the reproducibility of α angle measurement. However, even when the ScanIP

protocol was applied in a consistent manner, slight differences in the choice of vertex position or ray endpoints led to a variation of 16 to 31° (see Figure 4.9).

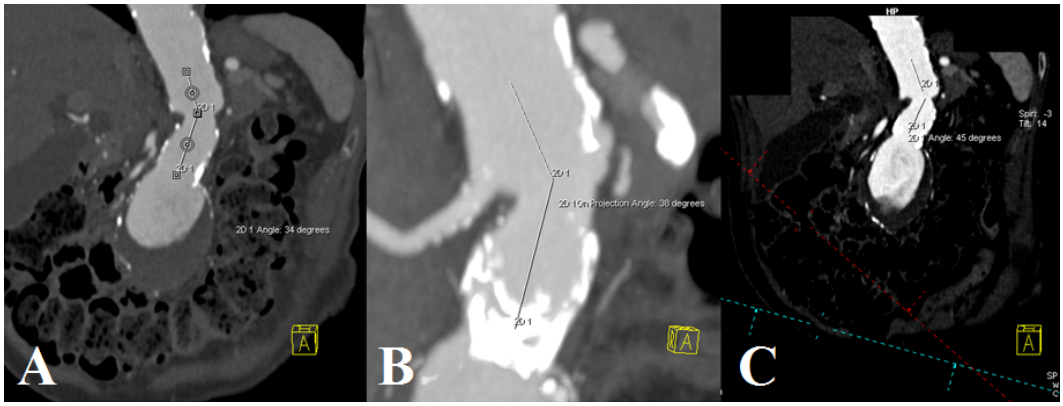

Figure 4.8 Case 4. The same α angle measured using different magnification with the Leonardo workstation (A: 34°, B: 38°, C: 45°)

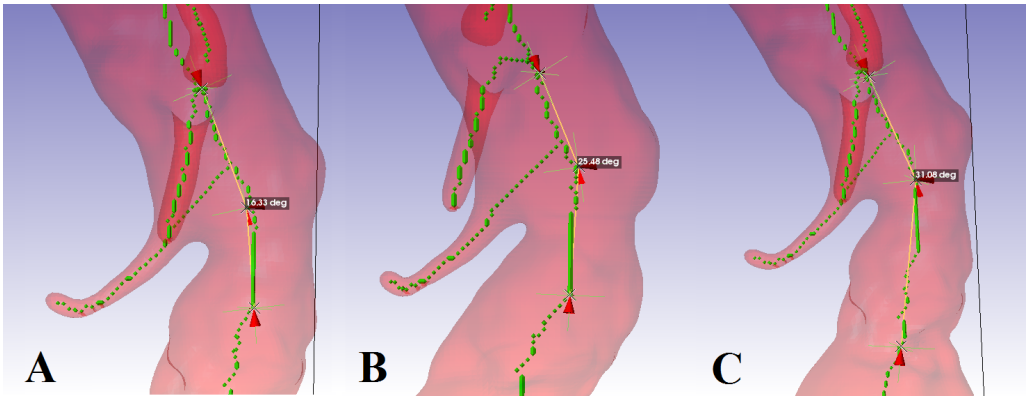

Figure 4.9 Case 4. Variation in α angle measured using ScanIP (A: 16°, B: 23°, C: 31°)

4.5 Discussion

The complex morphology of the aorta makes the measurement of angulation difficult. No standardised method exists despite the inclusion of maximum angulation within the instructions for use of all commercially available stent-grafts. An ideal method is consistent in terminology, applicable to anatomical variation and reproducible both in terms of image manipulation and actual

measurement technique. In this chapter a proposed new method of angle measurement (ScanIP) was assessed against the current method used in our unit (Leonardo). The new method included the use of three-dimensional reconstructed images, a central luminal line and three-dimensional calipers to reduce variability caused by image manipulation and measurement technique. It was written using standardised terms as a prescriptive protocol to improve overall reproducibility whilst still allowing for applicability to variation in normal anatomy.

Overall there were no statistically significant differences between α angles measured with Leonardo compared with those measured with ScanIP. There were also no significant differences between observers using either of the two methods. The results show non-inferiority of the ScanIP method and justify its use as a means to measure aortic angulation.

Examining the measurements qualitatively in section 4.4.3 revealed some variation in the application of protocol. This possibly contributed to the absence of the expected reduction in variation that was anticipated with the use of the ScanIP method with its prescriptive protocol, 3D reconstructed images, CLL and 3D calipers. Feedback training before another round of angle measurement using ten different aneurysms may have reduced variability but was beyond the scope of the current study.

In relating the current results to the measurement of angulation in the aorto-iliac vessels *after* fenestrated endovascular aneurysm repair for the purpose of determining an association with distraction force the following points should be considered:

1. One observer will be making the measurements providing no potential for interobserver variation.
2. A less prescriptive approach to describing the angles to be measured may be appropriate since this was not shown to improve variability.

3. Theoretical models include the angle of outlets in reference to the angle of the inlet therefore this needs to be measured for the complete fenestrated stent-graft and for each component in turn. Previous work from this unit has shown that the iliac vessels become significantly less tortuous following stent-graft deployment (190). This should improve the reproducibility of angle measurement as calipers are much easier to fit to straight lines rather than curves.
4. To enable comparison of Computational Fluid Dynamic (CFD) results with analytical models all angles will need to be measured in two separate planes. This will be the only way to ensure the three-dimensional arrangement of limbs in a bifurcated component can be accurately determined in relation to each other. One angle measurement as obtained using the ScanIP technique detailed above does not enable this. Two, two-dimensional angles will therefore need to be measured for each vessel angulation. Measuring angles in this way will require a simple and reproducible method of image manipulation to eliminate possible confounding factors.

The eventual method devised for angle measurement for the purpose of distraction force analysis is detailed in chapter five. α angle was retained as the angle describing the axis of blood flow into the proximal part of the stent-graft. It was adapted for use in fEVAR so that α angle became the angle between the axis of blood flow in the seal-zone of the proximal body component in relation to the abdominal aorta immediately above. Other angles measured include:

'β angle' – adapted from the Society for Vascular Surgery publication to define the axis of blood flow in the distal body component in relation to the visceral aorta (181). This is an approximation of the aneurysm angle in standard EVAR planning.

‘θ angle’ - defines the axis of blood flow at the outlet of a component in relation to its inlet. All rays were required to be at least as long as the corresponding sealing stent.

4.6 Conclusion

Variability in measurement of α angle was not improved with the use of a prescriptive protocol, 3D reconstructed images, CLL and 3D calipers. This approach is however at least as good as the current method in common use and has been developed further to define angles within the aorto-iliac arteries for the purpose of investigating the association between morphological features and distraction force.

5 Determining Distraction Force for Individual Components of the Fenestrated Stent-graft with Particular Reference to Morphological Features

5.1 Abstract

5.1.1 Background

Secure fixation of endovascular stent-grafts is essential for successful endovascular aneurysm repair. Haemodynamic distraction forces act against fixation force to encourage migration that may lead to stent-graft failure. The aim of this chapter was to quantify distraction forces acting on all fenestrated stent-graft components and determine which morphological factors were associated with greater force.

5.1.2 Method

Computer models of 54 fenestrated stent-grafts were constructed using image processing software (ScanIP, Simpleware Ltd). The models were exported into a finite-volume solver (FLUENT v6.2, ANSYS Inc.) for computational fluid dynamics analysis using boundary conditions representative of peak systole in a patient at rest. Distraction force results were obtained in three directions and used to calculate total Resultant Distraction Force (RDF). Cross-sectional area was measured and correlated with total RDF. Complete stent-grafts and components were grouped according to angulation ≥45° or <45° and total RDF was compared by non-parametric methods (Mann-Whitney U, MWU).

5.1.3 Results

Median total Resultant Distraction Force (RDF) acting on the complete stent-grafts was 6.0N (range 0.3-17.7N), on proximal bodies: 4.8N (range 1.3-15.7N), distal bodies 5.6N (range 1.0-8.0N) and limb extensions 1.7N (range 0.6-8.4N).

Inlet cross-sectional area (XSA) exhibited a strong, positive correlation with total RDF in complete stent-grafts, proximal body and distal body components (Spearman's Rho 0.814, 0.883, 0.802 respectively). Outlet XSA exhibited a similarly strong, positive correlation with total RDF in limb extension components (Spearman's Rho 0.822).

Outlet angulation ≥45° was significantly associated with greater total RDF in the most angulated groups i.e. complete stent-grafts and limb extension components (Median total RDF in complete stent-grafts with angle <45° = 2.6N vs 6.2N in those ≥45°, p<.001, MWU. Median total RDF in limb extensions with angle <45° = 1.4N vs 2.1N in those ≥45°, p=.004, MWU).

5.1.4 Conclusion

This chapter demonstrates a technique to obtain distraction force results for individual components of a fenestrated stent-graft using CT images and computational fluid dynamics.

For a given blood pressure cross-sectional area was the most important morphological determinant of total resultant distraction force. Angulation within the aorta was not large enough to significantly influence distraction force. Iliac angulation affecting outlet angles of complete stent-grafts and limb extension components was associated with significantly greater total resultant distraction force.

5.2 Introduction

Fenestrated endovascular aneurysm repair provides a less invasive alternative to open surgery in abdominal aortic aneurysms that are not suitable for standard EVAR. The Zenith fenestrated stent-graft (Cook Medical Inc., Bloomington, USA) has a modular design that comprises a customisable proximal body with fenestrations for visceral vessels, a bifurcated distal body and at least one tubular limb extension. Secure fixation of all components within the aorta and iliac arteries is essential for successful repair.

Clinical studies of standard stent-grafts have linked large diameter, conical and highly angulated aneurysm necks to migration, type I endoleak and increased rates of secondary interventions (45, 46, 48-52, 115, 142). A possible cause for this is the adverse effect that these unfavourable morphological features have on stent-graft fixation. In addition to the impact on fixation force, unfavourable morphology may also increase haemodynamic distraction forces acting against fixation force *in situ* (43, 158, 163, 172). Haemodynamic distraction forces are generated by blood pressure and blood flow and may lead to migration of the stent-graft. If distraction force overcomes fixation force in a fenestrated proximal body, migration carries the added risk of visceral vessel loss as well as type Ia endoleak, aneurysm expansion and subsequent rupture. Component distraction involving the distal body may lead to type IIIa endoleak and limb extension migration risks type Ib endoleak. Both types of endoleak may ultimately cause aneurysm expansion and rupture.

Chapter three outlined the evidence linking morphological features with greater distraction forces. Whilst larger proximal cross-sectional area was firmly associated with greater distraction force, the effect of angles was less obvious. Analytical models suggest that the larger the angle of bifurcation in a Y-shaped tube, the greater the forces are acting on that tube (44). This effect may be as much as a 52% increase in distraction force in stent-grafts with a bifurcation

angle of 80° compared with 10° (158). Computational fluid dynamics (CFD) studies in idealised stent-graft geometries have also shown the link between large bifurcation angles and greater forces but the effect of other angles within the stent-graft territory is less well defined (163, 165).

No previous *in silico* study has determined distraction forces for individual stent-graft components. This concept may be more relevant when considering a fenestrated stent-graft as opposed to a standard stent-graft due to its greater modularity.

5.3 Aim

The aim of this chapter is to use CFD to determine distraction force at constant blood pressure for each component of 54 fenestrated stent-grafts with particular reference to morphological features such as cross-sectional area and vessel angulation.

5.4 Hypothesis 1

Larger vessel angulation is associated with greater distraction force.

5.5 Methods

5.5.1 Model construction

Construction of computer models consisted of three distinct phases: Image acquisition, image manipulation (segmentation), and model construction (meshing).

5.5.1.1 Image acquisition

Arterial phase postoperative CT scans in Digital Imaging and Communications in Medicine (DICOM) format were imported into a commercially available image processing software (ScanIP, Simpleware Ltd). Axial slices were selected and cropped in anterio-posterior and lateral directions to include the distal thoracic aorta to the external iliac artery and at least the first order divisions of the visceral vessels. Two copies of these cropped axial slices were imported into ScanIP. Each was given different windowing (W) and level (L) settings in order to provide sharper detail of either the vessel lumen (W:L 900:300) or the stainless steel stent framework (W:L 4000:400).

5.5.1.2 Image manipulation (Segmentation)

Definition: the partitioning of a region of interest (ROI) from a background image.

5.5.1.2.1 Segmentation of lumen

Using the 900:300 background images, pixel greyscale density in the aorto-iliac lumen was sampled along its longitudinal axis. All pixels within the sampled greyscale range were then segmented.

The segmented lumen was smoothed and re-filled to remove unconnected pixels of similar density in the surrounding tissues. Metal artefacts caused by

radiopaque markers and visceral stents (as shown in Figure 5.1) were removed by manually segmenting pixels on sequential axial images.

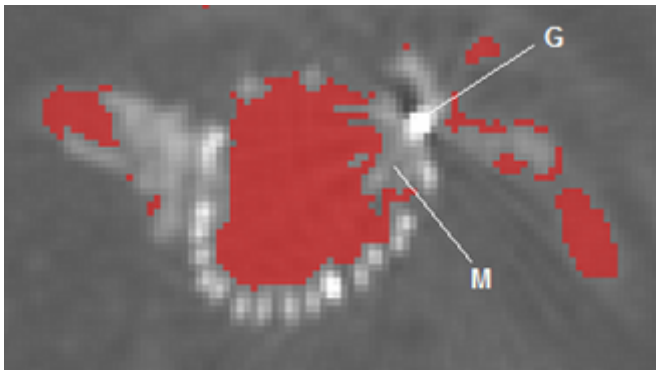

Figure 5.1 Axial image of 900:300 background at the level of the renal arteries showing metal artefact (M) caused by gold radiopaque marker (G). Lumen represented by red ROI

Some CT scans had different axial slice thickness, therefore all images were resampled with a pixel size of 0.4mm in x, y and z axes. The lumen was smoothed again and pixel greyscale density was sampled in transverse section of the distal thoracic aorta to ensure the remaining ROI was a true representation of the arterial contrast volume and therefore also of the vessel lumen.

5.5.1.2.2 Segmentation of model outlets

Using a cuboidal 3D editing tool, an artificial region of interest was segmented towards the distal extent of every outflow vessel (shown as multi-coloured parts in Figure 5.2 over page). The proximal surface was created perpendicular to its outflow vessel and the contact between that surface and the lumen ROI (shown in red in Figure 5.2) was assigned as 'outlet'.

5.5.1.2.3 Segmentation of radiopaque markers and stents

Pixels with greyscale density 220-255 were segmented from the 4000:400 background images to represent the radiopaque markers. Greyscale density of the stainless steel stents was sampled from the same background to create an

ROI representative of the stent framework. The average range of pixel greyscales in this ROI was approximately 140-220.

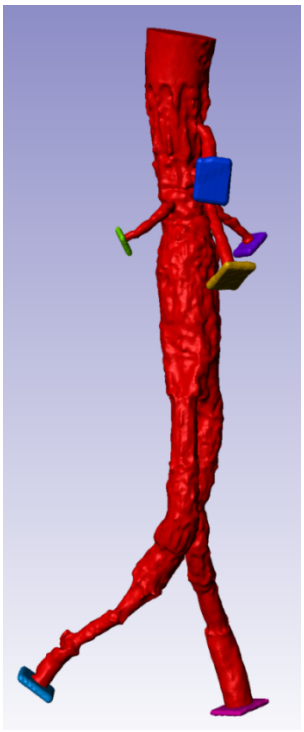

Figure 5.2 3D rendering of lumen (red) showing all outlet regions of interest (multi-coloured parts)

5.5.1.2.4 Segmentation of graft fabric

The lumen ROI was duplicated and dilated by two pixels in each direction to create a larger copy. The original lumen was subtracted from it to give a new ROI that completely enveloped the lumen. This formed the basis of the stent-graft fabric and further editing was then performed to create separate ROIs for each component based on the position of stents and radiopaque gold markers. The proximal body, distal body and limb extension ROIs that this process produced are shown in Figure 5.3. In those stent-grafts where the ipsilateral limb remained in close apposition to the contralateral limb some manual deletion of the graft fabric ROI was necessary to separate the limbs and complete the segmentation of the limb extension.

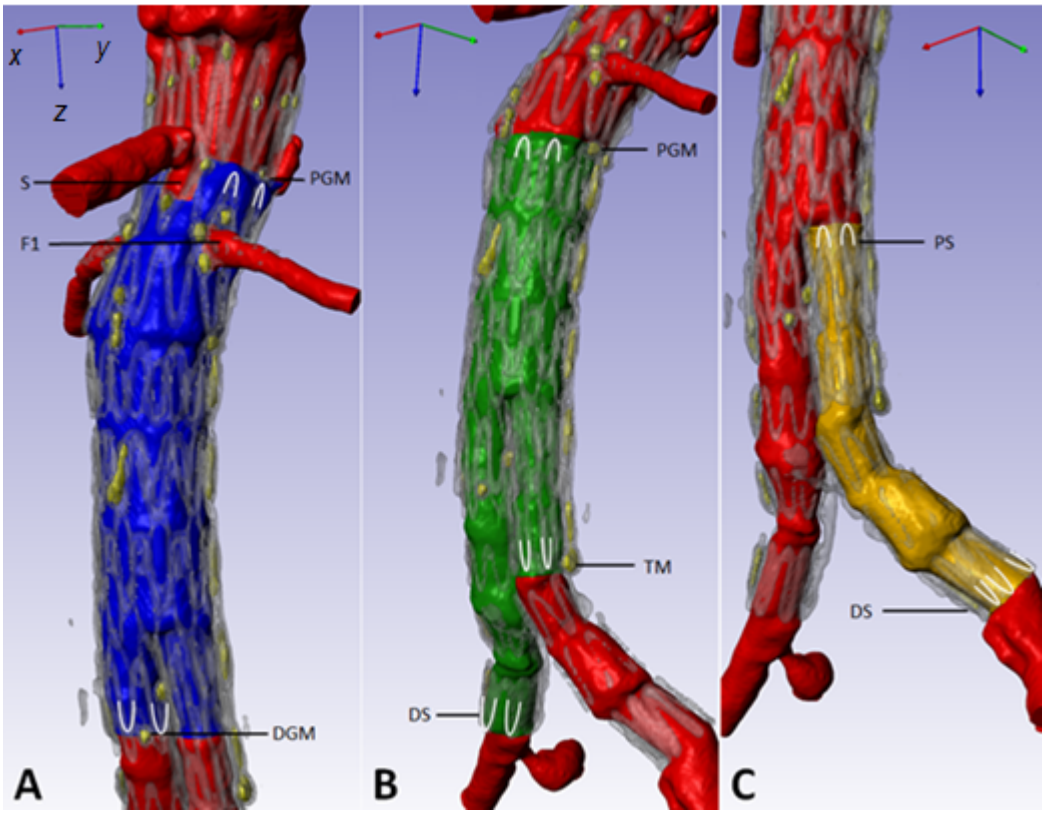

Figure 5.3 3D rendering of fenestrated stent-graft components

A: Proximal body (blue). Inlet: Upper margin of proximal gold radiopaque fabric markers (PGM). Outlet: lower margin of distal gold radiopaque marker (DGM). ROI cropped perpendicular to stent rows (white arcs) in each case. Fenestrations 'cut' according to position of gold radiopaque markers (S: scallop for superior mesenteric artery, F1: small fenestration for left renal artery).

B: Distal body (green). Inlet: Upper margin of proximal gold radiopaque marker (PGM) with ROI cropped perpendicular to 1st sealing stent (white arc). Outlets: lower extent of the radiopaque 'tick' marker (TM) perpendicular to the last stent of the contralateral gate and perpendicular to the distal sealing stent of the ipsilateral limb (white arcs).

C: Limb extension (orange): Inlet - Perpendicular to the upper extent of the proximal sealing stent (PS). Outlet - perpendicular to the lower extent of the distal sealing stent (DS).

Lumen shown in red. Arrows indicate directions in which force results were obtained: x (red arrow), y (green arrow), z (blue arrow).

5.5.1.2.5 Combining ROI

Because the CFD software could not recognise overlapping stent-graft components, the technique above required four separate models of each patient's lumen (i.e. one model each for proximal body, distal body and limb extension plus a complete stent-graft model). A different technique was used after the first 20 patients in order to make the process more efficient: By creating ROIs to represent the overlapping parts and by then subtracting them from each other it was possible to represent the complete stent-graft or any of its constituent components on the same lumen model. Figure 5.4 shows the arrangement of these ROIs for one fenestrated stent-graft. Appendix 8.3 compares both methods and confirms that this did not affect the distraction force results.

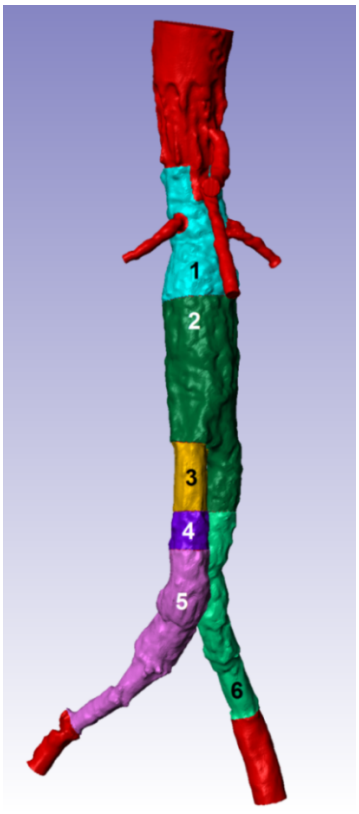

Figure 5.4 Regions of interest combine to represent the complete stent-graft or constituent components upon the same lumen model. Complete stent-graft: ROI 1, 2, 3, 4, 5, 6; Proximal body: ROI 1, 2, 3; Distal body: ROI 2, 3, 4, 6; Limb extension: ROI 3, 4, 5

5.5.1.3 Meshing

Definition: The construction of a three-dimensional model from the pre-segmented regions of interest using smaller tetrahedral building blocks or elements.

Computer models were constructed from the segmented regions of interest using a free mesh algorithm. This algorithm automatically choses small tetrahedral elements to preserve fine detail and uses large tetrahedral elements to reduce complexity and therefore file size in areas where detail is not required (i.e. the centre of the lumen). Mesh complexity was pre-set by selecting the 'compound coarseness'. Following a series of preliminary experiments (see appendix 8.4) compound coarseness of -20 was chosen. This gave tetrahedral elements with a minimum edge length of 0.76mm and maximum of 1.84mm. The average number of elements per model was approximately 1.4million.

5.5.1.4 Assigning model boundary conditions

5.5.1.4.1 Fluid region and wall

Only the region of interest representing the lumen was used to create a three-dimensional meshed volume. This volume was designated as 'fluid'. The volume of the stent-graft components ROIs was not used in the meshing process; only the surface area contact between the component and the lumen ROI was included and assigned as 'wall'. All walls were considered to be rigid with zero flow velocity (i.e. 'no-slip' conditions).

5.5.1.4.2 Inlets and outlets

The proximal extent of the lumen was assigned as the model 'inlet'. Model outlets were assigned to the surface area of contact between lumen and cubic outlet ROIs created for all patent major aortic branches (as shown in Figure 5.2). This included separate outlets for coeliac axis (CA), superior mesenteric artery

(SMA), left and right renal artery (RA), left and right common iliac (CIA) or - when the distal extent of the stent-graft was close to the bifurcation - internal and external iliac artery (IIA/EIA).

5.5.2 Computational Fluid Dynamics (CFD)

Models were exported into a finite-volume solver (FLUENT v6.2, ANSYS Inc.) for simulation of blood flow at steady-state using laminar flow. CFD uses numerical methods to solve the Navier-Stokes equations which are the governing equations of fluid motion. These equations are described in more detail in section 3.3.3 Computational Fluid Dynamics (CFD).

5.5.2.1 Assigning simulation boundary conditions

5.5.2.1.1 Fluid domain and Inlet conditions

Blood was represented by a Newtonian fluid with viscosity 0.0033Pa.s and density 1098 kg/m^3. Boundary conditions were representative of peak systole in a hypertensive patient at rest. Inlet pressure of the model was set at 160mmHg. Inlet volume flow rate was chosen to represent peak systole in the supracoeliac aorta at rest ($1.323x10^{-4}$ m^3/s) (191). Velocity was calculated by dividing the volume flow rate by the orthogonal cross-sectional area of the most proximal extent of the lumen.

5.5.2.1.2 Outlet conditions

Outlet weighting was assigned to outlet vessels to represent the division of blood flow at rest (192). The CA received 33% of supracoeliac blood flow, SMA: 7.4%, RAs: 14.8% equally divided between left and right, EIAs: 15.7% each and IIAs: 6.7% each. If one visceral artery was occluded its flow weighting was given to the contralateral patent vessel. In the case of aorto uni-iliac repair all infrarenal blood flow was assigned to the patent limb.

5.5.3 Validation

Prior validation of this method of blood flow simulation was carried out by comparison with analytical and pulsatile flow experimental models of simplified geometries:

5.5.3.1 Method

5.5.3.1.1 CFD model: Modelling, meshing and flow simulation

A computer model of a simplified bifurcated stent-graft was created by using ScanCAD – a computer aided design software from Simpleware Ltd – to combine three cylindrical shapes representing the aorto-iliac lumen. Dimensions were chosen to recreate the desktop experimental model used by Zhou *et al.* (154). The main body diameter was 30mm, length 150mm; Iliac limb diameter: 12mm with length: 150mm. Iliac angulation was 30° for each limb in the same plane (i.e. bifurcation angle: 60°). The bifurcated ROI were exported into ScanIP where a 3D computer model (Figure 5.5) was constructed using a free mesh algorithm without any further smoothing so as to preserve the original dimensions. Inlet and outlets were assigned in the same way as described in section 5.5.1.4.

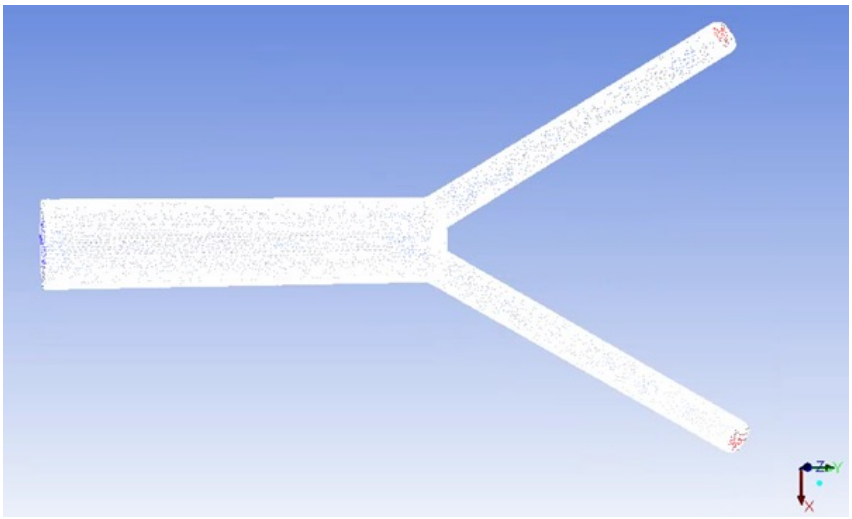

Figure 5.5 Simplified bifurcated model used in validation simulations

The finished model was imported into FLUENT v6.3 (ANSYS Inc., USA) for finite-volume analysis. Blood was represented by a Newtonian fluid with viscosity 0.0033Pa.s and density 1098kg/m^3. A separate steady state simulation was performed to reflect the boundary conditions found at each 0.1 second interval along the normal pulse wave used by Zhou *et al.* (154). Flow and pressure waveforms are shown in Figure 5.6. This approach enabled comparison between CFD and desktop experimental model as well as the intended comparison between CFD and analytical model. Equal flow weighting was given to each of the two outlets since the model was symmetrical. No-slip conditions were imposed at the wall i.e. the surface area of contact between lumen and stent-graft.

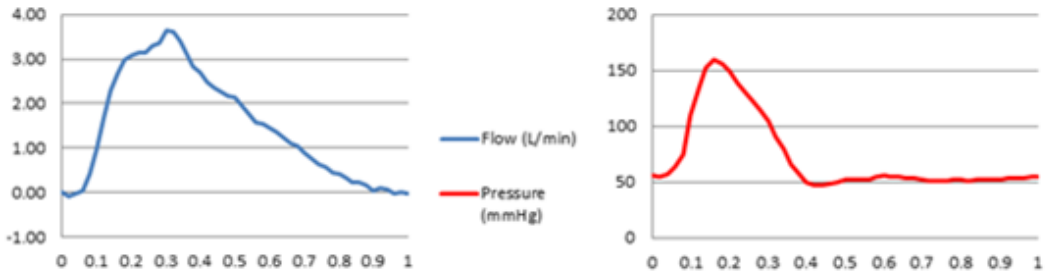

Figure 5.6 Normal flow (*Q*) and pressure waveforms. Adapted from Zhou *et al.* (154)

Distraction force results were obtained in three directions but only the longitudinal (z) forces were significant because the iliac limb angulation was in one plane only and the simplified model was symmetrical.

5.5.3.1.2 Analytical model

Equation 3.1 was written into Mathcad (PTC, USA) and was used to solve uni-directional distraction force for the same boundary conditions as the CFD model. U_1 (Inlet velocity m^3/s) was calculated from Q (volume flow rate L/min) and A_1 (Inlet cross-sectional area m^2) using the following equation:

$$U_1 = \frac{\left(\frac{\left(\frac{Q}{60}\right)}{1000}\right)}{A_1} \quad (5.1)$$

The angle of the iliac limb from the axis of the main body in degrees (θ_a=30°) was converted into radians (θ) using the following equation:

$$\theta = 2\pi \frac{\theta_a}{360} \quad (5.2)$$

5.5.3.1.3 Desktop experimental model

Results for the experimental model with pulsatile flow were obtained from the original thesis (193).

5.5.3.2 Validation results

There were no axial forces generated in the *x* and *y* directions. All forces acted in the longitudinal (*z*) plane. Table 5.1 shows the contribution of pressure and viscous forces to total force. Pressure forces were dominant. The magnitude of viscous force was always less than 0.1% of the total force.

Table 5.1 Longitudinal distraction force results for the simplified bifurcated model

Time (secs)	Pressure Force (N)	Viscous Force (N)	Total Force (N)
0	3.832	0.000	**3.832**
0.1	7.591	-0.001	**7.590**
0.2	10.328	-0.002	**10.326**
0.3	7.262	-0.003	**7.259**
0.4	3.467	-0.002	**3.465**
0.5	3.577	-0.002	**3.575**
0.6	3.833	-0.001	**3.832**
0.7	3.613	-0.001	**3.613**
0.8	3.562	0.000	**3.562**
0.9	3.599	0.000	**3.599**
1	3.758	0.000	**3.758**

Total force was compared with results of the analytical model obtained using Mathcad and the desktop experimental model data of Zhou *et al.* (193). The comparison shown in Figure 5.7 confirmed good agreement between all three methods.

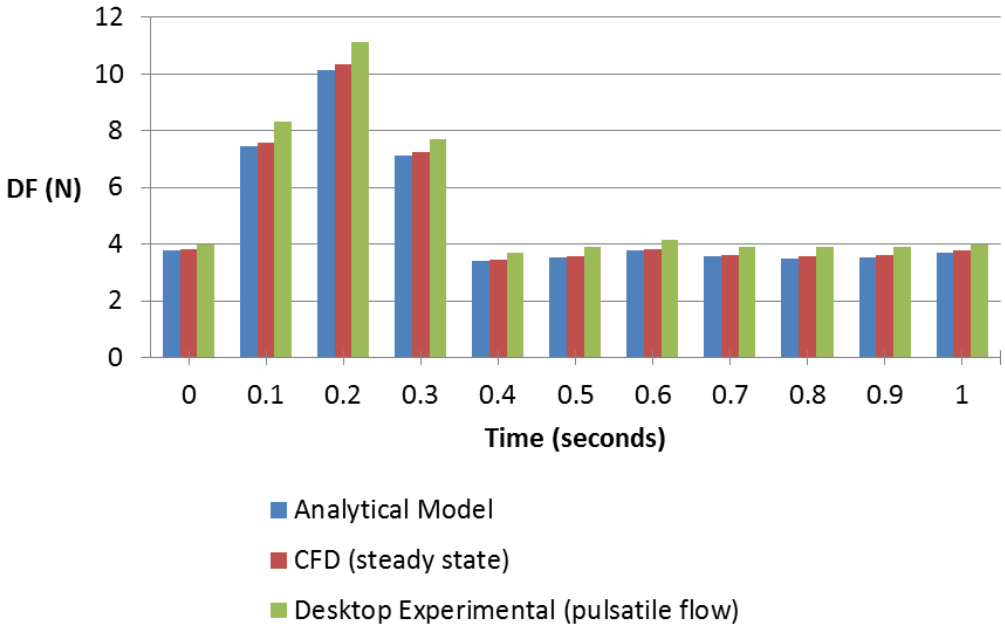

Figure 5.7 Comparison between distraction force (DF) results obtained via three different methods at 0.1 second intervals along a pulse wave

The results of this benchmarking show that CFD and analytical models agree to better than 2%. Some of this difference was thought to be due to the lack of viscous flow terms in the analytical model but inspection of the CFD results reveal that viscous forces are negligible in comparison with those derived from blood pressure. When CFD results were compared to distraction forces obtained using the experimental desktop model of the same bifurcated tube under physiological pulsatile flow conditions the difference was always less than 10%. Thus time dependent effects on distraction force are small compared to the other variables. The agreement between the three approaches justifies the use of steady state CFD analysis in the current study.

5.5.4 Format of results

Distraction force results for the patient-specific models were obtained for each stent-graft and their individual components in three directions: '*z*' – axial forces in the caudal direction; '*x*' – right lateral and '*y*' – posterior forces (see Figure 5.3). Unlike the simple bifurcated model used in the validation these models were asymmetrical and exhibited angulation in more than one plane therefore the *x*, *y* and z forces were used to calculate total Resultant Distraction Force (RDF) using the formula where *F* represents total force in a particular direction:

$$Total\ RDF\ (N) = \sqrt{(F_x^2 + F_y^2 + F_z^2)} \quad (5.3)$$

The term 'out-of-plane forces' was used to refer to the contribution of *x* and *y* directional force to the magnitude of total RDF. Total RDF comprised forces derived from blood pressure and blood flow (viscous friction).

5.5.5 Measurement of morphological features

5.5.5.1 Cross-sectional area

Lumen cross-sectional area (XSA) at the inlet and outlet of all components with the exception of the limb extension inlet was obtained from FLUENT v6.2 (ANSYS Inc.) by creating a plane through the lumen (Figure 5.8).

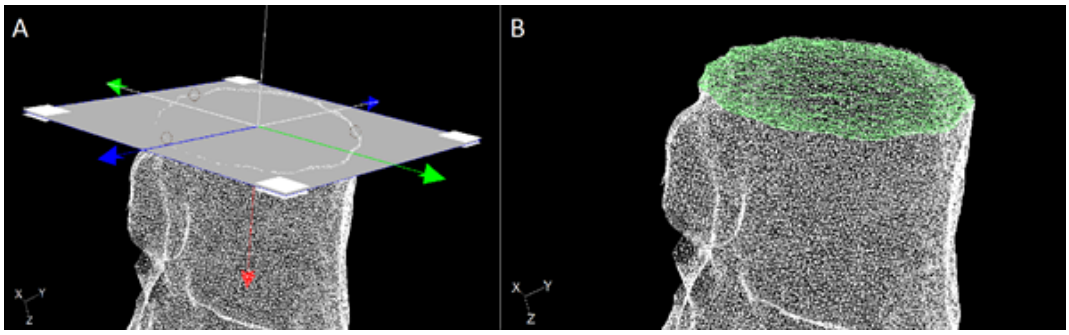

Figure 5.8 A: Plane created at the inlet of a component. B: Inlet cross-sectional area shown in green.

This method was not possible for the inlet to the limb extension components due to the close proximity of the two limbs at the bifurcation. For this inlet the average diameter as measured in ScanIP was used to calculate the approximate inlet XSA. For bifurcated components outlet XSA was the sum of left and right outlets. Inlet:Outlet area ratio was calculated by dividing the inlet XSA with that of the (combined) outlet.

5.5.5.2 Angle measurement

Angle measurement was performed in ScanIP. A CLL was created to guide the placement of a computerised caliper. Angles within each lumen model were measured in coronal and sagittal elevation by applying two-dimensional calipers onto the three-dimensional image. This gave two data points for each angle. Although it was possible to apply a 3D version of the calipers to the CLL to obtain one data point per angle this would not have provided any information regarding the position of one limb in relation to the other when considering bifurcated components. Calipers were applied over as much length of CLL as possible with each one covering at least the length of the respective sealing stent. Three types of angle were measured in both coronal elevation (as viewed from an anterior position) and sagittal elevation (as viewed from the patients' left, see Figure 5.9):

α angle: the angle between the axis of blood flow at the proximal body inlet from that of the aorta immediately above.

β angle: the angle between the axis of blood flow in the aneurysm lumen from that of the visceral aorta. Due to the effect of the stent-graft upon the native vessels the β angle was usually observed at the junction between proximal and distal bodies and was therefore a postoperative approximation of the angle between the aneurysm neck and the long axis of the aneurysm as described in the IFU document.

θ Angle: the angle between the axis of blood flow at the outlet of a component in relation to its inlet.

Bifurcation angle (the angle between two outlets of a bifurcated body or complete stent-graft in each plane) was calculated by taking the sum of left and right θ angles. Largest angle refers to the largest angle observed in either coronal or sagittal elevation.

α, β and θ angulation in a clockwise direction was initially assigned a negative value and counter-clockwise a positive value. Subsequent comparison was limited to *magnitude* only and therefore all values were considered as positive.

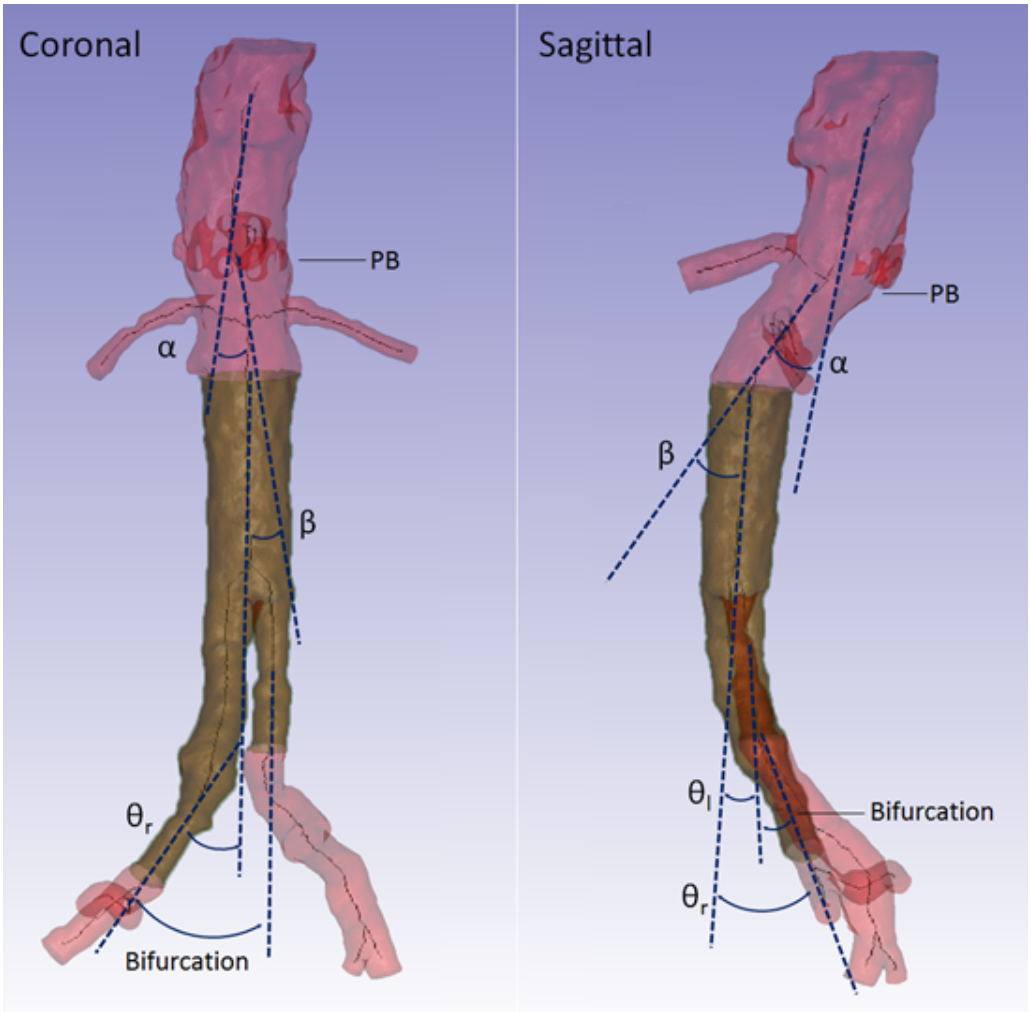

Figure 5.9 Angle measurement of one distal body in coronal and sagittal elevation. PB: Proximal extent of proximal body component. θl: Left outlet angle (demonstrated in sagittal elevation only), θr: Right outlet angle

5.5.6 Inclusion criteria

All patients who received fenestrated endovascular aneurysm repair at Royal Liverpool University Hospital between January 2006 and October 2011 were included in the study. Prior to 2006 images were not stored in the on-line repository but in hard copy or on compact discs which made retrieval and conversion to DICOM format difficult.

Ethical approval for the use of medical images and demographic data was granted by the North West – Liverpool East Research Ethics Committee.

5.5.7 Exclusion criteria

Patients without postoperative arterial phase contrast enhanced CT scans were excluded. Individual components where stents or gold radiopaque markers were not visible or obscured such that the inlet or outlet could not be identified were also excluded.

5.5.8 Statistical analysis

The correlation between XSA, actual component diameter and RDF was assessed using Spearman's correlation coefficient (Spearman's rho, ρ). Paired comparison between angulation or components within the same fEVAR were performed using Wilcoxon Signed Rank test (WSR). Complete stent-grafts and their individual components were grouped according to the presence of α, β, θ or bifurcation angles <45° or ≥45° in either sagittal or coronal plane. Total RDF in each group was compared by Mann-Whitney U test (MWU).

5.6 Results

59 patients were treated with fenestrated endovascular aneurysm repair between January 2006 and October 2011. Four patients were excluded due to no postoperative CTs being available. A further patient had no postoperative imaging with arterial phase contrast. Five limb extensions from two separate patients were excluded because the inlet or outlet could not be positively identified.

5.6.1 Morphological features

Appendix 8.5 details all morphological data for each complete stent-graft and all individual components. Table 5.2 summaries this data.

Table 5.2 Summary of morphological features for complete stent-grafts and components

Component	Complete Stent-graft	Proximal Body	Distal Body	Limb Extension
n	54	54	52	62
Inlet XSA (mm^2)	349.5 (111-907)	349.5 (111-907)	380.5 (160-501)	68.5 (44-104)
Outlet XSA (mm^2)	97 (25-400)	78 (35-356)	74 (23-393)	100 (25-400)
Combined Outlet XSA (mm^2)	198.5 (78-793)	163.5 (57-356)	156 (40-434)	-
Inlet:Outlet area ratio	1.62 (0.63-5.07)	1.95 (0.77-15.91)	2.29 (0.72-9.98)	0.71 (0.17-2.86)
θ angle	48° (1-140)	17° (0-69)	21° (0-89)	38° (2-116)
n (<45°/≥45°)	4/50	45/9	25/27	24/38
Bifurcation Angle	35° (0-167)	-	25.5° (0-85)	-
n (<45°/≥45°)	7/44◊	-	36/14ψ	-

Values given as median with range in parentheses. n: number, Inlet XSA: Inlet cross-sectional area post deployment (mm^2), Outlet XSA: Outlet cross-sectional area post deployment (mm^2), Inlet:Outlet area ratio (ratio of Inlet cross-sectional area:Outlet cross-sectional area) Largest θ angle: Largest outlet angle in either coronal or sagittal elevation, Largest Bifurcation angle: Largest Bifurcation angle in either coronal or sagittal elevation, ◊: total n=51 due to 1 tube graft and 2 ipsilateral limb occlusions where no bifurcation angle could be measured, ψ: total n=50 due to 2 ipsilateral limb occlusions.

5.6.1.1 Complete stent-grafts

5.6.1.1.1 Cross-sectional area

The inlet of the complete stent-graft in all cases was the inlet of the proximal body component. Fourty eight of the 54 complete stent-grafts had an inlet XSA larger than the combined outlet XSA, only six had outlets with larger XSA than the inlet (i.e. Inlet:Outlet area ratios less than 1). Overall median Inlet:Outlet area ratio was 1.62 (range 0.63-5.07).

5.6.1.1.2 Angulation

There were no α angles greater than 45° and there was no significant differences between α angles measured in coronal or sagittal elevation (median coronal α angle 8°, range 0-31° versus 8°, range 0-38, p=.704, WSR). Four of the 54 fEVARs had β angles greater than the maximum 45° stated in the IFU. β angulation was significantly greater in the coronal elevation (i.e. lateral angulation) than in sagittal elevation (antero-posterior angulation) with a median coronal β angle of 13°, range 0-58° versus 11°, range 0-42°, p=.021 (WSR).

Outlet angulation of complete stent-grafts in the coronal elevation (i.e. lateral angulation) was significantly less than in the sagittal elevation (antero-posterior) in both left (p=.000) and right limbs (p=.006, WSR). Median coronal outlet angle was 31°, range 1-83°(left), and 40°, 4-97°(right) versus median sagittal outlet angle 58°, 3-140°(left), and 56°, 12-120°(right). The degree of limb angulation in

sagittal elevation between the limbs did not differ significantly (p=.440, WSR). This is perhaps due to the similar posterior course taken by both common iliac arteries as they enter the pelvis and is supported by the finding of significantly lower bifurcation angle in this elevation (sagittal bifurcation angle: 11°, range 0-93° versus 78° coronal bifurcation angle, range 4-167, p=.000, WSR). There was a significant difference between left and right outlet angulation in coronal elevation (p=.003, WSR) which suggests that the iliac arteries had a more variable lateral - as compared to posterior - course.

5.6.1.2 Proximal bodies

5.6.1.2.1 Diameter and cross-sectional area

Proximal bodies were manufactured with proximal diameter (D1) of 24, 26, 28, 30, 32 and 36mm (Figure 5.10). In this cohort one custom-made device with a D1 of 40mm was used (fEVAR 55, Appendix 8.5.2).

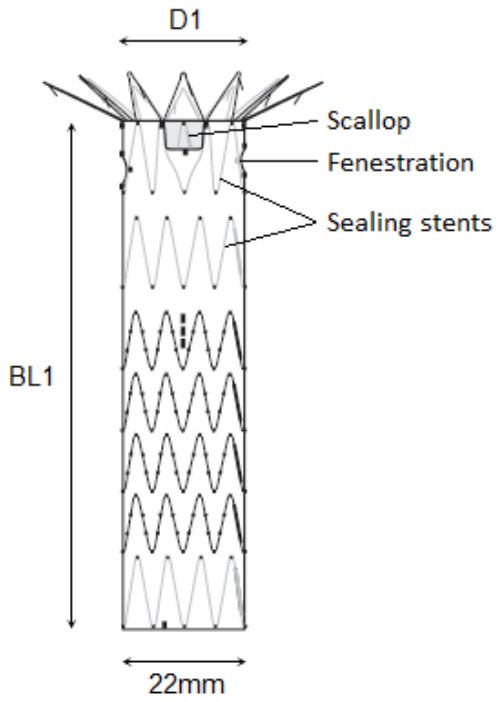

Figure 5.10 Proximal body configuration. Adapted from Cook Medical Inc. (72)

Median D1 of the proximal bodies used for CFD analysis was 30mm (range 24-40mm) and median post-deployment inlet cross-sectional area measured from the computer models was 349.5mm^2 (range 111-907mm^2). Post-deployment inlet cross-sectional area correlated strongly with pre-deployment proximal diameter (Spearman's rho, ρ 0.757, p<.01). This agreement suggests a consistent amount of oversizing was used in the planning stages and may also indicate consistency of the model construction process. The distal diameter of proximal bodies was usually 22mm although fEVAR 51 (tube graft only) had a distal diameter of 38mm. Two other non-standard devices were used: One had a distal diameter 30mm (fEVAR 28), the other was a custom-made single-piece bifurcated fenestrated stent-graft (fEVAR 7). The median combined outlet cross-sectional area was 163.5mm^2, range 57-356mm^2 which corresponds to an equivalent circular diameter of 14.2mm. The lower than expected value (i.e. less than 22mm shown in Figure 5.10) was due to the flow divider (bifurcation) of the distal body being placed above the distal extent of the proximal body in most cases in order to maximise component overlap. *In situ* this gave most proximal bodies two *functional* outlets as seen in fEVAR 36 (Figure 5.11A).

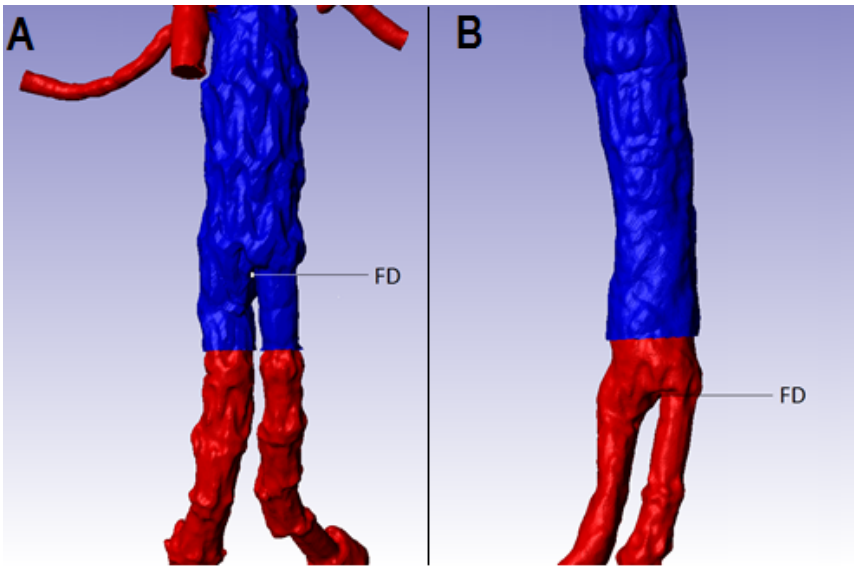

Figure 5.11 Two different proximal body components (blue) showing the distal body flow divider (FD) above (A) and below (B) the distal extent of the proximal body component. Red: lumen

The flow divider was distal to the proximal body fabric in only five of the fEVARs. One of these was fEVAR 37 shown in Figure 5.11B. A further two cases had one functional outlet due to an occluded stent-graft limb and one other due to the repair being performed with the tubular proximal body component only. The proximal body of fEVAR 55 had one functional outlet that was very close to the flow divider. The CLL was observed to have already bifurcated at the distal extent of the fabric and adherence to the protocol for angle measurement therefore produced four angle data points (two for each CLL).

5.6.1.2.2 Angulation

Median coronal and sagittal outlet angulation of the left functional outlet was 14° (range 0-45°) and 24.4° (0-58°) respectively. The difference between these distributions was significant (p=.007, WSR) but this difference was not observed with the right functional outlet (median coronal and sagittal outlet angle 16°, range 0-69° and 19°, range 2-50°, p=.627, WSR). The left side was the contralateral side in 40 of the 52 fEVARs and it is likely that the presence of the limb extension at the level of the contralateral functional outlet influenced its position causing an increase in angulation towards the origin of the iliac vessels.

5.6.1.2.3 Fenestrations

Table 5.3 summaries the scallop and fenestration configurations of all 54 fEVAR included in the distraction force analysis. fEVAR were numbered in chronological order and – as was the case with the French and Swedish series (106) – a trend to more complex fEVAR with more fenestrations was observed in the later cases. The most commonly used configuration was one scallop and two fenestrations (n=30).

Table 5.3 Summary of scallop and fenestration configurations

Scallop	**0**	**0**	**0**	**1**	**1**	**1**	**1**
Fenestration	**2**	**3**	**4**	**0**	**1**	**2**	**3**
n	1	4	2	2	4	30	11

5.6.1.2.4 Sealing stents and proximal body length

Usually two proximal sealing stents were used but fEVARs 6 and 24 included only one sealing stent. Two other fEVARs (34 and 58) had three sealing stents. Proximal bodies were available in lengths between 76-137mm (BL1, see Figure 5.10). Ten longer non-standard lengths were used (fEVAR 28, 37, 40, 51, 52, 53, 55, 56, 58 and 59).

5.6.1.3 Distal bodies

5.6.1.3.1 Diameter and cross-sectional area

Standard distal body proximal diameter was 24mm however one larger 32mm device was used in conjunction with a 30mm distal diameter proximal body (fEVAR 28, see Appendix 8.5.3). This device was also manufactured with non-standard lengths (DBL and DLL shown in Figure 5.12).

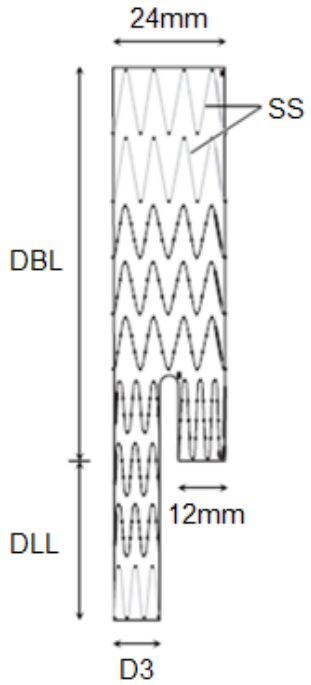

Figure 5.12 Distal body configuration.
Adapted from Cook Medical Inc. (72)

Median inlet cross-sectional area in the cohort of 52 distal bodies with postoperative imaging was 380.5mm^2 (range 160-501mm^2), this was the equivalent of a 22mm circular diameter. Contralateral gate diameter was a standard 12mm in all devices. The median contralateral outlet XSA was 70.5mm^2 (9.5mm circular diameter), range 23-100mm^2.

Forty of the 52 distal bodies were deployed from the right groin. The ipsilateral limb of the distal body component was available in diameters of 12, 16, 20 and 24mm. One custom made distal body with an ipsilateral limb diameter (D3) of 28mm was also used in this cohort to achieve distal seal in an ectatic common iliac artery (fEVAR 56). The median D3 used was 16mm (range 12-28mm) and median ipsilateral outlet XSA post-deployment was 85.5mm^2 (range 25-393mm^2). There was a moderate but significant positive correlation between these two distributions (ρ 0.607, $p<.01$).

5.6.1.3.2 Sealing stents and distal body length

Distal body lengths (DBL) were either 76, 94, 109 or 124mm. Only the 76mm version had two sealing stents (SS, Figure 5.12). All other lengths had three sealing stents as standard. Ipsilateral limbs lengths (DLL) were 28, 45 or 62mm. This enabled distal seal to be achieved at the chosen site in common iliac arteries of varying lengths. Apart from fEVAR 28, one other custom-made short distal body with slightly longer DLL was used (fEVAR 49). In this device the short DLL required an internalised contralateral gate to be manufactured inside the main distal body. In 13 cases the ipsilateral limb was extended further with a limb extension (see Appendix 8.5.4).

5.6.1.3.3 Angulation

Outlet angulation of the ipsilateral limb was significantly greater than the contralateral gate in both coronal and sagittal elevations (coronal: median=28°, range 0-85° versus 6.5°, range 0-58°, p=.000, and sagittal: 39.5°, range 7-89° versus 17°, range 2-49°, p=.000, WSR). This greater angulation was due to the

ipsilateral limb being deployed in the iliac arteries whilst the usual position for the contralateral gate was just proximal to the aortic bifurcation and therefore much more in line with the inlet. As with the complete stent-graft models, the bifurcation angle was significantly greater in the coronal elevation (28.5°, range 0-85° versus 25°, range 2-60°, p=.035, WSR). Overall however the bifurcation angle in the distal body models was significantly smaller than in the complete stent-grafts in both coronal and sagittal elevations. Median coronal bifurcation angle for distal bodies was 28.5°, range 0-85° versus 78° in complete stent-grafts, range 22-167°, p=.000 and median sagittal bifurcation angle 11°, range 0-93° versus 25°, range 2-60°, p=.012, WSR. This finding was also a consequence of the contralateral gate placement within the aortic lumen in the distal body component. In contrast, the configuration of the complete stent-graft included the contralateral limb extension and therefore had both outlets within the iliac arteries.

5.6.1.4 Limb extensions

5.6.1.4.1 Diameter and cross-sectional area

All limb extensions had a proximal diameter of 12mm to achieve seal within the contralateral gate of the distal body. All limb lengths (LL) in this cohort were between 56 and 107mm (Figure 5.13). Current standard LL lengths are 39, 56, 74, 90, 107 and 122mm although this changed slightly throughout the study period. LL was not inclusive of the 22mm proximal seal-zone.

The median outlet cross-sectional area for limb extensions was 99mm^2, range 25-400mm^2. This correlated well with the distal diameter (median D2 16mm, range 12-28mm, ρ=.829, P<.01). The standard range of available D2 diameters was 9-24mm. Two limb extensions were custom made 28mm D2 devices (fEVAR 25 and 56, see Appendix 8.5.4).

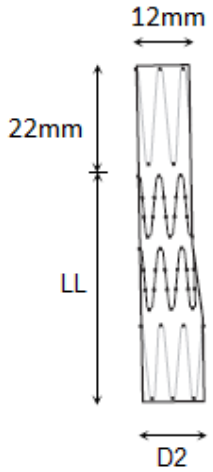

Figure 5.13 Limb extension configuration.
Adapted from Cook Medical Inc. (72)

5.6.1.4.2 Angulation

Median coronal outlet angle was 41° (range 2-116°). Median sagittal outlet angle was 38° (range 2-99°). There were no significant differences in the extent of angulation between these two elevations (p=.141, WSR).

5.6.2 Distraction force

Distraction force results for pressure and viscous friction forces were obtained in x, y and z directions and used to calculate total resultant distraction force (RDF). Appendix 8.6 details the *x*, *y* and *z* contributions of pressure and viscous force to total RDF for the complete stent-grafts and individual components of all fEVARs.

Median total RDF acting on the complete stent-grafts was 6.0N (range 0.3-17.7N), on proximal bodies 4.8N (range 1.3-15.7N), distal bodies 5.6N (range 1.0-8.0N) and limb extensions 1.7N (range 0.6-8.4N).

Pressure derived forces were the dominant contributor to total RDF. The contribution of viscous force was minimal: Median magnitude of viscous force was only 0.46% of total RDF (range 0.05-11.76%) and was inversely proportional to the overall magnitude of the total RDF (ρ=-0.690, p<.01) so that the smaller the total RDF the greater the magnitude of viscous friction.

Out-of-plane forces contributed a median 46% (range 4-100%) of total RDF in complete stent-grafts, 44% (range 3-99%) of total RDF in proximal bodies, 51% (12-100%) in distal bodies and 94% (36-100%) in limb extensions.

5.6.2.1 Cross-sectional area and total RDF

Inlet XSA showed a strong positive correlation with total RDF in complete stent-grafts (ρ=0.814), proximal bodies (ρ=0.883) and distal bodies (ρ=0.802). All values were significant to p<.01 (see Figure 5.14).

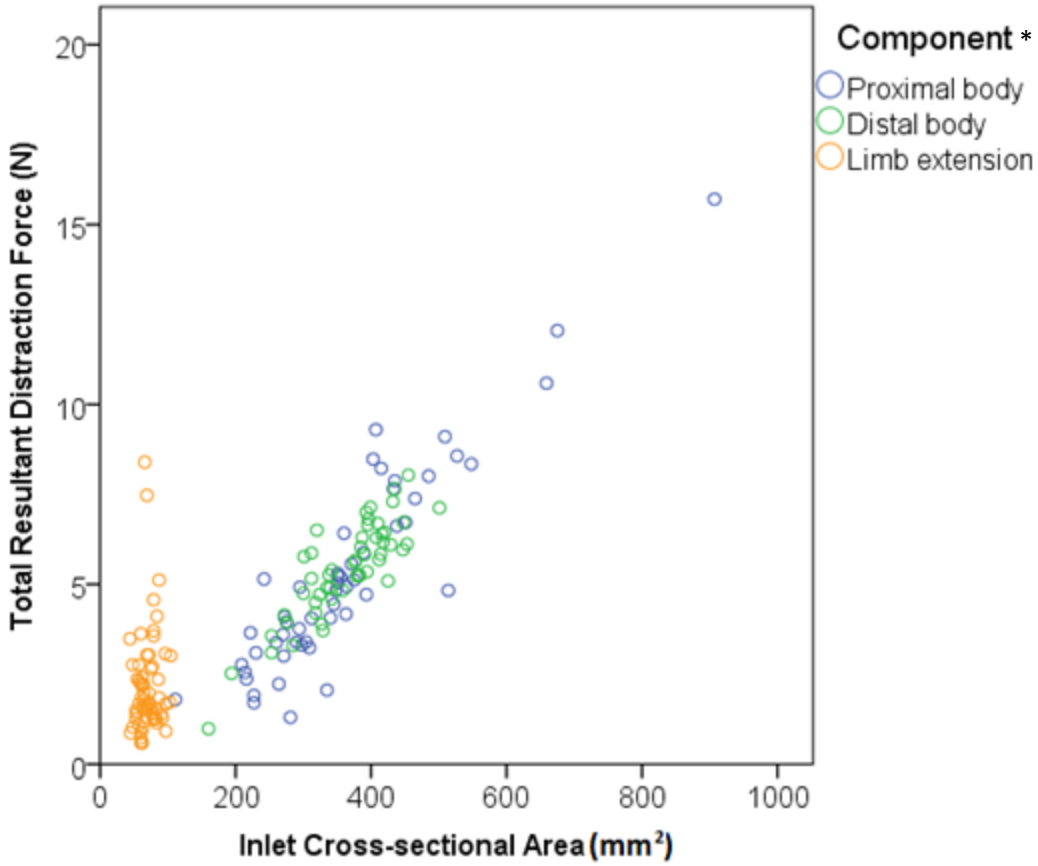

Figure 5.14 Correlation between inlet cross-sectional area and total resultant distraction force

*Complete stent-graft not included as inlet cross-sectional area was equivalent of proximal body inlet cross-sectional area

In the limb extension components where the outlet was predominantly larger than the inlet (See Table 5.2 Inlet:Outlet area ratio 0.71, range 0.17-2.86) there

was no correlation between inlet XSA and total RDF (ρ=0.179). This was the only component for which outlet XSA correlated significantly with total RDF (ρ=0.822, p<.01). Outlet XSA did not correlate with total RDF in any other component (ρ=0.153 in complete stent-graft, -0.165 in proximal bodies and -0.107 in distal bodies).

5.6.2.2 Inlet:Outlet area ratio

Inlet:Outlet area ratio showed a moderate positive correlation with total RDF in complete stent-grafts, proximal and distal bodies (ρ=0.438, 0.756 and 0.540, p<.01). In limb extensions the correlation between Inlet:Outlet area ratio and total RDF was negative (ρ=-0.756, p<.01).

5.6.2.3 Angulation and total RDF

5.6.2.3.1 β anglulation

Four of the 54 aortas had β angles greater than or equal to 45°. Median total RDF was not significantly larger in these complete stent-grafts (6.1N, range 0.3-17.7N) versus the other 50 with β angle less than 45° (median total RDF 3.2N, range 2.9-7.5N, p=.166, MWU). Similarly there was no significant difference in median total RDF acting upon the proximal bodies components of these fEVARs between β angle groups (4.6N, range 3.4-7.7N for β angle ≥45° versus 4.8N, range 1.3-15.7N for those <45°, p=.911, MWU).

5.6.2.3.2 θ angulation

Complete stent-grafts and components were also grouped according to the presence of outlet (θ) angle ≥45° or <45° (see Table 5.2). There were no significant differences in total RDF between proximal and distal bodies in either angulation group. This finding is shown in the box and whisker plot of Figure 5.15 where median total RDF for proximal bodies with a θ angle ≥45° was 4.4N (range 2.2-7.9N) compared with 4.8N (range 1.3-15.7N) for those with θ angle <45°,

p=.954. Distal bodies with θ angle ≥45° had a median total RDF of 5.7N (range 2.5-8.0N) compared with 5.3N (range 1.0-7.3N) for those <45°, p=.862, MWU.

In contrast, Figure 5.15 also shows that complete stent graft and limb extensions in the ≥45° θ angle group were exposed to significantly higher forces than those with θ angle <45°. For the complete stent-grafts the difference in median RDF was 6.2N (range 2.2-17.2N) versus 2.6N (range 0.3-3.1N), p=.001 and in limb extensions: 2.1N (range 0.9-8.4N) compared with 1.4N (range 0.6-4.6N), p=.004, MWU). Outliers represent stent-grafts or components at the extreme ends of available inlet/outlet diameters or observed cross-sectional areas.

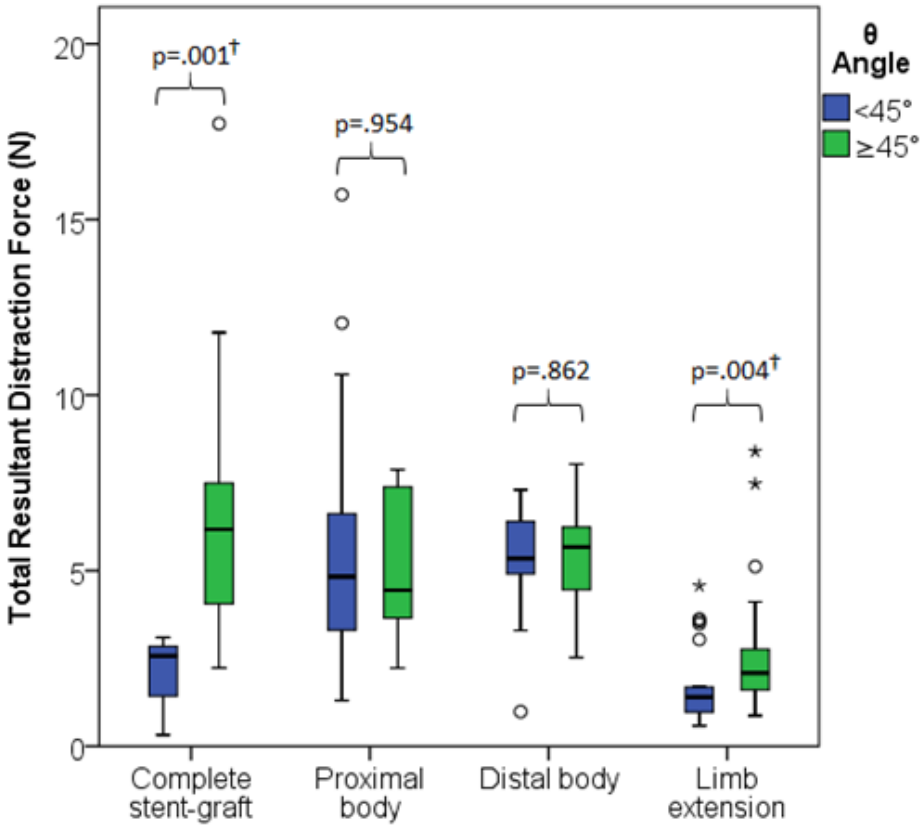

Figure 5.15 Comparison of total resultant distraction force between outlet (θ) angle groups in complete stent-grafts and components.

Boxes represent median total RDF and interquartile range, whiskers: 95% confidence interval, o: outlier at 95% CI, *: outlier at 99%CI, †indicates significance to p<.01, MWU.

5.6.2.3.3 Bifurcation angle

Fourty four complete-stent-grafts had bifurcation angles ≥45°. These stent-grafts were exposed to a median total RDF of 6.1N (range 2.2-11.8N). Complete stent-grafts with bifurcation angles <45° (n=7) were exposed to less total RDF (median 5.0N, range 0.3-7.3N) although this difference did not reach significance (p=.312, MWU). Similarly there was no significant differences between total RDF acting upon distal bodies with bifurcation angle ≥45° versus those with bifurcation angle <45° (median total RDF 5.7N, range 2.5-8.0 vs. 5.4N, range 1.0-7.1N, p=.503, MWU).

5.7 Discussion

Inlet cross-sectional area displayed the strongest correlation with total resultant distraction force in proximal body and distal body components. The relationship was linear. This finding is supported by one-dimensional analytical models based on conservation of linear momentum (43, 44, 158). Previous CFD studies have considered the stent-graft as a single piece (41, 161, 163-165) or have divided the stent-graft into arbitrary territories and in doing so biased results depending on the cross-sectional area at the choice of inlet position (41).

By considering each component separately we can compare total RDF with experimentally-derived fixation force. For a proximal body with one stented target vessel the initial fixation force was approximately 11.5N +/-1.5N (123). By contrast, distal bodies rely on the radial force of sealing stents alone and have a fixation force of approximately 6.5N (4.8-7.2N) (143). The fixation force at the distal seal-zone of a limb extension is approximately 9.6N +/-1.5N (84). In the current steady-state numerical simulations with constant pressure of 160mmHg there were two proximal bodies, 11 distal bodies and no limb extensions that were exposed to distraction forces in excess of their known fixation force.

5.7.1 Proximal and distal body

Fifty one of the 52 distal body components all had the same proximal diameter (24mm) for docking into the 22mm overlap zone of the proximal body. The range in inlet XSA observed in these components was much narrower than for the proximal body components (160-501mm^2 vs 111-907). A XSA of 380mm^2 approximates to a circular lumen diameter of 22mm therefore distal bodies with smaller XSA may have been deployed inside the 22mm portion of the proximal body. In aortas with a visceral segment luminal diameter greater than 22mm the sealing stents of the proximal body expand to a greater diameter than the overlap zone to approximate with the vessel intima. Landing a portion of the first distal body sealing stent in the wider segment may allow expansion up to the maximum diameter of 24mm. This diameter approximates to an equivalent circular XSA of 452mm^2 although the actual luminal XSA would be slightly less due to the thickness of the graft fabric (approximately 0.14mm as measured using a micrometer). Distal body XSA in excess of 380mm^2 were therefore most likely due to intentional maximisation of overlap.

5.7.2 Limb extension

When migration of limb extension components occurs it is usually in a cranial direction. This has been demonstrated experimentally by Volodos *et al.* (157) and by core lab analysis of follow-up images (194). The latter study observed an 8% incidence of migration greater than 4mm at 36 months follow-up. By considering total RDF for each component rather than for the stent-graft as a whole the reason for the cranial direction of migration can be explained: significantly higher θ angulation in the limb extensions compared with the proximal bodies (median 38° vs. 17° $p<.01$, WSR) led to significantly higher contribution of out-of-plane forces (94 vs. 44%, $p<.01$, WSR). This concept is illustrated in Figure 5.16B where the '*y*' axis force (green arrow) acting on the more angulated limb extension is almost twice the magnitude of the force acting axially in the '*z*' axis (blue arrow)

compared with the much smaller 'y' forces acting on the straighter proximal body component in Figure 5.16A. The effect on total RDF for limb extension components was to cause it to act in a more antero-posterior or lateral direction. In addition to the effect of angulation, a median Inlet:Outlet area ratio 0.71 confirmed that the outlet of the limb extension - designed for seal within iliac arteries of outer diameter 7-21mm - was usually larger than the standard 12mm diameter inlet. The effect of this was that pressure derived forces (and therefore total RDF) were reversed in relation to blood flow. This is also shown in Figure 5.16B where total RDF is seen to act parallel and in the opposite direction to the flow of blood in the distal part of the limb extension. Under these conditions the component outlet assumes primary importance as the main determinant of force magnitude.

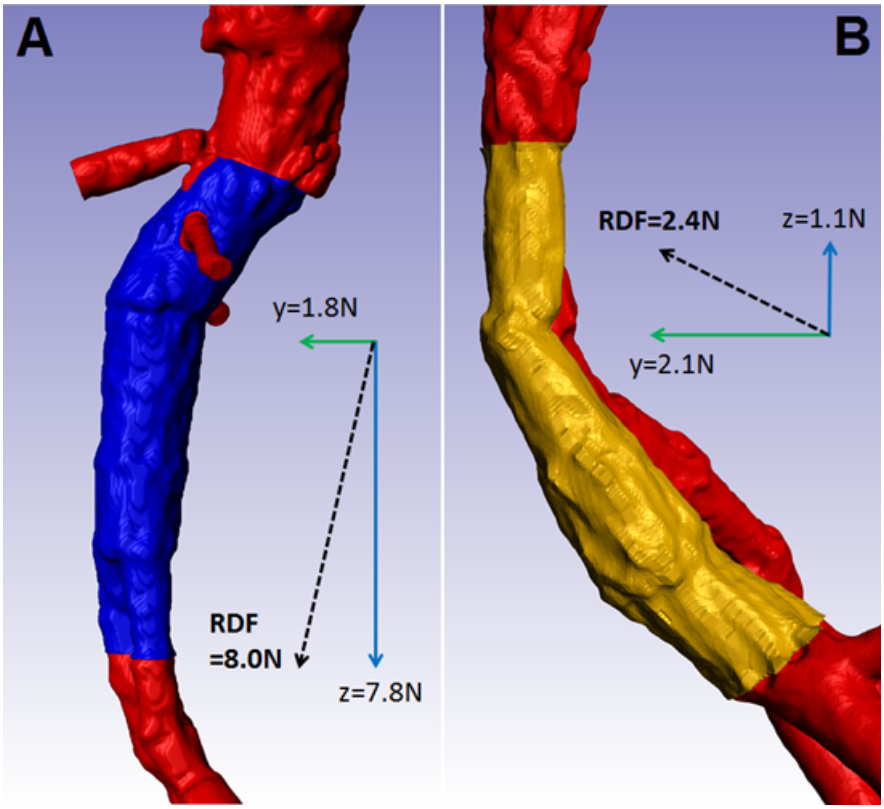

Figure 5.16 A: Total resultant distraction force for proximal body (blue) acting in predominantly longitudinal (z) axis versus B: Total RDF for limb extension (orange) acting more anteriorly and against the direction of blood flow

Images shown in sagittal elevation. *x* direction forces not shown. A: x=0.6N, B: x=0.2N.

5.7.3 Angulation

The α angle was above the graft fabric and theoretically should have no impact on the magnitude of total RDF however Molony *et al*. (165) and Kandail *et al.* (161) reported an association between anterio-posterior neck angulation and resultant distraction force following standard EVAR. An explanation may be that greater α angle may act as a surrogate marker for tortuosity which may also cause greater θ angulation. The effect of α angle upon total RDF was not assessed in this analysis since all were less than 45°.

Complete stent-grafts and limb extension components were the only groups for which θ angle was significantly associated with greater total RDF. There was a good distribution of limb extensions between angle groups (n=24 vs. 38) however there were only four complete stent-grafts with outlet angle <45° (see Table 5.2). The lack of significance when θ angle and total RDF were compared for the other components was probably as a result of smaller angulation. This assumption is supported by previous analytical and CFD analyses that show little effect upon force of angulation less than 35° (163).

The effect of bifurcation angle on force has been quantified analytically (158, 163, 172). An average distal body (Inlet XSA 380mm^2, equivalent to 22mm circular diameter) with a bifurcation angle of 80° would be exposed to 2N more distraction force than the same size component with a bifurcation angle of 10° (158). The lack of association found between bifurcation angle and total RDF in this analysis may be due to the small bifurcation angles. For example the median largest bifurcation angle was 35° for complete stent-grafts and 25.5° for distal bodies. The second value is predictably lower due to one of the distal body outlets (the contralateral gate) being situated within the aorta and therefore more in line with the inlet. It may also in part be due to the relatively greater importance of cross-sectional area as a determinant of force.

5.7.4 Predicting distraction force

Defining the relationship between morphological features and distraction force may be useful in the planning stage before endovascular aneurysm repair. The ability to predict distraction force using easily measured morphological features may allow the clinician to choose alternative treatment modalities or ensure close follow-up of those considered at a high risk of migration. It must be remembered however that an angle measured using the CLL on a planning CT may not represent the eventual angle formed by the stent-graft after deployment. Especially in tortuous anatomy the stent-graft may take what could be considered as the 'racing line'. Its mechanical properties and chosen site of deployment would also govern how much it conforms or deforms the original vessel morphology.

Based on the significant morphological features for complete stent-grafts and their individual components, a regression model was developed to predict total resultant distraction force (*F*) at constant blood pressure (160mmHg).

5.7.4.1 Complete stent-graft

For Complete stent-grafts, inlet XSA (A_1) alone predicted 81% of total RDF. Inlet:Outlet area ratio (A_1/A_2) and largest θ angle ($max[\theta]$) in sagittal or coronal elevation were also both independently significant (p=.001) and when combined with inlet XSA predicted 92% of total RDF (R^2 0.922):

$$F_{SG} = A_{SG} + B_{SG}A_1 + C_{SG}\frac{A_1}{A_2} + D_{SG}max[\theta] \quad \textbf{(5.4)}$$

where A_{SG}=4.109N, B_{SG}=0.017N/mm^2, C_{SG}=0.523N and D_{SG}=0.043N/deg. Inlet XSA in equation 5.4 refers to the lumen XSA at the inlet of the stent-graft following deployment. This should correspond well with the lumen XSA at the chosen proximal seal-zone as defined on the planning CT. The actual circular XSA of the

proximal body ($\pi D1^2/4$) would only act as a surrogate for this measurement if aortic wall thickness was uniform and consistent oversizing was employed.

5.7.4.2 Proximal body

In proximal body components inlet XSA (A_1) alone predicted 84% of total RDF. Inlet:Outlet area ratio (A_1/A_2) was also independently significant (p=.025) but only added another 1% to the overall predictive value of the following simple regression model (R^2 0.852):

$$F_{PB} = A_{PB} + B_{PB}A_1 + C_{PB}\frac{A_1}{A_2} \quad \textbf{(5.5)}$$

where A_{PB}=-1.305N, B_{PB}=0.017N/mm^2 and C_{PB}=0.239N. In regression models for both complete stent-grafts and proximal bodies every 1mm^2 increase in inlet XSA caused an approximate 0.017N increase in total RDF. For example a lumen of circular diameter 30mm has a cross-sectional area of 707mm^2. A 2mm increase in diameter leads to a cross-sectional area of 804mm^2 (an increase of 97mm^2). Using the simple linear regression model this would increase the distraction force acting on the complete stent-graft or proximal body by 1.8N assuming everything else held constant.

5.7.4.3 Distal body

Inlet XSA (A_1) alone predicted 74% of total RDF acting upon distal body components. Inlet:Outlet area ratio (A_1/A_2) was independently significant (p=.001) and although results above did not show any difference between distal bodies with θ angle ≥45° compared with those <45°, the largest θ angle in sagittal or coronal elevation ($max[\theta]$) was also independently significant (p<.001). Combined they contributed to a model that predicted 89% of total RDF (R^2 0.886):

$$F_{DB} = A_{DB} + B_{DB}A_1 + C_{DB}\frac{A_1}{A_2} + D_{DB}max[\theta] \quad \textbf{(5.6)}$$

where A_{DB}=-2.285N, B_{DB}=0.016N/mm^2, C_{DB}=0.048N and D_{DB}=0.004N/deg.

5.7.4.4 Limb extension

In limb extension components outlet XSA alone (A_2) predicted 85% of total RDF. Inlet:Outlet area ratio (A_1/A_2) and the largest θ angle ($max[\theta]$) were also independently significant and contributed to the most accurate simple regression model that predicted 95% of total RDF (R^2 0.953):

$$F_{LE} = A_{LE} + B_{LE}A_2 + C_{LE}\frac{A_1}{A_2} + D_{LE}max[\theta] \quad (5.7)$$

where A_{LE}=-1.69N, B_{LE}=0.001N/mm^2, C_{LE}=0.092N and D_{LE}=0.002N/deg.

5.8 Limitations

Limitations of this CFD study include the use of a steady-state blood flow rather than pulsatile flow. Previous experience with experimental models suggests that results are less than 10% higher at any given time along a pulse wave in pulsatile flow models compared with steady-state models. The difference is largest at peak systole due to the inertial effect of the pressure waveform (154). The validation experiment described earlier in this chapter (section 5.5.3) justifies the use of steady state blood flow. This approach was also used for practical reasons as - compared with pulsatile flow - the simulations take a tenth of the time to complete.

There were three limitations to the study design that were likely to have caused only minimal effect on distraction force results due to the insignificant contribution of viscous friction force (typically <1% of total RDF). These were the use of a Newtonian fluid model which was only an approximation of *in situ* conditions providing a less accurate representation of blood flow in areas with high velocity gradients; the assumption that all forces were transmitted through

the overlapping parts of the stent-graft (this was an oversimplification and in reality only pressure force was likely to be transmitted to those segments of a component not in direct contact with blood flow) and the exclusion of visceral stents from the stent-graft models due to limitations in CT imaging resolution. Whilst visceral stents would have affected the fixation force of an individual proximal body, their inclusion would only have likely led to more realistic local velocity profiles and no great affect upon distraction force results.

Use of a constant inlet pressure (160mmHg) was essential to investigate the effect of morphological features upon total RDF but this meant that the results did not reflect each patient-specific blood pressure. Pressure derived forces were the predominant force contributing to total RDF. A selection of simulations were carried out at 140mmHg where the 20mmHg pressure difference led to lower total RDF by a factor of 0.88 (i.e. 140/160). These findings suggest that control of hypertension should remain an important objective even after aneurysm exclusion.

No structural characteristics were modelled but the work of Molony *et al.* (178) supported the rigid wall ('no-slip') assumption and suggested that including compliance of the stent-graft in simulations had little effect upon the forces measured (178).

There was a small error introduced by the large variation in anatomy experienced during the modelling process. Occasionally the use of gold radiopaque markers to identify inlets or outlets led to larger than expected cross-sectional areas due to an overhang in the lumen (see Figure 5.17). The distal body illustrated in Figure 5.17B had an inlet XSA 501mm^2 and was the only distal body component significantly larger than the predicted approximate 452mm^2 XSA (equivalent to 24mm circular diameter). The affect this had upon distraction force can be estimated using equation 5.7 from the regression analysis. An

oversize of this magnitude is likely to add less than 0.8N - in this case 11% - to the total RDF.

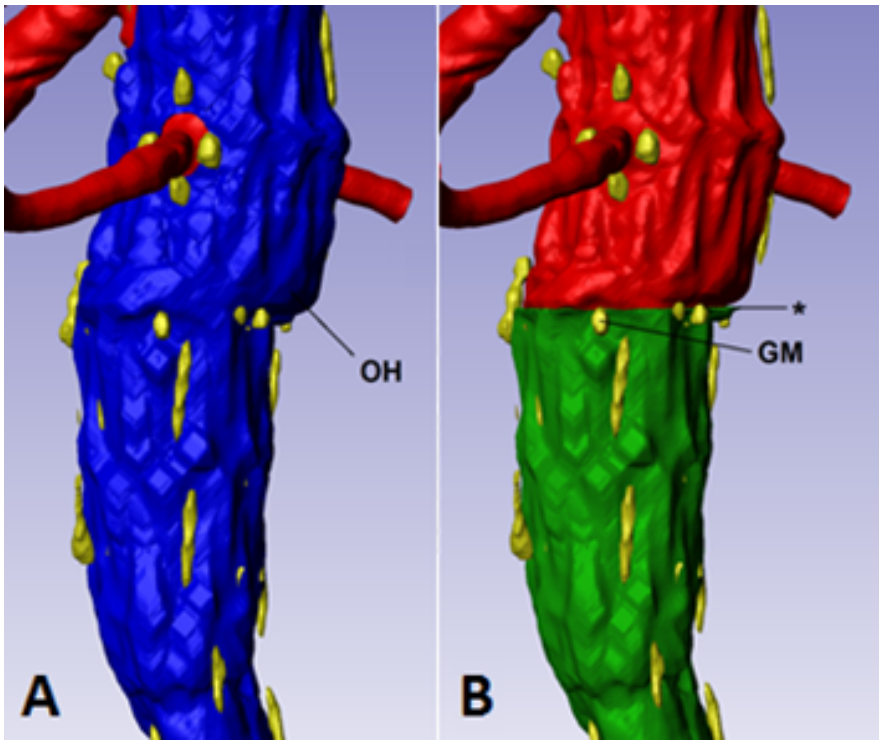

Figure 5.17 Proximal body (blue) and distal body (green) of fEVAR 47 showing inconsistency in inlet XSA (*) due to overhang (OH) secondary to modelling method. GM = Gold radiopaque Marker

Cross-sectional area of limb extension inlet was measured using a different technique to that used with other inlets and outlets. This was due to the close proximity of the other limb that interfered with the original software tool. Some measurements were smaller than expected for an inlet with a standard outer diameter of 12mm. These smaller measurements were probably due to the small amount of constriction of the 12mm seal-zone when deployed inside another 12mm diameter contralateral gate and also the artefact from the high concentration of metal stents and radiopaque markers that may have led to under-representation of the lumen during the segmentation process. The observed median inlet XSA was 68.5mm^2, range 44-104mm^2. An internal diameter of 11mm (which takes into account an estimated four graft thicknesses) would equate to a circular XSA of 95mm^2.

5.9 Conclusion

This study has demonstrated a technique to obtain distraction force results for individual components of a fenestrated stent-graft in patient-specific geometries using CT images and computational fluid dynamics. These simulations are the first to describe distraction force acting on the individual components of a fenestrated stent-graft. Given the potential for each component to move and the importance of inlet cross-sectional area in determining total resultant distraction force this approach is fundamental to achieving meaningful results.

At a given blood pressure the most important morphological determinant of total resultant distraction force was cross-sectional area (inlet for complete stent-grafts, proximal and distal bodies, outlet for limb extensions). No angles within the aorta were large enough to affect the total resultant distraction force. Angulation ≥45° was associated with significantly greater force in complete stent-grafts and iliac limb extension components. Therefore with regards to the original hypothesis, larger vessel angulation such as that caused by the iliac vessels in relation to the aorta was associated with significantly greater distraction forces following fenestrated endovascular aneurysm repair.

6 Relating Distraction Force to Migration and Component Distraction

6.1 Abstract

6.1.1 Background

Fixation force for proximal bodies, distal bodies and iliac limb extensions has been determined experimentally under ideal deployment conditions at 11.5N +/-1.5N, 6.5N (4.8-7.2N) and 9.6N +/-1.5N respectively (84, 123, 195). The second part of this thesis aims to quantify patient-specific distraction forces acting against fixation force for each component of the fenestrated stent-grafts and relate this to the incidence of migration and component distraction.

6.1.2 Method

Total resultant distraction force (RDF) results obtained in chapter five were corrected for patient-specific preoperative blood pressure. Core lab analysis of the patient cohort had already been performed to look for migration of proximal bodies and limb extensions (194). Data from this study was kindly contributed by the lead author.

A method for assessing component distraction between the proximal and distal body was developed from the migration analysis method detailed in the above study. Stent-graft components were grouped according to the presence of movement ≥4mm and the difference in total RDF was analysed by non-parametric statistical analysis (Mann Whitney U test, MWU).

6.1.3 Results

There were nine proximal bodies, three distal bodies and four limb extensions that exhibited movement of ≥4mm over a median follow-up period of 25 months

(range 4-72). All of these components were exposed to distraction forces less than the experimentally derived fixation force.

There was no significant difference between total RDF acting on either complete stent-grafts or proximal bodies in the migration and no migration groups (Median total RDF 6.0N, range 2.6-9.5N versus 5.0N, 2.1-13.1N, p=.295 for complete stent-grafts; 5.6N, range 1.7-8.6N versus 4.0N, 1.3-11.6N, p=.338 for proximal bodies). Likewise there was no significant difference between total RDF acting on either complete stent-grafts or distal bodies in the component distraction and no component distraction groups (Median total RDF 4.8N, range 4.2-5.1N versus 5.5N, 2.1-13.1N, p=.678 for complete stent-grafts and 4.3N, range 2.8-4.7N vs 4.8N, range 2.4-8.0N, p=.235 for distal bodies).

Limb extensions in the migration group were exposed to significantly greater total RDF compared to those that did not migrate (Median total RDF 2.9N, range 2.7-6.3N versus 1.6N, range 0.4-3.8N, p=.003). Median total RDF acting upon the complete stent-grafts in the limb migration group was 6.0N, range 2.4-13.1N versus 5.4N, range 2.1-7.8N for the no migration group. This difference was not significant (p=.747).

There was only one graft-related adverse event in all patients experiencing movement of a stent-graft component. This was a type IIIa endoloeak from the junction between the proximal body and left renal stent. It was treated at 14 months postoperatively with angioplasty of the renal stent.

6.1.4 Conclusion

Migration and component distraction may occur with distraction forces below the experimentally derived fixation force. In limb extension components greater distraction force was significantly associated with cranial migration from the distal seal-zone. The results suggest caution when planning distal seal in ectatic iliac vessels.

6.2 Introduction

In Chapter five, total Resultant Distraction Force (RDF) was determined for individual components of the fenestrated stent-graft using Computational Fluid Dynamics (CFD). The contribution of morphological features such as cross-sectional surface area and vessel angulation was quantified. Distraction force acting upon a component of the stent-graft is opposed by the fixation force of that component. Fixation force has been quantified by pullout studies in porcine and human cadaveric models (84, 124, 127, 135, 143, 145).

The Zenith proximal body with one visceral stent has an initial fixation force following deployment of approximately 11.5N +/-1.5N (123). The radial force of the sealing stent(s), the barbs on the bare metal stents and the visceral stent itself all contribute to this force. In situations where distraction force is greater than fixation force, movement of the stent-graft may occur. In fenestrated endovascular aneurysm repair caudal migration may lead to stenosis or occlusion of target vessels as well as compromise of the proximal seal with the potential for type Ia endoleak and AAA rupture. The cumulative incidence of proximal body migration reported in worldwide clinical series was approximately 2.3% (48, 59, 62, 64, 65, 67, 68, 80) but early subclinical or asymptomatic migration may occur more frequently. One recent retrospective core lab analysis suggested that proximal body migration of ≥4mm may occur in up 22% of cases by 36 months (194).

By contrast the distal body of the stent-graft relies upon the radial force of its sealing stents alone and is fixed inside the proximal body with median force of only 6.5N (interquartile range 4.8-7.2N) (143). Movement between the distal and proximal bodies (component distraction) may cause type IIIa endoleak, AAA expansion and subsequent rupture. The cumulative incidence of component distraction in reported fEVAR outcomes is approximately 1.5% (59, 64, 65, 67, 68, 80) however core lab analysis specifically for this complication has reported

movement of >10mm in 13% and distraction to less than two stents overlap in 7.5% (120). Interpretation of this is made more difficult by a redesign of the proximal body component in 2005 when the distal diameter was changed to 22mm from 24mm. The core lab analysis above was performed on 106 fenestrated stent-grafts deployed before 2006 and therefore most would have probably been the old 24/24mm configuration. All except one of the 43 stent-grafts in the current component distraction analysis are of the new 22/24mm configuration as was the device tested by Scurr *et al.* (143).

Limb extensions are fixed in the contralateral gate of the distal body with approximately 3.5N of fixation force (145) but since migration of this component is usually observed from the distal seal-zone in the cephalid direction, the distal fixation force in the iliac vessels of approximately 9.6N +/-1.5N is more clinically relevant (84). Cephalid migration of the limb extension may lead to kinking and occlusion. The reported incidence of Zenith limb occlusion following standard EVAR is approximately 3-5% (121). This figure may be higher in those deployed in the external iliac artery (196). Since fEVAR uses the same Zenith limbs as the standard repair a similar incidence may be expected however this outcome was not reported in any of the major fEVAR series reviewed in chapter two. Proximal migration of the iliac limb may also cause loss of distal seal, type Ib endoleak and subsequent AAA expansion and rupture.

6.3 Aim

The aim of this chapter is to quantify the *in situ* distraction force acting on each complete stent-graft and its individual components. These forces will then be compared with the incidence of graft-related adverse events (GRAE) including migration, component distraction, type I and III endoleak and target vessel compromise.

6.4 Hypothesis 2

Greater distraction force is associated with higher incidence of migration and component distraction.

6.5 Method

6.5.1 Calculating forces based on preoperative systolic blood pressure

Preoperative systolic blood pressure for each subject was used to calculate the *in situ* distraction force for each patient based on the results of the simulations in chapter five. Previous experimental and analytical studies have indicated that the relationship between blood pressure and pressure derived distraction force is linear (44, 155). In chapter five, distraction force results were obtained for a peak systolic blood pressure of 160mmHg (21332Pa). During these simulations, results were also obtained for a systolic pressure of 140mmHg (18665Pa). To prove the linear relationship between pressure and pressure derived forces, the results at 18665Pa were transformed by equation 6.1 and compared with actual results at 21332Pa from chapter five.

$$F_{RDF2} = F_{P1}\, x \frac{P_2}{P_1} + F_V \qquad (6.1)$$

where F_{RDF2} is the predicted total RDF in Newtons at 21332Pa (P_2) and F_{P1} is the pressure derived force at 18665Pa (P_1). Flow derived, viscous forces (F_V) were constant and independent of pressure forces. They were therefore added to the pressure force to give total resultant distraction force.

Table 6.1 shows the median error between the total RDF predicted by equation 6.1 and the actual observed total RDF at 21332Pa for all complete stent-grafts and components included in chapter five.

Table 6.1 Median error (%) of predicted versus observed total RDF at 21332Pa

	Median Error (%)	Range (%)
Complete stent-grafts	0.35	0.04-2.86
Proximal bodies	0.31	0.03-2.79
Distal bodies	0.31	0.02-2.82
Limb extensions	0.19	0.01-2.82

This error was considered acceptable and equation 6.1 was therefore used to translate force results at 18665Pa into patient-specific total RDF for each complete stent-graft and for the individual components as follows:

$$F_{IS} = \frac{F_{P1}}{P_1} x\ 133.32P_{PO} + P_V \quad (6.2)$$

where F_{IS} = in situ total RDF in Newtons and P_{PO} = preoperative systolic blood pressure in mmHg.

6.5.2 Analysis of component distraction

The method of England *et al.* (194) used in the analysis of proximal body migration had been previously validated by an intra and interobserver variability study (197). Using a computer generated central luminal line (CLL), electronic measuring tool and predefined anatomical markers, accuracy was observed to 4mm. The method described here for analysis of component distraction preserves as many of the features used in this migration analysis as possible.

6.5.2.1 Image acquisition and reconstruction

The first and last available postoperative CT scans were loaded onto a 3D workstation (Carestream PACS 10.2, Kodak, Rochester, NY). An in-built vessel analysis tool was used to generate a CLL from above the stent-graft to a point along the ipsilateral limb beyond the distal extent of the proximal body. The

ipsilateral limb was chosen for its smoother transition past the flow divider than the contralateral gate. Here the sudden reduction in luminal diameter caused by the proximal extent of the limb extension may cause sudden changes in the direction of the generated CLL.

The Maximum Intensity Projection (MiPPR) sagittal image was thickened to 25mm to more readily show the overall configuration of the stent-graft (see Figure 6.1B). Crosshairs were moved up and down the green CLL and were used to mark reference points as they appeared in the axial window (Figure 6.1C). The distance between reference points along the CLL was automatically calculated by the software. A 3D overview of the stent graft and vessel morphology was shown in the top left of the screen (Figure 6.1A).

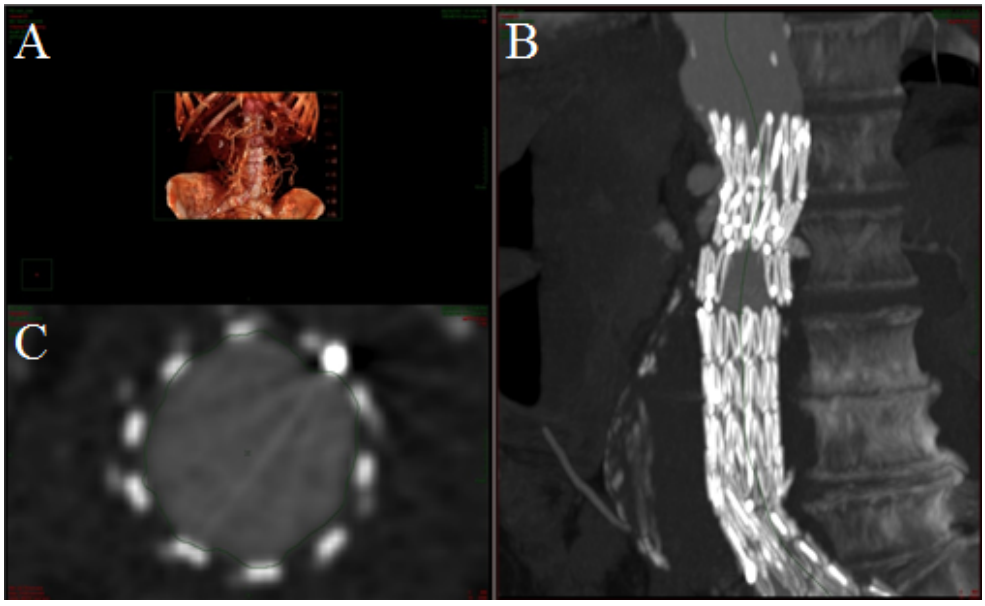

Figure 6.1 Carestream software set up for measurement of component distraction. A: 3D reconstruction, B: Sagittal MiPPR, C: axial window

6.5.2.2 Component distraction definition

One previous core lab analysis of 106 patients post fEVAR defined component *movement* as any movement of >10mm (120). Component *distraction* was defined as movement that had led to inadequate overlap length (less than two

stents as defined by IFU) or clinical symptoms or secondary intervention. Since the current method is based upon a previously described migration analysis method that has validated accuracy to 4mm, the term *component distraction* is used here to describe movement of ≥4mm of the distal body in relation to the proximal body.

6.5.2.3 Selection of reference points

For the measurement of proximal migration, England *et al*. (194) used the CLL distance between the first axial slice where there was clear separation of the SMA from the aortic wall and the appearance of at least two bare metal stents. Since the measurement of component distraction relies upon determining the position of one component in relation to another it was not necessary to include a native vascular reference point. All the reference points were therefore stents or markers on the proximal or distal body. These points are shown in Figure 6.2.

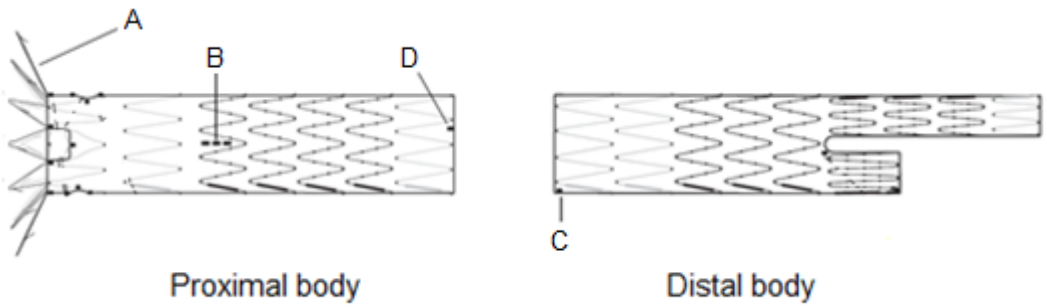

Figure 6.2 Reference points on the Zenith fenestrated proximal body and distal body for the measurement of component distraction.
Image adapted from Cook medical Inc. (72)

The most proximal reference point was the first appearance of at least two apices of the suprarenal bare metal stent (A). B is the anterior gold radiopaque markers of the proximal body. C is the proximal gold radiopaque marker of the distal body and D is the distal gold radiopaque marker of the proximal body.

6.5.2.4 Measurements

Four measurements were made on each CT scan. 'First appearance' in all cases refers to the identification of a reference point whilst moving through the images in a cranial to caudal direction.

6.5.2.4.1 Measurement 1 (M1)

The CLL distance between the first appearance of at least two struts of the bare metal stent (A, Figure 6.2 and Figure 6.3) to the first appearance of the proximal gold radiopaque marker on the distal body (C). This measurement was included as it uses one of the reference points from the previous proven methodology. Dowdall *et al.* (120) used the first contralateral gate radiopaque marker as the distal reference point but the extra distance between these points may lead to inaccuracy should there be any significant changes in aortic tortuosity or 'concertinering' of components. Concertinering refers to the potential for the z stents to move closer together thus closing the small 2mm gaps between them as a result of changes to the native vessel or migration of one end of a component in relation to the other. The net result is a shortening of the component. To address this point – and because identification of the maximum radiopacity of the gold markers may be less subjective than that of the stents – a second measurement was also taken (see M2).

6.5.2.4.2 Measurement 2 (M2)

The CLL distance between the first appearance of the most proximal of the three anterior vertical gold markers on the proximal body (B, Figure 6.2 and Figure 6.3) to the first appearance of the proximal gold radiopaque marker on the distal body (C). This distance was much shorter than M1 and in some cases negative i.e. when the distal body was overlapped to the lower margin of the lower most fenestration, reference point C was actually proximal to point B. M2 also quantified the amount of 'non-appositional overlap' present between the two components. The proximal of the three vertical markers identified the transition

point between the seal-zone above that may be up to 36mm in diameter depending on the size of device chosen and the overlap zone below where the diameter is always 22mm. Distal body sealing stents deployed above this point in large proximal body components may add little or no radial force to the component's fixation. Conversely with enough clearance below the visceral vessels, allowing a distal body sealing stent with a diameter of 24mm to fully deploy above the transition point may lead to more secure fixation since it would then be very difficult to distract it back down the 22mm overlap zone.

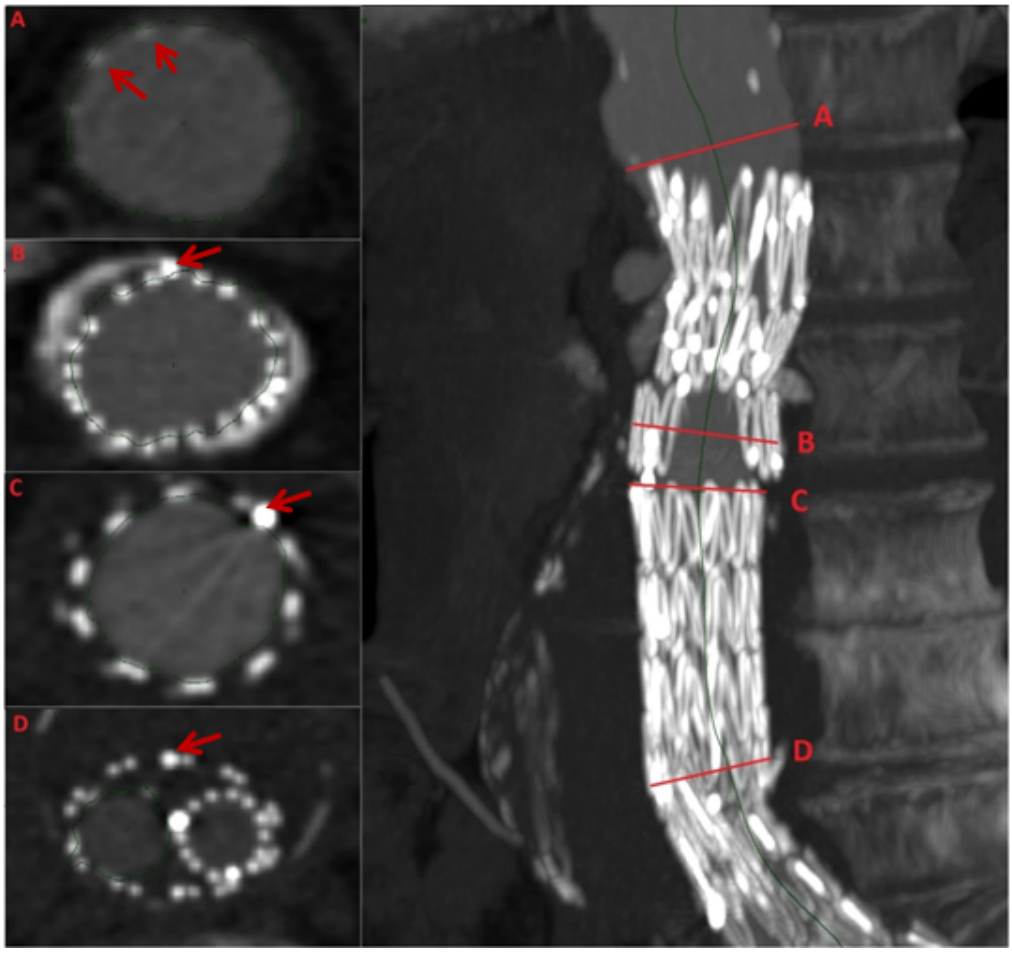

Figure 6.3 Axial views at positions A-D (left) and MiPPR (right) showing all reference points (indicated by red arrows). M1: A-C, M2: B-C, M3: B-D, M4: C-D

6.5.2.4.3 Measurement 3 (M3)

The CLL distance between the first appearance of the most proximal of the three anterior vertical gold markers on the proximal body (B, Figure 6.2 and Figure 6.3) to the first appearance of the distal gold radiopaque marker on the proximal body (D). While M3 gave no information in terms of component movement it was used to confirm that any changes in M4 were indeed due to distraction rather than a significant reduction in tortuosity or concertinering.

6.5.2.4.4 Measurement 4 (M4)

The CLL distance between the first appearance of the proximal gold radiopaque marker on the distal body (C, Figure 6.2 and Figure 6.3) to the first appearance of the distal gold radiopaque marker on the proximal body (D). M4 was a secondary measurement of movement between gold markers and also corresponded to the length of 'appositional overlap' between the proximal and distal bodies. This as opposed to 'non-appositional overlap' (see M2) was the length of distal body physically in contact with the 22mm diameter overlap zone of the proximal body.

Each measurement on the first postoperative CT scan was compared with the corresponding measurement on the last available CT scan and any difference ≥4mm was investigated further by visual comparison of images. A change of ≥4mm in M2 measurements was suggestive of component distraction and was confirmed by ensuring there were no significant differences in CLL morphology; by a ≥4mm change in M1 and M4 and a <4mm change in M3. A ≥4mm change in M3 would be suggestive of either a change in aortic tortuosity, inconsistencies with CLL generation or – in the case of reduction ≥4mm – concertinering.

6.5.3 Inclusion criteria

Patients were required to have an initial postoperative CT scan and at least one other separate surveillance episode with CT imaging. Ethical approval for the use

of medical images and demographic data was granted by the North West – Liverpool East Research Ethics Committee.

6.5.4 Statistical analysis

Continuous data was analysed using Mann Whitney U test (MWU), categorical data with Fisher's Exact test.

6.6 Results

6.6.1 Proximal body migration

6.6.1.1 Exclusions

Of 54 patients for whom flow simulations had been performed 43 had an initial postoperative CT plus one further surveillance episode with CT imaging. Eleven patients were excluded due to only having one available postoperative CT. This was either due to follow-up having been arranged elsewhere (n=6), short follow-up with only one completed imaging episode (n=2), mortality prior to second imaging episode (n=2) or poor renal function excluding further follow-up with contrast enhanced CT (n=1).

6.6.1.2 Migration analysis

Central luminal line analysis identified nine cases of migration ≥4mm (median distance migrated 6.1mm, range 4.1-12.5mm). There were 34 other proximal bodies in the 'no migration' group with a median migration distance of 1.7mm, range -3.2-3.8mm. Overall median time between imaging episodes was 25 months (range 4-72).

Demographics were obtained from departmental records. Both groups were well matched with the exception of BMI (see Table 6.2). Although the difference in BMI reached statistical significance (25 in the migration group versus 27.5 in the

no migration group) this is of little clinical significance since both are considered 'overweight' by the World Health Authority. There was a trend toward a longer time between imaging episodes in the migration group but this was not significant.

Table 6.2 Comparison of demographics between patients with proximal body migration versus no migration

	Migration	No Migration	p (MWU except [f]:Fisher's Exact)
n	9	34	
Distance Migrated, mm	6.1 (4.1-12.5)	1.8 (-3.2-3.8)	
Gender (M:F)	8:1	30:4	0.723[f]
Age	76 (65-86)	76 (62-85)	0.942
BMI	25.0 (22.6-34.3)	27.5 (19.7-40.9)	0.046*
Diabetes	1	3	0.624[f]
Ischaemic heart disease	5	20	0.575[f]
Heart failure	0	1	0.791[f]
Hypertension	4	20	0.345[f]
Preoperative systolic blood pressure, mmHg	135 (122-167)	140 (92-185)	0.567
Preoperative pulse rate, beats per minute	68 (50-90)	70 (53-118)	0.385
Chronic renal impairment	2	3	0.277[f]
Current smoker	3	6	0.463[f]
Peripheral vascular disease	1	4	0.723[f]
ASA (1/2/3/4)	0/2/7/0	1/10/23/0	
Imaging interval, months	44 (10-72)	24 (4-52)	0.295
Maximum preoperative AAA diameter (mm)	59 (55-80)	65 (55-86)	0.187
XSA of lumen at proximal body inlet (mm^2)	389 (209-659)	347 (214-907)	0.418

For full demographics see Appendix 8.8. Continuous variables expressed as median with range in parentheses, n given for categorical variables, ASA: American Society of Anaesthetists grading, BMI: Body mass index, n=Number of patients, XSA: Cross-sectional area, *denotes significance to p<.05

6.6.1.3 Total resultant distraction force (RDF)

Median total RDF acting on the complete stent-grafts in the migration group was 6.0N (range 2.6-9.5N). This figure was higher than in the no migration group (Median 5.0N, range 2.1-13.1N) but did not reach statistical significance. A similar trend was seen between proximal bodies in each group (5.6N, range 1.7-8.6N vs 4.0N, range 1.3-11.6N) (see Figure 6.4).

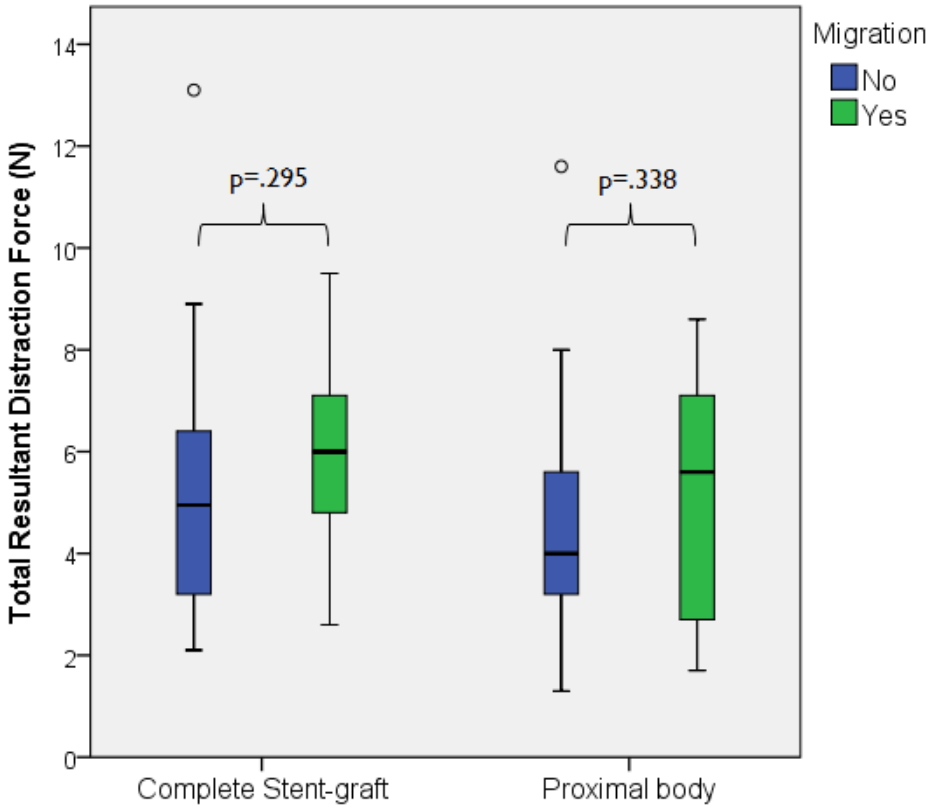

Figure 6.4 Comparison of total RDF between migration and no migration groups

Individual distraction force results for complete stent-grafts and proximal bodies are detailed in Appendix 8.7.1. Migration measurements and imaging intervals are also included.

6.6.1.4 Clinical sequelae

Only one of the nine patients with proximal body migration developed any target vessel problems. This was an ostial endoleak between the visceral stent of the left renal artery and the main stent-graft of fEVAR 53. It was treated with angioplasty of the original visceral stent at 14 months. One other patient (fEVAR 45) had suspected misalignment of the SMA scallop and was investigated with a digital subtraction angiogram. No significant stenosis was found and no secondary intervention was performed. Appendix 8.9 details the clinical outcomes for all patients in the cohort.

There were no late type I endoleaks in either group. Of the 34 patients in the no migration group there were two ostial type IIIa endoleaks between target vessel stents and the main stent-graft during the follow-up period (fEVARs 25 and 32). Three visceral vessels occluded without clinical consequences (fEVARs 29, 36 and 41), one associated with stent fracture and another with stent dislocation. Three other visceral stents remained patent but were noted to have fractured (fEVARs 25, 34 and 52) and one other had dislocated but also remained patent (fEVAR 25). There were two stenoses in scalloped target vessels (the right renal artery of fEVAR 21 and SMA of fEVAR 35).

Of the patients not included in the migration analysis (due to having only one available postoperative CT scan) one developed mesenteric ischaemia secondary to an SMA stent stenosis. This was treated unsuccessfully by angioplasty at one month and was followed by right external iliac artery to SMA bypass at 8 months. This patient (fEVAR 2) was lost to follow-up in another region at 28 months. One other had a right renal stent stenosis treated by angioplasty within the first postoperative month (fEVAR 24).

6.6.2 Proximal-distal body component distraction

6.6.2.1 Exclusions

One patient (fEVAR 7) was excluded from the 43 patients included in the proximal body migration analysis. This device was a custom made hybrid proximal/distal body component that was both fenestrated and bifurcated.

6.6.2.2 Distraction analysis

Three cases of component distraction ≥4mm between the distal and proximal bodies were identified (median distance 5.6mm, range 5.4-13.7mm). There were 39 other distal bodies in the 'no component distraction' group with a median distance of 0.4mm, range -3.2-3.0mm. Overall median time between imaging episodes was 24 months (range 4-52) and there were no significant demographic differences between groups (see Table 6.3). Likewise there was no significant difference between the groups in terms of preoperative AAA diameter or inlet cross-sectional area of the distal body component post-deployment.

The interval change between M1, 2, 3 and 4 measurements for each patient is shown in Appendix 8.7.2 along with patient-specific distraction forces acting on each distal body and fenestrated stent-graft as a whole.

Table 6.3 Comparison of demographics between patients with proximal-distal body component distraction versus no component distraction

	Component Distraction	No Component Distraction	p (MWU except [f]:Fisher's Exact)
n	3	39	
Distance distracted, mm Based on M2 measurements	5.6 (5.4-13.7)	0.4 (-3.2-3.0)	
Gender (M:F)	2:1	35:4	.323[f]
Age	76 (62-78)	76 (64-86)	.678
BMI	26.3 (19.7-27.6)	26.8 (20.3-40.9)	.371
Diabetes	0	4	1.000[f]
Ischaemic heart disease	1	23	.567[f]
Heart failure	0	1	1.000[f]
Hypertension	0	23	.084[f]
Preoperative systolic blood pressure, mmHg	117 (92-180)	140 (100-185)	.425
Preoperative pulse rate, beats per minute	65 (62-90)	70 (50-118)	.644
Chronic renal impairment	0	5	1.000[f]
Current smoker	2	7	.111[f]
Peripheral vascular disease	0	5	1.000[f]
ASA (1/2/3/4)	0/1/2/0	1/11/27/0	
Imaging interval, months	23 (21-49)	25 (4-52)	.577
Maximum preoperative AAA diameter (mm)	59 (57-62)	64 (55-86)	.298
XSA of lumen at proximal body inlet (mm^2)	340 (272-414)	382 (194-501)	.577

For full demographics see Appendix 8.8. Continuous variables expressed as median with range in parentheses, n given for categorical variables, ASA: American Society of Anaesthetists grading, BMI: Body mass index, n=Number of patients, XSA: Cross-sectional area

6.6.2.3 Visual image comparison for all measurement differences ≥4mm

Overall there were eight patients with ≥4mm change in M1, 2 or 4 measurements. Visual image comparison showed that only three of these were true cases of component distraction.

6.6.2.3.1 Cases where true component distraction was ruled out

fEVAR 19 (M4: -4.6mm): No component distraction.

Prior analysis of migration (see 6.6.1) had shown that fEVAR 19 underwent 4.1mm of proximal body migration between imaging intervals. This probably represented full engagement of the barbs into the aortic wall and can be seen in Figure 6.5 where the bare metal stents expanded and moved distally in relation to the superior border of the first lumbar vertebra (a).

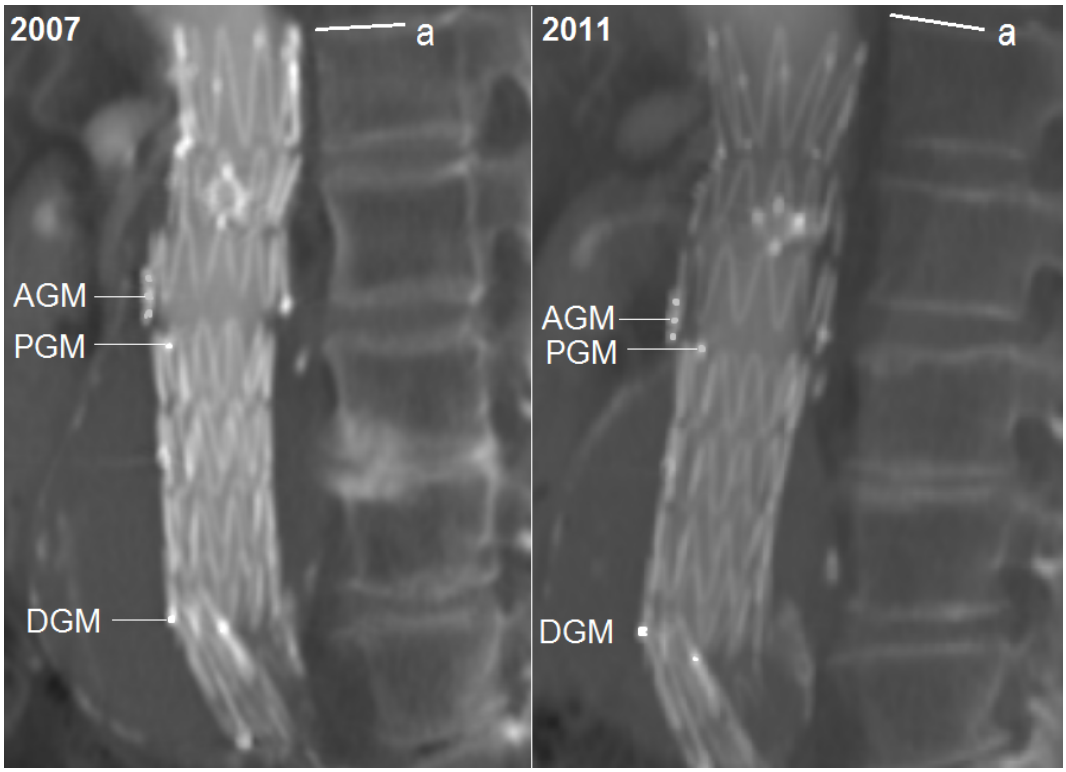

Figure 6.5 First and last available images for fEVAR 19

The distance between the proximal gold marker (PGM) of the distal body and the distal gold marker (DGM) of the proximal body reduced by 4.6mm but this probably represented the concertinering effect of the stents of both proximal and distal bodies due to the migration above rather than distraction between the two. The case for concertinering is supported by the 6.2mm reduction in distance between the anterior gold markers (AGM) and DGM (i.e. M3 measurement) and

by the small upward movement of the PGM in relation to AGM seen in Figure 6.5.

fEVAR 21 (M1: +6.6mm, M4: -5.3mm): No component distraction.

The distance between the appearance of two bare metal stents and the proximal gold marker (PGM) of the distal body increased by 6.6mm between imaging intervals. The anterior curvature of the stent-graft increased over this time period which would have contributed to the increase in the CLL distance between these two points (see Figure 6.6).

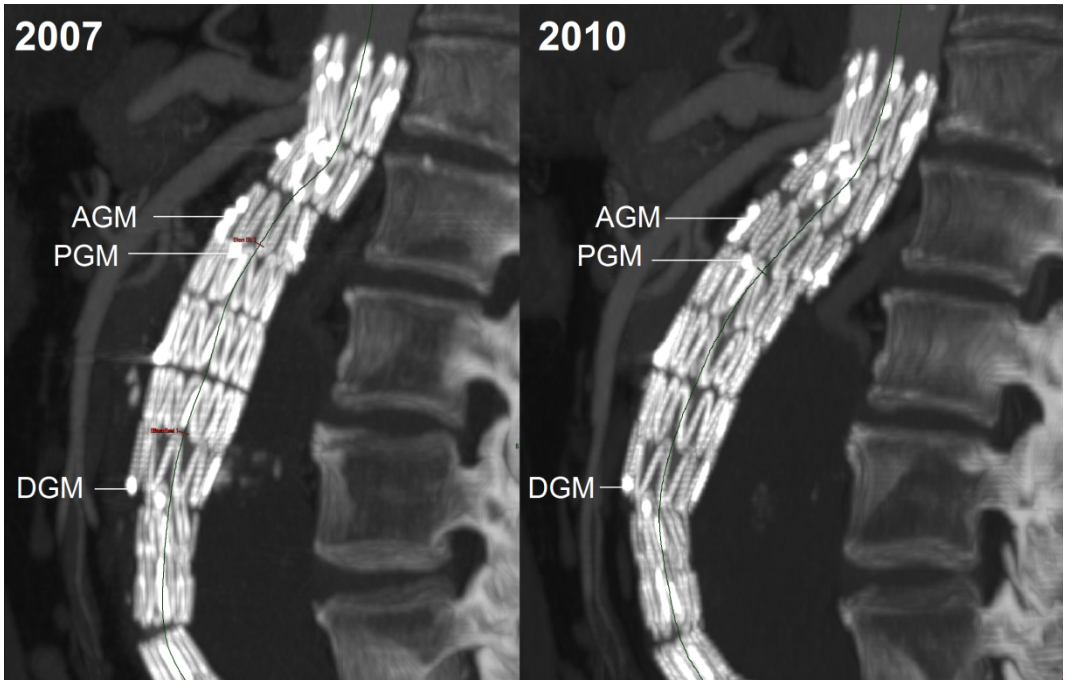

Figure 6.6 First and last available images for fEVAR 21

A further contributing factor was a 3.0mm increase in M2 distance, i.e. between the anterior gold markers (AGM) of the proximal body and PGM. This movement did not quite reach significance and although the measurement technique was not validated to prove such small movements, visual inspection of these points of interest does suggest a small amount of component distraction. The distance between the PGM and distal gold marker (DGM) of the proximal body (M4 distance) reduced by 5.3mm over the same imaging interval. The CLL curvature

throughout this segment did not change and the seemingly significant difference in M4 was probably as a result of the small amount (3.0mm) of component distraction together with the concertinering effect on the posterior aspect of the stents caused by the observed anterior displacement of the stent-graft.

fEVAR 26 (M1: +4.4mm): No component distraction.

This stent-graft exhibited significant (9.5mm) proximal body migration during the imaging interval. This can be seen in Figure 6.7 where the position of the bare metal stent moved from a to b in relation to the vertebral bodies between 2008 and 2012.

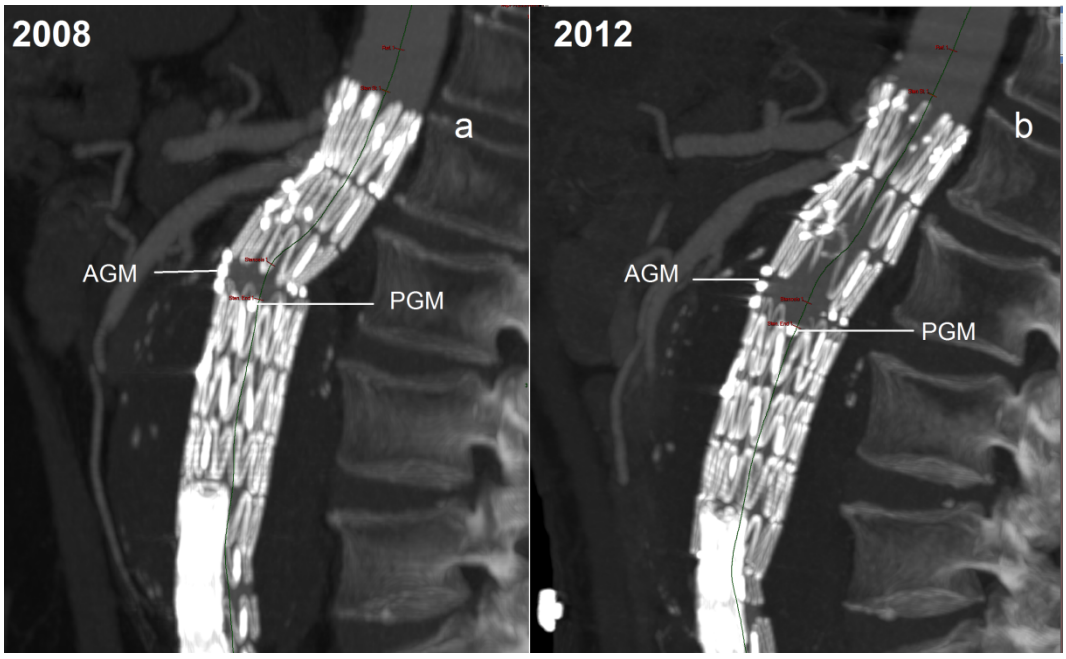

Figure 6.7 First and last available images for fEVAR 26

Despite significant proximal body migration the distance between the proximal bare metal stent and the proximal gold marker (PGM) increased by 4.4mm. Continued expansion of the first sealing stent may have contributed to this and visual inspection of images suggests that the PGM of the distal body remained at the same position in comparison with the three anterior gold markers (AGM) on the proximal body. This finding combined with no significant change in M2 or M4

distance confirmed the absence of component distraction. In this instance the proximal and distal bodies migrated distally *en mass*.

fEVAR 35 (M4: -4.4mm): No component distraction.

The M4 distance between the proximal gold marker (PGM) of the distal body and distal gold marker of the proximal body marker (DGM) in fEVAR 35 decreased by 4.4mm between imaging intervals but this was not accompanied by a significant change in M1 or M2 measurements (1.9 and 0.9mm respectively). A small amount of concertinering of the stent-graft may have contributed to the change in M4 measurement. This was suggested by the closer position of stents at point b compared with a (Figure 6.8) and by the -3.1mm change in the distance between AGM and DGM markers (i.e. M3). There is also no discernible change in the position of PGM in relation to AGM.

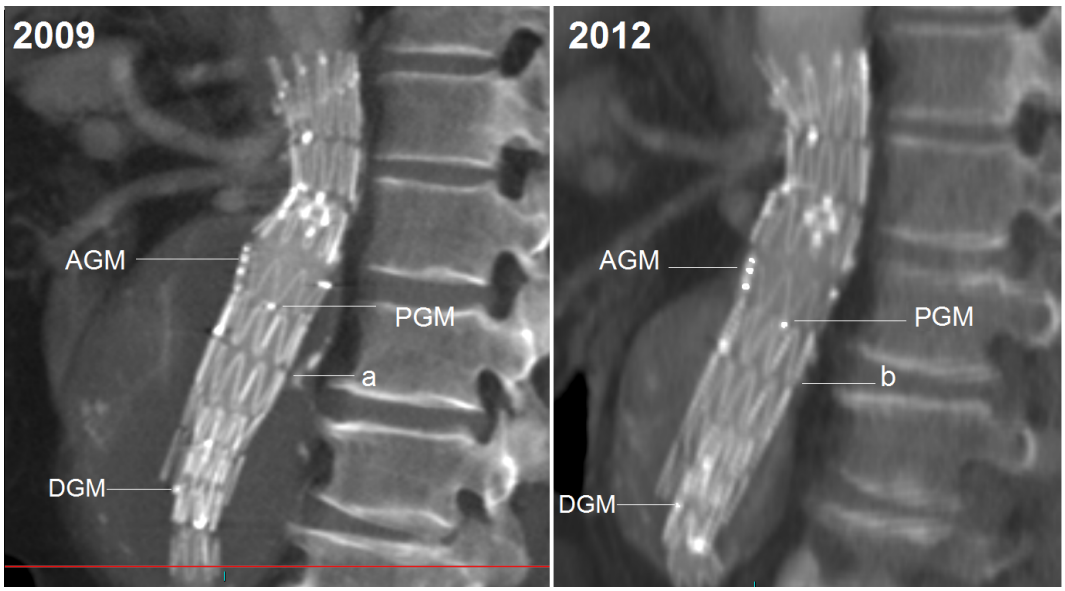

Figure 6.8 First and last available images for fEVAR 35

fEVAR 40 (M1: +7.8mm): No component distraction.

An isolated 7.8mm increase in the distance between the first appearance of two bare metal stents and the proximal gold marker (PGM) of the distal body was

observed for fEVAR 40. Visual inspection of images shows remodelling of the visceral aorta with reduction in aneurysm size. Although further expansion of the second sealing stent between imaging episodes has straightened the CLL there has been a little increase in the distance between this and the next stent at point b compared with point a (see Figure 6.9).

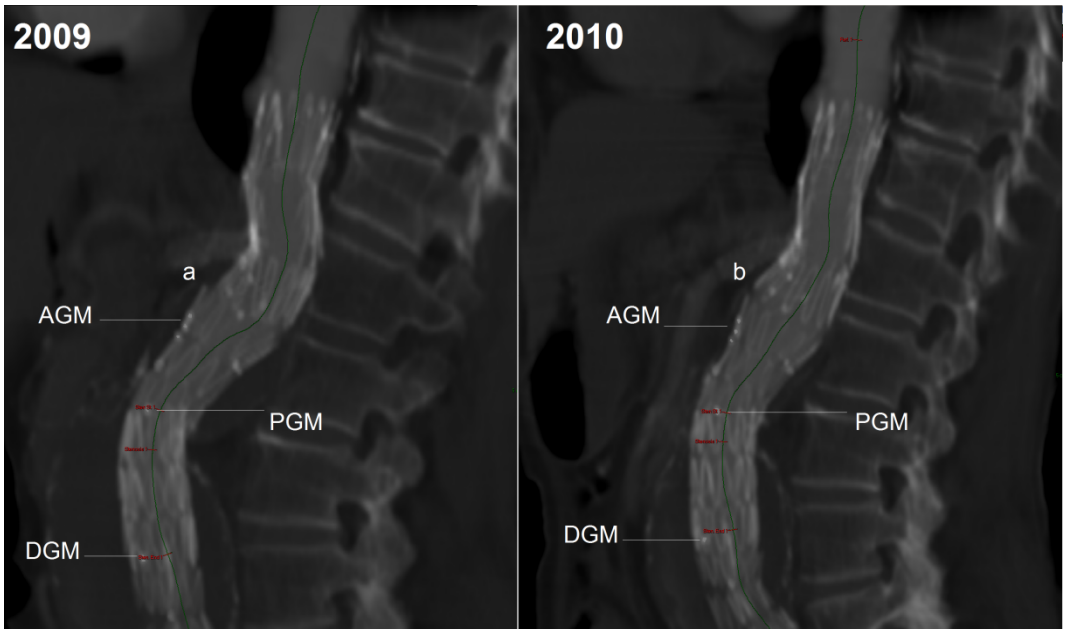

Figure 6.9 First and last available images for fEVAR 40

This slight moving apart of stent rows has caused all other reference points to be slightly lower against their respective vertebral bodies whereas the proximal bare metal stent remained at the same position. The lack of significant change in M1 and M2 measurements and the constant position of anterior gold markers (AGM), PGM and distal gold marker (DGM) confirmed that no distal body component distraction had occurred.

6.6.2.3.2 Cases where true component distraction was confirmed

fEVAR 22 (M1: +6.7mm, M2: +5.6mm, M4: -5.1mm): Confirmed component distraction.

All three measurements for fEVAR 22 showed significant change between imaging episodes and the length of the proximal body, i.e. the M3 distance between the anterior gold marker (AGM) and the distal gold marker (DGM) only changed by 0.5mm.

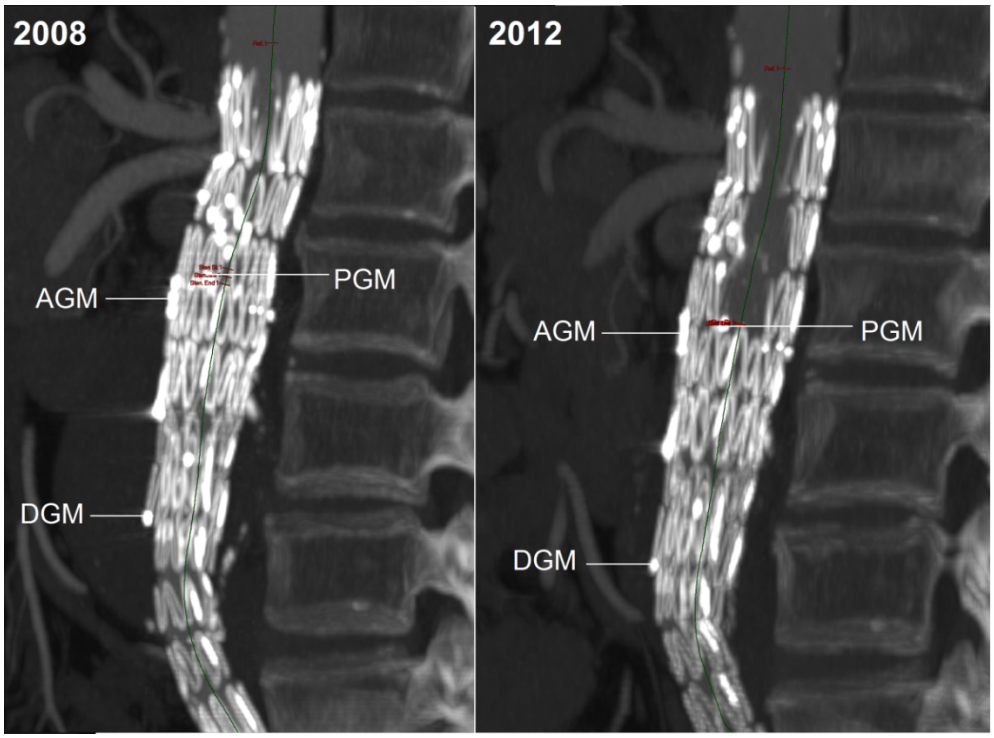

Figure 6.10 First and last available images for fEVAR 22

Visual inspection (see Figure 6.10) shows that the PGM of the distal body was initially proximal to the AGM in 2008 but by 2012 had moved to lie just distal to the upper edge of the first AGM. Although the change in position of the components in relation to the vertebral bodies was suggestive of a small amount of proximal body migration the movement was not significant (0.5mm, see Appendix 8.7.1). The observed changes in M1, 2 and 4 measurements in the absence of a significant change in M3 measurement confirmed the presence of component distraction.

fEVAR 43 (M1: +6.6mm, M2: +5.4mm, M4: -6.1mm): Confirmed component distraction.

Anterior displacement of the stent-graft was observed between imaging episodes. The proximal gold marker (PGM) of the distal body was proximal to the anterior gold markers (AGM) of the proximal body following deployment in 2009 but by 2012 had moved adjacent to the most proximal of the three AGM (see Figure 6.11). Although the CLL through the section of stent-graft between AGM and distal gold marker (DGM) appeared to straighten over the imaging interval there was only -0.6mm change in M3 measurement. This confirms that the reduction in M4 (PGM to DGM) was due to component distraction and not concertinering.

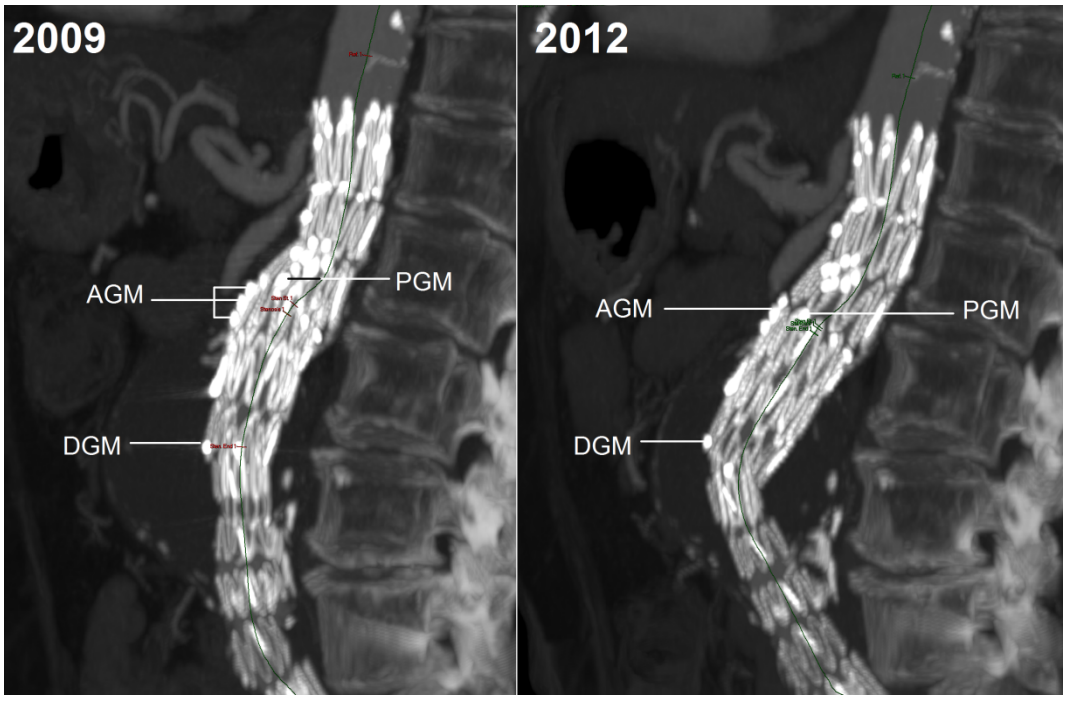

Figure 6.11 First and last available images for fEVAR 43

fEVAR 46 (M1: +11.3mm, M2: +13.7mm, M4: -9.6mm): Confirmed component distraction.

The proximal gold marker (PGM) of the distal body moved distally in relation to the anterior gold markers (AGM, see Figure 6.12). This resulted in an initial three-

stent overlap becoming only two-stents in the latter image. There was no significant proximal body migration (1.7mm) or change in the proximal CLL to affect the M1 measurements. The 9.6mm reduction in distance between PGM and DGM remained significant even after allowing for the apparent 4.2mm reduction in M3 measurement (i.e. length of proximal body or AGM to DGM).

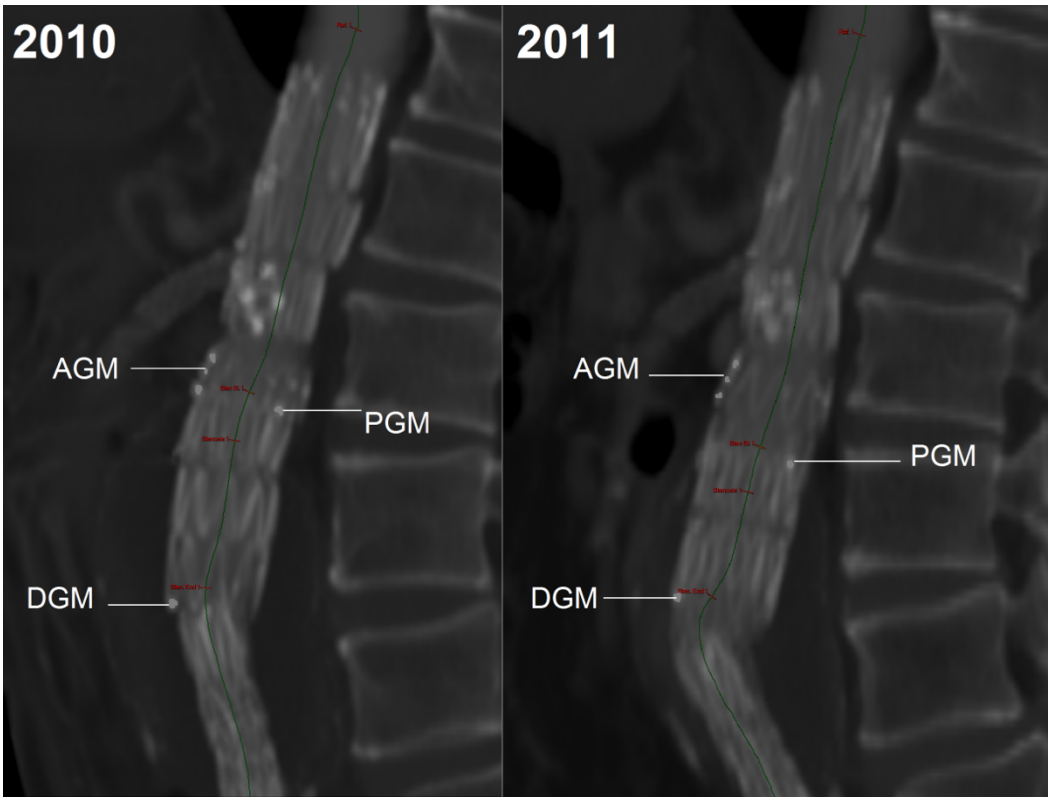

Figure 6.12 First and last available images for fEVAR 46

6.6.2.4 Total resultant distraction force

There was no observed trend towards greater total RDF in the component distraction group versus the no distraction group (see Figure 6.13). Total RDF was in fact non-significantly smaller in both complete stent-grafts with evidence of component distraction (median total RDF 4.8N, range 4.2-5.1N vs 5.5N, range 2.1-13.1N) and distal bodies (median 4.3N, range 2.8-4.7N vs 4.8N, range 2.4-8.0N).

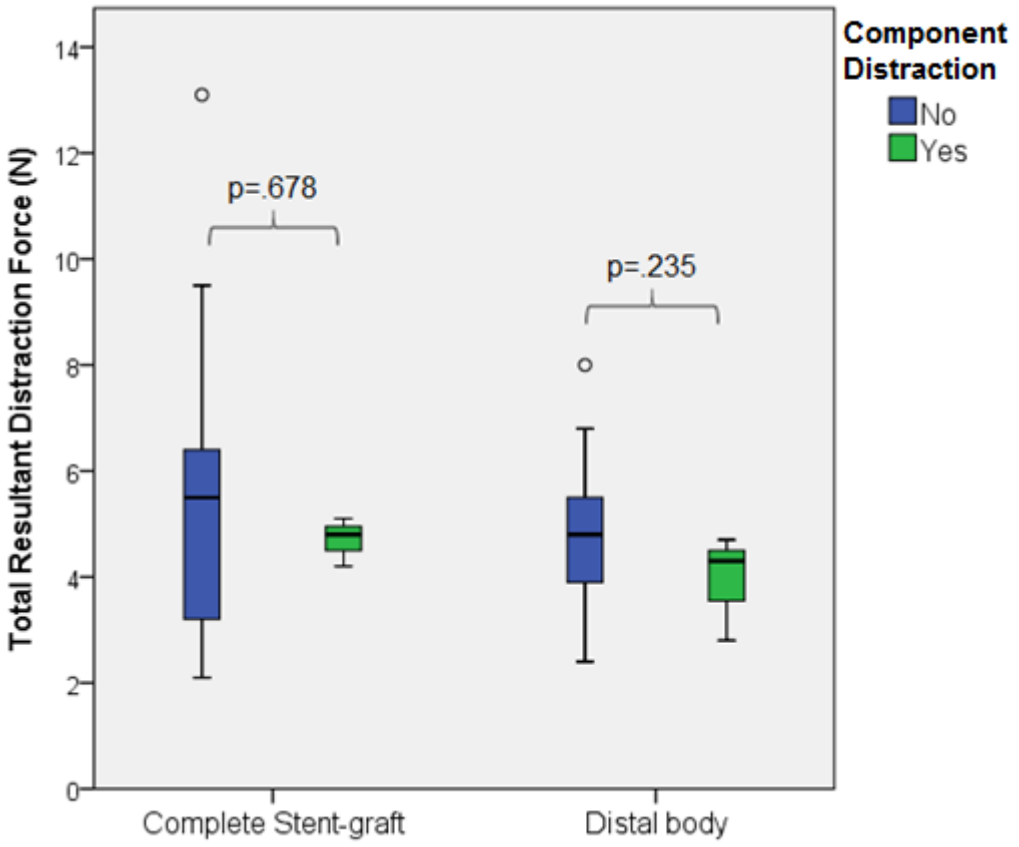

Figure 6.13 Comparison of total RDF between component distraction groups

6.6.2.5 Clinical sequelae

There were no clinical sequelae as a result of any of the three cases of component distraction. Two patients were alive at five and four years of follow-up with no graft-related adverse events (fEVAR 22 and 43). One patient died from non-aneurysm related causes after three years of follow-up (fEVAR 46). The distal body of this stent-graft moved 13.7mm caudally in relation to the proximal body between imaging episodes and although the initial three stent overlap was reduced to two stents, no type IIIa endoleak or other complication was identified. None of these patients underwent any secondary interventions. There were no graft-related adverse events in relation to the proximal-distal body junction within the 'no component distraction' group either. A full description of all clinical outcomes is included in Appendix 8.9.

6.6.3 Limb extension migration

6.6.3.1 Exclusions

One fenestrated stent-graft (fEVAR 15) was excluded from the 43 used in the proximal body analysis due to the presence of a Wallstent (Boston Scientific, France) in the contralateral limb. This uncovered stent placed at the time of the initial repair to correct a stenosis or kink in the limb extension would have had an unknown effect on the distal fixation force. It was not possible to identify the inlet and outlets of the limbs of one further stent-graft (fEVAR 49) due to the overlapping stents of three limb extensions deployed in the same common iliac artery. Five other stent-grafts were excluded due to no available migration data (fEVARs 40, 55-57 and 59). Thirty six fenestrated stent-grafts were therefore included in the analysis. These comprised 36 contralateral limb extensions plus an additional seven ipsilateral limb extensions (total 43 limb extensions).

6.6.3.2 Migration analysis

Prior central luminal line analysis had identified four cases of migration ≥4mm in a proximal direction from the distal seal-zone (194). There was also one migration of the distal body ipsilateral limb (fEVAR 39) but this case was not analysed with the limb extension components because the distraction force results were obtained for the entire component and would not have given a valid comparison. Likewise this case was not compared against other distal bodies without ipsilateral limb migration as no meaningful analysis could be achieved with only one case. Demographics are summarised in Table 6.4 and were similar between those patients with limb extension migration versus those without. The only significant difference was the duration of follow-up (i.e. the interval between imaging episodes). This was significantly higher in the migration group (see Table 6.4). Overall median time between imaging episodes was 26 months (range 4-72).

Table 6.4 Comparison of demographics between patients with limb extension migration versus no migration

	Migration	No Migration	p (MWU except [f]:Fisher's Exact)
No. of limb extensions (no. of complete stent-grafts)	4 (4)	39 (32)	
Distance migrated, mm	5.0 (4.4-10.6)	0.1 (-3.42-2.38)	
Gender (M:F)	3:1	29:3	.390[f]
Age	79.5 (72-86)	74.5 (62-85)	.092
BMI	25.0 (20.3-33.9)	27.0 (19.7-40.9)	.248
Diabetes	1	3	.390[f]
Ischaemic heart disease	2	19	.560[f]
Heart failure	0	1	.889[f]
Hypertension	1	18	.260[f]
Preoperative systolic blood pressure, mmHg	152.5 (120-164)	140 (92-180)	.421
Preoperative pulse rate, beats per minute	80 (66-90)	70 (50-118)	.315
Chronic renal impairment	1	4	.466[f]
Current smoker	0	7	.800[f]
Peripheral vascular disease	0	5	.534[f]
ASA (1/2/3)	0/1/3	1/9/22	1.000[f]
Imaging interval, months	46 (26-52)	24 (4-72)	.044*
Maximum preoperative AAA diameter (mm)	72 (57-85)	64 (55-86)	.292
XSA of limb extension outlet (mm^2)	183 (123-380)	95 (25-254)	.018*

For full demographics see Appendix 8.8. Continuous variables expressed as median with range in parentheses, n given for categorical variables, ASA: American Society of Anaesthetists grading, BMI: Body mass index, XSA: Cross-sectional area, *denotes significance to p<.05

Migration, total RDF and imaging interval data for individual patients is contained in Appendix 8.7.3.

6.6.3.3 Total resultant distraction force

Total RDF was non-significantly higher in the complete stent-grafts whose limbs were seen to undergo migration compared with those without limb migration (median total RDF 6.0N, range 2.4-13.1N vs 5.4N, 2.1-7.8N, p=.747). Limb extension components that underwent migration were exposed to significantly more distraction force than those that did not migrate (median 2.9N, range 2.7-6.3N vs 1.6N, 0.4-3.8N, p=.003, see Figure 6.14).

Chapter five showed that cross-sectional area of outlet was the most important factor contributing to total RDF in limb extensions and this was also significantly larger in the migration compared with the no migration group (see Table 6.4).

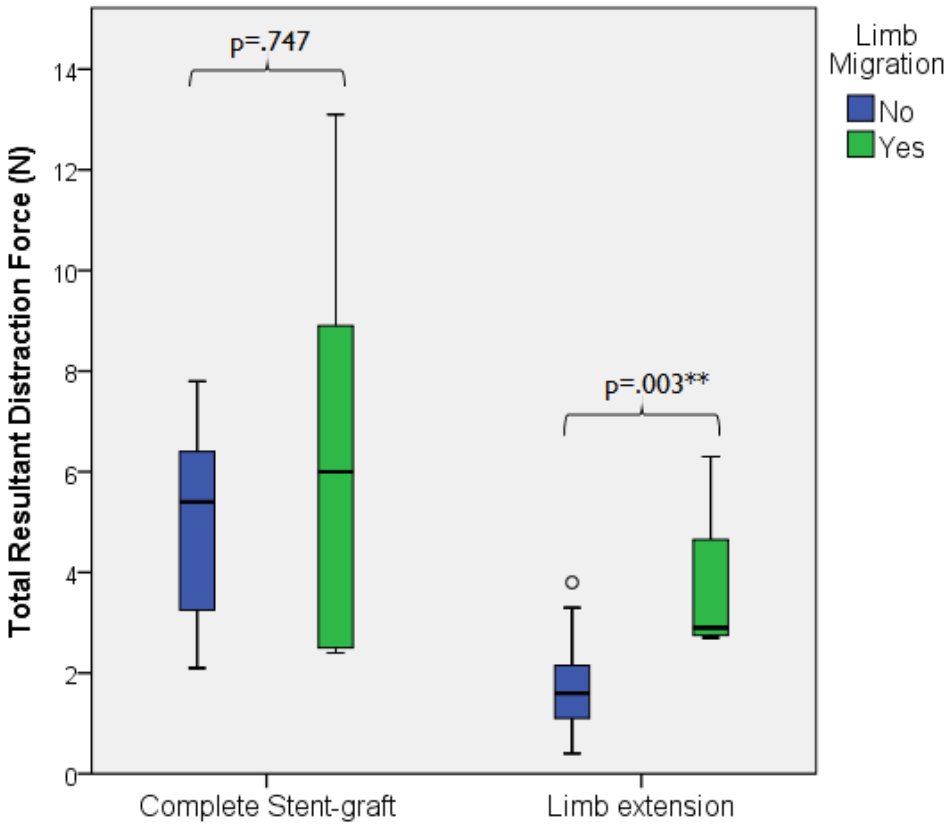

Figure 6.14 Total resultant distraction force in complete stent-grafts and limb extensions by group (denotes significance to p<.01)**

6.6.3.4 Clinical sequelae

Of the four patients within the migration group, one contralateral limb extension developed a stenosis at 14 months but was treated conservatively (fEVAR 25). The ipsilateral limb of this stent-graft was already known to have occluded prior to the first imaging episode and the patient was alive at five years follow-up. Another was noted to have poor apposition of limb extension and common iliac artery but no type Ib endoleak (fEVAR 41). This patient was alive at three years with no complications attributable to migration of the limb extension however the superior mesenteric artery stent had dislocated and occluded at 15 months. The other two cases of limb migration were free of complications and re-interventions. One died from non-aneurysm related causes at four years, the other was still alive at four years.

In the no migration group there were two occlusions in the ipsilateral limbs of distal body components. One occurred early before the first follow-up episode (fEVAR 28). The other (fEVAR 39) was the ipsilateral limb noted to have migrated cranially at 35 months, it then occluded and the patient died from unrelated causes shortly afterwards. There appears to be no unusual findings with regards to the direction or magnitude of the distraction forces acting on this particular distal body component (x: 2.0N y: -0.9N z: 3.3N, Total RDF: 4.0N, see Appendix 8.7.2).

6.7 Discussion

6.7.1 Proximal body migration

Proximal body migration is a serious and potentially fatal complication of endovascular repair therefore the incidence was expected to be low. There was a trend towards greater distraction forces in both proximal bodies and complete stent-grafts that underwent migration in comparison with those that did not migrate but the difference lacked significance. This may be due to the heterogeneity in configuration of proximal bodies within the cohort (see Appendix 8.5.2) or to a type two error. With a larger sample a significant difference may have been possible to prove.

In chapter five the inlet cross-sectional area of the proximal body was shown to be the most important morphological determinant of distraction force acting on this component. Analytical models and the predominance of pressure derived forces also show that blood pressure is of critical importance. Neither inlet XSA nor blood pressure was significantly different between migration and no migration groups.

Only one of the proximal body components that underwent migration developed a target vessel problem compared with nine patients in the no migration group. Statistical analysis of visceral vessel complications was not performed due to the small numbers involved and the presence of other variables such as the configuration of the devices and the choice of stents used. Of note is that the only custom-made single-piece bifurcated fenestrated main body (fEVAR 7) was one of the nine components in the migration group. This device migrated caudally 6mm over 72 months of follow-up. A contributory factor may have been the lack of proximal-distal body junction that would have resulted in the all of the distraction force (apart from that acting on the limb extension) having to be resisted by the proximal fixation force. In this case the potential for a small

amount of component distraction may have been protective. Despite the migration at the proximal seal-zone there were no target vessel complications.

In the no migration group, fEVAR 25 in particular was troubled with complications. It was a two scallop, one fenestration device that developed ipsilateral limb occlusion prior to the first CT scan and was then found to have a stenosis in the contralateral limb at 14 months. It developed one visceral stent fracture, one visceral stent dislocation and a type IIIa endoleak. A fracture of the bare metal stent was also found at 14 months (see Figure 6.15). Embolization of the inferior mesenteric artery was performed at 15 months for aneurysm enlargement in the presence of presumed type II endoleak.

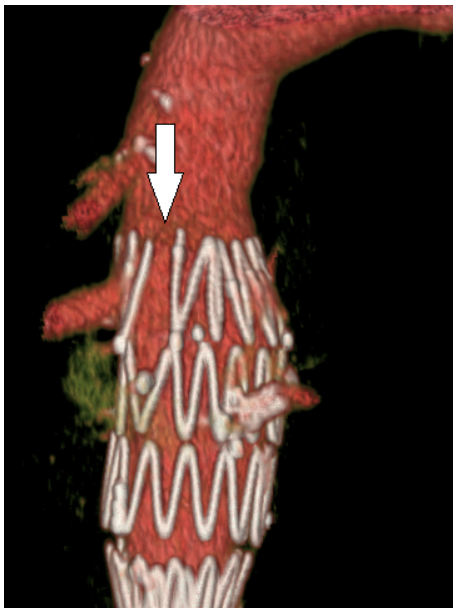

Figure 6.15 3D rendering of the proximal body stents of fEVAR 25 showing a fracture of the bare metal stent (white arrow).

Despite these complications no significant migration was noted. The migration analysis was performed 52 months after the first follow-up imaging and showed 3.2mm of *proximal* movement. It is possible that the fracture made the bare metal stent appear more proximal in relation to the SMA and therefore affected the validity of this result. Alternatively migration may have occurred before the

first follow-up imaging. It was noted that the proximal body of fEVAR 25 showed poor apposition with the visceral aorta. This may explain the apparent instability of the target vessel/main stent-graft interface. Verhoeven *et al.* (67) suspected that migration of <5mm had contributed to two cases of target vessel occlusion in their cohort. Even if the method used for migration analysis was able to confirm less than 4mm of movement, the direction would not have been consistent with the large, predominantly *caudal* direction of the distraction force (11.6N and the only outlier to the 95% confidence interval in the no migration group, see Figure 6.4). The results of Chapter five suggest that in addition to the large inlet cross-sectional area of the proximal body in fEVAR 25 (907mm^2), occlusion of the ipsilateral limb soon after deployment would also have contributed to the higher than average distraction force because of the increased Inlet:Outlet area ratio.

6.7.1.1 Fixation force

All nine cases of migration were exposed to *in situ* distraction forces smaller than the initial fixation force as determined by bovine pullout studies (123). This fixation force of 11.5N +/-1.5N was determined under experimental conditions in perfectly straight, non-diseased bovine aorta using a truncated Zenith fenestrated proximal body with one stented fenestration. Only three of the proximal bodies included in this analysis had one stented fenestration, two had no fenestrations (only a scallop). These devices may be expected to have a lower fixation force but none were among the nine cases of migration. It is uncertain how much the initial fixation force may be increased by adding further stented fenestrations to the Zenith device. As the target vessels were usually aligned to the inferior aspect of the fenestration in anticipation of a small degree of 'settlement' it may be anticipated that more stented fenestrations would not add to this initial fixation force but may add to the total fixation force once full engagement of the barbs had occurred. The initial *in situ* fixation force may be less by differing amounts than 11.5N in all patients depending on factors

affecting barb engagement such as the presence of thrombus, atherosclerosis and angulation.

6.7.2 Proximal-distal body component distraction

In chapter five the main determinant of total RDF acting on distal bodies was inlet cross-sectional area. This alone predicted 74% of distraction force at any given blood pressure. Because the proximal end of every distal body was 24mm diameter the range of inlet XSA was limited. Values above 380mm^2 (22mm diameter) were possible if the distal body was deployed with maximum overlap within the variable sized segment of proximal body above the 22mm diameter overlap segment. Although this would increase the distraction force acting on the distal body, experimental evidence confirms that a longer overlap also conveys greater fixation force (144). In this situation a greater distraction force may be effectively counteracted by greater fixation force. This may be the reason that no association was found between total RDF and component distraction.

All three values of total RDF in the distal bodies that underwent component distraction (4.3, 4.7 and 2.8N) were below the experimentally determined fixation force of 6.5N (4.8-7.2N) (195). Three distal bodies in the no component distraction group were exposed to total RDF above this figure.

6.7.2.1 Fixation force

Forty of the 42 proximal bodies included in the component distraction analysis had two sealing stents. In these patients it may be expected that inlet XSA of the distal body would be larger when the M1 distance (first appearance of two bare metal stent struts to the proximal gold radiopaque marker on the distal body) was shorter. This is because deploying the distal body partly within the visceral seal-zone of the proximal body may allow the proximal end to open out to its maximum 24mm diameter. No correlation was found between M1 distance and

distal body inlet XSA (Spearman's rho, ρ 0.143 p=.367). Likewise there was no correlation between M1 distance and total RDF acting on the distal bodies (ρ 0.014, p=.928). Conversely deploying the distal body within the 22mm overlap segment of proximal body may result in lower distraction force because of the restricted maximum cross-sectional area but also - and perhaps more importantly - lower fixation force due to less overlap. Initial M3 distance (i.e. the CLL distance from the anterior gold radiopaque marker to the distal gold radiopaque marker on the proximal body component) was synonymous with the length of available appositional overlap. When this was compared between groups it was significantly shorter in the three stent-grafts that exhibited component distraction (Median M3 53.2mm, range 41.6-67.3mm vs 73.3mm, range 53.8-119.9mm, p=.012 MWU, see Figure 6.16).

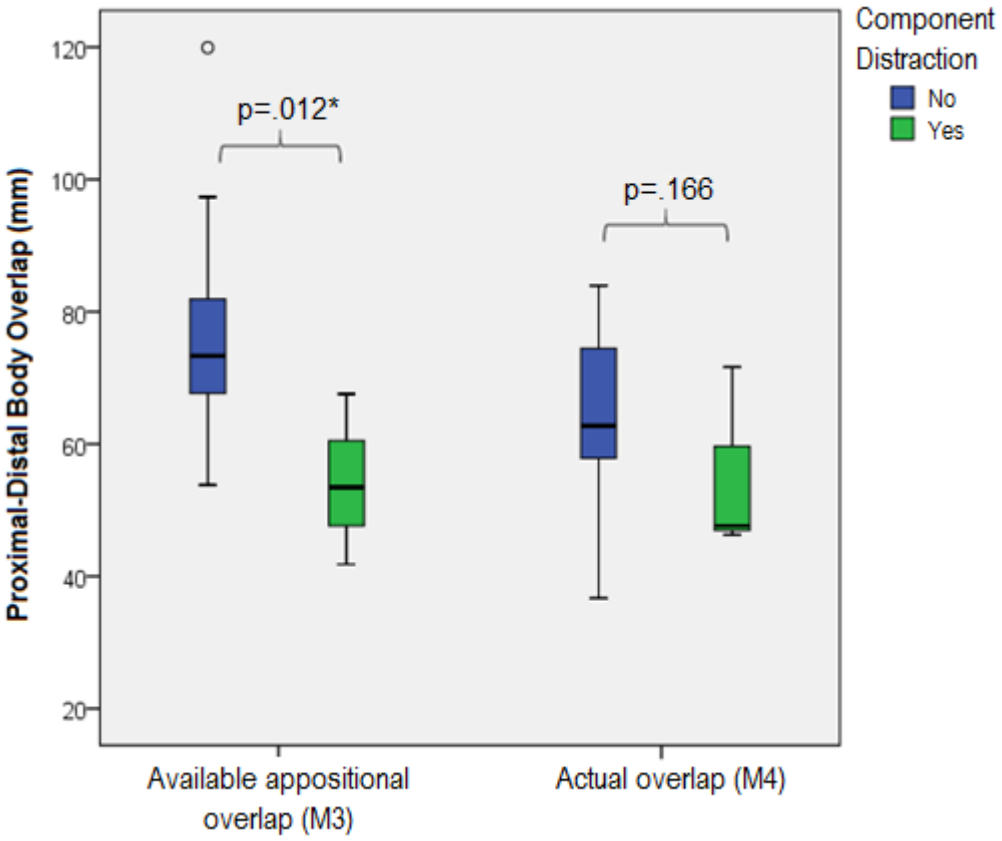

Figure 6.16 Comparison of available and actual overlap between proximal and distal body components by group

*denotes significance to p<.05

The length of the proximal body component as defined by the manufacturer was a less reliable surrogate for available overlap because two of the 42 proximal bodies had either one or three sealing stents that would have given them longer lengths with no increase in available appositional overlap. Consequently although the overall length of proximal body component (BL1, Figure 5.10) was shorter in the component distraction group (median BL1 109mm, range 94-109mm vs. 124mm, range 99-183mm) this did not quite reach statistical significance (p=.055 MWU).

Initial M4 distance (i.e. the CLL distance from the proximal gold radiopaque marker on the distal body to the distal gold radiopaque marker on the proximal body) represented the *actual* overlap between the two components (including appositional and non-appositional overlap). When this was analysed by group there was a trend towards less overlap in the distal bodies that underwent distraction (median M4 47.6mm, range 46.3-71.7mm vs 62.8mm, range 36.7-84.9mm) but this did not reach statistical significance (p=.166 MWU, see Figure 6.16).

Whilst there was no association between total RDF and component distraction, there was some evidence to suggest an association between shorter component overlap and the risk of component distraction. This would point towards fixation force being the most important factor governing the stability of the proximal-distal body junction.

There were no graft-related adverse events as a result of component distraction even though the maximum length of distraction was 13.7mm. This patient (fEVAR 46) died of non-aneurysm related causes at 40 months postoperatively. It is uncertain therefore whether the two stent overlap would have continued to distract or remained stable in the longer term. A small amount of distraction at this junction is probably useful in protecting the fenestrations above from migration.

6.7.3 Limb extension migration

The magnitude of total RDF acting upon limb extensions was significantly associated with limb migration. The same was not observed for total RDF acting upon complete stent-grafts. Chapter five showed that the forces acting on the complete stent-graft were in a more caudal direction with less contribution from out-of-plane forces. All significant migration of limb extension components occurred in the cranial direction. The difference between the direction of forces acting on the complete stent-grafts and the clinical observations suggests that overall forces on the complete stent-graft do not accurately describe the *in situ* conditions experienced by its individual components.

Limb extension migration occurred at forces much less than the apparent 9.6N +/-1.5N fixation force as determined by experimental models (84). This suggests that either our *in silico* model underestimates distraction force or that fixation force may be less than expected. Previous published work from our unit (123) suggests that steady state simulation of blood flow leads to an approximate 10% underestimation of distraction force. Use of pulsatile flow therefore may have only increased the largest forces acting on the limb extension to 7N. The experimentally derived figure of 9.6N +/-1.5N was taken from pullout studies in human cadaveric tissue. Attempts were made to classify the amount of atherosclerosis in the vessel wall however it is likely that the actual fixation force *in situ* is less than that measured experimentally under more ideal deployment conditions. More recent pilot study data using porcine aorta has suggested that a figure of 2.32N ±0.56N may be more realistic (198).

It is possible that dilatation of common iliac arteries during the follow up period may reduce the fixation force. The same process would also be expected to increase distraction force since outlet cross-sectional area was the main morphological determinant of force. The net effect of both would be to make migration more likely. We have no data to prove a significant change in diameter

occurred although one of the four cases of limb migration (and the one case of distal body ipsilateral limb migration) was noted to have lost apposition with the vessel wall at the level of the distal sealing stent. Another had a CIA diameter larger than the original limb chosen to achieve seal within it. These findings are highly suggestive of progressive vessel enlargement.

Clinical observational studies looking specifically at the issue of stent-graft deployment in ectatic iliac vessels have shown no associated increase in iliac limb related complications (152) or re-interventions (151). There were however only 11 Zenith stent-grafts used in ectatic iliac arteries in these studies, the majority being either Talent (Medtronic) or Excluder (Gore).

Standard Zenith stent-grafts accounted for 1988 (29%) of the 6787 stent-grafts in the EUROSTAR registry by 2005 (199). Of these, 803 limbs (40%) were deployed in iliac vessels greater than or equal to 16mm. The annual incidence of kinking in Zenith limbs was twice that of the Excluder (Gore) at 0.012% versus 0.006%. Likewise the annual incidence of occlusion was higher than other modern stent-grafts (Zenith: 0.035, Excluder: 0.011, Talent, 0.023%) and was only favourable when compared to outdated devices such as the Vanguard (0.053%) (199).

A recent analysis has shown that aorto-iliac tortuosity index was significantly reduced by EVAR deployment and that this reduction was maximal for Zenith limbs over Medtronic or Gore (190). The implication is that the Zenith limbs, similar to those used in this cohort may be stiffer with less conformability to native anatomy. Furthermore greater pre and postoperative aorto-iliac tortuosity index was significantly associated with complications such as limb kinking, occlusion and type Ib endoleak. Zenith stent-grafts comprised 59% of the endovascular arm of the EVAR trial (200) where the incidence of limb thrombosis was more than three times that observed in Talent devices (3.5 vs 1.1%). This also suggests that Zenith limbs may be less resilient to kinking caused by native vessel anatomy or movement at the distal seal-zone. All of the fenestrated

stent-grafts used in the current study included the 'TFLE' limb as illustrated in Figure 6.17A. More recently this has been superseded by the Spiral-Z limb (Figure 6.17B). The proximal and distal sealing stents are still of the same 'z' formation stainless steel construction but supporting the middle is a continuous spiral nitinol stent designed to improve its conformability and address some of the shortcomings of the old limb as detailed above.

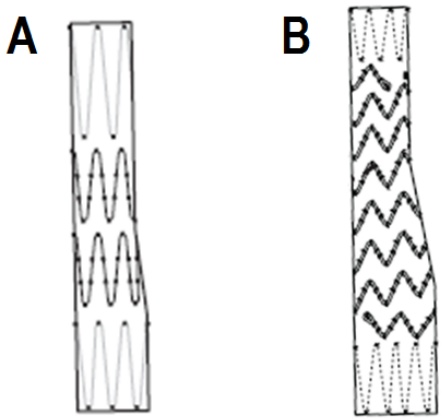

Figure 6.17 Zenith TFLE limb extension (A) and Spiral-Z ZSLE limb extension (B). Adapted from Cook Medical Inc. (72, 201)

The link between distraction force and graft-related adverse events could not be fully assessed because there were no type Ib endoleaks during the follow-up period. There were three late limb occlusions, one was in the migration group, one was in the no migration group and one in the ipsilateral limb of a distal body.

6.7.4 Limitations

A major limitation in this analysis was the small number of stent-grafts observed to have undergone movement, especially component distraction and migration of the distal limb extension seal-zone. Non-parametric statistical tests were used to limit the possibility of false positive results. The number of clinically significant complications was smaller still and no meaningful conclusions could be drawn from linking them with the magnitude of the total RDF. An alternative approach

would have been a case controlled study. Patients with proven migration, component distraction and graft-related adverse events could have been identified in advance and distraction force acting upon their stent-graft components then compared with a cohort of patient matched for demographics but without complications. A power calculation would have given an indication of the numbers required for such a study. The same patients could have been used for investigating the influence of morphological features upon distraction force as was described in chapter 5.

The definition of migration and component distraction was based on the accuracy of a validated technique. The figure of 4mm may result in clinically significant problems in relation to the proximal seal-zone and target vessel compromise but it is probably insignificant in the context of the proximal-distal body junction and the distal seal-zone of the limb extension. Within the confines of this study it was not possible to determine whether a small amount of movement predicts later, larger migration or distraction.

6.7.4.1.1 Local factors

No mechanical properties of the aorta were analysed but other studies suggest that higher pressure in the aneurysm sac such as the presence of an endoleak may reduce distraction force acting on the stent-graft and thereby convey some protection against migration (162). Fifteen of the 43 patients included in the proximal body migration analysis had an endoleak diagnosed during follow-up (14 type II and two type IIIa with one patient having both). There was no difference in the incidence of endoleak between migration and no migration groups (n=3 vs 12, p=.619, Fisher's exact test).

6.7.4.1.2 Boundary conditions

A single preoperative systolic blood pressure may not be indicative of prevailing physiological conditions following fenestrated endovascular aneurysm repair but a more robust measure of blood pressure was not available. An alternative

would have been to use 160mmHg for hypertensive patients and 120mmHg for normotensive patients but this approach would not have taken into consideration those patients with well controlled hypertension or those with undiagnosed hypertension. The use of preoperative blood pressure in simulations may have resulted in either an increase or a decrease in the difference between total RDF in the migration/component distraction and non-migration/component distraction groups.

As discussed in chapter five, steady state CFD simulations may underestimate distraction force by a small margin as compared with results obtained using pulsatile flow (see Validation, section 5.5.3).

6.8 Conclusion

This chapter has examined the relationship between patient-specific total resultant distraction force and movement of stent-graft components. Results suggest that movement at all three sites (caudal migration of the proximal seal-zone, component distraction at the proximal-distal body junction and cranial migration at the distal seal-zone) may occur at distraction forces lower than the experimentally derived fixation force.

Although there was a trend towards greater distraction forces in the proximal bodies that underwent migration this lacked statistical significance. No association was found between total resultant distraction force in distal bodies and the incidence of component distraction. Shorter available appositional overlap was significantly associated with component distraction, suggesting that the strength of fixation may be more important than distraction force at this site. Fixation force is increased with maximal overlap and the results support using the longest length of proximal body possible with maximum component overlap.

In limb extension components greater distraction force was significantly associated with cranial migration at the distal seal-zone. Results suggest that caution should be employed when planning to achieve distal seal in large calibre, ectatic iliac vessels. It is likely that such morphology will be associated with greater distraction force and may also be more likely to continue to dilate over time with subsequent increases in distraction force and compromise of fixation.

With regards to the second hypothesis, only in limb extension components was greater distraction force significantly associated with a higher incidence of migration.

7 Discussion

Device failure leading to reperfusion of the aneurysm is one of the biggest concerns following endovascular aneurysm repair. Movement of the stent-graft may lead to device failure and in *fenestrated* endovascular aneurysm repair this may carry the potentially serious added consequence of visceral vessel loss.

Fixation force resists movement of the stent-graft and hence protects against one mode of device failure. The strength of fixation is dependent upon the mechanical properties of the sealing stents and the presence of ancillary features such as hooks or barbs. Acting against the fixation force is the haemodynamic distraction force generated by blood pressure and blood flow. A greater understanding of the factors that contribute to distraction force should help to inform the clinician during the planning stage and help to avoid high-risk solutions that might predispose to device failure.

Chapter three set out the rationale for choosing the approach undertaken in this study both in terms of which factors to investigate and the methods used to assess them. Morphological features were investigated based on evidence from previous experimental, analytical and computational fluid dynamics models. The use of CFD enabled blood flow through complex patient-specific three-dimensional morphology to be modelled accurately and efficiently.

To enable lumen and stent-graft morphology to be compared with force results a reliable and reproducible method of measurement had to be devised. Cross-sectional area was easily measurable using software tools and although similar tools existed for the measurement of angulation, there was no common agreed method for their deployment. Chapter four defined one method of angle measurement and assessed it against another common method used in the planning stage of endovascular aneurysm repair. This new method was then

developed further with previous analytical and computational analyses of distraction force in mind for use in chapter five.

The CFD simulations in chapter five were performed at constant blood pressure and volumetric flowrate. They confirmed that cross-sectional area was the major contributing factor to distraction force. This factor was by no means the only important factor otherwise Figure 7.1 would show all the data points equal to unity. The significant variation from unity (up to 600%) confirms that other parameters do indeed influence the distraction force.

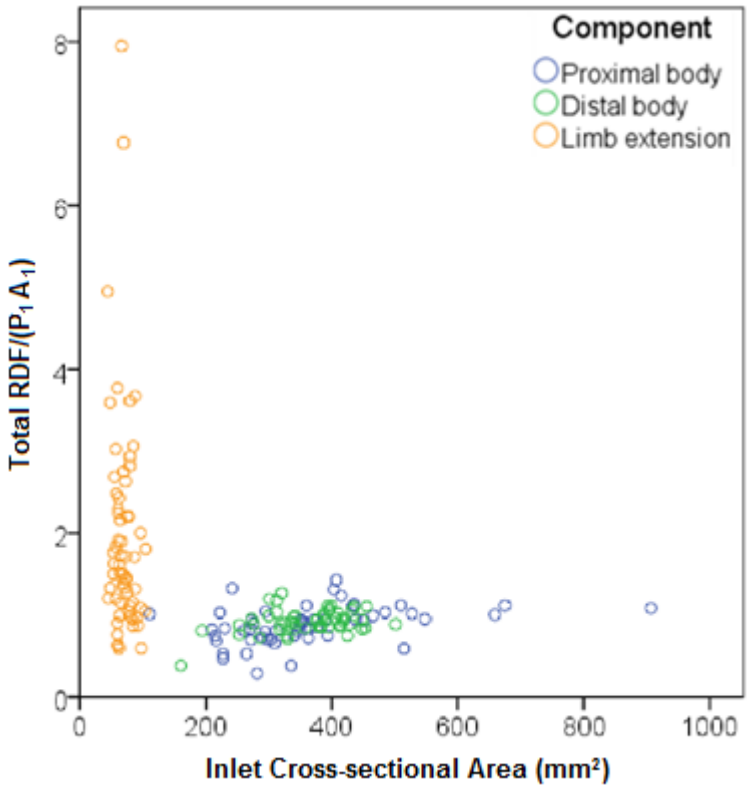

Figure 7.1 Plot of total resultant distraction force (RDF) normalised by the product of inlet pressure (P_1) and cross-sectional area (A_1).

The Bernoulli and continuity equations relate the inlet and outlet pressures and velocities of blood flow (43, 44, 202). Together they form the basis of a simple analytical model for determining distraction force (equation 3.1). From this analytical model it can be seen that distraction force is determined by: Inlet

pressure (P_1), inlet cross-sectional area (A_1), blood density (ρ), inflow velocity (U_1), outlet cross-sectional area (A_2), and outlet angle (θ). The only term not represented is viscosity but since this – as well as blood density, inlet volume flow rate (A_1U_1) and pressure – was kept constant for the CFD analysis, the remaining variables (all morphological terms A_1, A_2 and θ) must have been responsible for the variation in total resultant distraction force.

The relative importance of blood pressure was highlighted by the comparison of CFD results from chapter five at 21332Pa (160mmHg) with the same simulations at 18665Pa (140mmHg). By increasing the pressure by 20mmHg, the total resultant distraction force was increased by a factor of 1.14. This suggests that control of hypertension should remain an important objective even after aneurysm exclusion.

7.1 Limitations of the current study

7.1.1 Orthogonal versus resultant distraction force

Both migration and component distraction occur along the vessel lumen (i.e. orthogonal to the seal-zones of the stent-graft) yet only part of total RDF acts along this plane. Might this component of total RDF be more pertinent when considering migration and component distraction? In order to calculate this force the *x*, *y* and *z* directional forces have to be translated based upon the angle of each component's seal-zone from the vertical in coronal and sagittal elevation. In terms of the proximal body, this angle would be identical to α angle if the lumen of the distal thoracic aorta was precisely vertical within the computer generated model. *X* and *z* direction forces could be translated first using equation 7.1. This would give the component of distraction force acting along the seal-zone in coronal elevation (z_l):

$$z_I = z\cos\tau + x\sin\tau \quad (7.1)$$

This translation has been applied to the proximal body of fEVAR 12 in Figure 7.2 where the axis of blood flow within the proximal seal-zone is 35° anticlockwise from vertical. Applying equation 7.1 gives a coronal distraction force orthogonal to this proximal seal-zone (z_I) of 4.4N.

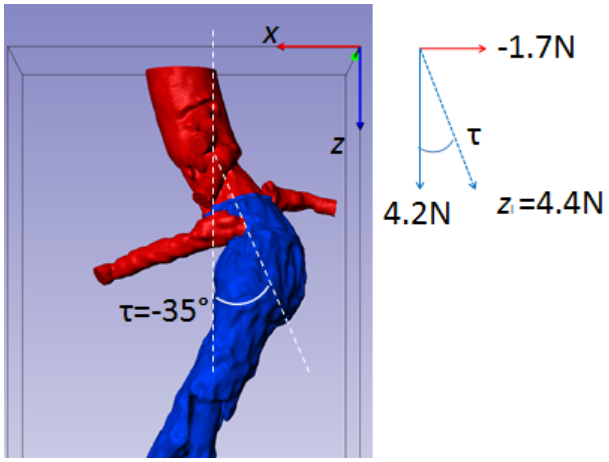

Figure 7.2 Translation in coronal elevation for proximal body (blue) of fEVAR 12. Red=lumen

z_I could then be used to translate the sagittal forces and calculate total orthogonal distraction force (z_{II}) using equation 7.2:

$$z_{II} = -y\,sin\,\varphi + z_I\,cos\,\varphi \quad (7.2)$$

Figure 7.3 shows equation 7.2 applied to the same proximal body in sagittal elevation. The total orthogonal distraction force (z_{II}) was 6.8N.

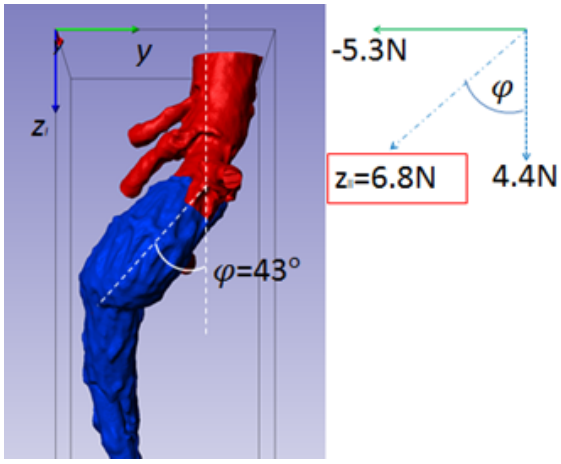

Figure 7.3 Translation in sagittal elevation for proximal body (blue) of fEVAR 12. Red=lumen

A similar set of equations can be applied to the *x*, *y* and *z* directional results for fEVAR 12 to show the magnitude (*z*) and direction (τ/φ) of the *resultant* forces in each elevation. Figure 7.4 shows a resultant force in coronal elevation of 4.5N acting at -22° from the *z* direction. These figures were obtained using the equations 7.3 and 7.4.

$$z_C = \sqrt{x^2 + z^2} \tag{7.3}$$

$$\tau = \tan^{-1}\left(\frac{x}{z}\right) \tag{7.4}$$

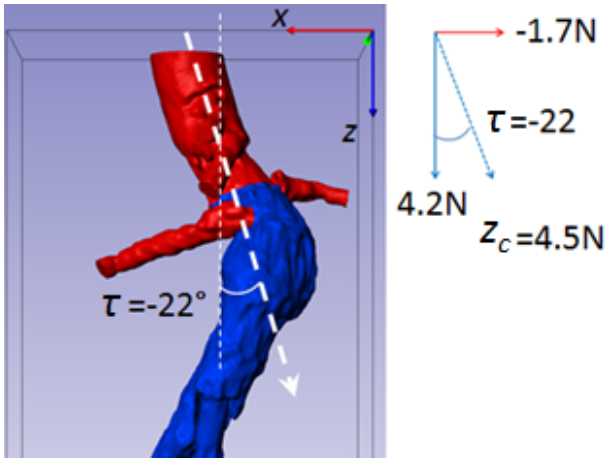

Figure 7.4 Magnitude and direction of coronal distraction force was similar to orthogonal coronal distraction force shown in Figure 7.2

Using the following two equations (7.5 and 7.6), the magnitude and direction of the total resultant distraction force can be resolved in the sagittal elevation.

$$z_S = \sqrt{{z_C}^2 + y^2} \tag{7.5}$$

$$\varphi = \tan^{-1}\left(\frac{-y}{z_C}\right) \tag{7.6}$$

These calculations are shown in Figure 7.5.

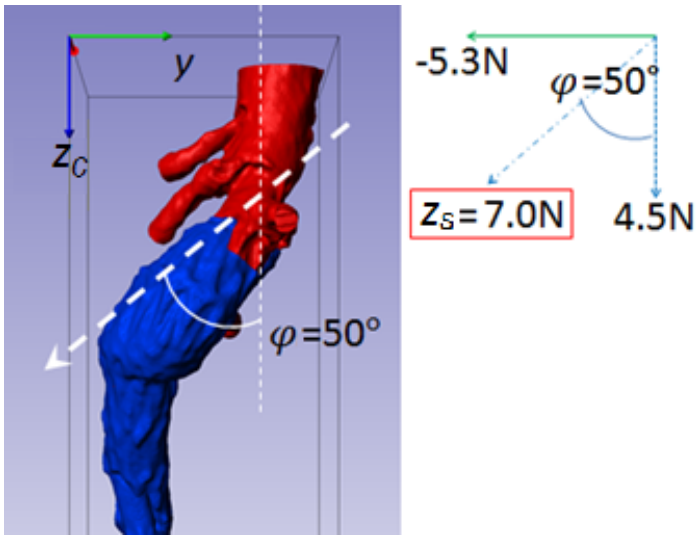

Figure 7.5 Magnitude and direction of total resultant distraction force shown in sagittal elevation was similar to the total orthogonal distraction force depicted in Figure 7.3

The magnitude and direction of resultant distraction force (7N acting at 50° to the vertical *z* axis) was very similar to the orthogonal forces obtained with equations 7.1-7.2 (6.8N at 43°). This confirms that most of the distraction force *did* act along the axis of blood flow at the seal-zone of the proximal body as was also noted by Molony *et al.* (165). The use of total orthogonal distraction force instead of total resultant distraction force therefore may not have made much difference to the results.

7.1.2 Measurement error

Any study that defines vessel angulation as a variable is limited by the method it uses to measure the angle or angles. In the current study attempts to identify potential weaknesses in the current methods of angle measurement were made and a new method was clearly defined before comparison with the old one. Error was minimised by clear definitions of angles and by the same observer taking all measurements. All images were manipulated in exactly the same way and there was a clear protocol for application of computerised calipers.

Because a small change in the placement of calipers may produce a relatively large variation in angle, all angles were compared in groups with relation to distraction force rather than as a continuous variable.

Sources of error in the measurement of XSA have been discussed in chapter five (section 5.8). These include the necessary use of a different method of measuring limb extension inlet XSA due to the close proximity of the other limb; the potential influence of metal artefact in underestimating the lumen XSA at this position and the potential overestimation of lumen XSA due to the modelling method as illustrated in Figure 5.17.

7.1.3 CFD analysis

Every effort was made to ensure realistic boundary conditions were used. This included the use of supracoeliac flow data from the investigational work performed at Stanford University (191, 192). The validity of a 'snapshot' preoperative systolic blood pressure is unknown but a more reliable measure of blood pressure was not available. The choice of a standard flow rate rather than standard velocity (velocity was calculated from the average orthogonal cross-sectional area at the model inlet divided by the flow rate) was intended to standardise as many variables as possible in order to best elucidate the effect of vessel geometry upon distraction force.

Steady-state blood flow was used rather than pulsatile flow. Previous experience with experimental models suggests that results are less than 10% higher at any given time along a pulse wave in pulsatile flow models compared with steady-state models. The difference was largest at peak systole due to the inertial effect of the pressure waveform (see Validation, section 5.5.3).

The current results represent a flow analysis of the fluid domain only. No biomechanical characteristics of the aneurysm sac or stent-graft were modelled. Previously published fluid/structure interactions have suggested a protective effect of type II endoleak in reducing distraction force (41, 162) and a negligible effect with the addition of stent-graft compliance (158, 178).

The use of a Newtonian fluid model, the assumption that all forces were transmitted through the overlapping parts of the stent-graft and the exclusion of visceral stents from the stent-graft models due to limitations in CT imaging resolution are limitations that would have only affected the shear/viscous flow derived forces and therefore would not have had a significant effect upon the results.

7.2 Further studies

7.2.1 Expanding the role of computer models

Previous work suggests that β angle and iliac tortuosity may reduce following standard EVAR deployment (190, 203). Conversely the diameter of the proximal seal-zone may increase by approximately 2mm in the first two years (204). Confirmation of how fenestrated stent-graft deployment affects blood vessel morphology could be obtained from pre and post-deployment CT images using the measuring methods developed for the current study. More complete data quantifying the effect of stent-graft deployment upon vessel morphology may facilitate the development of realistic 'virtual' stent-graft models enabling a

clinician to plan and deploy a stent-graft based on computerised models of the preoperative CT images. Recent studies have simply added a virtual stent-graft to a vessel lumen without taking into account what affect this may have on angulation and tortuosity (205). Simulator practice prior to undertaking the real intervention improves performance in endovascular procedures (206, 207) and benefits may be maximised by providing the most realistic simulator possible.

If the morphological changes following fEVAR can be anticipated it is also conceivable that CFD based upon these virtual models would allow accurate predictions of distraction force to be made *prior* to deployment. This could assist the clinician to choose alternative treatment modalities in high-risk morphology or ensure close follow-up of stent-grafts exposed to greater distraction force.

A mechanical solver that models the biomechanical properties of the aorta and stent-graft could be linked to the fluid solver used in the current studies. This may lead to a more accurate representation of patient-specific conditions but would be more complex to perform and may not significantly change any of the results obtained via fluid simulation alone (158, 178).

7.2.2 Distraction force prediction

Another option for prediction of distraction force would be to input morphological data in to the analytical model (equation 3.1). In simplified geometry the error between this approach and CFD is less than 2% however in complex three-dimensional anatomy the error may be much greater due to out-of-plane forces. To address this, the one-dimensional analytical model could be developed further. Equations 7.7-7.9 represent a proposed three-dimensional analytical model for total distraction force (*f*), inclusive of pressure and flow derived forces in *x, y* and *z* directions.

$$fz = P_1A_1 - P_3A_3\cos(\theta_{3x}) - P_2A_2\cos(\theta_{2x}) + \rho(U_1A_1)[-(U_3\cos(\theta_{3x}) + U_2\cos(\theta_{2x}))+U_1] \quad (7.7)$$

$$fx = P_2A_2\sin(\theta_{2x}) - P_3A_3\sin(\theta_{3x}) + \rho(U_1A_1)(U_2\sin(\theta_{2x}) - U_3\sin(\theta_{3x})) \quad (7.8)$$

$$fy = P_2A_2\sin(\theta_{2y}) - P_3A_3\sin(\theta_{3y}) + \rho(U_1A_1)(U_2\sin(\theta_{2y}) - U_3\sin(\theta_{3y})) \quad (7.9)$$

Where $U_2 = \frac{\frac{U1A1}{A2}}{2}$ and $U_3 = \frac{\frac{U1A1}{A3}}{2}$ and θ_2 and θ_3 refer to the left and right outlet angles in the coronal (*x*) and sagittal (*y*) elevation respectively.

fz can be solved for *x* as well as *y* angles and the difference between this force in each elevation is greater with larger differences in outlet angulation. Resolution of this problem was beyond the scope of this thesis and therefore a comprehensive comparison between 3D analytical model and CFD was not performed. An additional consequence of this was that the angle measurement technique described in Chapter five, designed to allow comparison in three-dimensions became obsolete. One angle per data point (instead of two) would therefore have been sufficient. This would not have given any information regarding the position of one outlet with regards to the other but would have made data analysis simpler. The 3D caliper used in the initial angle measurement study (see chapter four) would have provided this information and would have removed the potential error introduced by image manipulation prior to angle measurement in each elevation. This error was reduced in the current study by clearly defining the method to be used (see section 5.5.5.2).

A much simpler analytical model could be derived by combing the regression analysis in section 5.7.4. with equation 6.2 after first substituting P_1 (18665Pa) for P_2 (21332Pa). The only patient-specific parameters required would be the

predicted post-deployment cross-sectional area of the inlet and outlets, the largest outlet angle and the systolic blood pressure.

7.2.3 Expanding the current CFD methods to other stent-grafts

Since the start of this project other manufacturers have developed solutions for aneurysms with necks that are unsuitable for standard endovascular repair. One such device is the Nellix endovascular aneurysm sealing system from Endologix Inc., Irvine, USA. This consists of a polymer-filled endobag that sits within the aneurysm sac to provide fixation for two ePTFE-covered, cobalt chromium alloy balloon-expandable stents, each with little or no tapering between proximal and distal ends (see Figure 7.6). One retrospective review showed that it was suitable for use in more infrarenal aneurysms than any other manufacturer's standard stent-graft system (i.e. Cook, Zenith; Medtronic, Endurant and Gore, C3 Excluder) (208). Although it was only applicable to 8% of the aneurysms treated with fenestrated stent-grafts the original IFU is already being extended (209, 210). In the future it may offer a method of treating juxtarenal aneurysms without the need for complex EVAR planning or custom-made stent-grafts.

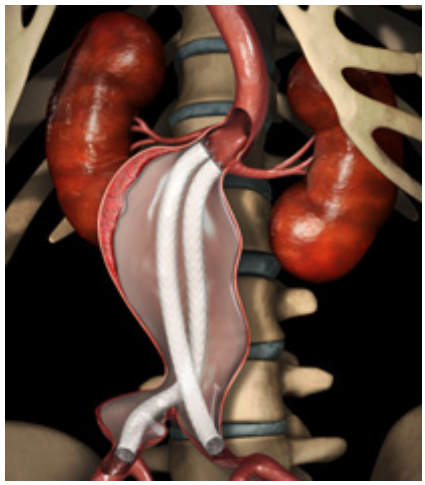

Figure 7.6 Nellix endovascular aneurysm sealing system.
Image from Endologix Inc. (211)

The design of the Nellix stent-graft represents a major change in approach to the issue of endovascular fixation and - given that the proximal inlet XSA of each conduit is much smaller that the Zenith device - it would be very interesting to determine the distraction force acting upon its components and compare it with the current work on the Zenith device. The modelling and CFD method described in Chapter five could be applied for this purpose.

7.2.4 Verifying fixation force

Median distraction force acting on limb extension components was 2.9N (range 2.7-6.3N). The distal fixation force was 9.6N +/-1.5N (84) yet four limbs migrated. Although all proximal and distal bodies that underwent migration and component distraction were also below the experimentally derived fixation forces, four components in the no migration groups (one proximal body and three distal bodies) were exposed to forces higher than this. In these two other components the discrepancy between distraction and fixation force was not as marked: Median total RDF in migrated proximal bodies 5.6N (range 1.7-8.6N) versus 11.5N +/-1.5N fixation force (123) and median total RDF in distracted distal bodies 4.3N (range 2.8-4.7N) versus 6.5N (4.8-7.2N) fixation force (195). This finding suggests that especially in regards to limb extension components, the reported fixation force may be too high and would support further investigation with additional pullout studies in porcine or cadaveric arteries.

7.3 Conclusion

7.3.1 Hypothesis 1

Larger angulation of vessels is associated with greater distraction force.

Only outlet (θ) angulation in complete stent-grafts and limb extension components was associated with greater distraction force. Inclusion of the largest θ angle also improved the predictive power of the regression analysis for distraction force acting on distal bodies.

The work outlined in this thesis is the first time that individual components of a stent-graft have been considered within a CFD analysis of distraction force. The results from this study thus enable the precise elucidation of which morphological factors are important in the generation of distraction force in each case. This comprehensive approach was chosen for the underlying reason that movement is possible at all component junctions. By focusing on the components in this way and defining more specific angles than in many previous analyses, hypothesis one has been tested in more depth than has hitherto been possible in the literature. This method provided the detail to be able to define inlet or outlet cross-sectional areas as the most important determinant of distraction force depending on which component was being considered. It also allowed a distinction to be made between the caudally directed forces acting on proximal and distal bodies with the more out-of-plane and cranial direction of force acting on limb extensions.

7.3.2 Hypothesis 2

Greater distraction force is associated with higher incidence of migration and component distraction.

The results of chapter six show the link between greater distraction force and migration of limb extension components. This intuitive link was not present in the migration of proximal body components perhaps due to the confounding effect of the many available configurations of stented fenestrations and scallops. Similarly it was not present in distal body components where it seems that the strength of the fixation as provided by overlap of components may be of more significance.

This is the first time that *in silico* distraction force results have been compared with migration and distraction analyses. The approach has enabled the cranial direction of distraction force in limb extensions to be directly related to their migration in the same direction.

8 Appendices

8.1 Planning document for Zenith fenestrated endovascular stent-graft

COOK MEDICAL

Zenith Fenestrated

FAX COMPLETED FORMS TO:
COOK AORTIC INTERVENTION PRODUCTS (EUROPE) +45 56868528

ALL information must be complete.

Date: _____ Patient ID: _____
Hospital: _____ Physician Name: _____
Physician Signature: _____ Physician Phone #: _____
Physician E-mail: _____

PROXIMAL BODY

One Internal Sealing Stent **or** **Two Internal Sealing Stents**

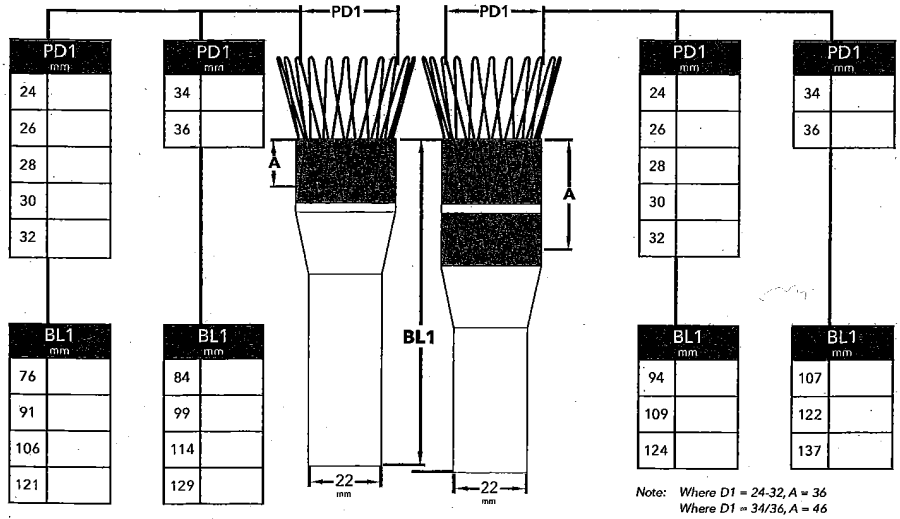

Note: Where D1 = 24-32, A = 16
Where D1 = 34/36, A = 21

Note: Where D1 = 24-32, A = 36
Where D1 = 34/36, A = 46

Proximal Main Body Order Number

ZFEN-P- ☐ - ☐☐ - ☐☐☐
(1) (2) Sealing Stents — PD1 — BL1

WILLIAM COOK EUROPE ApS
Sandet 6, DK 4632
Bjaeverskov, DENMARK
Phone +45 56868686
www.cookmedical.com

Page 1 of 3

AI-BOUSF-FENSZOOF-EN-201101

Patient ID: _____

CLOCK POSITION

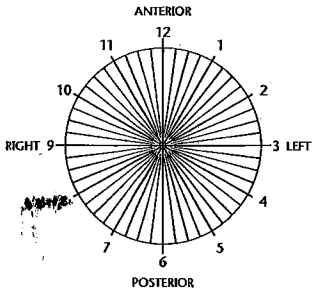

Clock positions are in 15 min increments.

GENERAL NOTES

Maximum number of fenestrations is 3. Maximum number of any particular type of fenestration is 2.

Bottom edge of all fenestrations must be within "A" dimension (see page 1). All measurements are in mm.

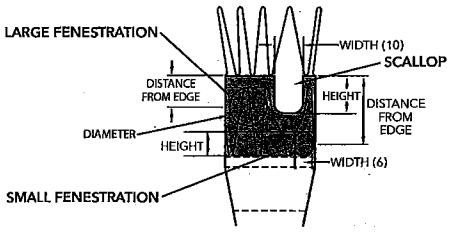

Internal Aortic Diameter	

REINFORCED SCALLOP FENESTRATION

All scallops are 10 mm wide.
Height ranges from 6 to 12 mm.

	#1	#2
Height		
Clock Position		

REINFORCED LARGE FENESTRATION

Diameters are 8, 10 or 12 mm.
Stent struts may cross large fenestration.
Distance from center to edge must be ≥ 10 mm.

	#1	#2
Diameter		
Clock Position		
Distance from Edge		

REINFORCED SMALL FENESTRATION

All small fenestrations are 6 mm wide.
Heights are either 6 or 8 mm.
Distance from center to proximal edge must be ≥ 15 mm.

	#1	#2
Height		
Clock Position		
Distance from Edge		

ALPHA CODE - ☐☐☐☐-☐☐☐☐-☐☐☐☐-☐☐

(For Cook internal use only)

WILLIAM COOK EUROPE ApS
Sandet 6, DK 4632
Bjaeverskov, DENMARK
Phone +45 56868686
www.cookmedical.com

AI-BOUSF-FENSZDOF-EN-201101

Patient ID: _____

DISTAL BODY

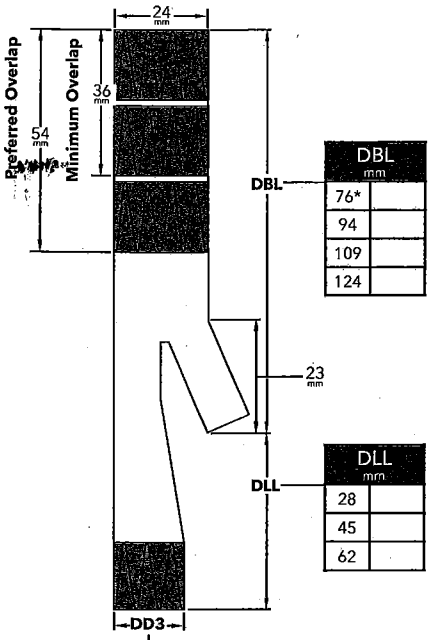

DBL mm	
76*	
94	
109	
124	

DLL mm	
28	
45	
62	

DD3 mm	
12	
16	
20	
24	

NOTE:
24 is not available
when DLL = 28 mm

CONTRALATERAL LEG

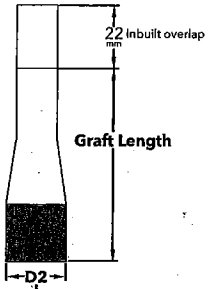

Contralateral Graft Diameter	
9	
11	
13	

Contralateral Graft Length	
39	
56	
74	
90	
107	
122	

Contralateral Graft Diameter	
16	
20	
24	

Contralateral Graft Length	
39	
56	
74	
90	

Distal Bifurcated Main Body Order Number

ZFEN - D - ☐☐ - ☐☐ - ☐☐☐
(DD3 - DLL - DBL)

Contralateral Iliac Leg Order Number

ZSLE - ☐☐ - ☐☐☐ - ZT
(Contralateral Graft Diameter - Contralateral Graft Length)

WILLIAM COOK EUROPE ApS
Sandet 6, DK 4632
Bjaeverskov, DENMARK
Phone +45 56868686
www.cookmedical.com

*Two internal sealing stents only.

AI-BOUSF-FENSZDOF-EN-201101

8.2 Instructions given to observers for α angle measurement using ScanIP

Terminology: All angles are made up of two *rays* that intersect at a *vertex*. For accurate angle measurement each ray must have a specified *endpoint* and be measured along a central luminal line (CLL).

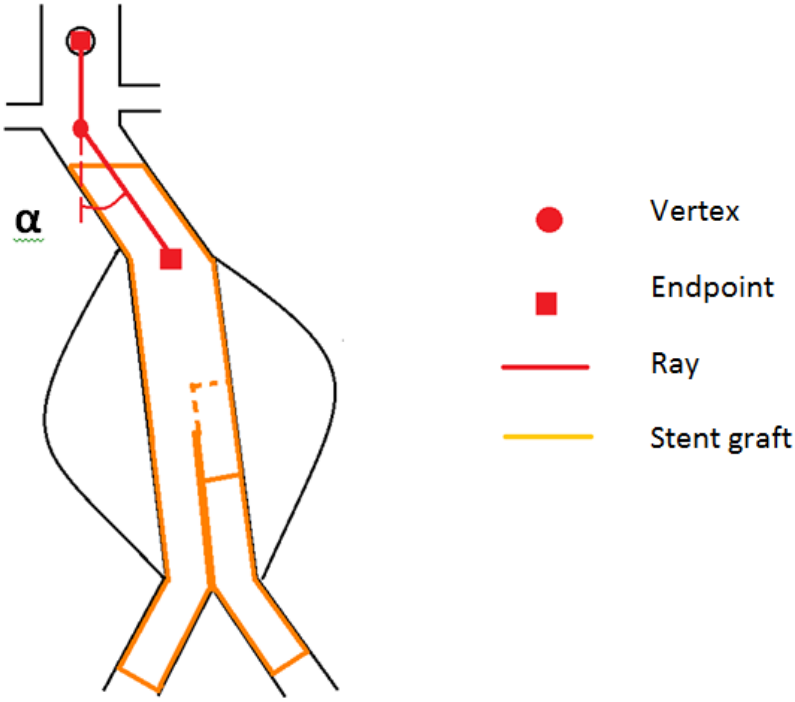

Supplementary angles are used (as opposed to inner or outer angles) as they represent blood flow in terms of deviation from 180°. A supplementary angle of 30° is equivalent to an inner angle 150° or an outer angle of 210°.

For the purpose of this study only α angle will be measured i.e. a proximal angle at or near the lowest renal artery that describes the angle of the aneurysm neck from the suprarenal aorta. In a post EVAR aorta the α angle would be at or just proximal to the proximal seal-zone.

The following points should be observed:

Proximal endpoint	**Vertex**	**Distal endpoint**
Where CLL of SMA joins aortic CLL	Major angulation of CLL nearest the lowest renal artery	Next major point of angulation or most distal extent of aneurysm neck

Step by step instructions for measuring α angle using ScanIP

1. Use the mouse to manipulate the model around the longitudinal axis of its lumen. Try to identify the likely position of the α angle vertex.

'Left click': rotates image; 'Scroll wheel': zooms in or out; 'Middle click'/clicking down scroll wheel and move: moves object around

The lumen model of 'exampleAAA' is shown below. The α angles appears quite small but there is a slight antero-(right)lateral deviation of the infrarenal aorta from the course of the suprarenal aorta which in itself angles anteriorly. This occurs at the point marked by the white arrow (the α angle vertex) just below the lowest renal artery.

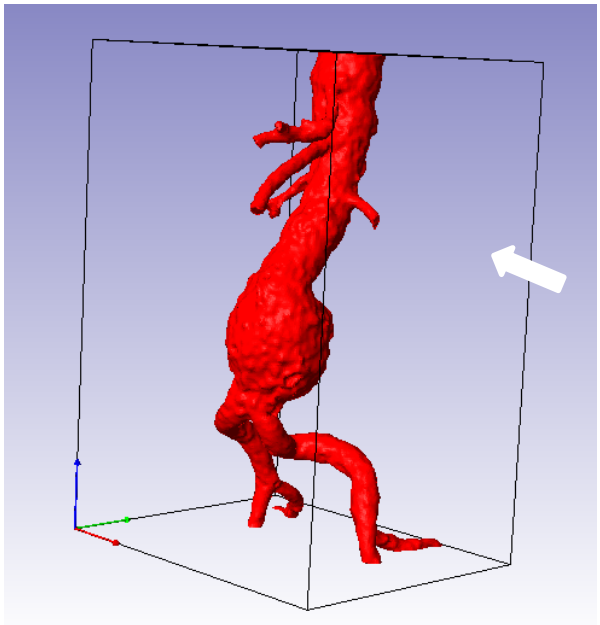

2. *Right click* on the 3D model to bring up the following box:

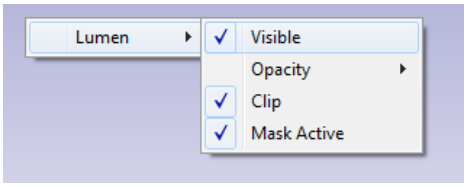

Hover the mouse over 'lumen' and *left click* over 'visible' to turn the view of the lumen off. This should bring the Centre Lumen Line (CLL) into view.

3. Left click on the measurements icon  in the second row from the top of the screen. A measurement toolbox should appear on the left hand side.

4. Select the angle measurement tool  from the measurement toolbox and the select 3D mode  which should make the angle measuring tool visible in the 3D pane.

5. *Right click* on 'Angle (deg)', hover over 'Set angle type' and *left click* to select 'Supplementary angle'

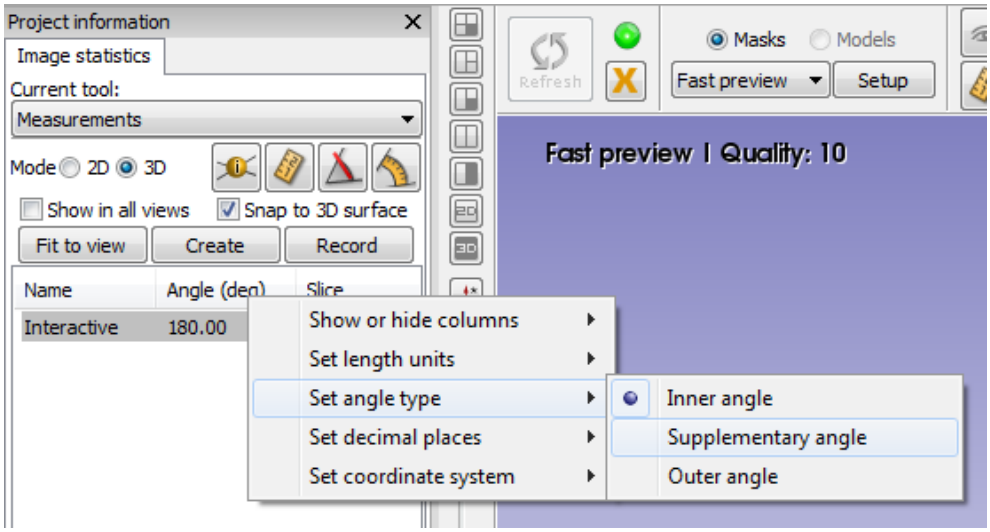

The angle measuring tool has proximal and distal endpoints plus a vertex that need to be 'snapped' onto the appropriate points along the aortic CLL.

6. Drag the proximal endpoint to near the SMA origin then zoom in to make placement more accurate. You should chose a point on the aortic CLL that best represents the origin of the SMA based on the direction of the SMA CLL.

In the diagram below the direction of the SMA CLL indicated by the green arrow suggests that either point 1 or 2 would be appropriate proximal endpoints.

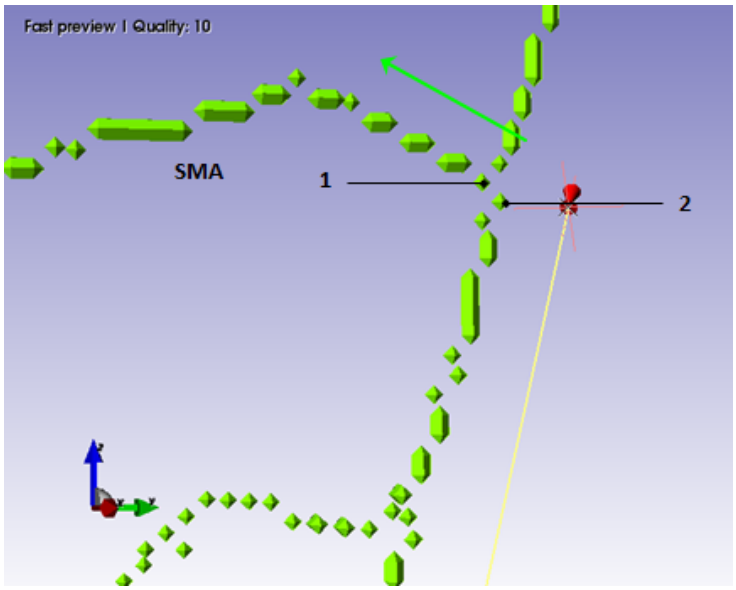

7. Drag the proximal endpoint marker to the chosen point (in the diagram below point 2 has been chosen). Release the left mouse button and the crosshair will change from red to green if it has been successfully 'snapped' to the CLL.

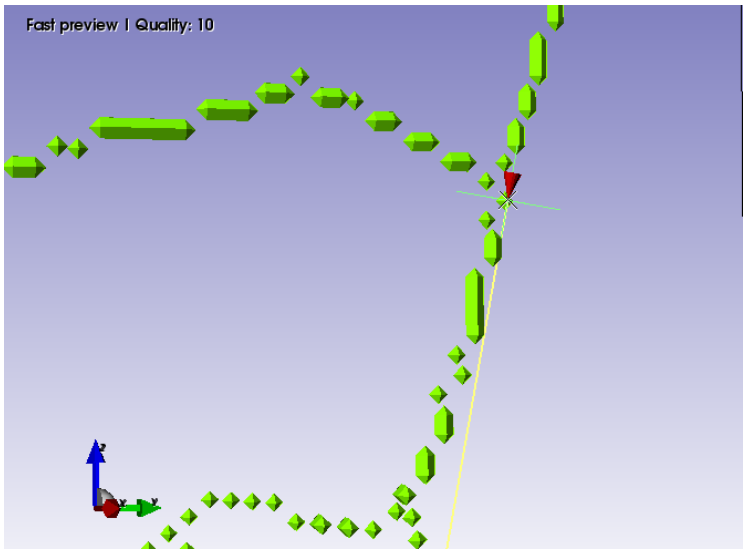

8. Zoom out to locate the vertex marker (black arrow)….

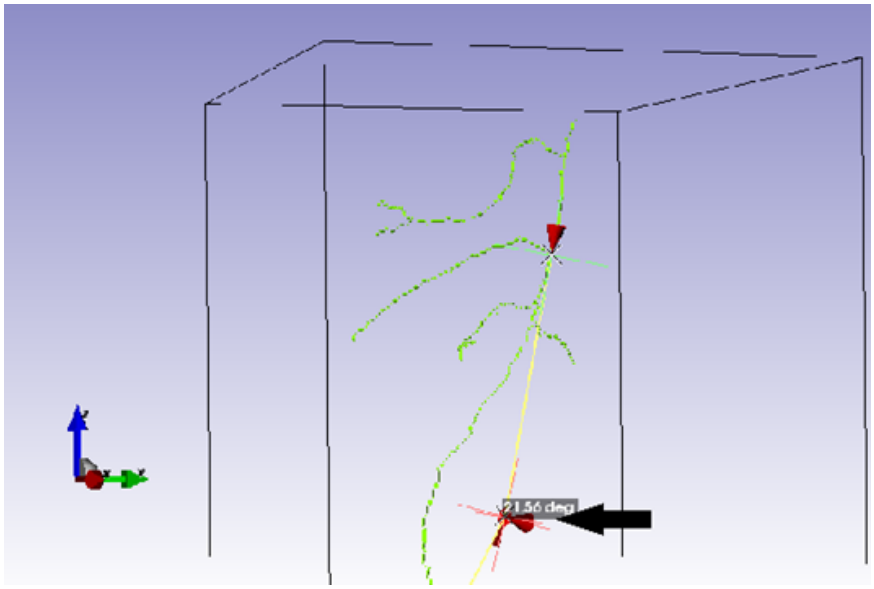

….drag it close to the lowest renal artery.

9. Zoom in and chose a suitable point to snap the vertex marker to. Based on our initial observations of the lumen model the α angle vertex looked to be just distal to the lowest renal artery. In the diagram below the point has been chosen to mark the α angle vertex.

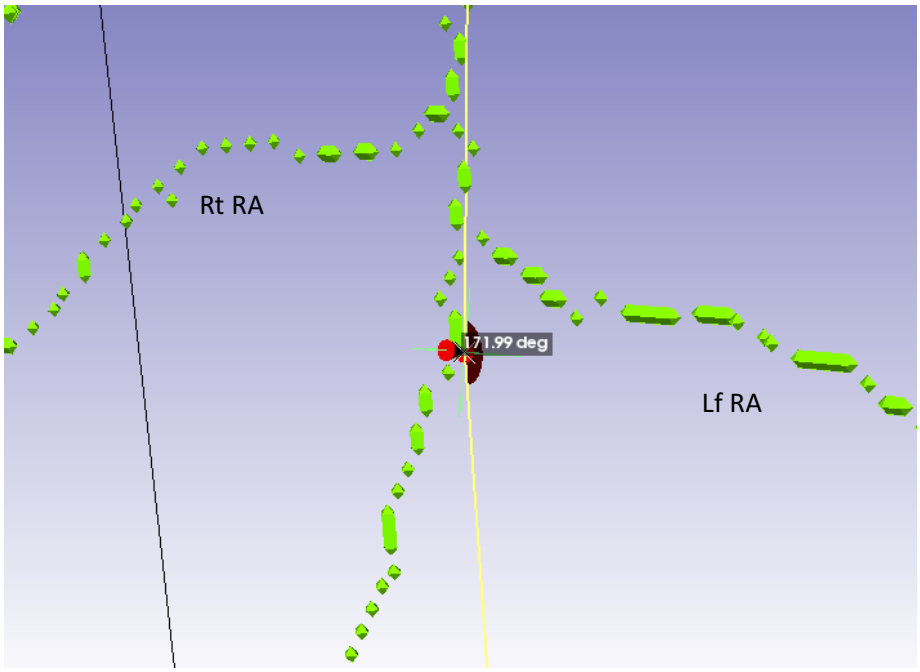

10. Repeat this process with the distal endpoint. You may need to *right click* on the 3D image and set 'visibility' to 'on' for the lumen model to remind yourself where the distal endpoint should be.

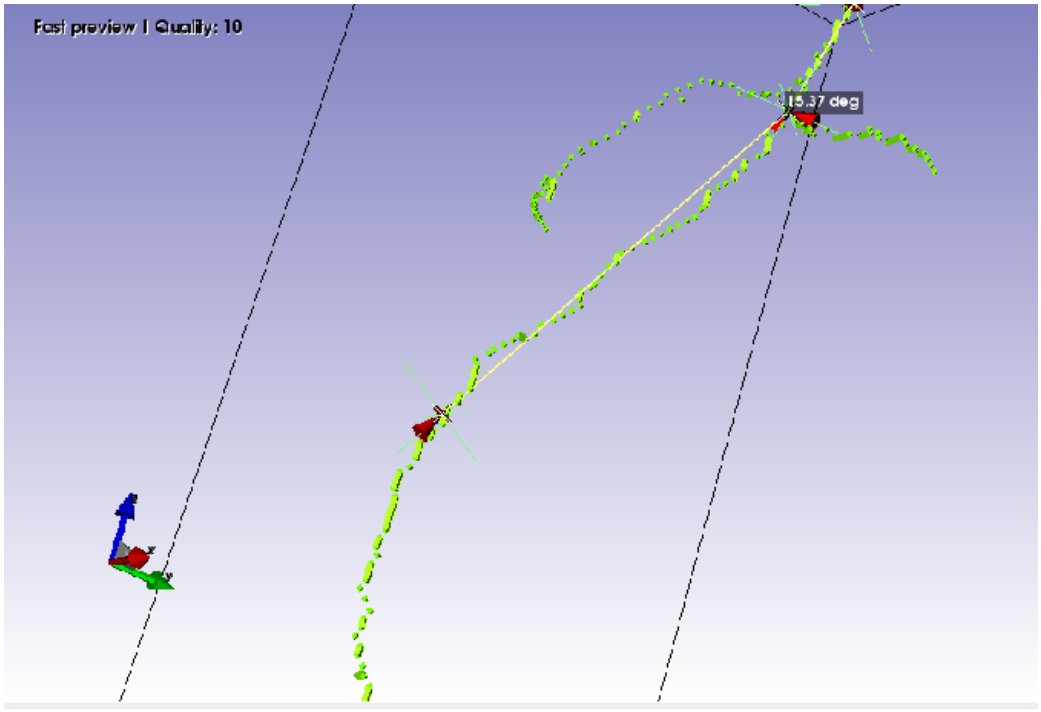

The rays (yellow lines) of the angle measuring tool should be a good fit to the course of the aortic CLL but do not have to exactly overlie every green marker.

11. Record the supplementary α angle (approx. 17-18° for 'exampleAAA') then right click on the temporary angle name to rename using the following nomenclature

EVAR/INITIALS/angle

E.g. I would rename the α angle measurement from EVAR 1 as 1SMJa

Angle Measurement with Leonardo

Consider the α angle in exactly the same way as above. Use your usual method for angle measurement with the following points in mind:

1. Whilst profiling the neck in the usual way ensure the blue box (bottom left) is also enlarged and that the blue crosshairs are moved to mark the level of the lowest renal artery.
2. Identify the intended site of the α angle vertex
3. Use the 'Angle' tool found in the 'Tools' menu. Ensure maximum length of lumen is demonstrated proximal and distal to the vertex and apply the tool to the centre of the lumen in either red or green boxes depending on which shows the larger angle. The proximal endpoint should be the approximate position of the SMA and the distal endpoint: the distal extent of aneurysm neck or the next major angulation along the centreline.
4. Record the angle: Highlight the box chosen for the angle measurement. Go to 'edit' and 'copy'. Press the windows key and under programmes open 'Paint'. Paste the image and save as file name: Number of EVAR/INITIALS/angle
e.g. 1SMJa

8.3 Validation of multiple stent-graft territories versus single component models

8.3.1 Aim

Section 5.5.1 described the model making process in full. Section 5.5.1.2.5 outlined how the number of simulations could be reduced four-fold by representing all stent-graft components on the same lumen. To confirm that this approach did not introduce bias a direct comparison was made between the two model techniques.

8.3.2 Method

Separate models for each component of fEVAR 18 were constructed in the same way as described in section 5.5.1. This approach yielded four models: A complete stent-graft, proximal body, distal body and limb extension model (see Figure 8.1).

One further model was constructed using the combined ROI approach described in section 5.5.1.2.5 (see Figure 8.1).

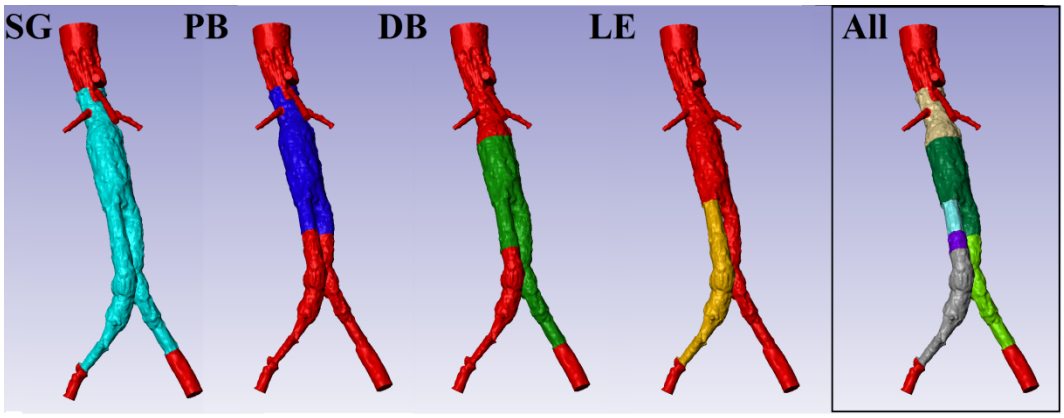

Figure 8.1 Separate models for each stent-graft component and combined ROI model

SG: Complete stent-graft, PB: Proximal body, DB: Distal body, LE: Limb extension, All: All components represented in combined region of interest approach.

CFD was performed for each model using the same boundary conditions as for previous simulations (i.e. blood viscosity 0.0033Pa.s and density 1098 kg/m^3 with a flow rate of 1.323x$10^{-4}$$m^3$/s). Blood pressure was set at 120mmHg (18665Pa).

8.3.3 Results

Table 8.1 shows the breakdown of all forces acting upon the single component and combined ROI models.

Table 8.1 Comparison between single component and combined ROI models

		Complete stent-graft		Proximal body		Distal body		Limb extension	
		Single component model	Combined ROI	Single component model	Combined ROI	Single component model	Combined ROI	Single component model	Combined ROI
x	pres	-0.063	-0.094	0.029	-0.020	-0.418	-0.400	-0.237	-0.226
	vis	-0.004	-0.004	0.001	0.001	0.005	0.005	-0.009	-0.009
	total	**-0.067**	**-0.098**	**0.030**	**-0.019**	**-0.413**	**-0.395**	**-0.247**	**-0.236**
y	pres	0.824	0.807	1.869	1.844	-1.813	-1.842	-0.484	-0.505
	vis	-0.003	-0.003	0.004	0.004	0.001	0.001	-0.005	-0.005
	total	**0.820**	**0.804**	**1.873**	**1.848**	**-1.811**	**-1.841**	**-0.489**	**-0.509**
z	pres	2.968	2.958	1.545	1.529	3.587	3.675	0.911	1.034
	vis	-0.041	-0.041	-0.014	-0.014	-0.023	-0.023	-0.020	-0.020
	total	**2.927**	**2.917**	**1.531**	**1.515**	**3.564**	**3.652**	**0.891**	**1.014**
Total RDF (N)		**3.04**	**3.03**	**2.42**	**2.39**	**4.02**	**4.11**	**1.05**	**1.16**
Error (%)			0.42		1.23		-2.23		-10.89

All of the difference in total RDF was due to pressure derived forces. Viscous friction forces were the same between all models.

8.3.4 Conclusion

Use of combined ROI models instead of single component models does not significantly affect distraction force results. The combined approach enables force results for all components of a fEVAR to be obtained with one simulation as opposed to four or more separate simulations. This saves a minimum of 12 hours of computational time per fEVAR. These results justify the use of combined ROI models.

8.4 Validation of model mesh complexity

8.4.1 Aim

When creating computer models of patient-specific aorto-iliac anatomy, regions of interest (ROI) segmented from CT images were converted into computer models by the process of meshing. This process was performed by ScanIP software (Simplware Ltd) and resulted in a 3-dimensional representation of the ROI built from smaller tetrahedral elements based on pre-set parameters. Free mesh algorithms were recommended for irregular biological morphology because they automatically use small tetrahedral elements to preserve fine detail and larger elements in areas that do not require detail to be preserved i.e. the centre of the lumen. Meshes that are too coarse potentially miss fine detail and may produce a poor representation of the actual anatomy. Meshes too complex require more processing power for both the meshing itself and the blood flow simulation. A balance must therefore be struck between accuracy and efficiency. The aim of this validation experiment was to assess the effect on distraction force of increasing mesh complexity.

8.4.2 Method

A patient-specific aorto-iliac ROI prepared using the method described in section 5.5.1 was meshed with standard settings recommended by the software provider with ‘compound coarseness’ set to -20 and then again with finer mesh parameters (compound coarseness=0).

Both standard and complex models were exported into FLUENT v6.2 (ANSYS Inc.) for blood flow simulation (see section 5.5.2). Mesh parameters were requested for each model including number of tetrahedral elements, number of faces comprising each model inlet and outlet and the actual surface area of the model inlet and outlets. Distraction force was determined for the distal body component and was compared between models.

8.4.3 Results

Table 8.2 shows mesh parameters for both the standard and complex model.

Table 8.2 Mesh parameters

	Standard mesh	Complex mesh
Total no. of tetrahedral elements	703287	2476618
No. of tetrahedral elements in lumen ROI	400882	1882302
No. of faces at model inlet **XSA (mm^2)**	1322 381	4996 382
No. of faces at right IIA outlet **XSA (mm^2)**	48 13	266 13
No. of faces at right EIA outlet **XSA (mm^2)**	124 47	873 47
No. of faces at left IIA outlet **XSA (mm^2)**	33 9	215 10
No. of faces at left EIA outlet **XSA (mm^2)**	124 42	802 42
No. of faces at right RA outlet **XSA (mm^2)**	24 6	141 7
No. of faces at left RA outlet **XSA (mm^2)**	37 7	166 7
No. of faces at SMA outlet **XSA (mm^2)**	44 19	431 20
No. of faces at CHA outlet **XSA (mm^2)**	26 12	271 12
No. of faces at SA outlet **XSA (mm^2)**	34 15	301 16

CHA: common hepatic artery, EIA: external iliac artery, IIA: internal iliac artery, SA: splenic artery, SMA: Superior mesenteric artery, RA: Renal artery

Table 8.3 Distraction force (N) acting on standard and complex models

		Standard Model	Complex Model
X	Pressure	0.968	0.960
	Viscous	0.006	0.006
	Total	**0.974**	**0.966**
Y	Pressure	-1.783	-1.776
	Viscous	-0.003	-0.004
	Total	**-1.786**	**-1.780**
Z	Pressure	1.506	1.499
	Viscous	-0.014	-0.014
	Total	**1.492**	**1.485**
Total RDF (N)		**2.523**	**2.511**

8.4.4 Discussion

Although the complex model had over three times the total number of tetrahedral elements and a maximum of ten times the number of outlet faces (common hepatic artery outlet) the maximum difference in any cross-sectional area was only $1mm^2$. Total resultant distraction force was 2.523N for the standard model and 2.511N for the complex model (see Table 8.3). The error was therefore 0.48%. Increasing the complexity of the mesh above the standard setting did not cause any significant difference in total RDF and this supports the use of standard mesh settings for determining distraction force in patient-specific anatomy.

8.4.5 Conclusion

Standard mesh settings are adequate to model patient-specific anatomy for the purpose of investigating distraction force.

8.5 Morphological features of stent-grafts and components

8.5.1 Complete stent-grafts

fEVAR	Cross-sectional area (mm2)			Angulation (degrees)									
	Inlet XSA	Left outlet XSA	Right outlet XSA	Cor α	Sag α	Cor β	Sag β	Left Cor θ	Left Sag θ	Right Cor θ	Right Sag θ	Cor Bif	Sag Bif
1	No postoperative CT imaging												
2	514	101	98	8	13	29	-10	-58	-63	26	-31	84	32
3	No postoperative CT imaging												
4	260	117	128	6	3	-9	-9	-37	-19	52	-48	89	29
5	675	201	278	0	0	5	-2	-29	-53	29	-60	58	7
6	355	214	165	-17	6	13	-28	-62	-35	19	-69	81	34
7	435	115	121	-7	7	0	0	14	-58	18	-67	4	9
8	345	37	65	-5	15	8	-13	-48	4	36	-86	84	90
9	275	84	254	-2	5	4	-4	-18	-57	40	-55	58	2
10	351	76*	72	-22	-1	-13	-21	8	-52	36	-58	28	6
11	485	120	78	-21	26	14	-34	-34	-82	51	-56	85	26
12	433	229	142	-1	24	58	-41	13	-60	64	-49	51	11
13	227	65	70	-12	18	-6	-15	-66	-62	28	-27	94	35
14	294	70	155	-26	38	43	-42	-62	-140	97	-120	159	20
15	295	71*	118	-8	11	14	-15	-53	27	51	-66	104	93
16	264	82	49	-14	29	41	-29	-4	-61	65	-60	69	1
17	271	124	37	-8	18	25	-7	-34	-64	30	-48	64	16
18	209	54	25	-2	9	5	4	-15	-20	52	-51	67	31
19	389	151	106	-12	13	9	-13	-37	-44	66	-43	103	1
20	309	33	217	4	5	24	0	-42	-35	36	-37	78	2
21	214	62	156	-2	23	4	-13	-23	-87	13	-91	36	4
22	375	87	83	-1	16	7	-8	-39	-59	32	-53	71	6
23	272	95	114	-19	8	13	-8	-14	-53	47	-54	61	1
24	111	72	56	-4	4	12	-11	-12	-37	19	-27	31	10
25	907	380	*	18	2	36	-16	-73	-114	Occluded limb			
26	290	78	86	3	13	0	-26	-2	-97	56	-99	58	2
27	438	95	59	-11	21	26	-22	-35	-83	66	-69	101	14
28	407	170	-	-11	5	23	2	-33	-70	Occluded limb			

	Cross-sectional area			Angulation									
	Inlet XSA	**Left outlet XSA**	**Right outlet XSA**	**Cor α**	**Sag α**	**Cor β**	**Sag β**	**Left Cor θ**	**Left Sag θ**	**Right Cor θ**	**Right Sag θ**	**Cor Bif**	**Sag Bif**
29	335	135	113	-15	-5	27	17	-13	-80	93	-76	106	4
30	312	59	30*	-1	-3	7	-9	-47	-43	46	-31	93	12
31	451	29	60	-8	9	15	10	6	-15	36	-60	30	45
32	340	125	97	-4	9	-11	-19	-80	-91	40	-64	120	27
33	No postoperative CT imaging with contrast												
34	360	114	194	-7	2	21	-7	-62	-71	4	-74	66	3
35	242	103	87	-4	8	10	23	3	-26	25	-20	22	6
36	348	70	35	-9	2	28	-8	-10	-59	40	-61	50	2
37	227	34	62	-14	7	18	-15	-28	-56	54	-48	82	8
38	281	28*	57	-22	-4	-3	-4	-7	-46	85	-12	92	34
39	222	91	104	-19	17	53	-27	-37	-87	45	-58	82	29
40	371	210	242	-24	-18	48	15	-5	-37	75	-37	80	0
41	527	96	123	2	11	-5	-1	-22	-82	26	-67	48	15
42	No postoperative CT imaging												
43	230	98	74	-13	9	-17	11	-44	-57	34	-50	78	7
44	216	41	112	-11	8	12	-1	-13	-44	40	-38	53	6
45	364	58	81	-12	18	19	-21	-22	-67	24	-42	46	25
46	415	33	80	1	3	13	-7	-83	-92	84	-95	167	3
47	351	84	92	6	8	-3	-2	-66	3	19	-24	85	27
48	298	209	263	-9	2	16	6	-63	-80	75	-67	138	13
49	351	131	216	11	9	-20	-23	-31	-61	38	-73	69	12
50	270	25	64	0	6	19	-21	1	-65	36	-74	35	9
51	304	356	-	-8	22	49	-38	22	-47	Tube graft only			
52	363	85	25	-9	-8	25	-24	-45	-60	77	-16	122	44
53	403	166	136	-19	0	24	-3	-34	-51	44	-58	78	7
54	No postoperative CT imaging												
55	659	132	128	-27	0	12	-28	-12	-44	57	-43	69	1
56	548	400	393	-3	-4	18	-1	-54	-31	56	-33	110	2
57	393	204	178	0	5	-12	4	-20	-65	27	-53	47	12
58	509	178	233	-31	1	-5	-10	-55	-59	58	-74	113	15
59	465	155	52	-15	14	26	-3	20	-49	64	-60	44	11

Cor/Sag α: α angle in coronal or sagittal elevation, β: β angle, θ: outlet angle, Bif: bifurcation angle (see Figure 5.9), XSA: cross-sectional area (mm^2), *:Wallstent across outlet

8.5.2 Proximal bodies

fEVAR	*D1*	Inlet XSA	*BL1*	*Seal stents*	*Scal*	*Fens*	Left Outlet XSA	Cor θ	Sag θ	Right Outlet XSA	Cor θ	Sag θ
1	*36*	-	*122*	*2*	*1*	*2*	No postoperative CT imaging					
2	*32*	514	*124*	*2*	*0*	*2*	330	29	-15	-	-	-
3	*28*	-	*124*	*2*	*1*	*2*	No postoperative CT imaging					
4	*26*	260	*109*	*2*	*1*	*2*	52	-6	-31	84	-15	-14
5	*36*	675	*122*	*2*	*1*	*2*	105	4	-3	78	11	-2
6	*34*	355	*99*	*1*	*1*	*0*	55	2	-30	97	10	-27
7	*32*	435	*181*	*2*	*1*	*3*	115	14	-58	70	0	-12
8	*28*	345	*109*	*2*	*0*	*3*	108	9	-28	45	18	-47
9	*28*	275	*109*	*2*	*1*	*2*	45	5	-15	92	17	-10
10	*28*	351	*124*	*2*	*0*	*3*	53	-2	-38	57	1	-38
11	*30*	485	*124*	*2*	*1*	*2*	62	15	-44	100	16	-44
12	*34*	433	*122*	*2*	*1*	*1*	89	43	-56	132	69	-50
13	*24*	227	*109*	*2*	*1*	*2*	109	-9	-15	100	0	-23
14	*28*	294	*124*	*2*	*1*	*2*	54	36	-48	66	58	-47
15	*26*	295	*109*	*2*	*1*	*2*	39	14	-24	42	1	-20
16	*28*	264	*124*	*2*	*1*	*2*	70	39	-25	101	49	-41
17	*30*	271	*124*	*2*	*0*	*3*	76	32	-24	97	37	-33
18	*24*	209	*109*	*2*	*1*	*2*	92	13	-11	58	6	2
19	*30*	389	*109*	*2*	*1*	*2*	51	10	-37	78	11	-16
20	*28*	309	*124*	*2*	*1*	*2*	113	15	-9	65	24	-15
21	*24*	214	*109*	*2*	*1*	*1*	51	7	-39	100	16	-32
22	*28*	375	*109*	*2*	*1*	*2*	70	0	-13	123	-2	-11
23	*28*	272	*109*	*2*	*1*	*2*	57	36	-23	54	25	-14
24	*24*	111	*76*	*1*	*1*	*1*	40	10	-15	103	20	-10
25	*36*	907	*137*	*2*	*1*	*2*	57	31	-23	Occluded		
26	*28*	290	*124*	*2*	*1*	*2*	111	2	-32	57	10	-32
27	*30*	438	*124*	*2*	*1*	*2*	48	25	-35	103	28	-19
28	*36*	407	*164*	*2*	*1*	*3*	78$^{\phi}$	32	-30	Occluded		
29	*32*	335	*124*	*2*	*1*	*2*	339	39	-8	-	-	-
30	*34*	312	*107*	*2*	*1*	*2*	54	8	-14	94	13	-12

fEVAR	*D1*	Inlet XSA	*BL1*	*Seal stents*	*Scal*	*Fens*	Left Outlet XSA	Cor θ	Sag θ	Right Outlet XSA	Cor θ	Sag θ
31	*30*	451	*124*	*2*	*1*	*3*	325	3	1	-	-	-
32	*30*	340	*124*	*2*	*1*	*3*	71	-17	-33	156	-12	-15
33	*32*	-	*124*	*2*	*1*	*3*	No postoperative CT imaging with contrast					
34	*32*	360	*129*	*3*	*1*	*3*	51	14	-25	143	36	-18
35	*28*	242	*124*	*2*	*1*	*2*	77	11	16	119	11	13
36	*30*	348	*109*	*2*	*1*	*2*	56	22	-23	110	28	-14
37	*26*	227	*139*	*2*	*1*	*3*	253	24	-16	-	-	-
38	*28*	281	*124*	*2*	*0*	*3*	50	25	-16	224	32	-29
39	*30*	222	*109*	*2*	*1*	*0*	45	45	-31	83	50	-16
40	*34*	371	*152*	*2*	*1*	*2*	153	37	0	58	53	4
41	*32*	527	*124*	*2*	*1*	*3*	344	-28	-7	-	-	-
42	*36*	-	*107*	*2*	*1*	*2*	No postoperative CT imaging					
43	*24*	230	*94*	*2*	*1*	*2*	71	5	-19	116	4	-9
44	*26*	216	*109*	*2*	*1*	*2*	57	8	-25	101	15	-16
45	*28*	364	*109*	*2*	*1*	*2*	62	19	-26	97	16	-29
46	*28*	415	*109*	*2*	*1*	*3*	50	16	-24	47	16	-29
47	*30*	351	*109*	*2*	*1*	*2*	50	-1	-22	103	0	-21
48	*26*	298	*124*	*2*	*1*	*2*	65	20	-3	107	23	-6
49	*34*	351	*108*	*2*	*1*	*1*	103	-21	-30	35	-15	-22
50	*28*	270	*109*	*2*	*1*	*2*	54	19	-34	86	23	-23
51	*28*	304	*153*	*2*	*1*	*3*	356$^{\Phi}$	22	-47	Tube graft only		
52	*30*	363	*139*	*2*	*1*	*2*	175	17	-29	52	30	-29
53	*28*	403	*139*	*2*	*1*	*3*	79	13	-20	56	22	-19
54	*34*	-	*137*	*2*	*0*	*3*	No postoperative CT imaging					
55	*40*	659	*171*	*2*	*1*	*2*	233	2	-36	-	23	-36
56	*36*	548	*183*	*2*	*0*	*4*	51	15	-15	100	23	-6
57	*28*	393	*109*	*2*	*1*	*2*	54	1	-31	122	8	-32
58	*36*	509	*174*	*3*	*1*	*3*	56	-9	-20	87	-8	-17
59	*32*	465	168	*2*	*0*	*4*	106	28	-14	59	47	-21

Data obtained from supply and manufacturing documents shown in italics. D1: Actual proximal diameter (mm), Inlet XSA: Inlet cross-sectional area post deployment (mm^2), BL1: Proximal body length (mm), Seal stents: no. of sealing stents, Scal: no. of Scallops, Fen: no. of Fenestrations, Outlet XSA: Outlet cross-sectional area post deployment (mm^2), Cor/Sag θ: Coronal/Sagittal outlet angle (degrees), $^{\Phi}$: non-standard distal diameter

8.5.3 Distal bodies

fEVAR	Inlet XSA	*DBL*	*DLL*	*D3 (R/L)*	Ipsilateral outlet			Contralateral outlet			Cor bif	Sag bif
					XSA	Cor θ	Sag θ	XSA	Cor θ	Sag θ		
1	-	*94*	*62*	*20*	No postoperative CT imaging							
2	420	*124*	*62*	*16 (R)*	101	-3	-22	71	-23	-33	20	11
3	-	*109*	*45*	*12*	No postoperative CT imaging							
4	376	*94*	*62*	*20 (R)*	128	61	-36	72	9	-29	52	7
5	453	*94*	*62*	*20 (L)*	202	-30	-54	100	9	-13	39	41
6	412	*94*	*45*	*20 (R)*	166	4	-44	76	-13	-10	17	34
7	Custom-made single-piece bifurcated fenestrated main body											
8	455	*94*	*62*	*12 (L)*	59*	-75	-57	72	5	-35	80	22
9	390	*94*	*28*	*12 (L)*	84	-26	-51	84	19	-26	45	25
10	342	*109*	*28*	*12 (R)*	50	47	-22	77	28	-27	19	5
11	448	*94*	*45*	*16 (R)*	79	39	-26	77	5	-13	34	13
12	447	*94*	*28*	*12 (R)*	90	3	-14	81	-11	-21	14	7
13	194	*94*	*45*	*12 (L)*	63	-61	-48	90	4	-19	65	29
14	327	*109*	*28*	*12 (R)*	79	24	-22	78	11	-3	13	19
15	377	*94*	*62*	*20 (R)*	118*	49	-51	27*	12	-16	37	35
16	416	*94*	*45*	*16 (R)*	49	24	-31	84	0	-15	24	16
17	408	*94*	*62*	*16 (R)*	36	6	-39	89	6	-22	0	17
18	342	*76*	*62*	*12 (L)*	55	-20	-23	79	1	-8	21	15
19	385	*94*	*62*	*16 (R)*	105	61	-31	82	25	-25	36	6
20	395	*94*	*45*	*16 (L)*	33	-68	-36	62	-1	-21	67	15
21	276	*94*	*28*	*12 (R)*	95	9	-56	72	-4	-31	13	25
22	414	*76*	*62*	*12 (R)*	124	26	-46	87	-6	-7	32	39
23	429	*76*	*28*	*12 (L)*	62	12	-27	68	13	-7	1	20
24	160	*76*	*45*	*12 (R)*	56	7	-16	61	4	-8	3	8
25	399	*109*	*62*	*12 (R)*	Occluded*‡			40	-2	-37	-	-
26	396	*94*	*62*	*12 (L)*	78	-2	-71	57	12	-14	14	57
27	393	*76*	*62*	*12 (R)*	59	37	-45	55	-2	-14	39	31
28	432ϕ	*97*	*30*	*12 (R)*	Occluded‡			65	8	-42	-	-
29	301	*109*	*62*	*20 (R)*	113	63	-89	51	8	-49	55	40
30	410	*76*	*62*	*12 (R)*	30*	41	-24	57	2	-4	39	20
31	285	*109*	*62*	*12 (L)*	109	-38	-30	66	-12	-25	26	5
32	382	*109*	*45*	*20 (R)*	97	53	-44	75	-6	-15	59	29

fEVAR	Inlet XSA	*DBL*	*DLL*	*D3 (R/L)*	Ipsilateral outlet			Contralateral outlet			Cor bif	Sag bif
					XSA	Cor θ	Sag θ	XSA	Cor θ	Sag θ		
33	-	*109*	*28*	*12*	No postoperative CT imaging with contrast							
34	387	*94*	*62*	*20 (R)*	194	-16	-67	66	-8	-23	8	44
35	383	*76*	*62*	*12 (R)*	87	16	-42	82	2	-10	14	32
36	253	*94*	*62*	*16 (R)*	35	12	-51	69	-7	-17	19	34
37	318	*109*	*45*	*12 (R)*	62	34	-30	61	-15	-4	49	26
38	320	*124*	*45*	*12 (R)*	57	85	-7	23*	58	-37	27	30
39	425	*76*	*62*	*12 (R)*	104	-8	-31	87	-7	-2	1	29
40	300	*94*	*45*	*22 (L)*	210	-53	-50	70	10	-21	63	29
41	312	*109*	*62*	*12 (R)*	77	57	-81	70	-28	-22	85	59
42	-	*76*	*62*	*12*	No postoperative CT imaging							
43	272	*76*	*62*	*16 (R)*	74	50	-58	83	19	-31	31	27
44	338	*94*	*45*	*12 (R)*	53	26	-40	66	-4	-34	30	6
45	394	*76*	*62*	*12 (R)*	82	5	-20	70	-3	-4	8	16
46	340	*76*	*28*	*12 (R)*	61	4	-25	57	4	-18	0	7
47	501	*76*	*62*	*16 (R)*	92	21	-23	70	-2	-21	23	2
48	435	*94*	*62*	*20 (R)*	263	59	-71	79	5	-11	54	60
49	379	*42*	*63*	*16 (L)*	131	-13	-40	23	6	-3	19	37
50	253	*76*	*45*	*16 (R)*	64	14	-52	82	2	-17	12	35
51	Fenestrated tube graft only											
52	318	*94*	*62*	*16 (R)*	25	52	-12	96	-4	-13	56	25
53	335	*76*	*45*	*20 (R)*	102	0	-38	68	-13	-17	13	21
54	-	*76*	*62*	*24*	No postoperative CT imaging							
55	358	*94*	*45*	*24 (R)*	128	38	-15	72	-3	-27	41	12
56	312	*109*	*62*	*28 (R)*	393	40	-34	41	2	-15	38	19
57	324	*76*	*62*	*16 (R)*	178	38	-55	62	14	-33	24	22
58	418	*94*	*62*	*22 (R)*	233	60	-62	70	-3	-16	63	46
59	329	109	45	*20 (L)*	155†	-8	-50	69	28	-21	36	29

Data obtained from supply and manufacturing documents shown in italics. Inlet XSA: Inlet cross-sectional area post deployment (mm^2), DBL: Actual distal body length to contralateral gate (mm), DLL: Actual ipsilateral limb length (mm), D3: Actual ipsilateral limb outlet diameter, (R/L): denotes laterality of ipsilateral limb, Ipsilateral/Contralateral XSA: limb outlet cross-sectional area post deployment (mm^2), Cor/Sag θ: Coronal/Sagittal outlet angle (degrees), Cor/Sag bif: Coronal/Sagittal bifurcation angle (degrees), *: Wallstent, †: Palmaz stent, ‡: Internal iliac artery coil embolization, ᶲ: non-standard inlet

8.5.4 Limb extensions

	Contralateral limb extension						Other limb extension					
fEVAR	**Inlet XSA**	***LL***	***D2***	**Outlet XSA**	**Cor θ**	**Sag θ**	**Inlet XSA**	***LL***	***D2***	**Outlet XSA**	**Cor θ**	**Sag θ**
1	-	*71*	*22*	No postoperative CT*								
2	65 (L)	*71*	*18*	100	-74	-20						
3	-	*71*	*12*	No postoperative CT*								
4	57 (L)	*71*	*16*	117	-32	15						
5	87 (R)	*88*	*22*	280	16	-56						
6	79 (L)	*54*	*20*	213	-64	-2						
7	86 (R)	*71*	*16*	121	17	-53						
8	48 (R)	*54*	*16*	65	17	-41	96 (L)	*54*	*12*	37*‡	2	60
9	79 (R)	*71*	*16*	254	21	-44						
10	60 (L)	*71*	*16*	76	16	-12	60 (R)	*54*	*16*	68	29	-16
11	103 (L)	*71*	*18*	120	-45	-35						
12	60 (L)	*88*	*24*	229	-33	-4	73 (R)	*71*	*24*	144	25	8
13	97 (R)	*54*	*12*	70	28	-9						
14	61 (L)	*71*	*16*	69	-116	-94	96 (R)	*88*	*16*	156	37	-75
15	(L)	*88* *71*	*12* *14*	Unable to identify inlet/outlet*‡								
16	63 (L)	*71*	*14*	82	-45	-21						
17	72 (L)	*71*	*22*	124	-57	-44						
18	65 (R)	*88*	*12*	25	47	-51						
19	48 (L)	*71*	*18*	148	-53	-5						
20	69 (R)	*54*	*24*	217	14	-31						
21	45 (L)	*71*	*14*	62	-28	-46	62 (R)	*54*	*20*	156	4	-57
22	68 (L)	*71*	*12*	83	-41	-50						
23	92 (R)	*71*	*18*	114	23	-39	75 (L)	*54*	*16*	95	-48	-26
24	62 (L)	*71*	*12*	61	-23	-17						
25	66 (L)	*93*	*28*	380	-106	-99	(R)	*71* *71*	*14* *12*	Occluded*‡		
26	65 (R)	*71*	*14*	86	45	-61						
27	64 (L)	*71*	*14*	95	-58	-46						
28	75 (L)	*56*	*24*	170	-55	-35	(R)	*90*	*12*	Occluded‡		
29	61 (L)	*71*	*18*	135	-50	-52						
30	79 (L)	*54*	*14*	59	-53	-28						
31	83 (R)	*73*	*12*	60	31	-45	83 (L)	*90*	*12*	29‡	29	13

fEVAR	Inlet XSA	*LL*	*D2*	Outlet XSA	Cor θ	Sag θ	Inlet XSA	*LL*	*D2*	Outlet XSA	Cor θ	Sag θ
32	58 (L)	*71*	*24*	125	-59	-59						
33	-	*54* *88*	*16* *16*	No postoperative CT with contrast								
34	72 (L)	*90*	*16*	114	-71	-45						
35	90 (L)	*90*	*14*	103	-13	-42						
36	57 (L)	*71*	*14*	70	-35	-32						
37	72 (L)	*71*	*12*	34	-63	-37						
38	53 (L)	*88*	*12*	28*	-39	-21						
39	61 (L)	*73*	*16*	91	-80	-55						
40	79 (R)	*73*	*24*	242	22	-41						
41	55 (L)	*90*	*16*	96	12	-60	104 (R)	*88*	*16*	123	-54	-55
42	-	*90*	*12*	No postoperative CT*								
43	70 (L)	*73*	*14*	98	-49	-38						
44	79 (L)	*90*	*16*	41	-23	-18	78 (R)	*71*	*14*	112	34	-18
45	83 (L)	*90*	*12*	58	-42	-42						
46	54 (L)	*90*	*16*	33	-98	-63	62 (R)	*73*	*16*	80	68	-63
47	87 (L)	*73*	*14*	84	-65	17						
48	84 (L)	*73*	*20*	209	-84	-75						
49	(R)	*56* *73* *90*	*12* *24* *24*	Unable to identify inlet/outlet								
50	60 (L)	*56*	*14*	25	-20	-26						
51	Tube graft only											
52	53 (L)	*73*	*16*	85	-62	-27						
53	57 (L)	*73*	*18*	166	-48	-29	69 (R)	*90*	*18*	136	25	-29
54	(L)	*73*	*20*	No postoperative CT								
55	64 (L)	*73*	*22*	132	-20	13						
56	69 (L)	*107*	*28*	400	-64	-14						
57	44 (L)	*73*	*18*	204	-20	-38						
58	77 (L)	*90*	*18*	178	-50	-40						
59	61 (R)	73	14	52‡	12	-38						

Data obtained from supply and manufacturing documents shown in italics. Inlet XSA: Inlet cross-sectional area post deployment (mm^2), (L/R) denotes laterality, LL: Actual length of limb extension (mm, not including 22mm proximal seal-zone), D2: Actual distal diameter of limb extension (mm), Outlet XSA: Outlet cross-sectional area post deployment (mm^2), Cor/Sag θ: Coronal/Sagittal outlet angle (degrees), *:wallstent, ‡: Internal iliac artery coil embolization.

8.6 Distraction force results for chapter 5

8.6.1 Complete stent-grafts

fEVAR	Pressure force (N)			Viscous Force (N)			Total Force (N)			Total RDF (N)
	x	y	z	x	y	z	x	y	z	
1	No results									
2	0.335	-3.245	7.017	0.001	-0.002	-0.018	0.336	-3.247	6.998	**7.7**
3	No results									
4	-0.439	-0.139	2.205	0.001	-0.005	-0.019	-0.438	-0.145	2.186	**2.2**
5	2.464	-7.018	7.444	-0.002	-0.002	-0.019	2.462	-7.020	7.425	**10.5**
6	5.372	-3.480	2.253	0.003	-0.005	-0.016	5.375	-3.485	2.237	**6.8**
7	-0.437	-1.700	7.121	0.002	0.000	-0.022	-0.435	-1.701	7.099	**7.3**
8	0.480	-0.885	6.424	0.012	-0.011	-0.035	0.492	-0.896	6.390	**6.5**
9	-1.391	-2.104	0.890	-0.002	-0.002	-0.019	-1.393	-2.106	0.871	**2.7**
10	-1.645	-2.404	4.462	-0.002	-0.003	-0.049	-1.647	-2.407	4.413	**5.3**
11	1.198	-3.473	8.163	0.000	-0.006	-0.021	1.198	-3.480	8.142	**8.9**
12	-0.618	-7.192	1.856	-0.008	-0.006	-0.027	-0.626	-7.198	1.829	**7.5**
13	0.500	0.253	3.182	0.004	-0.004	-0.021	0.504	0.249	3.161	**3.2**
14	-2.464	-6.042	3.819	-0.004	-0.007	-0.023	-2.468	-6.048	3.795	**7.6**
15	0.193	-0.139	3.955	0.008	0.000	-0.046	0.200	-0.139	3.910	**3.9**
16	-0.494	-1.336	3.092	-0.003	-0.004	-0.029	-0.496	-1.340	3.063	**3.4**
17	1.175	-1.600	3.596	-0.005	-0.002	-0.030	1.171	-1.602	3.566	**4.1**
18	-0.073	0.940	3.390	-0.004	-0.003	-0.041	-0.077	0.937	3.349	**3.5**
19	-0.974	-1.254	5.663	-0.004	-0.010	-0.024	-0.977	-1.264	5.638	**5.9**
20	-1.485	-0.275	2.062	-0.001	-0.002	-0.021	-1.486	-0.277	2.041	**2.5**
21	0.609	-3.369	2.191	0.000	-0.006	-0.028	0.610	-3.375	2.163	**4.1**
22	1.197	-1.450	6.270	0.001	-0.005	-0.019	1.197	-1.455	6.251	**6.5**
23	-0.212	-1.272	2.794	0.000	-0.003	-0.048	-0.212	-1.275	2.746	**3.0**
24	-0.279	0.130	-0.066	0.002	-0.006	-0.037	-0.278	0.124	-0.104	**0.3**
25	2.081	-9.641	14.76	0.008	-0.028	-0.052	2.089	-9.669	14.71	**17.7**
26	-1.009	-4.473	4.990	-0.005	-0.007	-0.028	-1.014	-4.479	4.962	**6.8**
27	-1.459	-2.670	7.889	-0.004	-0.012	-0.034	-1.462	-2.682	7.855	**8.4**
28	-0.988	1.930	7.368	0.005	-0.014	-0.035	-0.983	1.915	7.333	**7.6**

	Pressure Force (N) x,y,z			Viscous Force (N) x,y,z			Total Force (N) x,y,z			RDF
29	-1.593	-5.896	4.357	-0.003	-0.009	-0.025	-1.596	-5.905	4.332	**7.5**
30	0.112	-0.166	5.470	-0.004	-0.007	-0.041	0.107	-0.173	5.429	**5.4**
31	-1.149	3.500	7.444	0.006	-0.009	-0.057	-1.143	3.491	7.387	**8.2**
32	2.594	-2.413	5.454	0.001	-0.007	-0.031	2.595	-2.420	5.423	**6.5**
33	No results									
34	3.953	-2.059	5.779	-0.003	-0.005	-0.024	3.950	-2.064	5.755	**7.3**
35	-0.814	1.984	2.255	-0.005	0.002	-0.021	-0.818	1.986	2.234	**3.1**
36	0.610	-1.220	6.465	-0.002	-0.007	-0.028	0.607	-1.227	6.436	**6.6**
37	-0.885	0.111	3.357	0.002	-0.006	-0.044	-0.883	0.106	3.313	**3.4**
38	0.223	-1.032	4.915	-0.008	-0.009	-0.048	0.215	-1.041	4.867	**5.0**
39	-1.587	-2.294	1.335	-0.004	-0.006	-0.023	-1.590	-2.300	1.312	**3.1**
40	-0.761	-1.702	2.213	-0.001	-0.001	-0.028	-0.762	-1.704	2.185	**2.9**
41	1.342	-1.660	9.713	0.003	-0.009	-0.030	1.345	-1.668	9.683	**9.9**
42	No results									
43	1.210	-1.261	3.332	-0.001	-0.003	-0.023	1.209	-1.264	3.309	**3.7**
44	0.173	-0.829	2.485	-0.001	-0.006	-0.034	0.172	-0.835	2.451	**2.6**
45	0.862	-1.697	5.764	0.001	-0.007	-0.037	0.863	-1.705	5.727	**6.0**
46	-0.717	1.921	8.749	0.000	-0.012	-0.026	-0.717	1.909	8.724	**9.0**
47	2.446	1.724	5.261	0.001	-0.005	-0.029	2.447	1.719	5.231	**6.0**
48	-0.185	-4.852	1.769	-0.001	-0.003	-0.023	-0.186	-4.855	1.746	**5.2**
49	-3.101	-3.693	3.943	-0.005	-0.009	-0.039	-3.106	-3.702	3.903	**6.2**
50	-0.449	-1.460	4.797	-0.008	-0.009	-0.036	-0.456	-1.469	4.761	**5.0**
51	-3.287	0.429	0.743	-0.001	0.003	-0.009	-3.288	0.432	0.735	**3.4**
52	-0.179	1.442	6.735	-0.006	-0.010	-0.032	-0.186	1.432	6.702	**6.9**
53	2.094	0.612	5.376	-0.003	-0.003	-0.034	2.091	0.609	5.341	**5.8**
54	No results									
55	0.589	-0.714	11.75	0.004	-0.010	-0.020	0.593	-0.725	11.73	**11.8**
56	0.279	-6.130	0.019	0.000	-0.003	-0.030	0.279	-6.134	-0.011	**6.1**
57	0.241	-4.977	1.711	0.002	-0.004	-0.024	0.244	-4.981	1.687	**5.3**
58	3.600	-4.208	5.829	0.006	-0.005	-0.027	3.606	-4.212	5.802	**8.0**
59	-3.202	-2.005	6.286	-0.012	-0.003	-0.049	-3.214	-2.009	6.238	**7.3**

N: Newtons, RDF: Resultant distraction force, negative values indicate forces acting in the opposite direction to that of the x,y or z axis

8.6.2 Proximal bodies

fEVAR	Pressure force (N)			Viscous Force (N)			Total Force (N)			Total RDF (N)
	x	y	z	x	y	z	x	y	z	
1	No results									
2	-2.557	-2.068	3.539	-0.002	0.003	-0.003	-2.559	-2.064	3.535	**4.8**
3	No results									
4	0.213	1.111	3.196	0.001	-0.001	-0.010	0.214	1.109	3.187	**3.4**
5	2.529	-0.223	11.794	-0.002	0.003	-0.012	2.526	-0.220	11.782	**12.1**
6	2.343	-1.368	4.444	-0.001	-0.002	-0.009	2.342	-1.370	4.436	**5.2**
7	0.010	0.221	7.890	0.002	0.002	-0.018	0.012	0.224	7.872	**7.9**
8	-0.491	0.134	4.426	-0.001	0.001	-0.013	-0.492	0.135	4.412	**4.4**
9	0.948	1.475	3.560	-0.001	0.002	-0.008	0.947	1.477	3.552	**4.0**
10	-0.567	-1.373	5.053	0.006	0.004	-0.024	-0.562	-1.369	5.029	**5.2**
11	0.572	-1.753	7.804	0.000	0.000	-0.011	0.572	-1.753	7.793	**8.0**
12	-1.838	-5.831	4.615	-0.005	-0.001	-0.010	-1.843	-5.832	4.605	**7.7**
13	0.859	1.495	0.829	0.001	0.002	-0.011	0.860	1.497	0.818	**1.9**
14	-1.333	-1.764	3.056	0.000	0.002	-0.009	-1.333	-1.762	3.047	**3.8**
15	0.291	0.400	4.911	0.000	0.001	-0.015	0.291	0.401	4.895	**4.9**
16	-1.292	0.250	1.812	-0.002	0.002	-0.016	-1.294	0.252	1.796	**2.2**
17	-0.914	0.611	2.812	-0.004	0.004	-0.015	-0.917	0.615	2.796	**3.0**
18	0.032	2.134	1.766	0.001	0.004	-0.014	0.033	2.138	1.752	**2.8**
19	-1.616	0.895	5.593	0.000	-0.001	-0.010	-1.616	0.895	5.582	**5.9**
20	-0.715	1.028	2.996	-0.004	0.001	-0.014	-0.720	1.029	2.982	**3.2**
21	0.088	0.504	2.509	-0.001	0.003	-0.008	0.087	0.507	2.500	**2.6**
22	1.087	1.338	4.830	0.000	0.001	-0.009	1.087	1.339	4.820	**5.1**
23	-0.266	0.616	4.063	0.001	0.005	-0.024	-0.265	0.620	4.039	**4.1**
24	-0.569	1.672	-0.322	0.001	0.001	-0.012	-0.568	1.673	-0.334	**1.8**
25	-3.544	-3.721	14.86	-0.002	0.002	-0.021	-3.545	-3.719	14.84	**15.7**
26	-0.119	-0.920	3.273	0.001	0.002	-0.012	-0.119	-0.917	3.262	**3.4**
27	-2.065	-0.216	6.306	0.000	0.001	-0.018	-2.065	-0.215	6.288	**6.6**
28	-3.061	3.965	7.849	0.000	0.002	-0.014	-3.060	3.967	7.835	**9.3**

	Pressure Force (N) x,y,z			Viscous Force (N) x,y,z			Total Force (N) x,y,z			RDF
29	-1.905	-0.748	-0.223	0.000	0.003	-0.007	-1.905	-0.744	-0.230	**2.1**
30	-0.331	0.663	3.999	0.000	0.000	-0.011	-0.331	0.663	3.989	**4.1**
31	-0.362	6.157	2.666	0.001	0.004	-0.012	-0.362	6.162	2.654	**6.7**
32	2.295	0.748	3.283	0.001	0.002	-0.013	2.295	0.749	3.271	**4.1**
33	No results									
34	1.729	2.792	5.525	-0.003	0.002	-0.009	1.727	2.794	5.517	**6.4**
35	-0.426	4.688	2.082	-0.001	0.004	-0.011	-0.427	4.692	2.072	**5.1**
36	-0.538	0.705	4.757	-0.002	0.002	-0.012	-0.540	0.706	4.745	**4.8**
37	-1.112	1.223	-0.412	0.000	0.003	-0.014	-1.112	1.226	-0.426	**1.7**
38	0.975	-0.768	0.393	0.006	0.003	-0.012	0.981	-0.764	0.381	**1.3**
39	-3.228	-0.132	1.711	-0.004	0.000	-0.011	-3.232	-0.132	1.700	**3.7**
40	-0.834	4.058	3.720	0.002	0.006	-0.013	-0.833	4.063	3.707	**5.6**
41	4.569	3.962	6.072	0.001	0.002	-0.004	4.570	3.964	6.068	**8.6**
42	No results									
43	1.492	1.718	2.106	0.002	0.002	-0.010	1.494	1.720	2.096	**3.1**
44	0.905	0.999	1.957	0.000	0.002	-0.009	0.905	1.000	1.948	**2.4**
45	0.156	-0.124	4.955	-0.002	0.001	-0.015	0.154	-0.122	4.940	**4.9**
46	-0.252	3.702	7.345	-0.001	0.001	-0.009	-0.254	3.703	7.336	**8.2**
47	1.021	1.861	4.869	-0.002	-0.002	-0.013	1.019	1.860	4.856	**5.3**
48	-0.047	1.574	2.927	-0.001	0.003	-0.016	-0.047	1.577	2.911	**3.3**
49	-0.145	0.711	5.006	0.003	0.002	-0.020	-0.142	0.713	4.986	**5.0**
50	-0.526	0.332	3.559	-0.002	0.002	-0.012	-0.529	0.334	3.547	**3.6**
51	-3.287	0.429	0.743	-0.001	0.003	-0.009	-3.288	0.432	0.735	**3.4**
52	-1.473	1.998	3.363	0.000	0.001	-0.009	-1.473	1.999	3.354	**4.2**
53	1.007	3.815	7.525	-0.002	0.004	-0.019	1.005	3.820	7.506	**8.5**
54	No results									
55	0.726	0.701	10.54	0.001	-0.001	-0.007	0.728	0.700	10.54	**10.6**
56	-0.921	0.146	8.311	-0.002	0.001	-0.018	-0.923	0.147	8.293	**8.3**
57	0.343	-0.297	4.709	0.002	0.002	-0.015	0.345	-0.296	4.694	**4.7**
58	4.013	0.153	8.187	0.004	0.002	-0.017	4.016	0.155	8.170	**9.1**
59	-2.963	0.376	6.772	0.001	0.009	-0.021	-2.963	0.384	6.751	**7.4**

N: Newtons, RDF: Resultant distraction force, negative values indicate forces acting in the opposite direction to that of the x,y or z axis

8.6.3 Distal bodies

fEVAR	Pressure force (N)			Viscous Force (N)			Total Force (N)			Total RDF (N)
	x	y	z	x	y	z	x	y	z	
1	No results									
2	1.834	-3.088	5.365	-0.003	-0.002	-0.016	1.831	-3.091	5.349	**6.4**
3	No results									
4	-2.925	-1.487	4.554	-0.001	-0.005	-0.013	-2.927	-1.492	4.541	**5.6**
5	1.241	-5.094	3.170	0.000	0.001	-0.016	1.242	-5.093	3.153	**6.1**
6	0.613	-1.989	5.303	-0.002	-0.004	-0.014	0.611	-1.993	5.288	**5.7**
7	No distal body (custom-made single-piece bifurcated, fenestrated main body)									
8	1.053	-3.445	7.199	0.004	-0.010	-0.023	1.058	-3.454	7.177	**8.0**
9	0.194	-3.221	4.870	-0.001	-0.002	-0.017	0.193	-3.223	4.853	**5.8**
10	-2.486	-2.675	4.004	-0.001	-0.002	-0.035	-2.487	-2.676	3.969	**5.4**
11	-0.431	-0.993	6.652	-0.003	-0.004	-0.017	-0.434	-0.997	6.635	**6.7**
12	2.344	-1.385	5.327	-0.007	-0.006	-0.024	2.337	-1.391	5.303	**6.0**
13	0.968	-1.783	1.506	0.006	-0.003	-0.014	0.974	-1.786	1.492	**2.5**
14	-0.524	-1.631	3.515	-0.004	-0.001	-0.018	-0.528	-1.632	3.497	**3.9**
15	-0.480	-1.947	5.334	-0.006	-0.003	-0.030	-0.486	-1.951	5.304	**5.7**
16	0.473	-1.914	6.106	-0.007	-0.002	-0.021	0.466	-1.916	6.085	**6.4**
17	0.247	-3.997	4.882	-0.008	-0.001	-0.026	0.239	-3.998	4.856	**6.3**
18	-0.478	-2.073	4.100	0.005	0.001	-0.023	-0.472	-2.072	4.077	**4.6**
19	-2.130	-1.308	5.504	-0.008	-0.007	-0.020	-2.138	-1.315	5.484	**6.0**
20	2.246	-1.868	5.998	0.001	-0.001	-0.018	2.246	-1.869	5.979	**6.7**
21	0.384	-3.313	2.087	-0.001	-0.001	-0.020	0.382	-3.313	2.067	**3.9**
22	0.443	-2.514	5.265	-0.002	-0.001	-0.013	0.442	-2.515	5.252	**5.8**
23	-0.843	-1.813	5.800	-0.003	0.002	-0.036	-0.845	-1.811	5.764	**6.1**
24	-0.227	-0.492	0.846	-0.001	-0.003	-0.025	-0.228	-0.494	0.821	**1.0**
25	0.728	-1.927	6.871	-0.002	-0.005	-0.036	0.726	-1.932	6.835	**7.1**
26	-0.506	-3.318	5.954	-0.001	-0.005	-0.022	-0.507	-3.323	5.933	**6.8**
27	-0.959	-2.332	6.556	-0.008	-0.005	-0.026	-0.967	-2.338	6.530	**7.0**
28	0.244	-1.638	7.134	-0.003	-0.010	-0.025	0.241	-1.647	7.109	**7.3**
29	-1.848	-3.703	4.035	-0.006	-0.005	-0.020	-1.854	-3.708	4.014	**5.8**
30	-0.674	-0.920	6.628	-0.009	-0.005	-0.034	-0.683	-0.924	6.594	**6.7**
31	0.920	-2.283	2.220	0.008	-0.003	-0.028	0.927	-2.285	2.191	**3.3**
32	-0.859	-2.005	4.797	-0.001	-0.005	-0.026	-0.860	-2.010	4.771	**5.2**

	Pressure Force (N) x,y,z			Viscous Force (N) x,y,z			Total Force (N) x,y,z			RDF
33	No results									
34	0.750	-4.900	3.911	-0.007	-0.001	-0.018	0.743	-4.901	3.894	**6.3**
35	-0.173	-3.482	3.937	-0.004	0.002	-0.015	-0.177	-3.480	3.923	**5.2**
36	0.269	-1.645	3.173	-0.005	-0.003	-0.020	0.264	-1.649	3.153	**3.6**
37	-0.427	-1.176	4.336	-0.006	0.002	-0.019	-0.433	-1.173	4.317	**4.5**
38	-4.110	-1.198	4.912	-0.016	-0.002	-0.029	-4.126	-1.199	4.883	**6.5**
39	2.544	-1.201	4.268	-0.007	-0.003	-0.020	2.537	-1.204	4.248	**5.1**
40	2.118	-3.514	2.416	-0.003	-0.005	-0.021	2.115	-3.520	2.394	**4.8**
41	-1.120	-3.517	3.633	0.003	-0.001	-0.024	-1.117	-3.518	3.609	**5.2**
42	No results									
43	-1.887	-2.825	2.379	-0.003	-0.002	-0.015	-1.890	-2.827	2.363	**4.1**
44	-0.231	-2.801	4.467	-0.003	-0.003	-0.024	-0.234	-2.804	4.443	**5.3**
45	0.725	-1.597	5.077	-0.004	-0.001	-0.024	0.721	-1.598	5.052	**5.3**
46	0.313	-1.983	4.500	-0.003	-0.002	-0.017	0.310	-1.985	4.484	**4.9**
47	0.784	-1.804	6.869	-0.006	-0.005	-0.023	0.778	-1.809	6.846	**7.1**
48	-3.333	-5.591	4.036	-0.004	0.000	-0.018	-3.337	-5.591	4.017	**7.7**
49	-0.553	-2.044	4.815	0.005	-0.004	-0.024	-0.548	-2.048	4.792	**5.2**
50	0.108	-2.076	2.316	-0.008	-0.005	-0.023	0.100	-2.081	2.293	**3.1**
51	No distal body (fenestrated tube graft only)									
52	0.493	0.206	4.193	-0.012	-0.008	-0.025	0.482	0.197	4.168	**4.2**
53	0.583	-3.089	3.789	-0.004	0.000	-0.021	0.578	-3.089	3.768	**4.9**
54	No results									
55	-1.645	-0.840	4.474	-0.001	-0.007	-0.013	-1.646	-0.846	4.461	**4.8**
56	-4.507	-3.750	-0.038	-0.004	-0.002	-0.021	-4.511	-3.752	-0.060	**5.9**
57	-2.127	-3.931	1.519	0.001	-0.002	-0.018	-2.127	-3.933	1.501	**4.7**
58	-3.217	-3.639	3.831	-0.001	-0.003	-0.018	-3.218	-3.641	3.812	**6.2**
59	-0.394	-2.795	2.442	-0.008	-0.001	-0.030	-0.402	-2.797	2.412	**3.7**

N: Newtons, RDF: Resultant distraction force, negative values indicate forces acting in the opposite direction to that of the x,y or z axis

8.6.4 Limb extensions

fEVAR	Pressure force (N)			Viscous Force (N)			Total Force (N)			Total RDF (N)
	x	y	z	x	y	z	x	y	z	
1	No results									
2 L	1.767	-0.293	0.122	0.004	-0.004	-0.008	1.771	-0.296	0.113	**1.8**
3	No results									
4 L	1.414	0.140	-0.879	0.003	-0.004	-0.008	1.417	0.137	-0.887	**1.7**
5 R	-1.041	-4.103	-2.865	-0.002	-0.001	-0.009	-1.043	-4.104	-2.874	**5.1**
6 L	3.541	-0.436	-0.983	0.006	-0.003	-0.011	3.547	-0.439	-0.994	**3.7**
7 R	-0.262	-2.309	-0.358	0.001	0.000	-0.011	-0.262	-2.309	-0.369	**2.4**
8 R	0.320	-0.946	0.196	-0.003	-0.008	-0.009	0.317	-0.954	0.187	**1.0**
8 L	*-0.585*	*1.346*	*0.818*	*0.015*	*-0.002*	*-0.010*	*-0.570*	*1.344*	*0.808*	***1.7***
9 R	-2.733	-2.373	-2.781	-0.003	0.000	-0.006	-2.736	-2.373	-2.787	**4.6**
10 L	-0.459	-0.319	-0.195	-0.001	-0.004	-0.016	-0.459	-0.323	-0.211	**0.6**
10 R	*-0.689*	*-0.225*	*0.037*	*-0.006*	*-0.003*	*-0.016*	*-0.695*	*-0.228*	*0.021*	***0.7***
11 L	1.226	-1.096	0.502	0.003	-0.004	-0.009	1.229	-1.101	0.493	**1.7**
12 L	1.263	-1.207	-3.165	-0.001	-0.004	-0.011	1.262	-1.210	-3.176	**3.6**
12 R	*-1.217*	*0.082*	*-1.164*	*-0.002*	*-0.002*	*-0.009*	*-1.219*	*0.079*	*-1.173*	***1.7***
13 R	-0.636	-0.327	0.580	-0.002	-0.002	-0.010	-0.638	-0.329	0.570	**0.9**
14 L	0.669	-1.442	0.981	0.000	-0.004	-0.007	0.669	-1.446	0.975	**1.9**
14 R	*-1.050*	*-2.854*	*0.401*	*-0.005*	*-0.004*	*-0.010*	*-1.055*	*-2.858*	*0.391*	***3.1***
15	No results (unable to identify inlets/outlets)									
16 L	0.815	-0.557	-0.119	0.002	-0.004	-0.012	0.817	-0.561	-0.131	**1.0**
17 L	1.692	-0.923	0.444	0.001	-0.002	-0.014	1.693	-0.925	0.430	**2.0**
18 R	-0.271	-0.554	1.038	-0.009	-0.005	-0.020	-0.280	-0.559	1.018	**1.2**
19 L	2.435	-1.153	-0.569	0.002	-0.007	-0.011	2.438	-1.160	-0.579	**2.8**

	Pressure Force (N) x,y,z			Viscous Force (N) x,y,z			Total Force (N) x,y,z			RDF
20 R	-1.712	-1.141	-2.224	-0.003	-0.001	-0.008	-1.716	-1.143	-2.231	**3.0**
21 L	0.424	-0.711	0.246	0.003	-0.006	-0.011	0.427	-0.717	0.235	**0.9**
21 R	*-0.209*	*-2.109*	*-1.136*	*-0.001*	*-0.004*	*-0.009*	*-0.211*	*-2.112*	*-1.145*	***2.4***
22 L	0.944	-1.171	0.619	0.003	-0.003	-0.009	0.947	-1.174	0.610	**1.6**
23 R	-0.482	-1.178	-0.168	-0.004	-0.002	-0.020	-0.485	-1.180	-0.188	**1.3**
23 L	*1.272*	*-0.853*	*0.003*	*0.001*	*-0.005*	*-0.018*	*1.274*	*-0.858*	*-0.015*	***1.5***
24 L	0.182	-0.506	0.230	0.002	-0.004	-0.016	0.184	-0.511	0.214	**0.6**
25 L	5.597	-6.204	0.512	0.009	-0.029	-0.047	5.606	-6.233	0.465	**8.4**
26 R	-0.792	-1.511	0.999	-0.005	-0.003	-0.014	-0.798	-1.514	0.985	**2.0**
27 L	1.147	-1.740	0.729	0.003	-0.009	-0.016	1.150	-1.748	0.713	**2.2**
28 L	2.135	-1.539	-0.112	0.004	-0.017	-0.025	2.139	-1.557	-0.137	**2.6**
29 L	0.789	-2.090	0.131	0.000	-0.009	-0.013	0.789	-2.099	0.119	**2.2**
30 L	0.693	-0.538	0.890	0.005	-0.002	-0.015	0.698	-0.541	0.875	**1.2**
31 R	-0.501	-0.548	1.030	-0.004	-0.007	-0.016	-0.505	-0.556	1.013	**1.3**
31 L	*-0.891*	*0.355*	*0.681*	*0.008*	*-0.004*	*-0.024*	*-0.883*	*0.350*	*0.657*	***1.2***
32 L	1.272	-1.892	0.295	0.003	-0.005	-0.012	1.275	-1.897	0.282	**2.3**
33	No results									
34 L	2.288	-1.669	1.089	0.002	-0.005	-0.012	2.290	-1.674	1.076	**3.0**
35 L	0.091	-1.378	-0.167	-0.001	0.000	-0.009	0.090	-1.378	-0.176	**1.4**
36 L	0.820	-0.683	0.236	0.002	-0.005	-0.013	0.822	-0.688	0.223	**1.1**
37 L	0.718	-0.624	1.371	0.003	-0.009	-0.027	0.722	-0.633	1.345	**1.7**
38 L	0.198	-0.593	1.383	-0.003	-0.012	-0.027	0.195	-0.606	1.355	**1.5**
39 L	1.596	-1.292	0.775	0.002	-0.004	-0.010	1.598	-1.295	0.765	**2.2**
40 R	-1.680	-3.004	-0.911	-0.005	-0.003	-0.011	-1.685	-3.007	-0.921	**3.6**

	Pressure Force (N) x,y,z			Viscous Force (N) x,y,z			Total Force (N) x,y,z			RDF
41 L	-0.513	-2.266	0.439	0.005	-0.006	-0.010	-0.509	-2.272	0.429	**2.4**
41 R	*-1.988*	*-2.220*	*0.409*	*-0.003*	*-0.005*	*-0.015*	*-1.991*	*-2.226*	*0.394*	***3.0***
42	No results									
43 L	0.971	-1.118	0.198	0.002	-0.003	-0.010	0.973	-1.122	0.188	**1.5**
44 L	0.315	-0.383	1.325	0.003	-0.005	-0.014	0.318	-0.388	1.311	**1.4**
44 R	*-1.121*	*-0.536*	*-0.331*	*-0.004*	*-0.003*	*-0.013*	*-1.125*	*-0.539*	*-0.345*	***1.3***
45 L	0.532	-0.605	1.323	0.004	-0.006	-0.020	0.536	-0.612	1.303	**1.5**
46 L	0.592	-0.337	1.237	0.006	-0.007	-0.010	0.598	-0.344	1.227	**1.4**
46 R	*-0.970*	*-0.915*	*0.884*	*-0.005*	*-0.006*	*-0.010*	*-0.976*	*-0.921*	*0.874*	***1.6***
47 L	1.568	0.336	0.909	0.005	-0.002	-0.014	1.573	0.334	0.895	**1.8**
48 L	3.065	-2.685	0.543	0.001	-0.003	-0.011	3.066	-2.688	0.532	**4.1**
49	No results (unable to identify inlets/outlets)									
50 L	0.370	-0.257	0.754	-0.001	-0.007	-0.016	0.369	-0.263	0.739	**0.9**
51	No results (fenestrated tube graft only)									
52 L	1.074	-0.506	0.449	0.004	-0.007	-0.012	1.078	-0.513	0.437	**1.3**
53 L	2.020	-1.620	-0.930	0.002	-0.004	-0.013	2.021	-1.624	-0.943	**2.8**
53 R	*-1.023*	*-1.046*	*-0.429*	*-0.004*	*-0.003*	*-0.010*	*-1.027*	*-1.049*	*-0.440*	***1.5***
54	No results									
55 L	1.373	-0.423	-0.557	0.004	-0.007	-0.009	1.376	-0.430	-0.566	**1.5**
56 L	5.840	-2.621	-3.832	0.003	-0.004	-0.016	5.844	-2.625	-3.848	**7.5**
57 L	0.880	-2.893	-1.714	0.002	-0.003	-0.010	0.882	-2.896	-1.724	**3.5**
58 L	2.024	-1.791	-0.100	0.004	-0.005	-0.010	2.029	-1.796	-0.110	**2.7**
59 R	0.024	-0.308	0.555	-0.013	-0.009	-0.021	0.012	-0.316	0.533	**0.6**

L/R in fEVAR column refers to laterality of limb extension (Ipsilateral limbs in iltalics), N: Newtons, RDF: Resultant distraction force, negative values indicate forces acting in the opposite direction to that of the x,y or z axis

8.7 Detailed patient-specific results for chapter 6

8.7.1 Patient-specific total distraction force, migration distance and imaging interval for complete stent-grafts and proximal bodies

fEVAR	Systolic BP	Total distraction force acting on Complete stent-graft (N)				Total distraction force acting on Proximal body (N)				Proximal Body Migration (mm)	Imaging Interval
		x	y	z	Total RDF	x	y	Z	Total RDF		
1	No postoperative CT imaging										
2	Only 1 available postoperative CT (follow-up elsewhere)										
3	No postoperative CT imaging										
4	150	-0.4	-0.1	2.0	**2.1**	0.2	1.0	3.0	**3.2**	0.4	21
5	Only 1 available postoperative CT (follow-up elsewhere)										
6	140	4.7	-3.0	1.9	**5.9**	2.0	-1.2	3.9	**4.5**	1.8	26
7	167	-0.5	-1.8	7.4	**7.6**	0.0	0.2	8.2	**8.2**	6.0	72
8	160	0.5	-0.9	6.4	**6.4**	-0.5	0.1	4.4	**4.4**	2.6	19
9	134	-1.2	-1.8	0.7	**2.2**	0.8	1.2	3.0	**3.3**	3.1	45
10	100	-1.0	-1.5	2.7	**3.3**	-0.3	-0.8	3.1	**3.2**	2.0	17
11	112	0.8	-2.4	5.7	**6.2**	0.4	-1.2	5.4	**5.6**	1.3	4
12	147	-0.6	-6.6	1.7	**6.8**	-1.7	-5.3	4.2	**7.0**	2.8	12
13	150	0.5	0.2	3.0	**3.0**	0.8	1.4	0.8	**1.8**	0.6	26
14	129	-2.0	-4.8	3.0	**6.0**	-1.1	-1.4	2.4	**3**	2.7	13
15	134	0.2	-0.1	3.2	**3.3**	0.2	0.3	4.1	**4.1**	0.6	49
16	122	-0.4	-1.0	2.3	**2.6**	-1.0	0.2	1.4	**1.7**	4.6	51
17	Only 1 available postoperative CT (follow-up elsewhere)										
18	145	-0.1	0.8	3.0	**3.2**	0.0	1.9	1.6	**2.5**	5.0	52
19	164	-1.0	-1.3	5.8	**6.0**	-1.6	0.9	5.7	**6.0**	4.1	47
20	160	-1.5	-0.3	2.0	**2.5**	-0.7	1.0	3.0	**3.2**	1.8	45
21	137	0.5	-2.9	1.8	**3.5**	0.1	0.4	2.1	**2.2**	2.0	26
22	117	0.9	-1.1	4.6	**4.8**	0.8	1.0	3.5	**3.7**	0.5	49
23	Only 1 available postoperative CT (follow-up elsewhere)										
24	Only 1 available postoperative CT (poor renal function)										
25	120	1.6	-7.2	10.8	**13.1**	-2.6	-2.7	10.9	**11.6**	-3.2	52
26	130	-0.8	-3.6	4.0	**5.5**	-0.1	-0.7	2.6	**2.7**	9.5	44
27	135	-1.2	-2.3	6.6	**7.1**	-1.7	-0.2	5.3	**5.6**	12.5	10
28	140	-0.8	1.6	6.3	**6.6**	-2.6	3.4	6.7	**8.0**	0.8	22

fEVAR	Systolic BP	Total distraction force acting on Complete stent-graft (N)				Total distraction force acting on Proximal body (N)				Proximal Body Migration (mm)	Imaging Interval
		x	y	z	Total RDF	x	y	z	Total RDF		
29	145	-1.4	-5.3	3.9	**6.8**	-1.7	-0.7	-0.2	**1.9**	2.6	41
30	142	0.1	-0.1	4.7	**4.7**	-0.3	0.6	3.4	**3.5**	3.6	35
31	Only 1 available postoperative CT (follow-up elsewhere)										
32	150	2.4	-2.3	5.1	**6.1**	2.1	0.7	3.1	**3.8**	0.5	4
33	No postoperative CT imaging with contrast										
34	172	4.2	-2.2	6.2	**7.8**	1.9	3.0	5.9	**6.9**	3.5	38
35	148	-0.8	1.8	2.1	**2.9**	-0.4	4.3	1.9	**4.7**	0.0	36
36	143	0.5	-1.1	5.8	**5.9**	-0.5	0.6	4.2	**4.3**	0.4	34
37	125	-0.7	0.1	2.6	**2.7**	-0.9	1.0	-0.3	**1.3**	-1.5	35
38	Only 1 available postoperative CT (died at 1 month)										
39	125	-1.2	-1.8	1.0	**2.4**	-2.5	-0.1	1.3	**2.8**	2.6	35
40	120	-0.6	-1.3	1.6	**2.1**	-0.6	3.0	2.8	**4.1**	-2.0	5
41	145	1.2	-1.5	8.7	**8.9**	4.1	3.6	5.5	**7.7**	1.3	26
42	No postoperative CT imaging										
43	180	1.4	-1.4	3.7	**4.2**	1.7	1.9	2.4	**3.5**	3.3	23
44	Only 1 available postoperative CT (follow-up elsewhere)										
45	165	0.9	-1.8	5.9	**6.2**	0.2	-0.1	5.1	**5.1**	7.8	11
46	92	-0.4	1.1	5.0	**5.1**	-0.1	2.1	4.2	**4.7**	1.7	21
47	140	2.1	1.5	4.6	**5.3**	0.9	1.6	4.2	**4.6**	1.9	21
48	100	-0.1	-3.0	1.1	**3.2**	0.0	1.0	1.8	**2.1**	0.2	22
49	185	-3.6	-4.3	4.4	**7.1**	-0.2	0.8	5.7	**5.8**	3.3	25
50	Only 1 available postoperative CT										
51	Only 1 available postoperative CT										
52	150	-0.2	1.3	6.2	**6.4**	-1.4	1.9	3.1	**3.9**	-0.5	11
53	135	1.8	0.5	4.5	**4.8**	0.8	3.2	6.3	**7.1**	8.5	18
54	No postoperative CT imaging										
55	130	0.5	-0.6	9.5	**9.5**	0.6	0.6	8.5	**8.6**	6.1	11
56	123	0.2	-4.7	0.0	**4.7**	-0.7	0.1	6.4	**6.4**	-2.0	5
57	130	0.2	-4.0	1.4	**4.3**	0.3	-0.2	3.8	**3.8**	3.8	11
58	Only 1 available postoperative CT (died at 1 month)										
59	137	-2.7	-1.7	5.3	**6.2**	-2.5	0.3	5.7	**6.3**	2.3	4

Imaging interval in completed months, Systolic BP: Preoperative systolic blood pressure (mmHg), x,y,z forces and Total RDF include both pressure and viscous forces

8.7.2 Patient-specific total distraction force, interval change in M1, 2, 3 and 4 measurements and imaging interval for distal bodies

fEVAR	Systolic BP	Total RDF complete stent-graft*	Total distraction force acting on distal body (N)				M1 difference (mm)	M2 difference (mm)	M3 difference (mm)	M4 difference (mm)	Component distraction	Imaging interval
			x	y	z	Total RDF						
1	No postoperative CT imaging											
2	Only 1 available postoperative CT (follow-up elsewhere)											
3	No postoperative CT imaging											
4	150	**2.1**	-2.7	-1.4	4.2	**5.2**	-0.1	1.4	0.1	-0.8	No	21
5	Only 1 available postoperative CT (follow-up elsewhere)											
6	140	**5.9**	0.5	-1.7	4.6	**5.0**	3.9	2.5	1.2	-1.3	No	26
7	Custom made hybrid proximal/distal body component											
8	160	**6.4**	1.1	-3.4	7.2	**8.0**	1.3	1.7	1.1	0.5	No	19
9	134	**2.2**	0.2	-2.7	4.1	**4.9**	-0.5	-0.3	-0.3	0.1	No	45
10	100	**3.3**	-1.5	-1.7	2.5	**3.3**	1.6	-0.2	0.2	0.3	No	17
11	112	**6.2**	-0.7	-0.9	3.8	**4.0**	0.4	-0.8	-0.3	0.5	No	4
12	147	**6.8**	2.1	-1.3	4.9	**5.5**	2.7	-1.0	-1.7	-0.5	No	12
13	150	**3.0**	0.9	-1.7	1.4	**2.4**	0.7	0.9	-1.4	-2.3	No	26
14	129	**6.0**	-0.4	-1.3	2.8	**3.1**	-0.2	-1.0	-2.7	-1.6	No	20
15	134	**3.3**	-0.4	-1.6	4.4	**4.7**	0.6	-1.0	-2.3	-0.7	No	49
16	122	**2.6**	0.4	-1.5	4.6	**4.9**	-1.0	0.4	1.0	0.7	No	51
17	Only 1 available postoperative CT (follow-up elsewhere)											
18	145	**3.2**	-0.4	-1.9	3.7	**4.2**	2.2	1.0	0.5	-0.5	No	52
19	164	**6.0**	-2.2	-1.3	5.6	**6.2**	2.9	-1.6	-6.2	-4.6	No	47
20	160	**2.5**	2.2	-1.9	6.0	**6.6**	2.1	-1.6	1.1	2.7	No	45
21	137	**3.5**	0.3	-2.8	1.8	**3.3**	6.6	3.0	-2.3	-5.3	No	26
22	117	**4.8**	0.3	-1.8	3.8	**4.3**	6.7	5.6	0.5	-5.1	**Yes**	49
23	Only 1 available postoperative CT (follow-up elsewhere)											
24	Only 1 available postoperative CT (poor renal function)											
25	120	**13.1**	0.5	-1.4	5.0	**5.3**	1.9	-0.2	-1.7	-1.5	No	52
26	130	**5.5**	-0.4	-2.7	4.8	**5.5**	4.4	2.6	2.3	-0.3	No	44
27	135	**7.1**	-0.8	-2.0	5.5	**5.9**	-0.3	-0.3	-2.7	-2.2	No	10
28	140	**6.6**	0.2	-1.4	6.1	**6.3**	1.3	0.1	1.1	1.2	No	23

fEVAR	Systolic BP	Total RDF complete stent-graft*	Total distraction force acting on distal body (N)				M1 difference (mm)	M2 difference (mm)	M3 difference (mm)	M4 difference (mm)	Component distraction	Imaging interval
			x	y	z	Total RDF						
29	145	**6.8**	-1.7	-3.4	3.6	**5.2**	0.4	2.6	3.4	0.7	No	41
30	142	**4.7**	-0.6	-0.8	5.7	**5.8**	0.7	0.5	-0.6	-1.3	No	35
31	Only 1 available postoperative CT (follow-up elsewhere)											
32	150	**6.1**	-0.8	-1.9	4.5	**4.9**	-1.3	-0.4	0.6	1.3	No	5
33	No postoperative CT imaging with contrast											
34	172	**7.8**	0.8	-5.3	4.2	**6.8**	0.2	1.2	2.4	1.0	No	38
35	148	**2.9**	-0.2	-3.2	3.6	**4.8**	1.9	0.9	-3.1	-4.4	No	36
36	143	**5.9**	0.2	-1.5	2.8	**3.2**	0.3	-0.1	-2.4	-2.4	No	34
37	125	**2.7**	-0.3	-0.9	3.4	**3.5**	2.8	2.5	1.7	-0.9	No	35
38	Only 1 available postoperative CT (died at 1 month)											
39	125	**2.4**	2.0	-0.9	3.3	**4.0**	3.3	2.7	0.3	-2.5	No	35
40	120	**2.1**	1.6	-2.6	1.8	**3.5**	7.8	1.3	0.9	-0.7	No	5
41	145	**8.9**	-1.0	-3.2	3.3	**4.7**	-1.7	1.7	2.1	1.0	No	24
42	No postoperative CT imaging											
43	180	**4.2**	-2.1	-3.2	2.7	**4.7**	6.6	5.4	-0.6	-6.1	**Yes**	23
44	Only 1 available postoperative CT (follow-up elsewhere)											
45	165	**6.2**	0.7	-1.6	5.2	**5.5**	-1.8	-1.8	-1.2	0.6	No	11
46	92	**5.1**	0.2	-1.1	2.6	**2.8**	11.3	13.7	4.2	-9.6	**Yes**	21
47	140	**5.3**	0.7	-1.6	6.0	**6.2**	-1.3	-0.2	0.3	0.5	No	21
48	100	**3.2**	-2.1	-3.5	2.5	**4.8**	2.4	1.3	0.5	-0.9	No	22
49	185	**7.1**	-0.6	-2.3	5.5	**6.0**	0.3	2.8	0.4	-2.2	No	25
50	Only 1 available postoperative CT											
51	Only 1 available postoperative CT											
52	150	**6.4**	0.4	0.2	3.9	**3.9**	0.7	1.3	0.3	-1.0	No	11
53	135	**4.8**	0.5	-2.6	3.2	**4.1**	-2.6	-1.4	-3.9	-2.5	No	8
54	No postoperative CT imaging											
55	130	**9.5**	-1.3	-0.7	3.6	**3.9**	-2.7	-3.2	-2.9	0.3	No	11
56	123	**4.7**	-3.5	-2.9	-0.1	**4.5**	-0.6	-2.7	-2.1	0.7	No	5
57	130	**4.3**	-1.7	-3.2	1.2	**3.8**	3.7	0.4	0.8	0.8	No	4

fEVAR	Systolic BP	Total RDF complete stent-graft*	Total distraction force acting on distal body (N)				M1 difference (mm)	M2 difference (mm)	M3 difference (mm)	M4 difference (mm)	Component distraction	Imaging interval
			x	y	z	Total RDF						
58	Only 1 available postoperative CT (died at 1 month)											
59	137	**6.2**	-0.3	-2.4	2.0	**3.2**	-2.9	0.4	1.9	1.3	No	4

Imaging interval in completed months, M1-4: component distraction measurements (see 6.5.2.4), Systolic BP: Preoperative systolic blood pressure (mmHg), x,y,z forces and Total RDF include both pressure and viscous forces. *for full description of forces acting on complete stent-graft see 8.7.1

8.7.3 Patient-specific total distraction force, migration distance and imaging interval for limb extensions

fEVAR	Systolic BP	Total RDF complete stent-graft*	R/L	Total distraction force acting on limb extensions (N)				Migration (mm)	Imaging interval
				x	y	z	Total RDF		
1	No postoperative CT imaging								
2	Only 1 available postoperative CT (follow-up elsewhere)								
3	No postoperative CT imaging								
4	150	**2.1**	L	1.3	0.1	-0.8	**1.6**	0.1	21
5	Only 1 available postoperative CT (follow-up elsewhere)								
6	140	**5.9**	L	3.1	-0.4	-0.9	**3.3**	-1.3	26
7	167	**7.6**	R	-0.3	-2.4	-0.4	**2.5**	-0.1	72
8	160	**6.4**	R	0.3	-1.0	0.2	**1.0**	-0.1	19
9	134	**2.2**	R	-2.3	-2.0	-2.3	**3.8**	1.6	45
10	100	**3.3**	L	-0.3	-0.2	-0.1	**0.4**	2.4	17
			R	-0.4	-0.1	0.0	**0.5**	0.2	17
11	112	**6.2**	L	0.9	-0.8	0.3	**1.2**	2.2	4
12	147	**6.8**	L	1.2	-1.1	-2.9	**3.3**	-1.8	12
			R	-1.1	0.1	-1.1	**1.6**	1.0	12

fEVAR	Systolic BP	Total RDF complete stent-graft*	R/L	Total distraction force acting on limb extensions (N)				Migration (mm)	Imaging interval
				x	y	z	Total RDF		
13	150	**3.0**	R	-0.6	-0.3	0.5	**0.9**	1.2	26
14	129	**6.0**	L	0.5	-1.2	0.8	**1.5**	1.1	13
			R	-0.8	-2.3	0.3	**2.5**	1.6	13
15	Wallstent								
16	122	**2.6**	L	0.6	-0.4	-0.1	**0.8**	-3.4	51
17	Only 1 available postoperative CT (follow-up elsewhere)								
18	145	**3.2**	R	-0.3	-0.5	0.9	**1.1**	-0.6	52
19	164	**6.0**	L	2.5	-1.2	-0.6	**2.8**	-5.0	47
20	160	**2.5**	R	-1.7	-1.1	-2.2	**3.0**	-10.6	45
21	137	**3.5**	L	0.4	-0.6	0.2	**0.7**	-1.2	26
			R	-0.2	-1.8	-1.0	**2.1**	-2.2	26
22	117	**4.8**	L	0.7	-0.9	0.4	**1.2**	0.3	49
23	Only 1 available postoperative CT (follow-up elsewhere)								
24	Only 1 available postoperative CT (poor renal function)								
25	120	**13.1**	L	4.2	-4.7	0.3	**6.3**	-4.4	52
26	130	**5.5**	R	-0.6	-1.2	0.8	**1.6**	-0.3	44
27	135	**7.1**	L	1.0	-1.5	0.6	**1.9**	0.2	10
28	140	**6.6**	L	1.9	-1.4	-0.1	**2.3**	-1.9	22
29	145	**6.8**	L	0.7	-1.9	0.1	**2.0**	-0.9	41
30	142	**4.7**	L	0.6	-0.5	0.8	**1.1**	-1.6	35
31	Only 1 available postoperative CT (follow-up elsewhere)								
32	150	**6.1**	L	1.2	-1.8	0.3	**2.2**	1.1	4
33	No postoperative CT imaging with contrast								
34	172	**7.8**	L	2.5	-1.8	1.2	**3.3**	-3.4	38
35	148	**2.9**	L	0.1	-1.3	-0.2	**1.3**	-2.1	36
36	143	**5.9**	L	0.7	-0.6	0.2	**1.0**	-0.7	34
37	125	**2.7**	L	0.6	-0.5	1.0	**1.3**	0.5	35
38	Only 1 available postoperative CT (died at 1month)								

fEVAR	Systolic BP	Total RDF complete stent-graft*	R/L	Total distraction force acting on limb extension(N)				Migration (mm)	Imaging interval
				x	y	z	Total RDF		
39	125	**2.4**	L	1.2	-1.0	0.6	**1.7**	2.0	35
40	120	**2.1**	R	-1.3	-2.2	-0.7	**2.7**	No Data	
41	145	**8.9**	L	-0.5	-2.1	0.4	**2.1**	-1.0	26
			R	-1.8	-2.0	0.3	**2.7**	-4.9	26
42	No postoperative CT imaging								
43	180	**4.2**	L	1.1	-1.3	0.2	**1.7**	-2.9	23
44	Only 1 available postoperative CT (follow-up elsewhere)								
45	165	**6.2**	L	0.6	-0.6	1.3	**1.6**	-0.9	11
46	92	**5.1**	L	0.3	-0.2	0.7	**0.8**	-1.2	21
			R	-0.6	-0.5	0.5	**0.9**	1.2	21
47	140	**5.3**	L	1.4	0.3	0.8	**1.6**	-0.1	21
48	100	**3.2**	L	1.9	-1.7	0.3	**2.6**	0.7	22
49	Unable to identify inlet/outlets								
50	Only 1 available postoperative CT								
51	Only 1 available postoperative CT								
52	150	**6.4**	L	1.0	-0.5	0.4	**1.2**	-3.3	11
53	135	**4.8**	L	1.7	-1.4	-0.8	**2.3**	1.4	18
			R	-0.9	-0.9	-0.4	**1.3**	-0.4	18
54	No postoperative CT imaging								
55	130	**9.5**	L	1.1	-0.4	-0.5	**1.3**	No Data	
56	123	**4.7**	L	4.5	-2.0	-3.0	**5.8**		
57	130	**4.3**	L	0.7	-2.4	-1.4	**2.8**		
58	Only 1 available postoperative CT (died at 1 month)								
59	137	**6.2**	R	0.0	-0.3	0.5	**0.5**	No Data	

Imaging interval in completed months, Systolic BP: Preoperative systolic blood pressure (mmHg), *for full description of forces acting on complete stent-graft see 8.7.1, x,y,z forces and Total RDF include both pressure and viscous forces, negative values in Migration column indicate migration in proximal direction

8.8 Patient demographics

fEVAR	Gender	Age at fEVAR	BMI	Diabetes	IHD	LVF	Hypertension	CRF	Smoker	PVD	ASA grade	Systolic BP	Pulse rate	D3 (mm)
1	No postoperative CT imaging													
2	Only 1 available postoperative CT (follow-up elsewhere)													
3	No postoperative CT imaging													
4	M	76	29.1	Yes	Yes	No	Yes	Yes	Yes	No	3	150	99	76
5	Only 1 available postoperative CT (follow-up elsewhere)													
6	M	78	25.4	No	Yes	No	Yes	No	Yes	No	3	140	70	65
7	M	76	34.3	No	Yes	No	Yes	No	No	No	3	167	60	80
8	M	85	27.4	No	Yes	No	Yes	No	Yes	Yes	3	160	76	76
9	M	83	28.8	No	Yes	No	Yes	No	No	No	3	134	94	61
10	F	65	28.3	No	Yes	Yes	No	No	Yes	No	3	100	60	55
11	M	66	30.6	No	Yes	No	No	No	Ex	No	3	112	70	67
12	M	77	25.3	No	Yes	No	Yes	No	Yes	Yes	3	147	71	57
13	M	81	21.8	No	Yes	No	Yes	No	Yes	No	3	150	82	68
14	M	73	25.2	No	No	No	No	No	Yes	No	3	129	118	79
15	M	81	25.7	No	Yes	No	Yes	No	Yes	No	3	134	67	57
16	M	71	25.1	Yes	Yes	No	No	No	Ex	No	3	122	84	60
17	Only 1 available postoperative CT (follow-up elsewhere)													
18	M	65	25.3	No	Yes	No	Yes	No	Yes	Yes	2	145	50	55

fEVAR	Gender	Age at fEVAR	BMI	Diabetes	IHD	LVF	Hypertension	CRF	Smoker	PVD	ASA grade	Systolic BP	Pulse rate	D3 (mm)
19	F	86	25.0	No	Yes	No	No	No	Yes	No	3	164	90	57
20	M	81	20.3	No	No	No	No	No	Yes	No	3	160	75	70
21	M	70	27.2	No	Yes	No	Yes	No	No	No	2	137	85	57
22	M	62	26.3	No	Yes	No	No	No	Ex	No	3	117	65	62
23	Only 1 available postoperative CT (follow-up elsewhere)													
24	Only 1 available postoperative CT (poor renal function)													
25	M	78	24.9	No	No	No	No	No	No	No	2	120	66	85
26	M	78	23.7	No	Yes	No	No	Yes	Ex	No	3	130	68	68
27	M	76	24.5	No	No	No	No	No	No	No	3	135	65	57
28	M	75	25.1	No	No	No	Yes	No	Yes	No	2	140	70	64
29	M	65	40.9	No	No	No	Yes	No	Ex	No	3	145	90	80
30	M	68	26.8	No	No	No	Yes	No	No	No	2	142	62	56
31	Only 1 available postoperative CT (follow-up elsewhere)													
32	M	76	25.1	No	Yes	No	Yes	No	Yes	No	3	150	66	65
33	No postoperative CT imaging with contrast													
34	M	68	28.0	No	No	No	Yes	No	Yes	No	3	172	82	62
35	M	71	35.1	No	No	No	No	No	Yes	No	2	148	88	75
36	M	75	29.9	No	No	No	No	No	No	Yes	3	143	80	68
37	M	64	28.4	No	Yes	No	Yes	No	Yes	No	3	125	69	64
38	Only 1 available postoperative CT (died at 1 month)													
39	M	74	26.4	No	No	No	No	No	Ex	No	1	125	64	58
40	F	83	24.2	No	Yes	No	No	No	No	No	3	120	82	61

fEVAR	Gender	Age at fEVAR	BMI	Diabetes	IHD	Heart failure	Hypertension	CRF	Smoker	PVD	ASA grade	Systolic BP	Pulse rate	D3 (mm)
41	M	72	33.9	Yes	Yes	No	Yes	Yes	Yes	No	3	145	85	74
42	No postoperative CT imaging													
43	F	76	27.6	No	No	No	No	No	No	No	3	180	90	59
44	Only 1 available postoperative CT (follow-up elsewhere)													
45	M	74	22.6	No	No	No	Yes	Yes	Yes	No	3	165	65	64
46	M	78	19.7	No	No	No	No	No	Ex	No	2	92	62	57
47	M	85	26.8	No	Yes	No	No	No	Yes	Yes	2	140	69	62
48	F	64	28.3	No	Yes	No	Yes	No	Yes	No	3	100	53	66
49	M	77	35.4	No	Yes	No	Yes	No	Yes	No	3	185	70	71
50	Only 1 available postoperative CT													
51	Only 1 available postoperative CT													
52	M	82	31.4	Yes	Yes	No	Yes	Yes	Yes	No	2	150	60	86
53	M	71	28.6	No	No	No	No	No	Yes	No	2	135	75	58
54	No postoperative CT imaging													
55	M	76	23.9	No	No	No	Yes	No	Ex	No	3	130	75	59
56	M	68	30.6	No	No	No	No	No	Ex	No	2	123	68	70
57	M	82	28.6	No	No	No	Yes	No	Yes	No	3	130	76	55
58	Only 1 available postoperative CT (died at 1 month)													
59	M	76	30.4	No	Yes	No	Yes	No	Yes	No	2	137	62	58

Demographics for all patients included in chapter 6. BMI: Body mass index, IHD: Ischaemic heart disease, CRF: Chronic renal failure, PVD: Peripheral vascular disease, ASA: American Association of Anaesthetists, Systolic BP: Preoperative systolic blood pressure (mmHg), Pulse rate: Preoperative pulse rate (beats per minutes), D3: Maximum preoperative aneurysm diameter

8.9 Clinical outcomes

fEVAR	Proximal migration*	Comp. distraction*	Limb migration*	Graft-related adverse event	Reintervention	Other	Outcome	Follow-up (months)
1	Not assessed					MI 4 days post fEVAR	Died	0
2	Not assessed			SMA stenosis (mesenteric ischaemia)	Angioplasty 1mnth. REIA to SMA bypass, 8mnts		Lost to follow-up	28
3	Not assessed				Left hemi-colectomy within 30 days	Perforated colon due to fibro-matosis	Died NARC	18
4	No	No	No			type II, 2yrs	Died NARC	32
5	Not assessed					type II, 0-6yrs	Lost to follow-up	75
6	No	No	No				Died NARC	37
7	Yes	-	No		None		Alive	74
8	No	No	No				Died NARC	44
9	No	No	No				Alive	80
10	No	No	No				Alive	43
11	No	No	No				Died NARC	19
12	No	No	No				Died Unknown	39
13	No	No	No				Declined further follow-up	26
14	No	No	No				Died NARC	18
15	No	No	-				Died NARC	59
16	Yes	No	No		None		Declined further follow-up	53
17	Not assessed						Lost to follow-up	6
18	Yes	No	No		None		Alive	65
19	Yes	No	Yes		None	type II, 4yrs	Died NARC	57
20	No	No	Yes		None		Alive	59
21	No	No	No	Stenosis of RRA(scallop) AAA Expansion	RRA stent 8mnths	type II 1-27mnths	Alive	27

fEVAR	Proximal migration*	Comp. distraction*	Limb migration*	Graft-related adverse event	Reintervention	Other	Outcome	Follow-up (months)
22	No	Yes	No		None		Alive	63
23	Not assessed						Lost to follow-up	11
24	Not assessed			Early RRA stent stenosis	RRA stent angioplasty in 1st month	type II, 0-5yrs	Alive	61
25	No	No	Yes	Early occlusion Rt limb. Lf limb stenosis + BMS #, 14mnths. AAA expansion. RRA stent #, LRA stent dislocation + IIIa, 50mnths	IMA emboli-sation 15mnths	type II 2-14mnths	Alive	63
26	Yes	No	No		None		Died NARC	49
27	Yes	No	No		None		Died NARC	20
28	No	No	No	Early occlusion Rt limb			Lost to follow-up	24
29	No	No	No	RRA occlusion 43mnths	Ureteric stent	Transient type II, 1month. Ureteric obstruction due to fibrosis	Lost to follow-up	43
30	No	No	No			transient type II 1mnth	Alive	49
31	Not assessed						Died NARC	52
32	No	No	No	type IIIa from RRA	RRA stent angioplasty 12mnths		Lost to follow-up	15
33	Not assessed					type II 0-4yrs	Alive	50
34	No	No	No	SMA stent #	SMA re-stented 27mnths	type II 0-3yrs	Alive	39
35	No	No	No	SMA stenosis (scallop)	SMA stent 42mnths		Alive	49

fEVAR	Proximal migration*	Comp. distraction*	Limb migration*	Graft-related adverse event	Reintervention	Other	Outcome	Follow-up (months)
36	No	No	No	RRA stent # and occlusion	Diagnostic angiogram 39mnths	transient type II 1-8mnths	Alive	48
37	No	No	No			Pre-existing native REIA occlusion with fem-fem xover	Alive	36
38	Not assessed			Postoperative bleeding	Re-exploration of right groin	MI, MSOF	Died	1
39	No	No	No †	Ipsilateral limb occlusion, 36mnths	None	transient type II 1-12mnths	Died NARC	38
40	No	No	No				Died NARC	13
41	No	No	Yes	SMA stent dislocation + occlusion, 15mnths	None		Alive	38
42	Not assessed			Expanding AAA		transient type II, 2mnths	Lost to follow-up	9
43	No	Yes	No		None		Alive	39
44	Not assessed						Died NARC	13
45	Yes	No	No	High velocity in SMA	Diagnostic angiogram 10mnts (NAD)	transient type II 2mnts	Died NARC	24
46	No	Yes	No		None		Died NARC	40
47	No	No	No				Alive	23
48	No	No	No			transient type II 2mnths	Alive	36
49	No	No	-		None	type II 0-2yrs	Alive	25
50	Not assessed							24
51	Not assessed							16
52	No	No	No	SMA stent #	SMA re-stented 13mnths		Alive	24

fEVAR	Proximal migration*	Comp. distraction*	Limb migration*	Graft-related adverse event	Reintervention	Other	Outcome	Follow-up (months)
53	Yes	No	No	type IIIa from LRA	LRA stent angioplasty 14mnths	transient type II 6mnths	Alive	26
54	Not assessed							4
55	Yes	No	-		None		Alive	13
56	No	No	-				Alive	13
57	No	No	-				Alive	5
58	Not assessed						Died NARC	1
59	No	No	-			type II 1-12mnths	Alive	11

*as determined by CLL analysis, Comp. distraction: Component distraction of the distal body from the proximal body, Limb migration: Proximal migration of the distal iliac limb extension seal-zone, †only incidence of proximal migration of ipsilateral limb (distal body), L/RRA: Left/Right renal artery, MI: Myocardial infarction, MSOF: Multisystem organ failure, NAD: No Abnormality Detected, NARC: Non-aneurysm-related causes, SMA: Superior mesenteric artery, type I/II/III: endoleak classification, #: fracture

9 References

1. Bailey H, Love M, Mann CV, Russell RCG, Rains AJH. Bailey and Love's Short practice of surgery. 21st ed: London: Chapman & Hall; 1992.
2. Abdominal Aortic Aneurysm: Stanford Health Care; 2015 [31/12/2015]. Available from: http://stanfordhospital.org/clinicsmedservices/COE/surgicalservices/vascularsurgery/patienteducation/abdomin.html.
3. Thompson SG, Ashton HA, Gao L, Buxton MJ, Scott RAP. Final follow-up of the Multicentre Aneurysm Screening Study (MASS) randomized trial of abdominal aortic aneurysm screening. Br J Surg. 2012;99(12):1649-56.
4. Office for National Statistics, Mortality Statistics: Deaths Registered in England and Wales (Series DR) 2013 [31/12/2015]. Available from: http://www.ons.gov.uk/ons/publications/re-reference-tables.html?edition=tcm%3A77-325289.
5. Beard JD, Gaines PA, Loftus I. Vascular and Endovascular Surgery: A Companion to Specialist Surgical Practice. 5th Ed: Saunders Ltd; 2013.
6. Jones GT, Phillips VL, Harris EL, Rossaak JI, van Rij AM. Functional matrix metalloproteinase-9 polymorphism (C-1562T) associated with abdominal aortic aneurysm. J Vasc Surg. 2003;38(6):1363-7.
7. Wills A, Thompson MM, Crowther M, Sayers RD, Bell PRF, Wills A, et al. Pathogenesis of abdominal aortic aneurysms; Cellular and biochemical mechanisms. Eur J Vasc Endovasc Surg. 1996;12(4):391-400.
8. Grootenboer N, Bosch JL, Hendriks JM, van Sambeek MRHM. Epidemiology, Aetiology, Risk of Rupture and Treatment of Abdominal Aortic Aneurysms: Does Sex Matter? Eur J Vasc Endovasc Surg. 2009;38(3):278-84.
9. Scott RAP, Wilson NM, Ashton HA, Kay DN. Influence of screening on the incidence of ruptured abdominal aortic aneurysm: 5-year results of a randomized controlled study. Br J Surg. 1995;82(8):1066-70.
10. Thompson SG, Ashton HA, Gao L, Scott RAP. Screening men for abdominal aortic aneurysm: 10 year mortality and cost effectiveness results from the randomised Multicentre Aneurysm Screening Study. BMJ. 2009;338(7710):1538-41.
11. Darwood RJ, Brooks MJ. The Impact of Decreasing Abdominal Aortic Aneurysm Prevalence on a Local Aneurysm Screening Programme. Eur J Vasc Endovasc Surg. 2012;44(1):45-50.
12. Hager J, Länne T, Carlsson P, Lundgren F. Lower Prevalence than Expected when Screening 70-year-old Men for Abdominal Aortic Aneurysm. Eur J Vasc Endovasc Surg. 2013;46(4):453-9.
13. Lederle FA, Wilson SE, Johnson GR, Reinke DB, Littooy FN, Acher CW, et al. Immediate Repair Compared with Surveillance of Small Abdominal Aortic Aneurysms. New Engl J Med. 2002;346(19):1437-44.
14. Powell JT, Brown LC, Forbes JF, Fowkes FG, Greenhalgh RM, Ruckley CV, et al. Final 12-year follow-up of Surgery versus Surveillance in the UK Small Aneurysm Trial: UK Small Aneurysm Trial participants. Br J Surg. 2007;94(6):702-8.
15. Powell JT, Brown LC, Greenhalgh RM, Thompson SG. The Rupture Rate of Large Abdominal Aortic Aneurysms. Ann Surg. 2008;247(1):173-9.
16. Kirk RM, Winslet M. Essential General Surgical Operations. London: Churchill Livingstone; 2002.

17. Mike Wyatt SB, Ross Naylor, Simon Parvin, Jonothan Earnshaw, Vince Smith, Ian Loftus, Collette Marshall, Peter Barker, Julian Scott,Emily Diment, Graham Munneke, Adam Pichel. National Abdominal Aortic Aneurysm Quality Improvement Programme Interim Report: The Vascular Society of Great Britain and Ireland; 2011. Available from: http://www.vascularsociety.org.uk/wp-content/uploads/2012/11/National-AAA-QIP-Interim-Report.pdf.
18. Waton S, Johal A, Groene O, Cromwell D, Mitchell D, Loftus I. Outcomes after elective repair of infra-renal abdominal aortic aneurysm: London: The Royal College of Surgeons of England; 2013.
19. Tim Lees GS, Sara Baker, David Mitchell, Peter Holt, Peter Taylor, Ben Patterson, Jonothan Earnshaw, Peter Lamont. National Vascular Database Report 2009: The Vascular Society of Great Britain and Ireland; 2009. Available from: http://www.vascularsociety.org.uk/vascular/wp-content/uploads/2012/11/NVDREPORTFINAL-10Nov.pdf.
20. Parodi JC, Palmaz JC, Barone HD, Parodi JC, Palmaz JC, Barone HD. Transfemoral Intraluminal Graft Implantation for Abdominal Aortic Aneurysms. Ann Vasc Surg. 1991;5(6):491-9.
21. Aortic Intervention: Cook Medical Inc.; 2015 [31/12/2015]. Available from: https://www.cookmedical.com/aortic-intervention/abdominal-and-thoracic-aortic-disease-require-a-progressive-approach-to-treatment/.
22. Keefer A, Hislop S, Singh MJ, Gillespie D, Illig KA. The influence of aneurysm size on anatomic suitability for endovascular repair. J Vasc Surg. 2010;52(4):873-7.
23. The UK EndoVascular Aneurysm Repair (EVAR) trials: randomised trials of EVAR versus standard therapy. Health Technol Assess. 2012;16(9):1-218.
24. Lederle FA, Freischlag JA, Kyriakides TC, Padberg FT, Matsumura JS, Kohler TR, et al. Outcomes Following Endovascular vs Open Repair of Abdominal Aortic Aneurysm A Randomized Trial. JAMA. 2009;302(14):1535-42.
25. Prinssen M, Verhoeven ELG, Buth J, Cuypers PWM, van Sambeek MRHM, Balm R, et al. A Randomized Trial Comparing Conventional and Endovascular Repair of Abdominal Aortic Aneurysms. New Engl J Med. 2004;351(16):1607-18.
26. Becquemin JP, Pillet JC, Lescalie F, Sapoval M, Goueffic Y, Lermusiaux P, et al. A randomized controlled trial of endovascular aneurysm repair versus open surgery for abdominal aortic aneurysms in low- to moderate-risk patients. J Vasc Surg. 2011;53(5):1167-73.
27. Epstein D, Sculpher MJ, Powell JT, Thompson SG, Brown LC, Greenhalgh RM. Long-term cost-effectiveness analysis of endovascular versus open repair for abdominal aortic aneurysm based on four randomized clinical trials. Br J Surg. 2014;101(6):623-31.
28. White HA, MacDonanld S. Estimating risk associated with radiation exposure during follow-up after endovascular aortic repair (EVAR). J Cardiovasc Surg. 2010;51(1):95-104.
29. Richenberg J. How to reduce nephropathy following contrast-enhanced CT: A lesson in policy implementation. Clin Radiol. 2012;67(12):1136-45.
30. Bobadilla JL, Suwanabol PA, Reeder SB, Pozniak MA, Bley TA, Tefera G. Clinical Implications of Non–Contrast-Enhanced Computed Tomography for Follow-Up After Endovascular Abdominal Aortic Aneurysm Repair. Ann Vasc Surg. 2013;27(8):1042-8.
31. Harrison GJ, Oshin OA, Vallabhaneni SR, Brennan JA, Fisher RK, McWilliams RG, et al. Surveillance after EVAR Based on Duplex Ultrasound and Abdominal Radiography. Eur J Vasc Endovasc Surg. 2011;42(2):187-92.
32. Cantisani V, Ricci P, Grazhdani H, Napoli A, Fanelli F, Catalano C, et al. Prospective Comparative Analysis of Colour-Doppler Ultrasound, Contrast-enhanced Ultrasound,

Computed Tomography and Magnetic Resonance in Detecting Endoleak after Endovascular Abdominal Aortic Aneurysm Repair. Eur J Vasc Endovasc Surg. 2011;41(2):186-92.
33. Millen A, Canavati R, Harrison G, McWilliams RG, Wallace S, Vallabhaneni SR, et al. Defining a role for contrast-enhanced ultrasound in endovascular aneurysm repair surveillance. J Vasc Surg. 2013;58(1):18-23.
34. White GH, Yu W, May J, Chaufour X, Stephen MS. Endoleak as a Complication of Endoluminal Grafting of Abdominal Aortic Aneurysms: Classification, Incidence, Diagnosis,and Management. J Endovasc Surg. 1997;4(2):152-68.
35. White GH, May J, Waugh RC, Chaufour X, Yu W. Type III and Type IV Endoleak: Toward a Complete Definition of Blood Flow in the Sac After Endoluminal AAA Repair. J Endovasc Surg. 1998;5(4):305-9.
36. Brunicardi FC, Anderson DK, Billiar TR, Dunn DL, Hunter JG, Pollock RE, et al. Schwartz's Principles of Surgery. 9th ed. Brunicardi FC, editor2010.
37. Chung R, Morgan R, Chung R, Morgan RA. Type 2 Endoleaks Post-EVAR: Current Evidence for Rupture Risk, Intervention and Outcomes of Treatment. Cardiovasc Intervent Radiol. 2015;38(3):507-22.
38. Jones SM, Vallabhaneni SR, McWilliams RG, Naik J, Nicholas T, Fisher RK. Type IIIb Endoleak Is an Important Cause of Failure Following Endovascular Aneurysm Repair. J Endovasc Ther. 2014;21:723-7.
39. Gilling-Smith G, Brennan J, Harris P, Bakran A, Gould D, McWilliams R. Endotension After Endovascular Aneurysm Repair: Definition, Classification, and Strategies for Surveillance and Intervention. J Endovasc Surg. 1999;6(4):305-7.
40. Chaikof EL, Blankensteijn JD, Harris PL, White GH, Zarins CK, Bernhard VM, et al. Reporting standards for endovascular aortic aneurysm repair. J Vasc Surg. 2002;35(5):1048-60.
41. Howell BA, Kim T, Cheer A, Dwyer H, Saloner D, Chuter TA. Computational Fluid Dynamics Within Bifurcated Abdominal Aortic Stent-Grafts. J Endovasc Ther. 2007;14(2):138-43.
42. Resch T, Ivancev K, Brunkwall J, Nyman U, Malina M, Lindblad B. Distal Migration of Stent-Grafts after Endovascular Repair of Abdominal Aortic Aneurysms. J Vasc Interv Radiol. 1999;10(3):257-64.
43. Liffman K, Lawrence-Brown MMD, Semmens JB, Bui A, Rudman M, Hartley DE. Analytical Modeling and Numerical Simulation of Forces in an Endoluminal Graft. J Endovasc Ther. 2001;8(4):358-71.
44. Mohan IV, Harris PL, van Marrewijk CJ, Laheij RJ, How TV. Factors and forces influencing stent-graft migration after endovascular aortic aneurysm repair. J Endovasc Ther. 2002;9(6):748-55.
45. Abbruzzese TA, Kwolck CJ, Brewster DC, Chung TK, Kang J, Conrad MF, et al. Outcomes following endovascular abdominal aortic aneurysm repair (EVAR): An anatomic and device-specific analysis. J Vasc Surg. 2008;48(1):19-28.
46. Albertini JN, Kalliafas S, Travis S, Yusuf SW, Macierewicz JA, Whitaker SC, et al. Anatomical Risk Factors for Proximal Perigraft Endoleak and Graft Migration Following Endovascular Repair of Abdominal Aortic Aneurysms. Eur J Vasc Endovasc Surg. 2000;19(3):308-12.
47. Boult M, Babidge W, Maddern G, Barnes M, Fitridge R, on behalf of the Audit Reference G. Predictors of Success Following Endovascular Aneurysm Repair: Mid-term Results. Eur J Vasc Endovasc Surg. 2006;31(2):123-9.

48. Chisci E, Kristmundsson T, de Donato G, Resch T, Setacci F, Sonesson B, et al. The AAA With a Challenging Neck: Outcome of Open Versus Endovascular Repair With Standard and Fenestrated Stent-Grafts. J Endovasc Ther. 2009;16(2):137-46.
49. Fulton JJ, Farber MA, Sanchez LA, Godshall CJ, Marston WA, Mendes R, et al. Effect of challenging neck anatomy on mid-term migration rates in AneuRx endografts. J Vasc Surg. 2006;44(5):932-7.
50. Hobo R, Kievit J, Leurs LJ, Buth J. Influence of Severe Infrarenal Aortic Neck Angulation on Complications at the Proximal Neck Following Endovascular AAA Repair: A EUROSTAR Study. J Endovasc Ther. 2007;14(1):1-11.
51. Stather PW, Sayers RD, Cheah A, Wild JB, Bown MJ, Choke E. Outcomes of Endovascular Aneurysm Repair in Patients with Hostile Neck Anatomy. Eur J Vasc Endovasc Surg. 2012;44(6):556-61.
52. Waasdorp E, Vries J-P, Hobo R, Leurs L, Buth J, Moll F. Aneurysm Diameter and Proximal Aortic Neck Diameter Influence Clinical Outcome of Endovascular Abdominal Aortic Repair: A 4-Year EUROSTAR Experience. Ann Vasc Surg. 2005;19(6):755-61.
53. Crawford E, Beckett W, Greer M. Juxtarenal infrarenal abdominal aortic aneurysm. Special diagnostic and therapeutic considerations. Ann Surg. 1985;203(6):661-70.
54. Cross J, Gurusamy K, Gadhvi V, Simring D, Harris P, Ivancev K, et al. Fenestrated endovascular aneurysm repair. Br J Surg. 2012;99(2):152-9.
55. Torsello G, Troisi N, Donas KP, Austermann M. Evaluation of the Endurant stent graft under instructions for use vs off-label conditions for endovascular aortic aneurysm repair. J Vasc Surg. 2011;54(2):300-6.
56. Lee JT, Ullery BW, Zarins CK, Olcott C, Harris EJ, Dalman RL, et al. EVAR Deployment in Anatomically Challenging Necks Outside the IFU. Eur J Vasc Endovasc Surg. 2013;46(1):65-73.
57. Landry G, Lau I, Liem T, Mitchell E, Moneta G, Landry G. Open Abdominal Aortic Aneurysm Repair in the Endovascular Era : Effect of Clamp Site on Outcomes. Arch Surg. 2009;144(9):811-6.
58. Park JH, Chung JW, Choo IW, Kim SJ, Lee JY, Han MC. Fenestrated Stent-Grafts for Preserving Visceral Arterial Branches in the Treatment of Abdominal Aortic Aneurysms: Preliminary Experience. J Vasc Interv Radiol. 1996;7(6):819-23.
59. Semmens JB, Lawrence-Brown MM, Hartley DE, Allen YB, Green R, Nadkarni S. Outcomes of Fenestrated Endografts in the Treatment of Abdominal Aortic Aneurysm in Western Australia (1997-2004). J Endovasc Ther. 2006;13(3):320-9.
60. Zenith Fenestrated AAA Endovascular Graft Cook Medical Inc.; 2013 [13/08/2013]. Available from: https://www.cookmedical.com/products/adc82bec-ce78-46fd-8df0-0c78e4c6ebd3/#tab=specifications.
61. Amiot S, Haulon S, Becquemin JP, Magnan PE, Lermusiaux P, Goueffic Y, et al. Fenestrated Endovascular Grafting: The French Multicentre Experience. Eur J Vasc Endovasc Surg. 2010;39(5):537-44.
62. Greenberg RK, Sternbergh Iii WC, Makaroun M, Ohki T, Chuter T, Bharadwaj P, et al. Intermediate results of a United States multicenter trial of fenestrated endograft repair for juxtarenal abdominal aortic aneurysms. J Vasc Surg. 2009;50(4):730-7.
63. Kristmundsson T, Sonesson B, Malina M, Björses K, Dias N, Resch T. Fenestrated endovascular repair for juxtarenal aortic pathology. J Vasc Surg. 2009;49(3):568-75.
64. O'Neill S, Greenberg RK, Haddad F, Resch T, Sereika J, Katz E. A Prospective Analysis of Fenestrated Endovascular Grafting: Intermediate-term Outcomes. Eur J Vasc Endovasc Surg. 2006;32(2):115-23.

65. Scurr JR, Brennan JA, Gilling-Smith GL, Harris PL, Vallabhaneni SR, McWilliams RG. Fenestrated endovascular repair for juxtarenal aortic aneurysm. Br J Surg. 2008;95(3):326-32.
66. Tambyraja AL, Fishwick NG, Bown MJ, Nasim A, McCarthy MJ, Sayers RD. Fenestrated aortic endografts for juxtarenal aortic aneurysm: Medium term outcomes. Eur J Vasc Endovasc Surg. 2011;42(1):54-8.
67. Verhoeven ELG, Vourliotakis G, Bos WTGJ, Tielliu IFJ, Zeebregts CJ, Prins TR, et al. Fenestrated Stent Grafting for Short-necked and Juxtarenal Abdominal Aortic Aneurysm: An 8-Year Single-centre Experience. Eur J Vasc Endovasc Surg. 2010;39(5):529-36.
68. Ziegler P, Avgerinos ED, Umscheid T, Perdikides T, Stelter WJ. Fenestrated endografting for aortic aneurysm repair: A 7-year experience. J Endovasc Ther. 2007;14:609-18.
69. Cook Medical Inc. Zenith Fenestrated AAA Endovascular Graft Summary of Safety and Effectiveness Data 2012. Available from: http://www.accessdata.fda.gov/cdrh_docs/pdf2/P020018S040b.pdf.
70. Oderich GS. Diameter-Reducing Wire to Facilitate Deployment of a Modified Zenith Fenestrated Stent Graft. Ann Vasc Surg. 2010;24(7):980-4.
71. Cross J, Raine R, Harris P, Richards T. Indications for fenestrated endovascular aneurysm repair. Br J Surg. 2012;99(2):217-24.
72. Zenith Fenestrated AAA Endovascular Graft Instructions for Use: Cook Medical Inc.; 2012 [03/01/2016]. Available from: https://www.cookmedical.com/data/IFU_PDF/IFU-FU_V3.PDF.
73. Kan C-D, Lee H-L, Yang Y-J. Outcome after endovascular stent graft treatment for mycotic aortic aneurysm: A systematic review. J Vasc Surg. 2007;46(5):906-12.
74. Michel M, Becquemin JP, Clement MC, Marzelle J, Quelen C, Durand-Zaleski I, et al. Editor's Choice - Thirty day Outcomes and Costs of Fenestrated and Branched Stent Grafts versus Open Repair for Complex Aortic Aneurysms. Eur J Vasc Endovasc Surg. 2015;50(2):189-96.
75. Moll FL, Powell JT, Fraedrich G, Verzini F, Haulon S, Waltham M, et al. Management of Abdominal Aortic Aneurysms Clinical Practice Guidelines of the European Society for Vascular Surgery. Eur J Vasc Endovasc Surg. 2011;41, Supplement 1:S1-S58.
76. Sobocinski J, Chenorhokian H, Maurel B, Midulla M, Hertault A, Le Roux M, et al. The Benefits of EVAR Planning Using a 3D Workstation. Eur J Vasc Endovasc Surg. 2013;46(4):418-23.
77. Kitagawa A, Greenberg RK, Eagleton MJ, Mastracci TM. Zenith p-branch standard fenestrated endovascular graft for juxtarenal abdominal aortic aneurysms. J Vasc Surg. 2013;58(2):291-300.
78. Sobocinski J, d'Utra G, O'Brien N, Midulla M, Maurel B, Guillou M, et al. Off-the-Shelf Fenestrated Endografts: A Realistic Option for More Than 70% of Patients With Juxtarenal Aneurysms. J Endovasc Ther. 2012;19(2):165-72.
79. On behalf of the British Society for Endovascular Therapy and the Global Collaborators on Advanced Stent-Graft Techniques for Aneurysm Repair R. Early Results of Fenestrated Endovascular Repair of Juxtarenal Aortic Aneurysms in the United Kingdom / Clinical Perspective. Circulation. 2012;125(22):2707-15.
80. Troisi N, Donas KP, Austermann M, Tessarek J, Umscheid T, Torsello G. Secondary Procedures After Aortic Aneurysm Repair With Fenestrated and Branched Endografts. J Endovasc Ther. 2011;18(2):146-53.

81. de Souza LR, Oderich GS, Banga PV, Hofer JM, Wigham JR, Cha S, et al. Outcomes of total percutaneous endovascular aortic repair for thoracic, fenestrated, and branched endografts. J Vasc Surg. 2015 (in Press).
82. Harrison GJ, Thavarajan D, Brennan JA, Vallabhaneni SR, McWilliams RG, Fisher RK. Fascial Closure Following Percutaneous Endovascular Aneurysm Repair. Eur J Vasc Endovasc Surg. 2011;41(3):346-9.
83. Moore R, Hinojosa CA, O'Neill S, Mastracci TM, Cin, agrave, et al. Fenestrated endovascular grafts for juxtarenal aortic aneurysms: A step by step technical approach. Catheterization and Cardiovascular Interventions. 2007;69(4):554-71.
84. Melas N, Saratzis A, Saratzis N, Lazaridis J, Psaroulis D, Trygonis K, et al. Aortic and Iliac Fixation of Seven Endografts for Abdominal-aortic Aneurysm Repair in an Experimental Model Using Human Cadaveric Aortas. Eur J Vasc Endovasc Surg. 2010;40(4):429-35.
85. Oshin O, Brennan J, McWilliams R, Fisher R, Gilling-Smith G, Vallabhaneni S. Modes and mechanisms of threat to target vessel patency following fenestrated endovascular repair of juxtarenal aneurysms. Br J Surg. 2010;97:7-.
86. Oshin OA, How TV, Brennan JA, Fisher RK, McWilliams RG, Vallabhaneni SR. Magnitude of the Forces Acting on Target Vessel Stents as a Result of a Mismatch Between Native Aortic Anatomy and Fenestrated Stent-Grafts. J Endovasc Ther. 2011;18(4):569-75.
87. Ullery BW, Lee GK, Lee JT. Shuttering of the superior mesenteric artery during fenestrated endovascular aneurysm repair. J Vasc Surg. 2014;60(4):900-7.
88. Ricotta JJ, Oderich GS. Fenestrated and Branched Stent Grafts. Perspectives in Vascular Surgery and Endovascular Therapy. 2008;20(2):174-87.
89. Di X, Ye W, Liu C-W, Jiang J, Han W, Liu B. Fenestrated Endovascular Repair for Pararenal Abdominal Aortic Aneurysms: A Systematic Review and Meta-Analysis. Ann Vasc Surg. 2013;27(8):1190-200.
90. Linsen MAM, Jongkind V, Nio D, Hoksbergen AWJ, Wisselink W. Pararenal aortic aneurysm repair using fenestrated endografts. J Vasc Surg. 2012;56(1):238-46.
91. Nordon IM, Hinchliffe RJ, Holt PJ, Loftus IM, Thompson MM. Modern Treatment of Juxtarenal Abdominal Aortic Aneurysms with Fenestrated Endografting and Open Repair – A Systematic Review. Eur J Vasc Endovasc Surg. 2009;38(1):35-41.
92. Sun Z, Mwipatayi BP, Semmens JB, Lawrence-Brown MMD. Short to midterm outcomes of fenestrated endovascular grafts in the treatment of abdominal aortic aneurysms: a systematic review. J Endovasc Ther. 2006;13(6):747-53.
93. Ou J, Chan YC, Cheng SW. A Systematic Review of Fenestrated Endovascular Repair for Juxtarenal and Short-Neck Aortic Aneurysm: Evidence So Far. Ann Vasc Surg. 2015.
94. Rao R, Lane TR, Franklin IJ, Davies AH. Open repair versus fenestrated endovascular aneurysm repair of juxtarenal aneurysms. J Vasc Surg. 2015;61(1):242-55.
95. Belczak SQ, Lanziotti L, Botelho Y, Aun R, Silva ES, Puech-Leao P, et al. Open and endovascular repair of juxtarenal abdominal aortic aneurysms: a systematic review. Clinics (Sao Paulo). 2014;69(9):641-6.
96. Bicknell CD, Cheshire NJW, Riga CV, Bourke P, Wolfe JHN, Gibbs RGJ, et al. Treatment of Complex Aneurysmal Disease with Fenestrated and Branched Stent Grafts. Eur J Vasc Endovasc Surg. 2009;37(2):175-81.
97. Manning BJ, Agu O, Richards T, Ivancev K, Harris PL. Early Outcome Following Endovascular Repair of Pararenal Aortic Aneurysms: Triple- Versus Double- or Single-Fenestrated Stent-Grafts. J Endovasc Ther. 2011;18(1):98-105.

98. Halak M, Goodman MA, Baker SR. The Fate of Target Visceral Vessels After Fenestrated Endovascular Aortic Repair—General Considerations and Mid-term Results. Eur J Vasc Endovasc Surg. 2006;32(2):124-8.
99. Constantinou J, Giannopoulos A, Cross J, Morgan-Rowe L, Agu O, Ivancev K. Temporary axillobifemoral bypass during fenestrated aortic aneurysm repair. J Vasc Surg. 2012;56(6):1544-8.
100. Metcalfe MJ, Holt PJ, Hinchliffe RJ, Morgan R, Loftus IM, Thompson MM. Fenestrated Endovascular Aneurysm Repair: Graft Complexity Does Not Predict Outcome. J Endovasc Ther. 2012;19(4):528-35.
101. Canning C, Martin Z, Colgan MP, Abdulrahim O, McCafferty M, Fitzpatrick J, et al. Fenestrated endovascular repair of complex aortic aneurysms. Ir J Med Sci. 2015;184(1):249-55.
102. Ronchey S, Serrao E, Kasemi H, Pecoraro F, Fazzini S, Alberti V, et al. Endovascular treatment options for complex abdominal aortic aneurysms. J Vasc Interv Radiol. 2015;26(6):842-54.
103. Coscas R, Becquemin JP, Majewski M, Mayer J, Marzelle J, Allaire E, et al. Management of perioperative endoleaks during endovascular treatment of juxta-renal aneurysms. Ann Vasc Surg. 2012;26(2):175-84.
104. Donas KP, Eisenack M, Panuccio G, Austermann M, Osada N, Torsello G. The role of open and endovascular treatment with fenestrated and chimney endografts for patients with juxtarenal aortic aneurysms. J Vasc Surg. 2012;56(2):285-90.
105. Kristmundsson T, Sonesson B, Malina M, Bjorses K, Dias N, Resch T. Fenestrated endovascular repair for juxtarenal aortic pathology. J Vasc Surg. 2009;49(3):568-74.
106. Sveinsson M, Sobocinski J, Resch T, Sonesson B, Dias N, Haulon S, et al. Early versus late experience in fenestrated endovascular repair for abdominal aortic aneurysm. J Vasc Surg. 2015;61(4):895-901.
107. Kristmundsson T, Sonesson B, Dias N, Tornqvist P, Malina M, Resch T. Outcomes of fenestrated endovascular repair of juxtarenal aortic aneurysm. J Vasc Surg. 2014;59(1):115-20.
108. Mastracci TM, Eagleton MJ, Kuramochi Y, Bathurst S, Wolski K. Twelve-year results of fenestrated endografts for juxtarenal and group IV thoracoabdominal aneurysms. J Vasc Surg. 2015;61(2):355-64.
109. Canavati R, Millen A, Brennan J, Fisher RK, McWilliams RG, Naik JB, et al. Comparison of fenestrated endovascular and open repair of abdominal aortic aneurysms not suitable for standard endovascular repair. J Vasc Surg. 2013;57(2):362.
110. Shahverdyan R, Majd MP, Thul R, Braun N, Gawenda M, Brunkwall J. F-EVAR does not Impair Renal Function more than Open Surgery for Juxtarenal Aortic Aneurysms: Single Centre Results. Eur J Vasc Endovasc Surg. 2015;50(4):432-41.
111. Martin-Gonzalez T, Pincon C, Maurel B, Hertault A, Sobocinski J, Spear R, et al. Renal Outcomes Following Fenestrated and Branched Endografting. Eur J Vasc Endovasc Surg. 2015;50(4):420-30.
112. Bakoyiannis CN, Economopoulos KP, Georgopoulos S, Klonaris C, Shialarou M, Kafeza M, et al. Fenestrated and Branched Endografts for the Treatment of Thoracoabdominal Aortic Aneurysms: A Systematic Review. J Endovasc Ther. 2010;17(2):201-9.
113. Boyle JR, Thompson MM, Vallabhaneni SR, Bell RE, Brennan JA, Browne TF, et al. Pragmatic minimum reporting standards for endovascular abdominal aortic aneurysm repair. J Endovasc Ther. 2011;18(3):263-71.

114. Grimme FAB, Zeebregts CJ, Bekkema F, Tielliu IFJ, Reijnen MMJP, Verhoeven ELG. Visceral stent patency in fenestrated stent grafting for abdominal aortic aneurysm repair. J Vasc Surg. 2014;59(2):298-306.
115. O'Callaghan A, Greenberg RK, Eagleton MJ, Bena J, Mastracci TM. Type Ia endoleaks after fenestrated and branched endografts may lead to component instability and increased aortic mortality. J Vasc Surg. 2015;61(4):908-14.
116. England A, Garcia-Finana M, McWilliams RG. Multicenter retrospective investigation into migration of fenestrated aortic stent grafts. J Vasc Surg. 2015;62(4):884-92.
117. Haddad F, Greenberg RK, Walker E, Nally J, O'Neill S, Kolin G, et al. Fenestrated endovascular grafting: The renal side of the story. J Vasc Surg. 2005;41(2):181-90.
118. Greenberg RK, Sternbergh WC, 3rd, Makaroun M, Ohki T, Chuter T, Bharadwaj P, et al. Intermediate results of a United States multicenter trial of fenestrated endograft repair for juxtarenal abdominal aortic aneurysms. J Vasc Surg. 2009;50(4):730-7.
119. Resch T, Sonesson B, Malina M. Incidence and management of complications after branched and fenestrated endografting. J Cardiovasc Surg. 2010;51(1):105-13.
120. Dowdall JF, Greenberg RK, West K, Moon M, Lu Q, Francis C, et al. Separation of Components in Fenestrated and Branched Endovascular Grafting – Branch Protection or a Potentially New Mode of Failure? Eur J Vasc Endovasc Surg. 2008;36(1):2-9.
121. Oshin OA, Fisher RK, Williams LA, Brennan JA, Gilling-Smith GL, Vallabhaneni SR, et al. Adjunctive iliac stents reduce the risk of stent-graft limb occlusion following endovascular aneurysm repair with the Zenith stent-graft. J Endovasc Ther. 2010;17(1):108-14.
122. Malina M, Brunkwall J, Ivancev K, Jonsson J, Malina J, Lindblad B. Endovascular Healing Is Inadequate for Fixation of Dacron Stent-grafts in Human Aortoiliac Vessels. Eur J Vasc Endovasc Surg. 2000;19(1):5-11.
123. Zhou SS, How TV, Rao Vallabhaneni S, Gilling-Smith GL, Brennan JA, Harris PL, et al. Comparison of the Fixation Strength of Standard and Fenestrated Stent-Grafts for Endovascular Abdominal Aortic Aneurysm Repair. J Endovasc Ther. 2007;14(2):168-75.
124. Bosman WMPF, Steenhoven TJvd, Su, aacute, rez DR, Hinnen JW, et al. The Proximal Fixation Strength of Modern EVAR Grafts in a Short Aneurysm Neck. An In Vitro Study. Eur J Vasc Endovasc Surg. 2010;39(2):187-92.
125. Zenith Flex: Cook Medical Inc.; 2013 [07/01/2016]. Available from: https://www.cookmedical.com/zenithflex/.
126. Talent Abdominal Stent Graft: Medtronic; 2014 [cited 2013]. Available from: http://www.medtronic.com/patients/abdominal-aortic-aneurysm/device/abdominal-stents/talent/.
127. Resch T, Malina M, Lindblad B, Malina J, Brunkwall J, Ivancev K. The Impact of Stent Design on Proximal Stent-graft Fixation in the Abdominal Aorta: an Experimental Study. Eur J Vasc Endovasc Surg. 2000;20(2):190-5.
128. Murphy EH, Johnson ED, Arko FR. Device-Specific Resistance to In Vivo Displacement of Stent-Grafts Implanted With Maximum Iliac Fixation. J Endovasc Ther. 2007;14(4):585-92.
129. Arko FR, Heikkinen M, Lee ES, Bass A, Alsac JM, Zarins CK. Iliac fixation length and resistance to in-vivo stent-graft displacement. J Vasc Surg. 2005;41(4):664-71.
130. Heikkinen MA, Alsac JM, Arko FR, Metsanoja R, Zvaigzne A, Zarins CK. The importance of iliac fixation in prevention of stent graft migration. J Vasc Surg. 2006;43(6):1130-7.

131. Waasdorp EJ, de Vries JPPM, Sterkenburg A, Vos JA, Kelder HJC, Moll FL, et al. The Association between Iliac Fixation and Proximal Stent-graft Migration during EVAR Follow-up: Mid-term Results of 154 Talent Devices. Eur J Vasc Endovasc Surg. 2009;37(6):681-7.
132. Benharash P, Lee JT, Abilez OJ, Crabtree T, Bloch DA, Zarins CK. Iliac fixation inhibits migration of both suprarenal and infrarenal aortic endografts. J Vasc Surg. 2007;45(2):250-7.
133. Scurr JR, How TV, McWilliams RG, Lane S, Gilling-Smith GL. Fenestrated stent-graft repair: which stent should be used to secure target vessel fenestrations? J Endovasc Ther. 2008;15(3):344-8.
134. Dyet J, Watts W, Ettles D, Nicholson A. Mechanical properties of metallic stents: How do these properties influence the choice of stent for specific lesions? Cardiovasc Intervent Radiol. 2000;23(1):47-54.
135. Linsen MA, Vos AW, Diks J, Rauwerda JA, Wisselink W. Fenestrated and Branched Endografts: Assessment of Proximal Aortic Neck Fixation. J Endovasc Ther. 2005;12(6):647-53.
136. Kratzberg JA, Golzarian J, Raghavan ML. Role of graft oversizing in the fixation strength of barbed endovascular grafts. J Vasc Surg. 2009;49(6):1543-53.
137. Sternbergh W, Sternbergh WC, III, Money SR, Greenberg RK, Chuter TAM. Influence of endograft oversizing on device migration, endoleak, aneurysm shrinkage, and aortic neck dilation: results from the zenith multicenter trial. J Vasc Surg. 2004;39(1):20-6.
138. Kim DB, Choi H, Joo SM, Kim HK, Shin JH, Hwang MH, et al. A Comparative Reliability and Performance Study of Different Stent Designs in Terms of Mechanical Properties: Foreshortening, Recoil, Radial Force, and Flexibility : Reliability and performance of different stent designs. Artificial Organs. 2013;37(4):368-79.
139. Bastos Gonçalves F, Verhagen HJM, Chinsakchai K, van Keulen JW, Voûte MT, Zandvoort HJ, et al. The influence of neck thrombus on clinical outcome and aneurysm morphology after endovascular aneurysm repair. J Vasc Surg. 2012;56(1):36-44.
140. Choke E, Munneke G, Morgan R, Belli AM, Loftus I, McFarland R, et al. Outcomes of Endovascular Abdominal Aortic Aneurysm Repair in Patients with Hostile Neck Anatomy. Cardiovasc Intervent Radiol. 2006;29(6):975-80.
141. Sternbergh 3rd WC, Carter G, York JW, Yoselevitz M, Money SR. Aortic neck angulation predicts adverse outcome with endovascular abdominal aortic aneurysm repair. J Vasc Surg. 2002;35(3):482-6.
142. Boult M, Babidge W, Maddern G, Barnes M, Fitridge R. Predictors of Success Following Endovascular Aneurysm Repair: Mid-term Results. Eur J Vasc Endovasc Surg. 2006;31(2):123-9.
143. Scurr JRH, McWilliams RG, How TV. How Secure is the Anastomosis between the Proximal and Distal Body Components of a Fenestrated Stent-Graft? Eur J Vasc Endovasc Surg. 2012;44(3):281-6.
144. Liffman K, Sutalo ID, Lawrence-Brown MM, Semmens JB, Aldham B. Movement and Dislocation of Modular Stent-Grafts Due to Pulsatile Flow and the Pressure Difference Between the Stent-Graft and the Aneurysm Sac. J Endovasc Ther. 2006;13(1):51-61.
145. Cina DP, Grant G, Peterson M, Campbell V, Garrido-Olivares L, Cina CS. A Study of Pullout Forces of the Components of Modular Multi-manufacturer Hybrid Endografts Used for Aortic Aneurysm Repair. Eur J Vasc Endovasc Surg. 2009;37(6):671-80.
146. Peripheral Vision: W.L. Gore & Associates Inc.; 2009 [07/01/2016]. Available from: http://www.goremedical.com/newsletters/peripheral-vision/issue-2/news1.html.

147. Anaconda AAA Stent Graft System: Vascutek; 2011 [cited 2013]. Available from: http://www.vascutek.com/vascutek/products/item/anaconda-aaa-stent-graft-system.
148. Media Kits Aortic Aneurysm - Abdominal: Medtronic; 2015 [07/01/2015]. Available from: http://newsroom.medtronic.com/phoenix.zhtml?c=251324&p=irol-mediakit&ID=AorticAneurysmAbdominal.
149. Raza I, Badran MF, McWilliams R, Gould D, Harris PL, Gilling-Smith GL, et al. Common iliac artery engagement: an important concept in relation to endovascular aortic aneurysm repair (EVAR). Annals of the Royal College of Surgeons of England. 2002;84(4):282.
150. Coulston J, Baigent A, Selvachandran H, Jones S, Torella F, Fisher R. Lack of Iliac Engagement Correlates With Iliac Limb Complications Following Standard EVAR. Vascular and Endovascular Surgery. 2015;49(7):201-5.
151. England A, Butterfield J, McCollum C, Ashleigh R. Endovascular Aortic Aneurysm Repair with the Talent Stent-Graft: Outcomes in Patients with Large Iliac Arteries. CardioVascular and Interventional Radiology. 2008;31(4):723-7.
152. Malagari K, Brountzos E, Gougoulakis A, Papathanasiou M, Alexopoulou E, Mastorakou R, et al. Large Diameter Limbs for Dilated Common Iliac Arteries in Endovascular Aneurysm Repair. Is It Safe? Cardiovasc Intervent Radiol. 2004;27(3):237-42.
153. Filis KA, Arko FR, Rubun GD, Raman B, Fogarty TJ, Zarins CK. Aortoiliac angulation and the need for secondary procedures to secure stent graft fixation: Which angle is important? International angiology : a journal of the International Union of Angiology. 2002;21(4):349-54.
154. Zhou SN, How TV, Black RA, Vallabhaneni SR, McWilliams R, Brennan JA. Measurement of pulsatile haemodynamic forces in a model of a bifurcated stent graft for abdominal aortic aneurysm repair. Proceedings of the Institution of Mechanical Engineers Part H Journal of Engineering in Medicine. 2008;222(4):543-9.
155. Volodos SM, Sayers RD, Gostelow JP, Bell P. Factors Affecting the Displacement Force Exerted on a Stent Graft after AAA Repair; An In vitro Study. Eur J Vasc Endovasc Surg. 2003;26(6):596-601.
156. Corbett TJ, Callanan A, McGloughlin TM. In vitro measurement of the axial migration force on the proximal end of a bifurcated abdominal aortic aneurysm stent-graft model. Proceedings of the Institution of Mechanical Engineers Part H, Journal of Engineering in Medicine (Professional Engineering Publishing). 2011;225(H4):401-9.
157. Volodos SM, Sayers RD, Gostelow JP, Bell PRF. An investigation into the cause of distal endoleaks: Role of displacement force on the distal end of a stent-graft. J Endovasc Ther. 2005;12(1):115-20.
158. Morris L, Delassus P, Walsh M, McGloughlin T. A mathematical model to predict the in vivo pulsatile drag forces acting on bifurcated stent grafts used in endovascular treatment of abdominal aortic aneurysms (AAA). J Biomech. 2004;37(7):1087-95.
159. Avrahami I, Brand M, Meirson T, Ovadia-Blechman Z, Halak M. Hemodynamic and mechanical aspects of fenestrated endografts for treatment of Abdominal Aortic Aneurysm. European Journal of Mechanics - B/Fluids. 2012;35:85-91.
160. Figueroa CA, Taylor CA, Yeh V, Chiou AJ, Zarins CK. Effect of Curvature on Displacement Forces Acting on Aortic Endografts: A 3-Dimensional Computational Analysis. J Endovasc Ther. 2009;16(3):284-94.

161. Kandail H, Hamady M, Xu XY. Patient-specific analysis of displacement forces acting on fenestrated stent grafts for endovascular aneurysm repair. J Biomech. 2014;47(14):3546-54.
162. Li Z, Kleinstreuer C. Computational analysis of type II endoleaks in a stented abdominal aortic aneurysm model. J Biomech. 2006;39(14):2573-82.
163. Li Z, Kleinstreuer C, Farber M. Computational analysis of biomechanical contributors to possible endovascular graft failure. Biomechanics and Modeling in Mechanobiology. 2005;4(4):221-34.
164. Segalova PA, Xiong G, Venkateswara Rao KT, Zarins CK, Taylor CA. Evaluating Design of Abdominal Aortic Aneurysm Endografts in a Patient-Specific Model Using Computational Fluid Dynamics. Journal of Medical Devices. 2011;5(4):041005.
165. Molony DS, Kavanagh EG, Madhavan P, Walsh MT, McGloughlin TM. A Computational Study of the Magnitude and Direction of Migration Forces in Patient-specific Abdominal Aortic Aneurysm Stent-Grafts. Eur J Vasc Endovasc Surg. 2010;40(3):332-9.
166. Tu J, Yeoh GH, Liu C. Computational fluid dynamics. [electronic book] : a practical approach: Amsterdam ; Elsevier/Butterworth-Heinemann, 2013. 2nd ed.; 2013.
167. Ray G, Davids N. Shear stress analysis of blood-endothelial surface in inlet section of artery with plugging. J Biomech. 1970;3(1):99-110.
168. Taylor CA, Hughes TJ, Zarins CK. Finite element modeling of three-dimensional pulsatile flow in the abdominal aorta: relevance to atherosclerosis. Ann Biomed Eng. 1998;26(6):975-87.
169. Fillinger MF, Marra SP, Raghavan ML, Kennedy FE. Prediction of rupture risk in abdominal aortic aneurysm during observation: wall stress versus diameter. J Vasc Surg. 2003;37(4):724-32.
170. Fillinger MF, Raghavan ML, Marra SP, Cronenwett JL, Kennedy FE. In vivo analysis of mechanical wall stress and abdominal aortic aneurysm rupture risk. J Vasc Surg. 2002;36(3):589-97.
171. Venkatasubramaniam AK, Fagan MJ, Mehta T, Mylankal KJ, Ray B, Kuhan G, et al. A comparative study of aortic wall stress using finite element analysis for ruptured and non-ruptured abdominal aortic aneurysms. Eur J Vasc Endovasc Surg. 2004;28(2):168-76.
172. Li Z, Kleinstreuer C. Analysis of biomechanical factors affecting stent-graft migration in an abdominal aortic aneurysm model. J Biomech. 2006;39(12):2264-73.
173. Long Q, Xu XY, Collins MW, Bourne M, Griffith TM. Magnetic resonance image processing and structured grid generation of a human abdominal bifurcation. Computer Methods and Programs in Biomedicine. 1998;56(3):249-59.
174. Raghavan ML, Vorp DA, Federle MP, Makaroun MS, Webster MW. Wall stress distribution on three-dimensionally reconstructed models of human abdominal aortic aneurysm. J Vasc Surg. 2000;31(4):760-9.
175. Redaelli A, Rizzo G, Arrigoni S, Martino ED, Origgi D, Fazio F, et al. An assisted automated procedure for vessel geometry reconstruction and hemodynamic simulations from clinical imaging. Computerized Medical Imaging and Graphics. 2002;26(3):143-52.
176. Georgakarakos E, Xenakis A, Manopoulos C, Georgiadis GS, Tsangaris S, Lazarides M. Geometric Factors Affecting the Displacement Forces in an Aortic Endograft With Crossed Limbs: A Computational Study. J Endovasc Ther. 2013;20(2):191-9.
177. Molony DS, Callanan A, Morris LG, Doyle BJ, Walsh MT, McGloughlin TM. Geometrical Enhancements for Abdominal Aortic Stent-Grafts. J Endovasc Ther. 2008;15(5):518-29.

178. Molony DS, Callanan A, Kavanagh EG, Walsh MT, McGloughlin TM. Fluid-structure interaction of a patient-specific abdominal aorticaneurysm treated with an endovascular stent-graft. BioMedical Engineering OnLine. 2009;8(1):24-35.
179. Morris L, Delassus P, Grace P, Wallis F, Walsh M, McGloughlin T. Effects of flat, parabolic and realistic steady flow inlet profiles on idealised and realistic stent graft fits through Abdominal Aortic Aneurysms (AAA). Medical Engineering & Physics. 2006;28(1):19-26.
180. Nichols WW, Nichols WW, McDonald DA. McDonald's blood flow in arteries : theoretic, experimental, and clinical principles. 6th ed. London: Hodder Arnold; 2011.
181. Chaikof EL, Fillinger MF, Matsumura JS, Rutherford RB, White GH, Blankensteijn JD, et al. Identifying and grading factors that modify the outcome of endovascular aortic aneurysm repair. J Vasc Surg. 2002;35(5):1061-6.
182. Diehm N, Katzen BT, Samuels S, Pena C, Powell A, Dick F. Sixty-four-detector CT angiography of infrarenal aortic neck length and angulation: Prospective analysis of interobserver variability. J Vasc Interv Radiol. 2008;19(9):1283-8.
183. Kramer SC, Seifarth H, Pamler R, Fleiter T, Gorich J. Geometric Changes in Aortic Endografts Over a 2-year Observation Period. J Endovasc Ther. 2001;8(1):34-8.
184. Kritpracha B, Wolfe J, Beebe HG. CT Artifacts of the Proximal Aortic Neck: An Important Problem in Endograft Planning. J Endovasc Ther. 2002;9(1):103-10.
185. Ouriel K, Tanquilut E, Greenberg RK, Walker E. Aortoiliac morphologic correlations in aneurysms undergoing endovascular repair. J Vasc Surg. 2003;38(2):323-8.
186. Parra JR, Ayerdi J, McLafferty R, Gruneiro L, Ramsey D, Solis M, et al. Conformational changes associated with proximal seal zone failure in abdominal aortic endografts. J Vasc Surg. 2003;37(1):106-11.
187. White RA DC, Walot I, Woody J , Kim N, Kopchok GE. Computed tomography assessment of abdominal aortic aneurysm morphology after endograft exclusion. J Vasc Surg. 2001;33(2 Suppl):1-10.
188. van Keulen JW, Moll FL, Tolenaar JL, Verhagen HJM, van Herwaarden JA. Validation of a new standardized method to measure proximal aneurysm neck angulation. J Vasc Surg. 2010;51(4):821-8.
189. Ullery BW, Suh GY, Lee JT, Liu B, Stineman R, Dalman RL, et al. Geometry and respiratory-induced deformation of abdominal branch vessels and stents after complex endovascular aneurysm repair. J Vasc Surg. 2015;61(4):875-84.
190. Coulston J, Baigent A, Selvachandran H, Jones S, Torella F, Fisher R. The impact of endovascular aneurysm repair on aortoiliac tortuosity and its use as a predictor of iliac limb complications. J Vasc Surg. 2014;60(3):585-9.
191. Suh GY, Les AS, Tenforde AS, Shadden SC, Spilker RL, Yeung JJ, et al. Hemodynamic Changes Quantified in Abdominal Aortic Aneurysms with Increasing Exercise Intensity Using MR Exercise Imaging and Image-Based Computational Fluid Dynamics. Ann Biomed Eng. 2011;39(8):2186.
192. Les AS, Shadden SC, Figueroa CA, Park JM, Tedesco MM, Herfkens RJ, et al. Quantification of Hemodynamics in Abdominal Aortic Aneurysms During Rest and Exercise Using Magnetic Resonance Imaging and Computational Fluid Dynamics. Ann Biomed Eng. 2010;38(4):1288-313.
193. Zhou SS. Biomechanical investigations of endografts for abdominal aortic aneurysm repair: Liverpool : Thesis M.D., 2009.; 2009.
194. England A, García-Fiñana M, Fisher RK, Naik JB, Vallabhaneni SR, Brennan JA, et al. Migration of fenestrated aortic stent grafts. J Vasc Surg. 2013;57(6):1543-52.

195. Scurr JR, McWilliams RG, How TV. How secure is the anastomosis between the proximal and distal body components of a fenestrated stent-graft? Eur J Vasc Endovasc Surg. 2012;44(3):281-6.
196. Conway AM, Modarai B, Taylor PR, Carrell TWG, Waltham M, Salter R, et al. Stent-graft limb deployment in the external iliac artery increases the risk of limb occlusion following endovascular AAA repair. J Endovasc Ther. 2012;19(1):79-85.
197. England A, García-Fiñana M, How TV, Vallabhaneni SR, McWilliams RG. The accuracy of computed tomography central luminal line measurements in quantifying stent graft migration. J Vasc Surg. 2012;55(4):895-905.
198. Shah S, Jones SM, How TV, Williams RL, Fisher RK. Distal fixation forces of different endovascular limb extensions in an experimental porcine model. Br J Surg. 2015;102:15.
199. van Marrewijk CJ, Leurs LJ, Vallabhaneni SR, Harris PL, Buth J, Laheij RJ. Risk-Adjusted Outcome Analysis of Endovascular Abdominal Aortic Aneurysm Repair in a Large Population: How Do Stent-Grafts Compare? J Endovasc Ther. 2005;12(4):417-29.
200. The ETP. Secondary Interventions and Mortality Following Endovascular Aortic Aneurysm Repair: Device-specific Results from the UK EVAR Trials. Eur J Vasc Endovasc Surg. 2007;34(3):281-90.
201. Zenith Spiral-Z AAA Iliac Leg Graft Instructions for Use: Cook Medical Inc.; 2013 [07/01/2016]. Available from: https://www.cookmedical.com/data/IFU_PDF/T_ZAAASZ_REV3.PDF.
202. Poullis MP, Warwick R, Oo A, Poole RJ. Ascending aortic curvature as an independent risk factor for type A dissection, and ascending aortic aneurysm formation: a mathematical. Eur J Cardiothorac Surg. 2008;33(6):995-1001.
203. Hoshina K, Akai T, Takayama T, Kato M, Nakazawa T, Okamoto H, et al. Outcomes and Morphologic Changes After Endovascular Repair for Abdominal Aortic Aneurysms With a Severely Angulated Neck - A Device-Specific Analysis. Circulation. 2013;77(8):1996-2002.
204. Badran MF, Gould DA, Raza I, McWilliams RG, Brown O, Harris PL, et al. Aneurysm neck diameter after endovascular repair of abdominal aortic aneurysms. J Vasc Interv Radiol. 2002;13(9 Pt 1):887-92.
205. Xiong G, Taylor CA. Virtual stent grafting in personalized surgical planning for treatment of aortic aneurysms using image-based computational fluid dynamics2010. 375-82 p.
206. Chaer RA, DeRubertis BG, Lin SC, Bush HL, Karwowski JK, Birk D, et al. Simulation improves resident performance in catheter-based intervention: Results of a randomized, controlled study. Ann Surg. 2006;244(3):343-9.
207. Kendrick DE, Gosling AF, Nagavalli A, Kashyap VS, Wang JC. Endovascular Simulation Leads to Efficiency and Competence in Thoracic Endovascular Aortic Repair Procedures. Journal of Surgical Education. 2015 In press.
208. Karthikesalingam A, Cobb RJ, Khoury A, Choke EC, Sayers RD, Holt PJ, et al. The Morphological Applicability of a Novel Endovascular Aneurysm Sealing (EVAS) System (Nellix) in Patients with Abdominal Aortic Aneurysms. Eur J Vasc Endovasc Surg. 2013;46(4):440-5.
209. Krievins DK, Holden A, Savlovskis J, Calderas C, Donayre CE, Moll FL, et al. EVAR Using the Nellix Sac-anchoring Endoprosthesis: Treatment of Favourable and Adverse Anatomy. Eur J Vasc Endovasc Surg. 2011;42(1):38-46.
210. Torella F, Chan TY, Shaikh U, England A, Fisher RK, McWilliams RG. ChEVAS: Combining Suprarenal EVAS with Chimney Technique. Cardiovasc Intervent Radiol. 2015;38(5):1294-8.

211. Nellix Endovascular Anuerysm Sealing System: Endologix Inc.; 2016 [09/01/2016]. Available from: http://www.endologix.com/investigational_devices/nellix/.